DEVELOPMENT OF EROSION RESISTANT NITRONIC STEEL

A THESIS

Submitted in partial fulfilment of the
requirements for the award of the degree
of
DOCTOR OF PHILOSOPHY
in
METALLURGICAL AND MATERIALS ENGINEERING

by

AKHILESH KUMAR CHAUHAN

DEPARTMENT OF METALLURGICAL AND MATERIALS ENGINEERING
INDIAN INSTITUTE OF TECHNOLOGY ROORKEE
ROORKEE - 247 667 (INDIA)

AUGUST, 2008

INDIAN INSTITUTE OF TECHNOLOGY ROORKEE
ROORKEE

CANDIDATE'S DECLARATION

I hereby certify that the work which is being presented in the thesis entitled **DEVELOPMENT OF EROSION RESISTANT NITRONIC STEEL,** in partial fulfilment of the requirements for the award of the Degree of Doctor of Philosophy and submitted in the Department of Metallurgical & Materials Engineering of the Indian Institute of Technology Roorkee, Roorkee, is an authentic record of my own work carried out during a period from Jan. 2004 to Aug. 2008 under the supervision of Dr. D.B. Goel, Emeritus Fellow and Dr. S. Prakash, Professor, Metallurgical and Materials Engineering Department, Indian Institute of Technology Roorkee, Roorkee.

The matter presented in this thesis has not been submitted by me for the award of any other degree of this or any other institute.

AKHILESH KUMAR CHAUHAN

This is to certify that the above statement made by the candidate is correct to the best of our knowledge.

(S. Prakash)
Supervisor

(D.B.Goel)
Supervisor

Date: 11.08.08

The Ph.D. Viva-Voce Examination of **Mr. Akhilesh Kumar Chauhan**, Research Scholar, has been held on 24.10.2008

Signature of Supervisors

24-10-2008

Signature of External Examiner

(D. H. SASTRY)
I.I. Sc.

Synopsis

Erosive wear is caused by the impact of abrasive particles against a solid surface. Erosion is rapid and severe forms of wear and can results in significant costs if not adequately controlled. Erosive wear occurs in a wide variety of machineries and typical examples are the damage to gas turbine blades when an aircraft flies through dust clouds, hydro turbine under water parts when silt laden water flows through it and the wear of pump impellers in mineral slurry processing systems. It is seen that hydro power plants suffer a serious setback due to rapid erosion of underwater parts by silt laden water and cavitation.

The 13Cr-4Ni (termed as 13/4 or CA6NM) steel is currently being used for fabrication of underwater parts in hydroelectric projects. There are, however, several maintenance problems associated with the use of this steel. In this research attempts are made to develop an erosion resistant material called 21-4-N steel as an alternative to 13/4 steel. So far no investigation has been reported on the comparative study on erosion behaviour of 13/4 and 21-4-N steel. 21-4-N steel is a nitrogen strengthened austenitic stainless steel. The role of nitrogen in 21-4-N steel is to stabilize the austenitic structure at room temperature, strengthen the austenitic matrix by solid solution hardening and decrease the stacking fault energy, which results in improving the strain hardening ability. By alloying with nitrogen, the strength of the alloy can exceed than that of martensitic steel. Due to higher strain hardening ability, the strength of nitronic steels can be enhanced by mechanical deformation.

Bars of 40 × 40 mm cross section of as cast 13/4 steel and 21-4-N steel in as cast and hot rolled conditions were received from M/S Star Wire (India) Ltd. Ballabhgarh

(Haryana). The heat treatment of as cast 13/4 steel involved austenitizing at 1050°C, followed by oil quenching, followed by tempering at 620°C for 4 hrs. The heat treatment of as cast 21-4-N steel consisted of heating at various austenitizing temperatures (950°C, 1000°C, 1050°C and 1100°C) for 2 hr, followed by water quenching (WQ). A few specimens of 21-4-N steel were solution treated at 1100°C, followed by WQ, followed by aging at 700°C for 20 hrs. To investigate the effect of deformation on mechanical properties and erosion behaviour 8% reduction in thickness was given to as cast 13/4 and 21-4-N steels at 700°C. Studies were also conducted on 21-4-N steel, which was subjected to 89% reduction in cross sectional area by hot rolling at 1180°C.

The erosion rate or weight loss for all the samples was determined by means of solid particle erosion using gas jet. The erodent particles used were SiC of size 500-700 μm. Particle velocity of 120 ms^{-1} at a constant feed rate of 5 g min^{-1} has been employed. The erosion experiments were conducted at 30° and 90° impingement angles at room temperature. The samples were cleaned in acetone, dried, weighed to an accuracy of 1×10^{-4} g using an electronic balance, eroded in the test rig for 10 min and then weighed again to determine weight loss. The ratio of this weight loss to the weight of the eroding particles causing the loss (i.e., testing time × particle feed rate) was then computed as the dimensionless incremental erosion rate. The cavitation erosion tests were performed using ultrasonic vibration processor for total duration of 32 hr. The scanning electron microscopy was used to study the mechanisms of erosion. To study the effect of surface coatings on erosion behaviour, D-Gun spray coatings of stellte-6, Cr_3C_2-NiCr and WC-Co-Cr were provided on the hot rolled 21-4-N steel, which has excellent erosion resistance.

The microstructure of 13/4 steel consists of martensitic laths and δ-ferrite. However, these martensitic laths are observed to be thickened after tempering as well as after 8% rolling operation. The microstructure of 21-4-N steel in various conditions consists of precipitates of carbides in the matrix of austenite. During solution annealing treatment most of the carbides are dissolved in austenitic matrix. The extent of carbide precipitation is increased during aging of 21-4-N steel. Small deformation (8%) does not cause any appreciable change in the microstructure of as cast 21-4-N steel. The microstructure of hot rolled 21-4-N steel consists of fine grains of austenite and precipitates of carbides along the grain boundaries.

The 13/4 steel in as cast condition possesses significantly higher values of impact energy, YS and UTS than the corresponding values in the 21-4-N steel in as cast condition. The hardness, ductility (% elongation), tensile toughness and strain hardening exponent in 13/4 steel in as cast condition are lower than that for as cast 21-4-N steel in as cast condition. Due to austenitizing and tempering of 13/4 steel (termed as tempered 13/4 steel), there is significant increase in YS, UTS and impact energy, and the value of hardness is decreased, while minor changes occur in ductility, tensile toughness and strain hardening exponent. Drastic fall in the values of ductility, impact energy, tensile toughness and considerable increase in the values of YS, UTS and hardness are observed, while strain hardening exponent remains almost unchanged in 13/4 steel as a result of 8% rolling. The solution annealing treatment of as cast 21-4-N steel shows the increased value of YS, UTS, ductility and tensile toughness, whereas these are decreased as a result of 8% rolling. Hardness and strain hardening exponent of as cast 21-4-N steel are observed to decrease by the solution annealing treatment, but increase in hardness and

strain hardening exponent is seen after aging treatment; while minor change is seen in impact energy. After 8% rolling of 21-4-N steel, there is remarkable increase in YS, UTS and hardness; whereas the values of ductility, tensile toughness, impact energy and strain hardening exponent decrease considerably.

It is seen that erosion damage in both the 13/4 and 21-4-N steels is lower at 30° impingement angle than that at 90° impingement angle, which corresponds to erosion of brittle materials. The erosion behaviour in 13/4 and 21-4-N steels are observed to be affected by heat treatments and deformation by rolling. Cumulative weight losses of all the samples eroded at 30° impingement angle give straight line relationship with time, which indicates that the mechanism of erosion is same throughout the erosion test. Maximum weight loss is observed at 30° impingement angle in tempered 13/4 steel; while at 90° impingement angle maximum weight loss is observed in 8% rolled 13/4 steel. The least cumulative weight loss is observed in hot rolled 21-4-N steel at both the impingement angles.

The erosion resistance of as cast 21–4–N steel investigated by means of solid particle impingement is higher than that of as cast 13/4 martensitic stainless steel, because of its austenitic matrix, which is less prone to erosion damages as compared to the stressed and untempered martensitic matrix of 13/4 steel. Mechanical properties significantly affect the erosion resistance of target material. In 21–4–N steel, high resistance to erosion is due to (i) high hardness coupled with high ductility, (ii) high tensile toughness and (iii) high rate of strain hardening in comparison to 13/4 martensitic stainless steel.

Remarkable improvement is observed at 90° impingement angle in the erosion resistance of as cast 13/4 steel; whereas erosion resistance slightly deteriorates at 30° impingement angle as a result of solutionizing at 1050 °C and tempering at 620 °C. At 90° impingement angle the increased erosion resistance of 13/4 steel as result of tempering treatment is due to relieving of internal stresses and thickening of martensitic laths.

As a result of tempering at 620 °C there are certain changes in mechanical properties of 13/4 steel. Due to tempering the hardness decreases from 305 to 289 VHN and the tensile toughness increases slightly (from 68 to 71 MJm^{-3}). The values of ductility and strain hardening exponent (n) almost remain unchanged. The decrease in erosion resistance at 30° impingement angle is attributed to decrease in hardness whereas increase in erosion resistance at 90° impingement angle is correlated with slightly increase in tensile toughness.

Substantial improvement in the erosion resistance of 21-4-N steel at both the impingement angles of 30° and 90° is observed as a result of solution annealing at 1100 °C. However, aging treatment of solution annealed 21-4-N steel causes deterioration in erosion resistance at both impingement angles. The improved erosion resistance of 21-4-N steel as a result of solution annealing at 1100 °C is due to substantial dissolution of carbides in the austenitic matrix. Again reprecipitations of carbides in the aged 21-4-N steel are responsible for decreased erosion resistance.

The mechanical properties resulting from solution annealing significantly affect the erosion resistance of 21-4-N steel. The increased values of ductility and tensile toughness as a result of solution annealing of 21-4-N steel increase the erosion resistance.

However, lowering of hardness and strain hardening exponent of 21-4-N steel as result of solution annealing may cause reduction in erosion resistance; but cumulative effect of all mechanical properties results in increased erosion resistance.

Mechanical working (by rolling) significantly affects properties and erosion resistance of 13/4 and 21-4-N steels. In 13/4 steel the martensitic laths are thickened whereas in 21-4-N steel no significant change is observed in the microstructure as a result of 8% rolling at 700 °C. The values of YS, UTS, and hardness increase and the values of tensile toughness, ductility, impact energy and strain hardening exponent in both 13/4 and 21-4-N steels as a result of 8% rolling at 700 °C. The values of hardness, impact energy, YS, UTS, tensile toughness and strain hardening exponent increase in 21-4-N steel as a result of hot rolling.

As a result of 8% reduction in thickness by rolling, for both 13/4 and 21-4-N steels there is improvement in erosion resistance at 30° impingement angle, whereas at 90° impingement angle there is a deterioration in the erosion resistance. Hot rolling to 21-4-N steel causes improvement in erosion resistance at both impingement angles. By 8% rolling the improved erosion resistance of 13/4 and 21-4-N steel at 30° impingement angle is attributed to overwhelming effect of increased hardness; whereas, the deterioration in erosion resistance of both the steels at 90° impingement angle is attributed to decreased values of ductility, tensile toughness and strain hardening exponent, in addition to internal stresses induced during rolling. By hot rolling at 1180 °C the improved erosion resistance of 21-4-N steel at both 30° and 90° impingement angles is attributed to (i) fine grain structure of austenite and (ii) increased values of hardness, ductility, tensile toughness and strain hardening exponent.

The cavitation erosion resistance of 13/4 steel investigated by means of ultrasonic vibration processor is less than that of 21-4-N steel in both as cast and hot rolled conditions. However, hot rolled 21-4-N steel exhibits excellent cavitation erosion resistance. From the microstructure view point, the untempered martensitic laths of 13/4 steel exhibit more cavitation erosion than the austenitic structure of 21-4-N steel. The martensitic laths, already associated with internal stresses, are less able to absorb the strain energy due to transient stresses in the material induced by cavitation impact wave. It can also be inferred that the carbides present in 21-4-N steel are detrimental to cavitation erosion resistance leading to more erosion in as cast condition. In 21-4-N steel in both as cast and hot rolled conditions, the cavitation erosion damages occur along the grain boundaries and the carbides are the first to be dislodged from the specimens. In 21-4-N steel higher resistance to cavitation erosion is associated with high hardness coupled with high ductility, high tensile toughness and high strain hardening exponent in comparison to those in 13/4 steel.

The stellite-6 coating on 21-4-N steel substrate exhibits maximum damage due to erosion at 30° and 90° impingement angles. Minimum erosion losses are observed in WC-Co-Cr coating at 30° impingement angle. The analysis of the influence of various parameters on erosion behaviour of surface coatings poses a complex problem. It is not possible to quantify the role of individual parameters like microstructural features, microhardness and porosity in affecting the erosion behaviour of coating. It is, however, observed that the nature and extent of porosity affect to a large extent the erosion rate of coatings. Maximum concentration of porosity is observed in stellite-6 coating. Scanning electron microscopic study of eroded surfaces on coated components reveals that at 30°

impingement angle erosion occurs by a shear process involving formation of lips and ploughs on the target surface. Existence of deep craters in the SEM micrographs at 90° impingement angle indicate knocking out of chunk of material from the target surface resulting in high rates of erosion.

The entire work has been presented over nine chapters in the thesis. **Chapter 1** presents a critical review of the available literature on nitrogen strengthened austenitic stainless steels, solid particle erosion, erosion resistant engineering materials, cavitation erosion, cavitation erosion resistant engineering materials, and erosive wear of surface coatings. **Chapter 2** deals with the formulation of problem and planning of experiments. **Chapter 3** deals with the experimental study employed in the present study. Details of air jet erosion test rig, ultrasonic processor for cavitation erosion test have been described. Details of various treatments given to the steels under study have been described. Details of instruments/machines and the techniques employed in the mechanical testing and metallographic study are given. **Chapter 4** consists of characterization (microstructural and mechanical properties) and solid particle erosion behaviour of as cast 13/4 and 21-4-N steels. **Chapter 5** describes the effect of heat treatment on the solid particle erosion behaviour of as cast 13/4 and 21-4-N steels. **Chapter 6** describes the effect of deformation on the solid particle erosion behaviour of as cast 13/4 and 21-4-N steels. The erosion test was also conducted on hot rolled 21-4-N steel and comparative study has been made with that of as cast 21-4-N steel. **Chapter 7** gives the cavitation erosion behaviour of as cast 13/4 steel and 21-4-N steel in as cast and in hot rolled conditions. **Chapter 8** describes the characterization and erosive wear behaviour of surface coated hot rolled 21-4-N steel. **Chapter 9** presents the conclusions and scope for future works.

Acknowledgement

Throughout this work, Prof. D.B. Goel and Prof. S. Prakash, Department of Metallurgical and Materials Engineering, Indian Institute of Technology Roorkee, Roorkee, have been sources of inspiration. Their guidance, stimulating discussions with them and their painstaking efforts in organizing the thesis are gratefully and thankfully acknowledged. I do not have the words to express by obligation for their benevolent gesture of support and motivation provided through the course of this research work.

Thanks are due to Prof. S.K. Nath, Head of Department and Prof. P.S. Misra, former Head, Department of Metallurgical and Materials Engineering, Indian Institute of Technology Roorkee, Roorkee for providing necessary facilities in the department during my experimental work.

The steels used in this investigation were received from M/S Star Wire (India) Ltd Ballabhgargh (Haryana). I wish put on record the kind help I received from Mr. M. K. Gupta, Managing Director and Dr. S. K. Goel, Executive Director of this organization as also the keen interest they took in this study. They are also making sincere efforts for field trial of the nitronic steel developed in this investigation. Shri S. Kasana and Shri Rajnish Bhardwaj of M/S Star Wire (India) Ltd have rendered useful help in various experimental studies. The study on surface coatings was conducted with the kind assistance of Shri M. Nageshwara Rao, Managing Director, M/S Sai Surface Technologies, Hyderabad.

The investigation reported in this thesis form part of a larger R&D project funded by the Ministry of Power, Government of India. The assistance rendered by Ministry of

Power through Central Power Research Institute, Bangalore is gratefully acknowledged. I am also thankful to Government of India for taking keen interest in the field study of the nitronic steel developed in this investigation.

Help of Mr. K.V. Ojha, Mr. Anil K Chaturvedi, Mr Rajendra Prasad, Mr. Vikash Narayan and Mr. Mahesh R Anwar, Research Scholars, Department of Metallurgical and Materials Engineering, Indian Institute of Technology Roorkee, Roorkee during experimental work is gratefully acknowledged. Thanks are also due to M/S. S.S. Gupta, B.D. Sharma, Samsher Singh, Rajendra Singh Sharma, S.M. Giri and H.K. Ahuja of this department for necessary help during experimental work in their respective laboratories.

Special thanks are due to my wife Sushila Chauhan, son Matransh Chauhan and brothers and sisters for leaving me undisturbed and alone since past one year.

Last but not the least, I wish to place on record my deep sense of gratitude to my grandmother, parents and parents in-laws without whose blessings I would not have been able to join this prestigious department for higher studies to enrich myself with the latest knowledge. I dedicate this work and thesis to fond memories of Shri Ram Brikch Chauhan, my departed grandfather. He had been a source of motivation and inspiration due to which this work could be completed.

Roorkee Akhilesh K Chauhan

August, 2008.

Contents

List of figures

List of tables

Chapter 1

Literature review

1.1 Introduction

Erosion of underwater parts is a serious problem encountered in hydro power plants. In Indian context the problem is much serious and grave in the perennial Himalayan rivers which have a very high quartz rich silt content (fairly ranging between 5000 ppm to as high as 20000 ppm in monsoon). In India, 80% of available hydro power resources are from Himalayan region and Himalayan silt contains nearly 90% of quartz which is 7 on Moh's scale compared with 10 for diamonds and any particle having Moh's hardness of more than 5 is extremely harmful [1, 2].

Continuous demand of electrical energy in India has necessitated a smooth work of various power plants mainly in the Himalayan region. Various techniques have been reported to reduce the loss of material due to erosion [3-6]. Cavitation erosion and solid particle erosion often co-exist causing severe damage. According to **ASTM G76-02** [7], erosion is the progressive loss of original material from a solid surface due to mechanical interaction between that surface and a fluid, a multi-component fluid, or impinging liquid or solid particles. The cavitation is the formation and subsequent collapse, within a liquid, of cavities or bubbles that contain vapor or gas or both. Cavitation erosion is the progressive loss of original material from a solid surface due to continued exposure to cavitation **(ASTM G40)** [8]. Cavitation erosion is a type of wear in systems in which a material comes into contact with a flowing liquid, e.g. hydro turbines, ship propellers etc [9-19]. The bubble explode during cavitation generates very high and transient stresses,.

which strains the materials in a particular way [9]. Cavitation originates from a local decrease in hydrostatic pressure in the liquid; it is also produced by motion of the liquid i.e. decrease in static pressure induced by changes in velocity of a flowing liquid or cavitation caused by the pressure fluctuations within a liquid, induced by the vibration of a solid surface immersed in the liquid **(ASTM G32-06)** [20].

Initially the cavitation erosion is not too much dangerous for the hydro turbine under water parts, but in the presence of silt erosion damage, cavitation enhances the erosion damages. This is called synergetic erosion i.e. erosion due to silt as well as cavitation [5-6]. For efficient operation of a hydro turbine, it must have specific shape and contour. Cavitation erosion leaves behind cavities or pits which affect these important contours, creating obstacles to smooth flow of water through the turbine. This leads to a loss of operating efficiency of the turbine. Considering the cost of electrical energy, even a relatively small change in the operating efficiency can be very expensive. Cavitation causes surface penetration damage of up to 10 mm per year to critical components such as impellors, turbine blades, and casings [21].

The cast martensitic stainless steel containing 13%Cr and 4%Ni currently finds wide applications in many hydro turbine and other industrial applications facing damages due to erosion [22]. At present attempts are concentrated on techniques to reduce the erosion damages namely, reduce the silt content by sedimentation, providing hard surface coatings and development of erosion resistant materials. Sedimentation techniques suffer from the limitation that concentration of particles below 300 ppm cannot be eliminated

[23]. Improving the erosion resistance of engineering materials requires an understanding of the mechanism by which the material is removed. In case of ductile materials, the material removal is through cutting and ploughing while in case of brittle materials it is through flake fragmentation and removal of flakes [24-50]. The work hardening characteristic of the material also plays an important role in reducing the erosion. **Goretta et al** [51] have investigated the erosion of copper, nickel and 304 stainless steel with sharp alumina particles. They concluded that work hardening improves the erosion resistance of the copper, which has high ductility. Higher hardness also improves the erosion resistance of the material if it retains sufficient ductility. The role of ductility, which facilitates plastic flow of the target material by the impingement of abrasive particles, becomes very important. Poor ductility leads to tendency for localization of strains and development of cracks. As far as cavitation erosion is concerned, the characteristic of a ductile material exposed to cavitation is to be progressively hardened by the successive collapses. So any measure to allow some plastic deformation in the target material is expected to improve its erosion resistance. The erosion resistance can be increased by any treatment which improves the ductility. This has been theoretically predicted by **Hutchings** [52]. **Naim and Bahadur** [53] found in maraging steel that erosion increases with the increasing hardness at constant ductility, which is in conflict with the results of **Finnie** [54], who showed that erosion decreases with increasing hardness. **Naim and Bahadur** [53] also noted an increase in erosion rate as the ductility was reduced by cold working essentially at high strength.

Ductile failure mechanism is observed for most engineering metallic materials which are not very sensitive to strain rate. Metals with an fcc structure are generally not sensitive to strain rate. **Chen and Mongis** [55] reported that the response of fcc materials to cavitation is often similar to their static mechanical behaviour. For metals with bcc structure, the deformation is generally strain rate sensitive. So their reaction to cavitation is always a competition between flow and fracture. Brittle materials exhibit often brittle failure behaviour because of weak capability of energy absorption during deformation by impact. In this case most impact energy is dissipated by crack formation, which leads to more frequent material removal. The absorbed energy to remove a given volume of material by cracking is much less than that necessary to remove the same volume of material by plastic deformation. Tensile toughness is indicative of the ability of a material to absorb the energy of the abrasive particles impacted. **Levin et al** [56] have shown that a material having higher tensile toughness possesses higher erosion resistance.

Coatings provide a way of extending the limits of use of materials at the upper end of their performance capabilities, by allowing the mechanical properties of the substrate materials to be maintained while protecting them against wear [57]. Coating technology is one of the more rapidly growing technologies in the field of materials. A combination of the development of materials specifically erosion resistance and the appropriate technique for the application of these materials, as a coating would be the optimum solution. Suitable coating technique also allow for regeneration of parts that have been rendered unusable by erosion. Coatings are primarily used to restrict surface

damage of components in practice [58]. It has been reported that thermal spray is a technique that produces a wide range of coatings for diverse applications. Thermal spray coating represents an important and cost effective technique for tailoring the surface properties of engineering components with a view to enhancing their durability and performance under a variety of operating conditions. Among the commercially available thermal spray coating techniques, detonation spray and high velocity oxy fuel spray are the best choices to get hard, dense and consequently wear resistant coatings [59-61].

1.2 Hydro turbine steels

The stainless revolution began when it was observed that addition of 12% Cr imparts good corrosion resistance and avoids the rust formation over steels. As we all know today stainless steels are classified into different types and classes based on the phases present and the microstructure obtained.

There are over 150 grades of stainless steel, of which fifteen are most common. The AISI (American Iron and Steel Institute) defines the following grades among others:

- 200 Series—austenitic iron-chromium-nickel-manganese alloys
- 300 Series—austenitic iron-chromium-nickel alloys
    - Type 301—highly ductile, for formed products. Also hardens rapidly during mechanical working.
    - Type 303—free machining version of 304 via addition of sulfur
    - Type 304—the most common; the classic 18/8 stainless steel

- Type 316—Alloy addition of molybdenum to prevent specific forms of corrosion

- 400 Series—ferritic and martensitic alloys

Selection of proper stainless steel for hydro turbine underwater parts operating in silty water is important for ensuring their longer life. The material should be erosion resistant and should be weldable quality to enable repair at site. The most commonly used 13/4 Martensitic stainless steels for critical hydro turbine components is a better comprise against cavitation erosion as well as erosion due to silt laden water [22, 62-65]. Based on Indian experience, following materials are recommended for critical turbine components;

1.2.1 13/4 martensitic stainless steel

CA6NM is a 13Cr-4Ni cast grade of martensitic stainless steel that is widely used throughout the hydro turbine and pump industry [22, 62-65]. CA6NM is the result of material development efforts conducted at a Swiss foundry in the early 1960's, with the following aims:

- Increase impact strength and improve weldability by lowering carbon content
- Attain a microstructure free of delta ferrite by increasing the nickel content
- Suppress temper embrittlement and improve corrosion resistance by suitable molybdenum content

Conventionally produced CA6NM has a carbon content of 0.06% maximum. In fact, foundries employing argon-oxygen-decarburization (AOD) refining routinely produce CA6NM castings with even lower carbon content in the vicinity of 0.03% or less. The relatively low level of carbon in CA6NM facilitates welding in several ways. Low carbon retards the formation of a brittle heat affected zone consisting of untempered martensite. Preheat is usually only 200°F, compared with 400°F minimum for CA-15. Postweld heat treat temperature is also some 250°F lower. And, minor repairs can be made without postweld heat treatment, a distinct advantage for finish machined castings. Despite its weldability, CA6NM repair welds made with matching filler metal have been consistently harder than the base metal. The higher hardness can cause machining difficulties. In addition, many CA6NM pump castings are used in oil industry applications where exposure to hydrogen sulfide and the potential for sulfide stress corrosion cracking dictate that the weld and heat affected zone not exceed 255 BHN in hardness [65]. In practice, it has proven difficult to consistently meet this 255 BHN hardness requirement in welds. In fact, the lowest attainable hardness of repair welds is near this 255 BHN limit.

1.2.2 Nitronic steels

Nitronic steels are the austenitic stainless steel containing nitrogen as alloying element. This is also known as high nitrogen austenitic stainless steels. Steels and stainless steels are considered high nitrogen varieties if they contain N content well above that present in conventional steels and stainless steels. For example, steels contain 0.1

Table 1.1. Selection of material for critical turbine components [63]

Si. No.	Component	Material
1	Runner	13%Cr, 4% Ni stainless steel
2	Labyrinth seals	13%Cr, 4%Ni or 18%Cr, 10%Ni stainless steel
3	Guide vane	13%Cr, 4% Ni stainless steel
4	Guide vane bush housing	Cast steel
5	Liners for top cover and pivot ring	18%Cr, 10%Ni stainless steel
6	Fasteners in water path	Stainless steel
7	Tubes for bearing coolers	Cupro-Nickel (80% Cu-20%Ni)
8	Rubber seals	Neoprene synthetic rubber

mass % of N in creep resistance varieties [66, 67], 0.9 mass% in the normal grades or 2 mass% in tool steels are considered high nitrogen (HNS) steels. According to **Speidel** [68], if the steels contain more than 0.08 wt% N in a martensitic matrix or more than 0.4 wt% N in austenitic matrix are termed as high nitrogen stainless steels. According to **Mudali** [69], the word high can be used to refer a concentration where N added to steels or stainless steels achieves properties glaringly different as compared to the alloy without N. The main driving force in the development of HNS alloys is the improvement in the mechanical properties as well as in the corrosion resistance. The YS and UTS of HNS alloys can exceed than those of conventional AISI 200 and 300 series by 200% to 350% in the annealed condition without sacrificing toughness. Due to a high strain hardening potential, cold deformation could further enhance YS above 2 GPa. The combination of YS and fracture toughness which can be achieved at room temperature with HNS is better than any other steel can provide [69].

According to **Mudali** [69], N alloying in steel was never popular due to skepticism associated with N causing brittleness in ferritic steels and the problems involved in introducing N into steel melt. The beneficial effect of N was recognized only in the beginning of twentieth century. In late 1930s and 1940, the shortage of Ni during world war inspired research on the possible replacement of Ni with N to stabilize austenite. The renewed interest in these alloys arises from two facts: concern over diminishing supplies of alloying elements such as Ni and the unfulfilled dream of a high strength face centered cubic steels [70].

Alloying stainless steels with N become common in the United States when the argon oxygen decarburization (AOD) process made it possible for the first time to introduce N as a gas instead of different alloy systems. Replacing Ni with a combination of N and Mn had lead to the additional advantage of increasing solubility of N and this research resulted in standardized new alloy of AISI 200 series. In the late 1960s, the first commercial introduction of N-bearing stainless steels "Nitronic" with 0.18N and German grade 1.4439 (AISI 317LMN stainless steel) were introduced in steel market [71]. The nitronic steels contained high Mn and N (21Cr-9Mn-7Ni-0.32N) and exhibit high strength and toughness at low temperatures and good corrosion resistance.

The scientific community of HNS alloys evolved series of International conferences on the topic since the first conference at Lillie, France in 1988 (HNS 88), followed by HNS 90 in Germany, HNS 93 in Ukrain, HNS 95 in Japan, HNS 98 in Finland and Sweden, HNS 2001 in India and HNS 2003 in Switzerland. **Mudali** [69] has reported that high nitrogen steels are being transformed into "high interstitial alloys" with addition of C to HNS alloys. Addition of C probably would avoid steel making HNS with very high N contents (about 0.9 wt %) and the possibility of having new class of alloys with C (0.4 wt %) and N (0.4 wt %) together. The high nitrogen contents in the austenitic stainless steels decreases the stacking fault energy and stabilize austenitic structure so that no strain induced transformation to α-martensite and ε-martensite occurs [71-74]. The best known application of HNS alloys is retaining rings for power generating sector, but many other application exist (bolts, spring, turbine blades, washing troughs,

protective liners etc). The largest use for N-alloyed stainless steels is for replacement of Ni and this area will probably grow with time, because Ni is a potential allergic and carcinogenic element that is restricted for biomedical applications, and the developments and applications of HNS alloys in this area will be more attractive too [71, 75].

Solubility of nitrogen in austenitic stainless steels

Pure iron has low solubility (0.044% N) in the molten as well as in the solid state. Increasing the Cr content increases the nitrogen solubility as shown in Fig. 1.1 [76]. When there is δ-ferrite formation during transformation from molten to solid state, the solubility of nitrogen decreases to a value far below the equilibrium solubility in the molten state. However, in the solid state, further lowering of temperatures results in the formation of austenite phase, in which nitrogen solubility increases remarkably to values well above that in the liquid state. Like Cr, the presence of Mn has also been reported to enhance the solubility of nitrogen. Nitrogen solubility in the presence of both Cr and Mn in steel shows deviation from Sievert's law [76]. Thus, it is understood that to achieve high nitrogen content in steels, the presence of large amounts of Cr and Mn is required.

Steels are generally reported to acquire corrosion resistance, when Cr content is greater than 12%. Conventional austenitic stainless steels have metastable austenite phase [77]. Nickel in these steels expands the austenite phase field and promote sluggishness of phase transformation. Other economically viable austenite stabilizers are carbon, copper, manganese and nitrogen. Among these, carbon has a tendency to sensitize the steel,

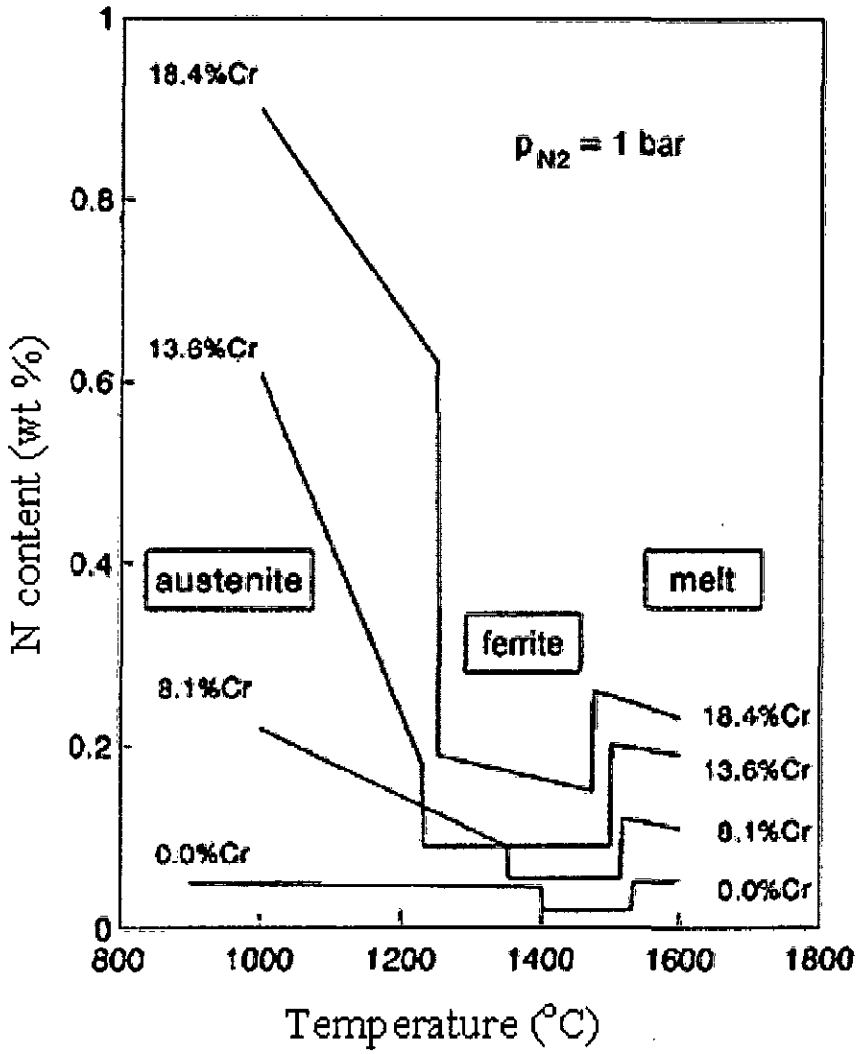

Fig. 1.1. Nitrogen solubility in steel as a function of temperature and Cr content [76]

copper leads to hot shortness and manganese alone cannot totally replace Ni to form austenite phase. This leads to nitrogen as the best alloying additive.

Thermodynamics of Fe–Cr–N system [78] show that for 12% Cr content, the austenite phase exists in a narrow range of nitrogen composition, which increases with increasing Cr content. Beyond the range, Cr_2N and CrN phases are formed. At high Cr levels, there is the formation of ferrite, austenite and Cr_2N type nitrides. The problem with this system is that the nitride can precipitate out readily at lower temperature aging [79] and they are not stable against martensitic transformation [80]. Hence, one of the alternatives was to have Mn in the Fe–Cr–N system. Then, it is necessary to know the minimum limits of N and Mn contents required to make stable austenitic stainless steel. Analysis of the Fe–Cr–Mn phase diagram at temperatures of 800 to 1200°C shows that, when Cr is greater than 13%, Mn alone cannot produce a fully austenitic structure. At Cr contents greater than 15 %, there is the formation of sigma phase. This necessitates addition of other austenite stabilizers such as Ni or N or both. Thus, an 18% Cr steel with 0.1% C and 8% Mn requires 4 to 5% Ni and 0.15% N for getting stable austenitic microstructure at room temperature. Each 0.05% N is found to be equivalent to 1% Ni in its austenite stabilizing effect. In steels with 10 to 35% Cr and 2 to 23% Mn, increasing nitrogen content expanded the austenite field and shifted the sigma phase to higher Cr contents.

Alloying with nitrogen has several advantages over alloying with carbon:

(1) Nitrogen is a more effective solid-solution strengthener than carbon and also enhances grain size (Hall-Petch) strengthening.

(2) Nitrogen is a strong austenite stabilizer thereby reducing the amount of nickel required for stabilization.

(3) Nitrogen reduces the tendency to form ferrite and deformation-induced and ε martensites.

(4) Nitrogen has greater solid-solubility than carbon, thus decreasing the tendency for precipitation at a given level of strengthening.

1.3 Erosion

Erosive wear is caused by the impact of particles against a solid surface. Erosion is rapid and severe forms of wear and can results in significant costs if not adequately controlled. Erosive wear occurs in a wide variety of machineries and typical examples are the damage to gas turbine blades when an aircraft flies through dust clouds, hydro turbine under water parts when silt laden water flows through it and the wear of pump impellers in mineral slurry processing systems. In common with other forms of wear, mechanical strength does not guarantee wear resistance and a detailed study of material characteristics is required for wear minimization. The properties of the eroding particle are also significant and are increasingly being recognized as a relevant parameter in the control of this type of wear.

Erosion of metallic components occurs by many different mechanisms depending upon material, environment, operating conditions and geometry of the wearing bodies. These mechanisms can be classified into two broad groups: first those dominated primarily by the mechanical and physical behaviour of solids and second, those dominated primarily by chemical behaviour of materials.

1.3.1 Mechanisms of erosion

In erosion, the detailed process that cause material removal is still poorly understood [40]. **Finnie's** [81] analysis of the cutting action of a single particle launched against a ductile target was the first model of the solid particle erosion capable of predicting erosion rate. **Ruff and Wiederhorn** [82] developed two models for erosion of brittle materials: one is the based on assumption that erosion occurs entirely by crack propagation and chipping and the other is based on the assumption that plastic deformation contributes to the process of crack formation and surface chipping.

Material removal is mainly the result of particle impacts as the jet delivers abrasive particles at high velocities to the target surface. Fig. 1.2 shows the hierarchy of this process.

These mechanisms are cutting, fatigue, brittle fracture, and melting. Clearly, these mechanisms generally do not act separately, but in combination. Their importance for the particular erosion process depends on several factors, such as the impact angle, the

particle kinetic energy, the particle shape, target-material properties, and environmental conditions [83].

In order to compare solid particle erosion, a non-dimensional erosion number, E_N, is defined by Equation (1.1).

$$E_N = \frac{m_M}{m_P} \qquad ..(1.1)$$

Here m_M is the mass of the material removed and m_P is the mass of the abrasive particle. Thus, the removed volume of the material is

$$V_M = \frac{E_N \cdot m_P}{\rho_M} \qquad ..(1.2)$$

The term 'erosive wear' refers to an unspecified number of wear mechanisms which occur when relatively small particles impact against mechanical components. This definition is empirical by nature and relates more to practical considerations than to any fundamental understanding of wear. The known mechanisms of erosive wear are illustrated in Fig. 1.3 [84]. The angle of impingement is the angle between the eroded surface and the trajectory of the particle immediately before impact. A low angle of impingement favours wear processes similar to abrasion because the particles tend to track across the worn surface after impact. A high angle of impingement causes wear mechanisms which are typical of erosion.

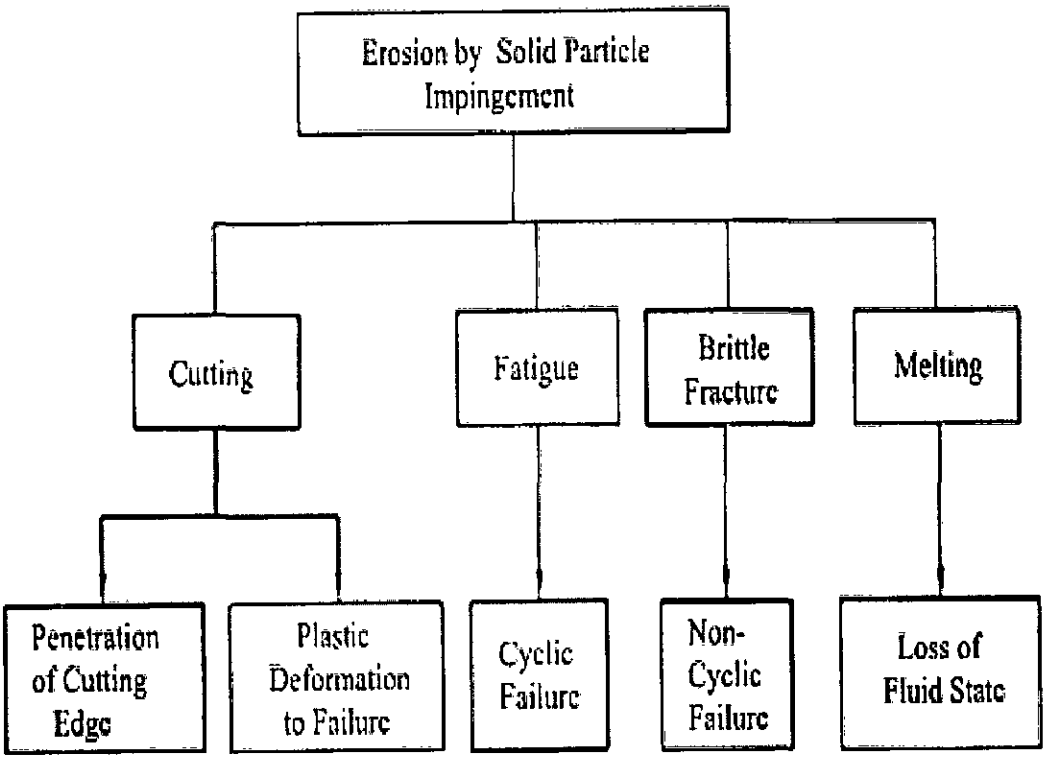

Fig. 1.2. Mechanisms of material-removal by solid-particle erosion [83]

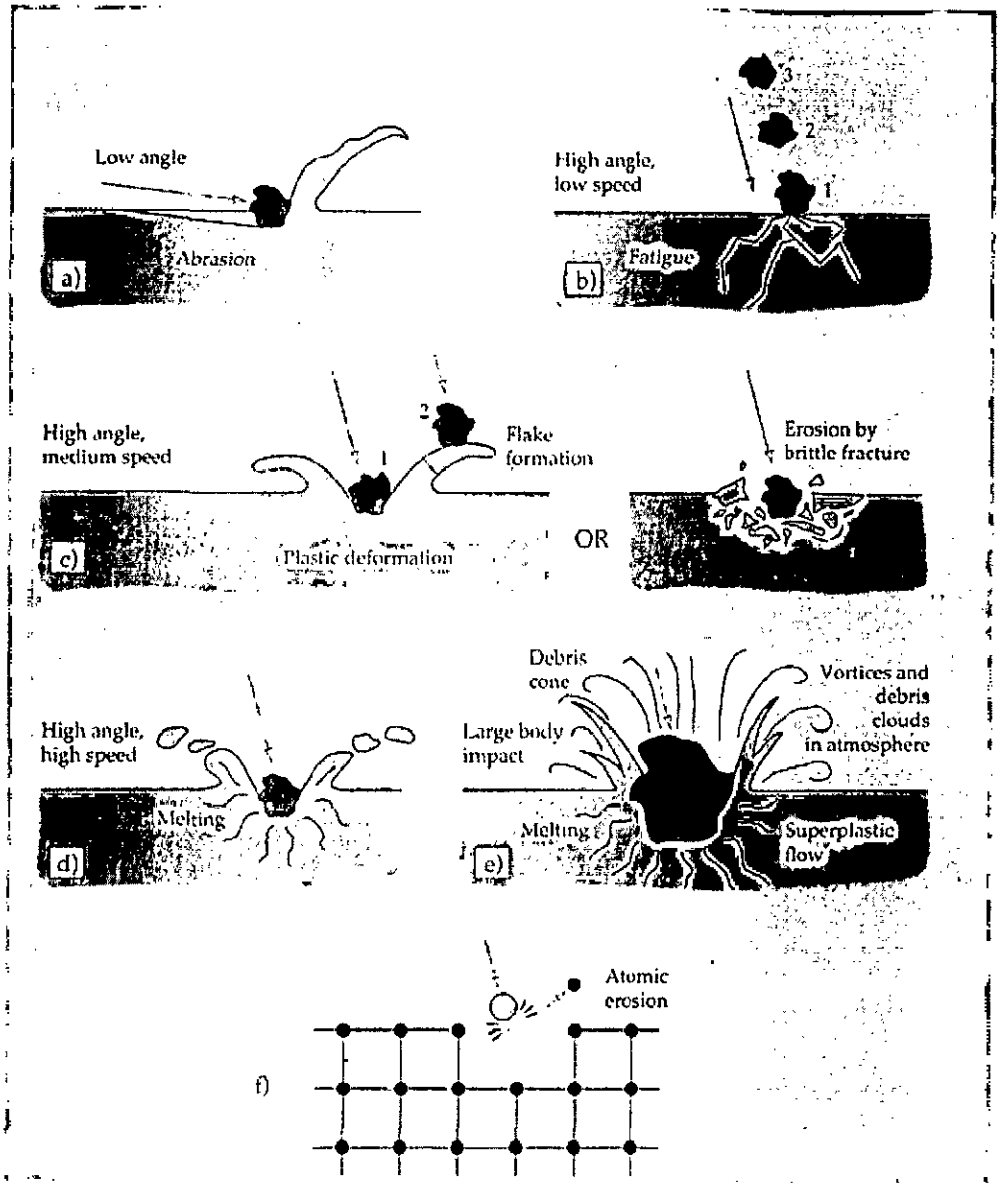

Fig. 1.3. Possible mechanisms of erosion (a) abrasion at low impact angles, (b) surface fatigue during low speed, high impingement angle impact, (c) brittle fracture or multiple plastic deformation during medium speed, large impingement angle impact, (d) surface melting at high impact speeds, (e) macroscopic erosion with secondary effects and (f) crystal lattice degradation from impact by atoms [84]

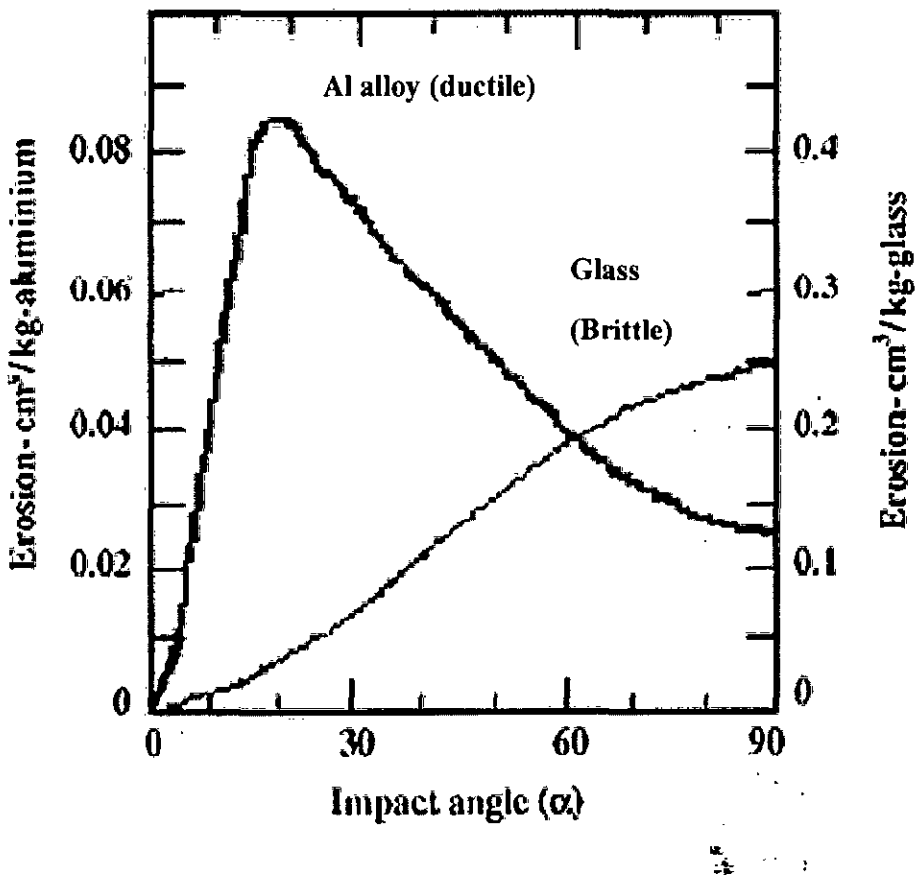

Fig. 1.4. Erosion behavior of brittle and ductile materials [50]

Erosive wear involves several wear mechanisms which are largely controlled by the particle material, the angle of impingement, the impact velocity and the particle size. Two different modes of erosion response of a material are defined: ductile and brittle. The main difference between these two modes is the manner in which the erosion rate varies with the angle of impact. For brittle layers maximum erosion occurs at normal impact but for ductile materials maximum erosion occurs at glancing angles. The failure is mainly due to extensive plastic deformation of surface material. The erosion rate vs angle of impingement for ductile and brittle materials is shown in Fig. 1.4 [50].

Erosion mechanisms of ductile materials

A model for the erosion of ductile material was first developed by **Finnie [81]**. He treated the problem by assigning a plastic response character to the material through a flow stress σ_F. He calculated the trajectory of a particle cutting and removing material, and determined the eroded volume (V_M) given by the expression:

$$V_M = (mv^2/\sigma_f Kd)\, g(\theta) \qquad (1.3)$$

Where m is the particle mass,

v is the impact velocity,

K is the ratio of vertical force to horizontal force on the particle,

d the depth of cut, and

$g(\theta)$ is a function describing the effect of attack angle θ.

But this model could not be used for attack angle $\theta = 90^0$ and also quantitative discrepancies arise concerning the effect of flow stress and the velocity exponent. **Bitter** [85, 86] developed a model to account for erosion at all attack angles. He considered erosion to consist of two simultaneous processes, indentation deformation wear for high angle of attack and cutting wear for low angles of attack. This theory requires experimentally determined parameters for complete applications. **Tilly** [87] proposed a two-stage mechanism of erosion recognizing explicitly that particles impacting at near-normal incidence may fragment and the fragments may subsequently erode exposed surface features.

Levy [88] has reported that how specific steel microstructures affect the erosion; he used an erosion weight loss curve that resulted in basic doubt concerning the validity of micro cutting mechanism. In order to learn more about the initiation of erosion that occurred, the erosion was conducted on steel; incrementally 60 g of particles at a time, and weight loss caused by each 60 g increment was measured and plotted as shown in Fig. 1.5.

The initial erosion rate caused by the first 60 g of SiC particles was much lower than that of subsequent 60 g batches of erodent. Also, extrapolating the curves down to zero erosion shows that a number of grams of SiC particles have impacted the surface before erosion losses began. With subsequent increments of impacting particles, the

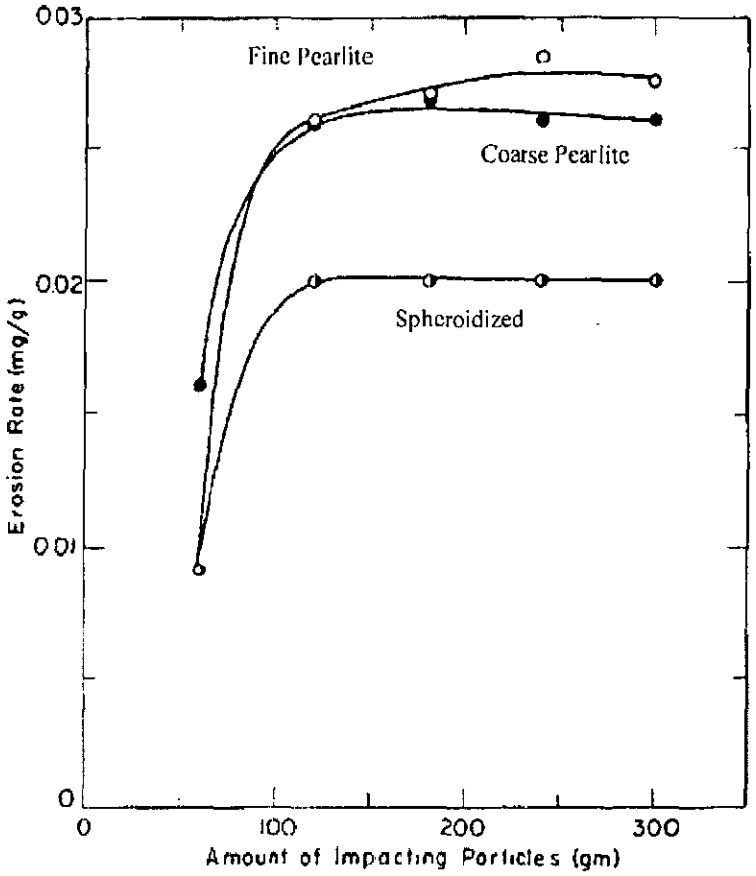

Fig. 1.5. Plot of erosion rate verses mass of impacting particles for 1075 steel (SiC particles 240 μm in diameter; $v = 30.5$ m s^{-1}; $\theta = 30^{\circ}$) [88]

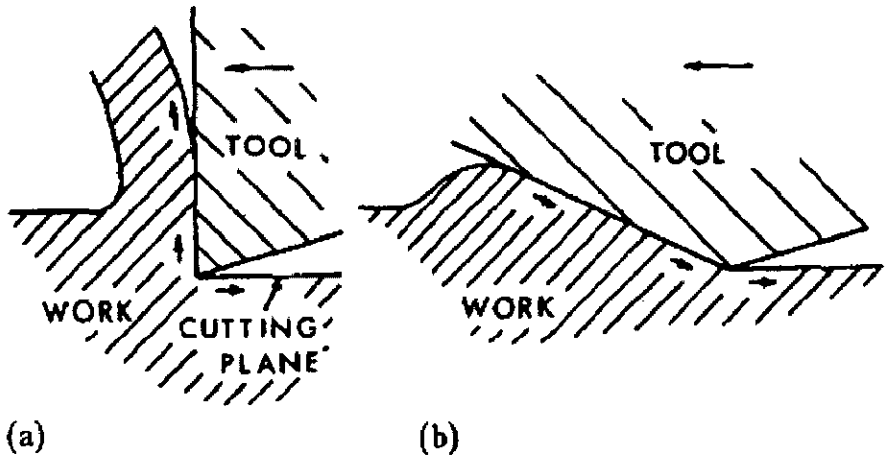

Fig. 1.6. The two modes of surface deformation considered (a) cutting, in which the metal flow bifurcates at the cutting edge, (b) ploughing, in which the metal flows continuously past the cutting edge [91]

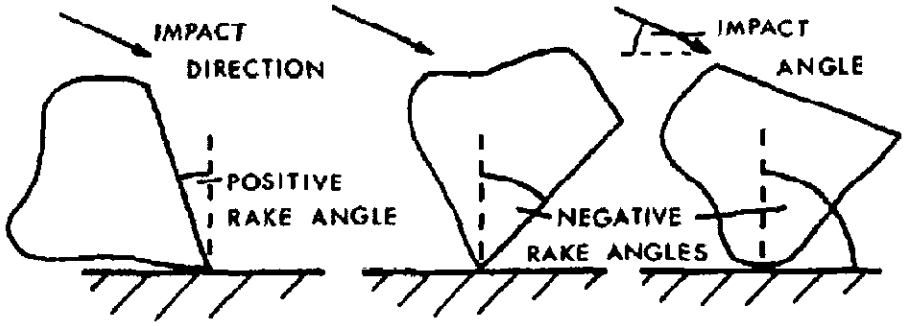

Fig. 1.7. A typical sand grain striking a surface at different orientations. The rake angle as defined here varies with particle orientation [91]

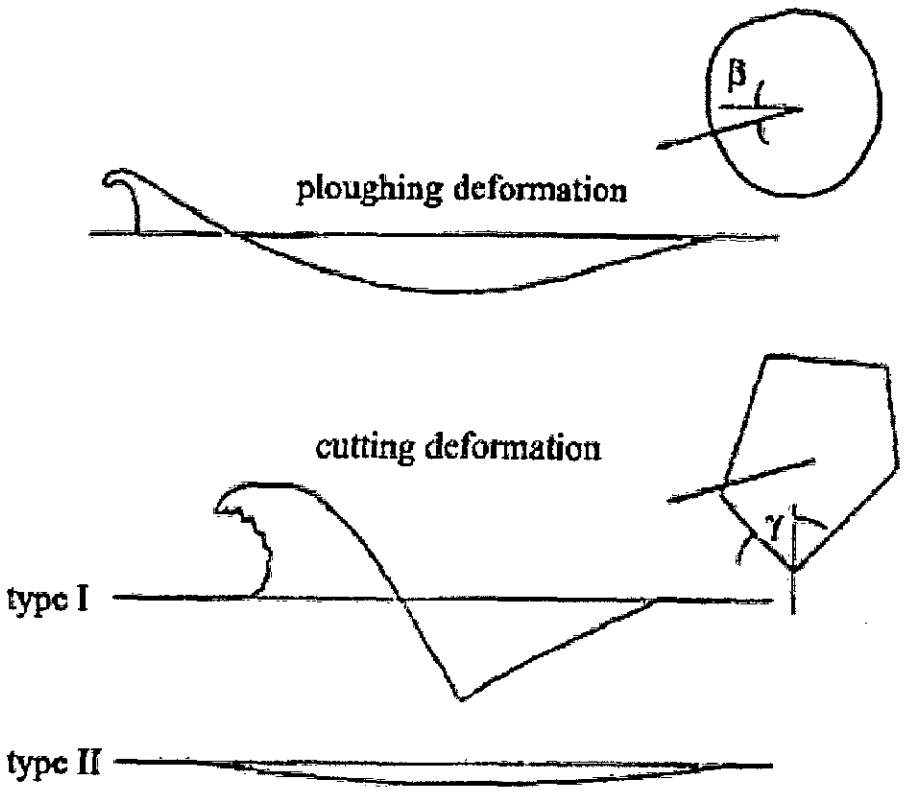

Fig. 1.8. Cutting and ploughing by solid particles at oblique impact angles [94]

metal loss rate increased until it reached steady state conditions. **Levy** [88] further reported that if micro cutting was the primary mechanism of erosion, the erosion rate of initial, uneroded surface should be higher than subsequent incremental rates because work hardening of the surface due to machining action would have reduced the machinability of the surface and the resulting amount of material loss.

Some researchers [89-93] have used the large single particle, millimeter in diameter, and impacted them individually at the target surface to study the mechanism of erosion from a physical standpoint. **Winter and Hutchings** [91] have identified the two different regimes of deformation ploughing and cutting (Fig.1.6). According to them at rake angles more positive than a critical angle, cutting occurs; material flows up the rake face of the tool and the flow of metal bifurcates at the cutting edge of the tool producing a cutting plane. On the other hand, at rake angles more negative than this critical angle, ploughing dominates; in this case material probably flows down the tool face and the flow of metal is continuous over the cutting edge. Fig. 1.7 shows the rake angles for a typical sand grain striking a surface at different orientations. If other impact conditions are kept constant, material is removed by ploughing when a critical impact velocity is exceeded. They further added that ploughing deformation is, however, discouraged if the particle executes a rolling type rotation during its time of contact with the surface rather than sliding along it.

Hutchings [94] developed a model for volume removal due to the action of the abrasive water jet which is based on observations obtained by high-speed photography and SEM. He also defined two modes of cutting. One is cutting deformation and the other is ploughing deformation as shown in Fig. 1.8. As can be seen the ploughing deformation mode works best with blunt shaped abrasive particles. It is noticed that as the abrasive particle interacts with the target material, a lip of material is formed. However, not every abrasive particle will "plough" into the material. Some may rotate in the opposite direction in which case the Type II cutting profile is valid.

A theoretical model which predicts the extent of lip formation as well as the weight loss using the single impact experiments is presented by **Sundararajan** [95]. The model postulates that the lip formation is the result of localization of deformation in the near-surface regions of the target and the lip is removed either by inertial-stress-induced tensile fracture or by separation across adiabatic shear bands formed at the base of the lip. He used the single impact data's for copper, brass, thoria dispersed nickel and nickel targets. **Sundararajan and Shewmon** [96] had proposed the new theoretical model for the erosion of metals by particles at normal incidence which employs a criterion for critical plastic strain to determine when the material will be removed. This critical plastic strain is defined as the strain at which the deformation in the target localizes and hence results in the lip formation. **Brach** [97] has developed an analytical model for the energy loss suffered by an arbitrarily shaped, rigid particle impacting the surface of a massive target material at any impact angle. He further assumed that the erosion rate is proportional to the energy loss

suffered by the particle during impact, he had demonstrated that the erosion response will be ductile (i.e. a maximum erosion rate at glancing impact angles) or brittle (maximum erosion rate at normal impact angle), depending on the relative magnitudes of the energy absorbed due to tangential (i.e. frictional) and normal inelasticity effects.

Hutchings and Levy [98] had discussed the mechanisms of erosion in ductile metals subjected to the impact of solid particles and reported the possible effects associated with the local temperature rise caused by particle impact. They found that heat conduction play an important role in reducing the maximum temperature rise in all practical cases of erosion and had reported the negligible cumulative effect on the temperature rise of successive impacts. They described the observed erosion mechanisms in three distinct phases, which occurred sequentially at any one location. According to them in the steady state condition all the three phases occur simultaneously at different locations over the surface. In the initial phase an impacting particle forms a crater and material is extruded or displaced from the crater to form a raised lip. In the second phase the displaced metal is deformed by subsequent impacts; this may lead to lateral displacement of the material and can be accompanied by some ductile fracture in heavily strained regions. Finally after a few impacts, the displaced material becomes so severely strained that it is detached from the surface. They reported this mechanism of erosion as the platelet mechanism defined by **Levy** [88] and differs from the micro cutting model proposed by **Finnie** [81] in that it is postulated that in most cases the impact of several particles is necessary in order to remove a fragment of metal from the surface [97].

Sundararajan [99] developed a model valid for all impacts angles as an extension of the earlier model [96] proposed specifically for normal impact erosion. This model [99] is based on the assumption that the localization of plastic flow underneath the particle impact is responsible for lip formation and hence erosion. He reported that it is capable of rationalizing the important experimental observations related to erosion, namely the effects of material properties, impact velocity, impact angle and particle shape. **Sundararajan and Shewmon** [100] developed a simplified model for the oblique impact of a hard ball against a ductile material. The model correctly predicts the magnitude of crater dimension and volume, and also their variation with impact angle and velocity, but it cannot predict correctly the energy absorbed per impact.

Erosion mechanisms of brittle materials

When the impact of an erodent particle causes brittle fracture, material is removed by the formation and intersection of cracks. If the mechanism responsible for material removal by brittle fracture, there is often also be some plastic flow in the material around the point of contact of the erodent particle. The extent of cracking due to particle impact is most severe when the impact direction is normal to the surface, and erosion under these conditions is then most rapid (curve for brittle materials in Fig. 1.4). Erosion falls monotonically with angle away from 90°, in contrast to the behaviour when erosion occurs by cutting and ploughing mechanisms (curve for ductile material in Fig. 1.4).

The model proposed by **Sheldon and Finnie** [101] assumes that erosion occurs as the result of Hertzian contact stresses during impact. In their analysis they considered dynamic forces between the surface and particle and this resulted in a prediction in the volume removed for a material with specific properties. They also concluded that the fracture at the surface is function of the volume of material constrained in the primary erosion zone in relation to the surface and volume flows. The theory by **Evans and Wilshaw** [102] explains erosion in terms of experimental crack behavior during single particle impact events, and thus takes into account lateral crack formation during erosion. The erosion model assumes that the erosion rate is proportional to the amount of material removed by each impact event. **Ruff and Wiederhorn** [82] developed two models for erosion of brittle materials: one is based on the assumption that erosion occurs entirely by crack propagation and chipping and the other is based on the assumption that plastic deformation contributes to the process of crack formation and surface chipping.

Zambelli and Levy [103] investigated the erosion behaviour of brittle oxide scales on ductile alloy substrates. They interpreted the erosion damage of the NiO scales using simplified postulates based on the fracture propagation concepts. They reported the removal of NiO duplex scale in a two step mechanism. Plastic flow indentation and lateral crack growth in the columnar outer layer is the first step in the erosion mechanism. In the second step, pits are produced from Hertzian cone fractures formed in the inner layers, which enlarges the pits. At greater velocities, particle sizes and impingement angles, the erosion of the thinner oxide scales to the bare Ni occurred in times of the

order of seconds. It is suggested that the strengths of the bonds between the two scale layers and between the scale and metal substrate are directly related to the erosion behaviour.

Hutchings [104] has pointed out that the angular dependence of erosion is not a characteristic of the material alone, but depends also on the conditions of erosion. For example, although most metals eroded by angular particles do show typical ductile behaviour of erosion (Fig.1.4), erosion by spherical particles, even of a ductile metal such as mild steel, can lead to apparently brittle angular dependence, although wear still occurs by purely plastic processes. Alloys of high hardness and low ductility may also show their maximum erosion rate at normal incidence; an example, for a low alloy bearing steel after different heat treatments, is shown in Fig.1.9. At comparatively low hardness and high ductility, the steel shows characteristic ductile behaviour, while with high hardness it shows apparently brittle behaviour, although microscopic observation shows no sign of brittle fracture.

1.3.2 Erosive wear resistance of materials

Material characteristics exert a strong effect on erosive wear and have been extensively studied [105]. In a similar manner to abrasive wear, it is found that improvements in mechanical properties do not always coincide with superior erosive wear resistance. For example, erosive wear rates may increase when a material is deliberately hardened. An illustration of this rule is provided by the comparison of the

relative erosion resistance of metals as a function of impingement angle. When the impingement angle is shallow, hardened steel shows lower erosion than a soft steel; the converse is true at high impingement angles. This is illustrated in Fig. 1.10, where the erosive wear rate, at two different impingement angles of 15° and 90°, is shown as a function of material hardness for various metals and grades of steel hardness. The abrasive used was silicon carbide of diameter about 1 mm impinging at a velocity of 30 (m/s).

Heat treatment of steel to increase hardness improves erosive wear resistance at low impact angles but lessens the erosive wear resistance at high impact angles. There is no general recipe for a high level of erosive wear resistance. Because of the two different erosive wear protection mechanisms that can take place, high wear resistance can be achieved by more than one type of material. In some cases the material can be extremely hard and tough so that the impacting particle is unable to make any impression on the surface. Alternatively, the material can be tough but with an extremely low elastic modulus so that the kinetic energy of the particles is harmlessly dissipated. These contrasting wear protection mechanisms are illustrated in Fig. 1.11 [84]. Rubber is generally believed to provide good erosion resistance by elastic absorption of particle energy although this has not been demonstrated experimentally. It has been shown that the first particle impact causes no visible damage to a rubber surface and that wear depends on slow fatigue processes [106].

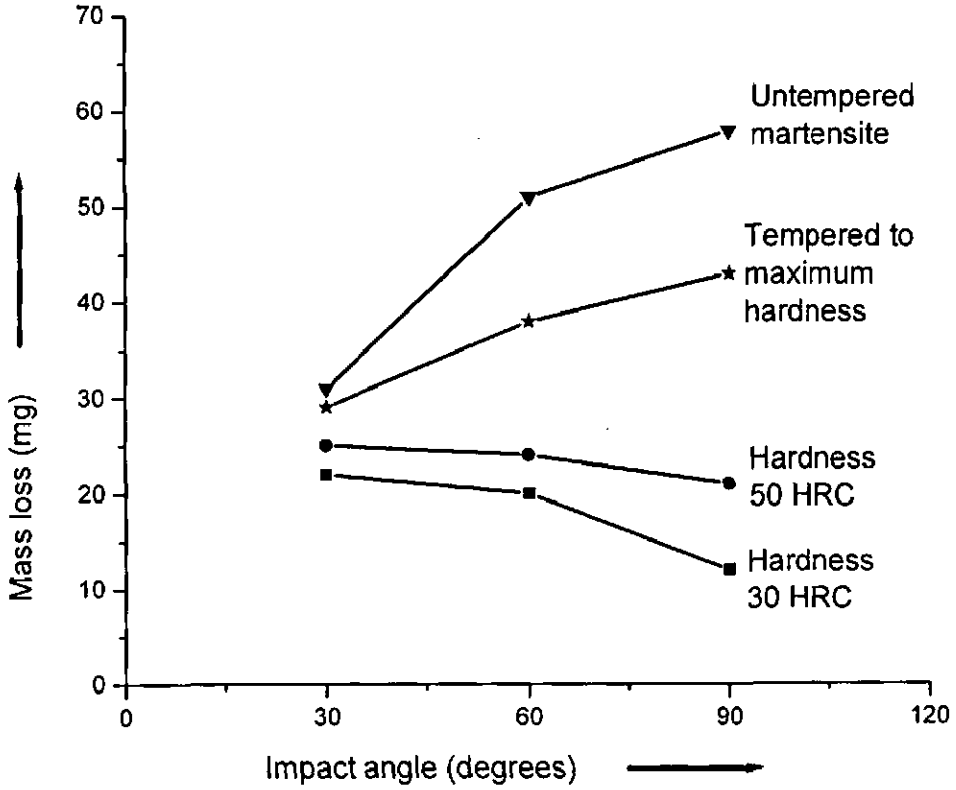

Fig. 1.9. Erosion rate of AISI 52100 steel samples (1%C, 1.5%Cr) with different microstructures as a function of impact angle. Silica particles were used at 153 ms^{-1} [104]

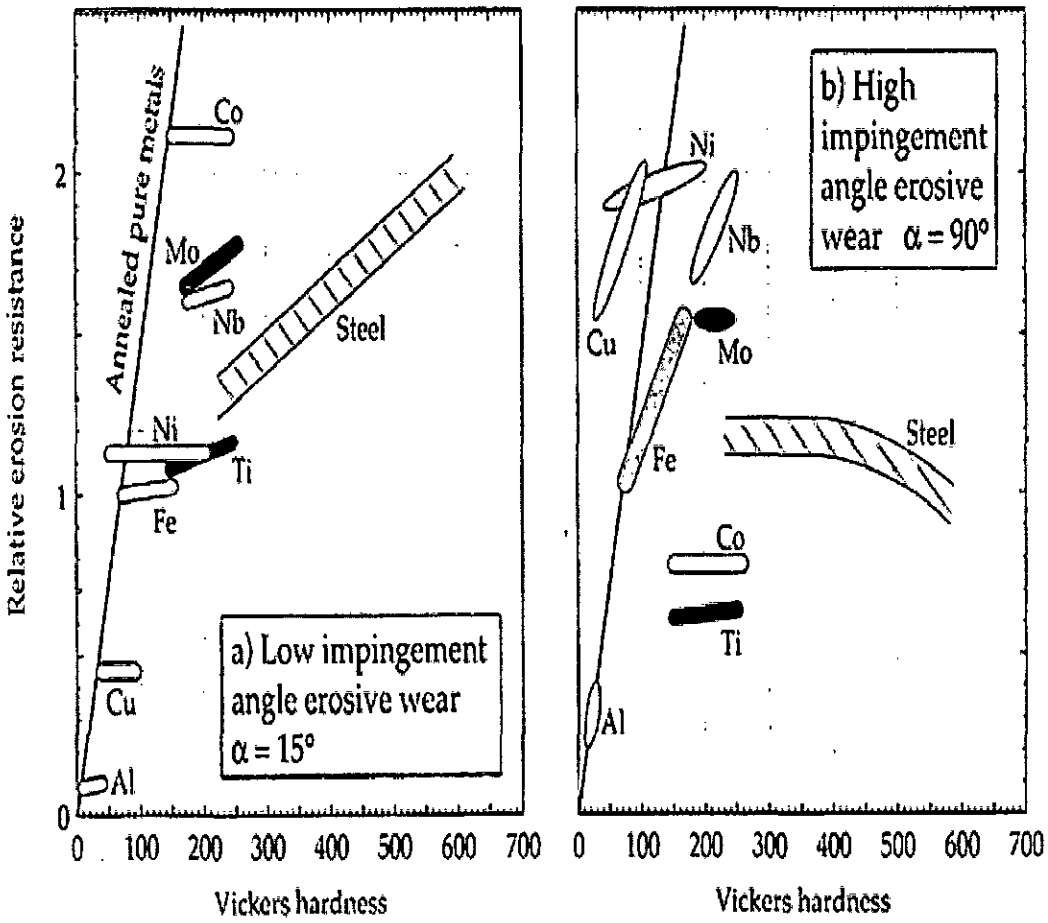

Fig. 1.10. Effect of primary material characteristics and erosion parameters on erosion rate [105]

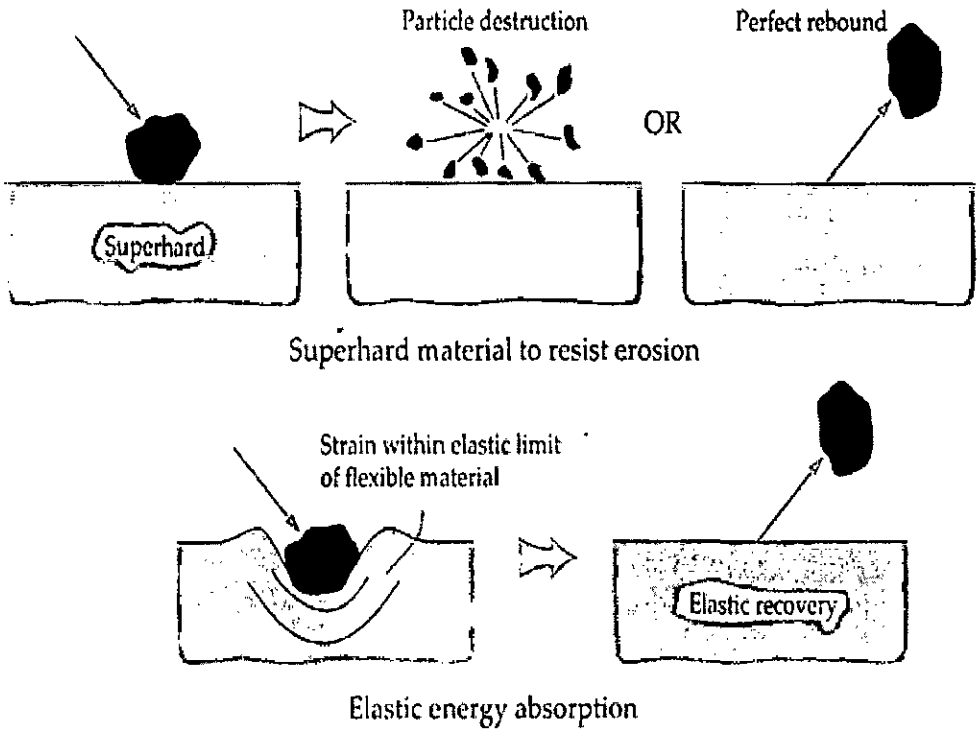

Fig. 1.11. Comparison of the high and low elastic modulus modes of erosive wear protection [84]

The choice of erosion resistant material may also be compromised by other considerations such as operating temperature or material transparency. Clearly, temperatures in excess of 200°C preclude polymers from service, but if a transparent material is required for a specific application then metals are not particularly useful. For example, materials for aircraft windscreens, apart from being transparent, are required to be resistant to high speed erosion by sand, dust and rain [107]. **Rao and Buckley** [107] found that polymethylmethacrylate is the best candidate for this application since it is both tough and shows a minimum of transparency loss by erosion damage.

1.3.3 Erosive wear resistance of steels

The literature available on the effect of steel microstructure on erosive wear rates suggests that ductile steel is the most wear resistant. Hardening of steel to form martensite offers little improvement except at very low impingement angles, and the formation of massive or lamellar carbides reduces erosive wear resistance. The selection of steel for erosive wear minimization is therefore different from the case of abrasive wear. For low alloy carbon steels, the ferritic phase with sufficient spheroidal carbide inclusions to induce strengthening is very effective against erosive wear [88]. Pearlitic steels show inferior wear resistance to spheroidized steels. That the erosive wear of steels shows the classical ductile erosion characteristic, i.e., a maximum wear rate at low impingement angles with subsurface and surface cracking [88]. This suggests that the erosive wear resistance of steels is limited by a lack of ductility. For very soft erosive particles such as coal, the inclusion of carbides promotes wear resistance slightly [108].

Alloying of steel or cast iron to obtain a microstructure containing a significant amount of retained austenite is an effective means of reducing erosive wear. Adding about 2.5 wt% of silicon to 0.7 wt% carbon steel or about 0.45 wt% of silicon to 2.54 wt% cast iron results in good erosive wear resistance [109, 110]. The optimum heat treatment of this steel or cast iron includes a relatively long austempering time where all the martensite is removed and only retained austenite and bainitic ferrite are present. As a general rule, however, ductility rather than hardness should be enhanced in steels for improved erosive wear resistance.

1.4 Cavitation erosion

Cavitation is defined by **Dular et al** [111] as the condition when a liquid reaches a state at which vapour cavities are formed and grow due to dynamic-pressure reductions to the vapour pressure of the liquid at constant temperature. In a flowing liquid, these cavities are subjected to a pressure increase that stops and reverses their growth, collapsing implosively and disappearing. The violent process of cavity collapse takes place in a very short time of about several nanoseconds and results in the emission of large amplitude shock-waves, as demonstrated by **Avellan and Farhat** [112]. A high-speed reentrant liquid micro-jet directed towards the boundary can also occur for cavities collapsing close to a solid surface [113]. If the amplitude of the resulting pressure pulse is larger than the limit of the material mechanical strength, a hollow or indentation of several micrometers called "pit" will be formed on the surface. If an accumulation of pits takes place in a narrow area, the material is finally eroded and mass loss occurs due

to the repetitive action of the cavity collapses. In a flowing liquid, these cavities can take different forms that can be described as travelling bubbles, attached cavities or cavitating vortices. Cavitation erosion is usual damage phenomenon in flow handling parts of hydraulic turbines, and service life and capability of such parts are reduced by the damage [9].

1.4.1 Mechanism of cavitation erosion

The characteristic feature of cavitation is the cyclic formation and collapse of bubbles on a solid surface in contact with a fluid. Bubble formation is caused by the release of dissolved gas from the liquid where it sustains a near-zero or negative pressure. Negative pressures are likely to occur when flow of liquid enters a diverging geometry, i.e., emerging from a small diameter pipe to a large diameter pipe. The down-stream face of a sharp sided object moving in liquids, e.g., ship propeller, is particularly prone to cavitation. The ideal method of preventing cavitation is to avoid negative pressures close to surfaces, but in practice this is usually impossible.

When a bubble collapses on a surface, the liquid adjacent to the bubble is at first accelerated and then suddenly decelerated as it collides with the surface. The collision between liquid and solid generates large stresses which can damage the solid. Transient pressures as high as 1.5 GPa are possible. The process of bubble collapse together with experimental evidence of a hole formed in a metal surface by bubble collapse are shown in Fig. 1.12 [114]. The cavitation crater, shown in Fig. 1.12, was produced on the surface of indium which is soft. Harder materials such as ceramics are unlikely to form a deep

hole under the same conditions. Cracking and spallation are the predominant modes of wear for hard brittle materials. Almost all materials suffer some kind of subsurface damage by cavitation erosion; and accumulated work hardening and crack formation are commonly observed [115]. In some cases when the cavitation is intense, the density of holes may be sufficient to reduce the worn material to a porous matrix or 'sponge'. Although cavitation involves a similar process of collision between a liquid and a solid as occurs in erosion by liquids, however, there are some significant differences. Cavitation erosion is a much milder process than erosive wear. In cavitation wear particles are detached per millions of cavitations whereas only a few thousand impacts by droplets are enough to cause erosive wear [116]. Cavitation wear has an 'incubation period' like erosive wear but the weight gain found in erosive wear is not possible unless the cavitated material absorbs liquid.

Cavitation wear can be accelerated by the simultaneous occurrence of erosive wear, in other words synergetic interaction between these two wear mechanisms is possible. If the cavitating fluid contains erosive particles, then the collapsing bubbles cause the particles to hit the worn surface at high velocity. The rate of wear in synergetic erosion is higher than either cavitation or erosion alone. For example, this phenomenon takes place in hydraulic turbines operating in sandy water [117]. The turbine, operating at a head of 900 m and utilizing water containing mainly fine particles (<0.060 mm), was suffering minor silt erosion at the needle tip after 300 h of operation, as shown by Fig. 1.13(a). This was caused by the strong turbulence in the boundary layer at the tip.

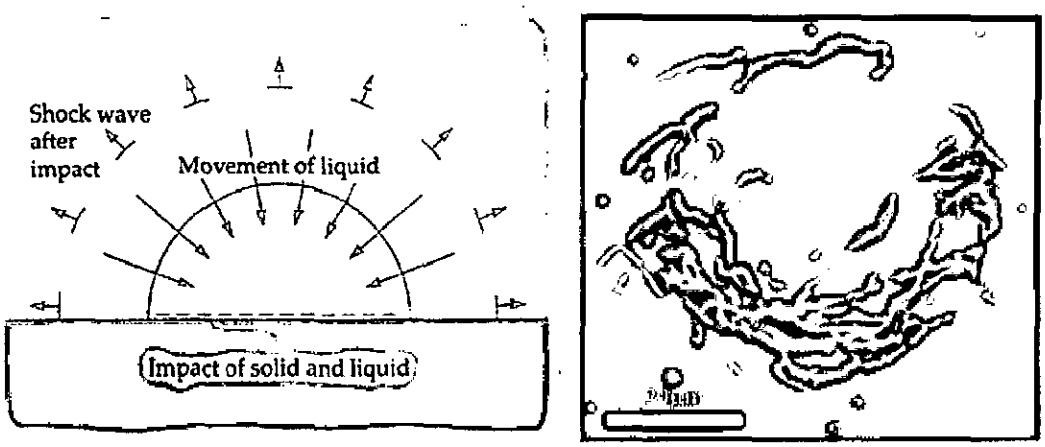

Fig. 1.12. Mechanism of cavitation wear (a) mechanism of bubble collapse and (b) experimental evidence of damage by cavitation to a metallic (indium) surface [114]

Fig. 1.13. Synergetic erosion in a Pelton turbine (a) (left) Initial stage: silt erosion on needle tip (300 h); (b) (middle) subsequent synergetic erosion (600 h) on needle tip; (c) (right) no noticeable erosion on buckets. Material: stainless steel (13Cr 4Ni) [5]

However, owing to the initial damage to the very streamlined and smooth surface, subsequent cavitation set in, which acted in concert with the silt erosion process, significantly enhancing the damage rate. Only after a similar time interval of operation, did the resultant damage to the tip become very severe such that the needle had to be replaced, as shown by Fig. 1.13(b) [5].

Taking the components of a turbine working in silt-laden water as an example, in most cases there are stagnation points (lines) on the bodies immersed in the flow. These stagnation points will be severely eroded owing to the impingement of particles at large angles (≈90°). This might be the initial cause of erosion, following which cavitation usually sets in owing to the deterioration of the streamlined profile. Then the synergetic erosion starts, such as in the example shown above, referring to Fig.1.13. Alternatively, when cavitation already exists, the synergetic erosion starts from the very beginning. However, no matter whether it is a subsequent phenomenon or not, the synergism mechanism is virtually the same [5].

1.4.2 Cavitation erosion resistant materials

A basic determinant in the choice of material for protection against cavitation erosion is the physical scale of the device where the cavitation takes place. Cavitation can occur in components ranging from propellers to dam spillways. For large-scale structures, concrete based materials are often used, e.g., concrete reinforced with chopped steel fibres, polymer impregnated concrete or concrete coated with epoxy resin. More

information on these materials can be found elsewhere [118, 119]. A material with good cavitation wear resistance is rubber since its low modulus of elasticity allows the bubble collapse energy to be dissipated harmlessly.

A basic feature of cavitation is its preferential attack on the weakest phase of a material. An example of this is found in the significance of graphite inclusions on the cavitation wear of cast iron. The graphite inclusions provide the required crack initiation centres for rapid wear by brittle fracture [120]. A similar process affects cermets which often contain a hard material such as tungsten carbide particles surrounded by a softer metallic matrix. Cavitation can dislodge the tungsten carbide by gradual removal of the surrounding matrix. **Heathcock et al** [121] have observed the improvement in cavitation erosion resistance, which is dependent on the properties of the binder rather than the tungsten carbide. Materials which protect against cavitation usually have a uniform microstructure with absence of large mechanical differences between phases. The mechanism of cavitation wear in multi-phase materials is schematically illustrated in Fig. 1.14.

Of the ferrous metals, stainless steels are more resistant to cavitation than cast iron. Plain carbon steels are not often considered as materials providing protection against cavitation erosion. With stainless steels, the ferrite phase is inferior to the austenite phase and the martensitic phase has the best resistance. Austenitic chromium-manganese-nitrogen (Cr-Mn-N) stainless steels have been found to offer better resistance to cavitation than conventional chromium-nickel-molybdenum stainless steels. The

additional benefit of Cr-Mn-N stainless steel is that the substitution of manganese and nitrogen as alloying elements reduces the cost of the stainless steel. It is believed that the pronounced work hardening characteristics of the austenitic (but not ferritic) Cr-Mn-N stainless steels promotes the resistance to cavitation wear [122]. Hadfield steel or the manganese steels provide the best cavitation erosion resistance of the austenitic steels. Of the more recently developed materials, high-nitrogen austenitic steels (HNAS) offer attractively high levels of resistance to cavitation erosion. HNAS are characterized by low carbon contents and nitrogen content exceeding 0.4%, while mechanical properties combine high yield strength with good ductility and toughness. Vigorous strain hardening of these steels under bubble impact is attributed as the cause for the high resistance to cavitation erosion by HNAS [123].

For severe cavitation problems, cobalt alloys such as 'stellite' are particularly useful. **Karimi and Martin** [9] have mentioned that cobalt is more wear resistant to cavitation erosion than to solid particle erosion. In ductile materials plastic deformation occurs under cavitation and key characteristics of plastic deformation are dynamic recovery and work-hardening. Materials with high stacking fault energy (SFE) display rapid dynamic recovery and poor work-hardening characteristics. For alpha aluminum bronzes, SFE is inversely related to cavitation wear resistance [124]. This indicates that for alpha aluminum bronzes, plastic deformation under bubble collapse is significant and that the energy of bubble collapse is not entirely absorbed by plastic deformation.

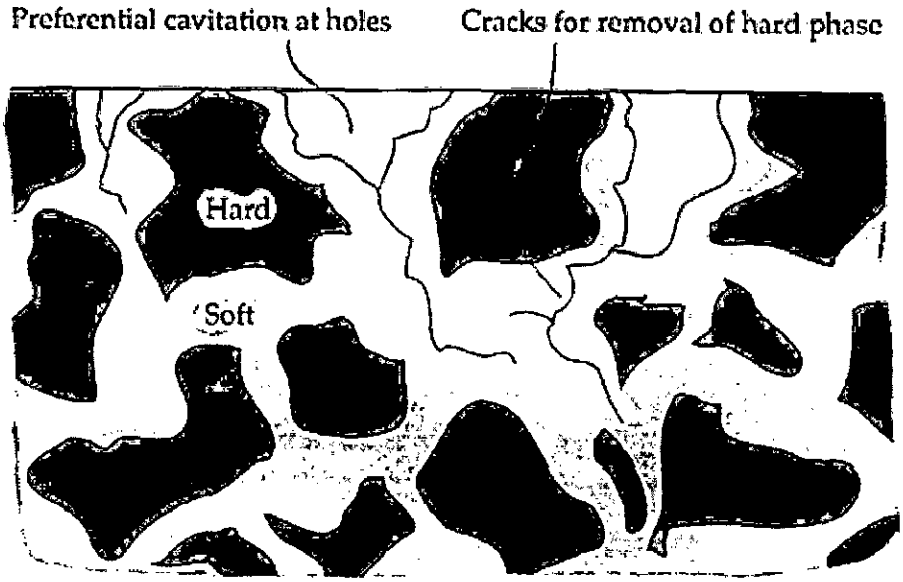

Fig. 1.14. Preferential attack by cavitation of the weaker phase in a microstructure [84]

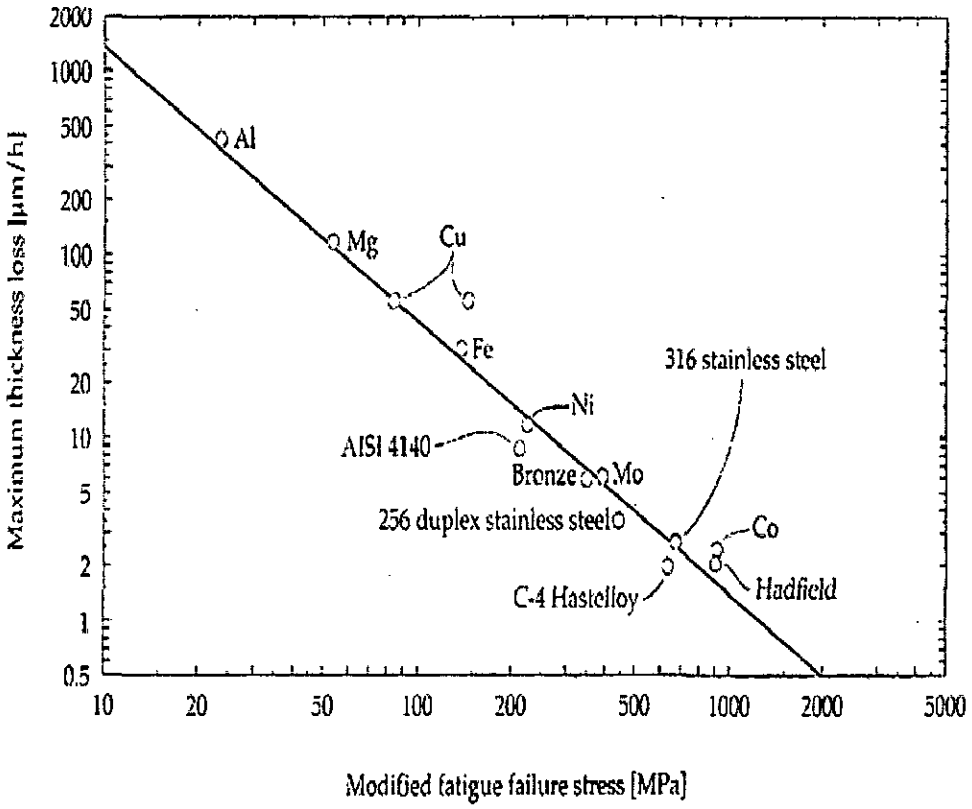

Fig. 1.15. Relationship between the cavitation wear resistances expressed in terms of maximum thickness loss and modified fatigue failure stress [125]

One of the fundamental characteristics of cavitation erosion is a fatigue-type damage process which allows some useful comparisons of the relative wear resistances of metals based on metal fatigue theory [125]. It is found that the cavitation erosion rates of a range of pure metals correlate well with a fatigue strength parameter which is the product of the nominal fatigue failure stress at zero cycles and the exponent of stress increase during cyclic plastic strain. The relationship, obtained from experimental data, between the cavitation erosion resistances expressed in terms of maximum thickness loss and modified fatigue failure stress is shown in Fig. 1.15.

1.5 Factors affecting erosion

The material removal during erosion is dependent on many interrelated factors that include metallurgical as well as operating parameters [34, 50, 51, 56, 84, 88, 126-144]. The main metallurgical factors affecting erosion are mechanical properties and microstructure of target material.

1.5.1 Mechanical properties

Metal hardness and impact strength are among the most important characteristic to consider when selecting the metals for minimum erosion. Hardness appears to be a dominant factor governing the erosion resistance of various materials in specific applications [50, 51, 56, 126-130]. In general wear resistance tends to increase with hardness and it decreases as impact strength increases. But in case of erosion, high hardness increases the erosion rate and it decreases as impact strength increases. This is

an important relationship in application that requires both wear resistance and impact resistance. If the material is sufficiently hard, it will have more resistance to erosion and also resistance to crack propagation. The material having higher impact strength poses more resistance to erosion. The impact strength of metals is closely related to the crack propagation rate, which also affects the rate of erosion.

Goretta et al [127] studied the solid particle erosion behaviour of AISI 4140 steel heat treated to have Vickers hardness of 288-650 HV. They concluded that erosion rate was nearly independent of hardness for HV $\leq$ 365, but increased with HV $\geq$ 365. **Divakar et al** [50] have studied the effect of surface hardness on the erosion behaviour of AIAI 316 steel. They reported that increase in the hardness shows higher erosion resistance of AIAI 316 steel as a result of compressive stresses, which is induced in to the target surface by the cold rolling.

The work hardening behaviour of the target material during solid particle impact also appears to be of critical importance. The austenitic grades of steels usually owe their wear resistance to their work hardening characteristics [51]. Development of wear resistant Hadfield steel, for example, is primarily based on its self work hardening characteristics. **Richmann and McNaughton** [128] have reported the correlation of cavitation erosion behavior with mechanical properties of metals. They observed that the predominant property in cavitation erosion resistance is the fatigue strength coefficient (σ_f) which accounts for most of the differences among materials. Correlations

are further improved by incorporating the strain hardening exponent n' in a combined parameter "$\sigma_f n$".

Levin et al [56] have reported that tensile toughness is indicative of the ability of a material to absorb energy of the abrasive particles impacted and have shown that a material having higher tensile toughness possesses higher erosion resistance. **O'Flynn et al** [130] have reported that the erosion rate increases as $1/U_T\varepsilon_u$ increases; where U_T is tensile toughness and ε_u is uniform strain. This is to say that erosion resistance increases as the product of tensile toughness and uniform strain (strain up to UTS) increases.

1.5.2 Microstructures

Metallurgically hardness and microstructures are commonly interrelated and both have importance as factors in resistance to erosion. Increasing the carbon content of steel results in microstructural alteration that increases hardness and decreases ductility, impact strength and tensile toughness. The maximum hardness depends on the carbon content of the steel and the amount of martensite. Carbon content also affects erosion resistance through formation of various carbides [64].

Effect of microstructure on erosion has been studied by various authors [34, 88, 131-140]. **Pugsley and Allen** [132] have studied the cavitation erosion performance of a range of tungsten carbide–cobalt (WC–Co) composites of varying grain sizes and cobalt contents has been evaluated using a stationary-specimen vibratory cavitation erosion rig. They observed that the erosion resistance increases with increasing cobalt content and is

not dependent on either the bulk material deformation parameters or the fracture toughness. The effects of the microstructure of two ductile steels on their behavior under solid particle erosion were determined by **Levy** [88]. **Levy** [88] presented that the erosion rate is directly related to the distribution of hard, brittle and soft, ductile phases in the alloy. He further emphasized that within limits, the more continuous the ductile matrix, the lower the erosion rate is. However, when the ductile matrix becomes the predominant phase and the resulting strength of the steel is markedly reduced, strength and not ductility becomes the dominant factor in erosion. **Wang et al** [133] have investigated the erosion-corrosion resistance of 1018 plain carbon steel and 2.25Cr lMo steel, two commonly used boiler tubing steels in five different conditions, i.e. annealed, hot rolled, normalized, quenched-tempered and cold rolled at room and elevated temperatures using SiO, particles at V= 20 ms^{-1} and $\theta = 30^{o}$. They presented the similar observations reported by **Levy** [88] that the influence of microstructure on the room temperature erosion depends on the distribution of hard, brittle and soft, ductile phases in the steel, which determined their combination of ductility and strength.

The microstructure of target material plays an important role in solid particle erosion. In solid particle erosion austenite is considered to be beneficial constituent because (i) austenite is plastic and tough; (ii) the strength at the interface between carbide and austenite is high [134] and (iii) localized strength of austenite increases with strain hardening [135]. In hot rolled 21-4-N steel the austenitic matrix is continuous and the strength is high too, which are beneficial parameters for erosion resistance [87].

Kwok et al [136] have studied the cavitation erosion characteristics of alloys with duplex structures such as super duplex stainless steel (UNS S32760) and α + β brass (Cu–40%Zn) in 3.5% NaCl solution at 23°C by means of a 20 kHz ultrasonic vibrator at peak-to-peak amplitude of 50 μm and compared with that of austenitic stainless steel (UNS S30400). They concluded that cavitation erosion behaviour of α + β brass, S30400 and S32760 is significantly influenced by the deformation mechanism and the microstructure of the alloys. They explained that for alloys with duplex structure like α + β brass and super duplex stainless steel S32760, the weaker phase is attacked selectively. For α + β brass, the α phase, which is lower in hardness than the β phase, is attacked selectively, whereas for S32760, the strain rate sensitive ferritic (α) phase is attacked selectively by brittle fracture mechanism. The initiation sites for cavitation erosion are at the inter phase boundaries and the damage spreads through the weaker phase. For austenitic stainless steel S30400, the initiation of cavitation attack is at the twin boundaries by ductile fracture mechanism.

Bregliozzia et al [137] have studied the cavitation erosion behaviour of two different austenitic stainless steels (AISI 304 and high nitrogen steel) in water with different pH values at room temperature by means of a 20-kHz ultrasonic vibrator operating at peak-to-peak amplitude of 40 μm. They reported that for both steels, the initiation of cavitation attack is at the grain boundaries and slip bands and results in the formation of surface undulations. Cavitation cracks start generally from these defects, which represent origins of stress concentration. They explained that the material removal

is by ductile fracture. The high nitrogen steel, due to enhanced mechanical properties, exhibits higher cavitation erosion resistance than AISI 304 steel.

1.5.3 Operating variables

Effect of erodent velocity

The velocity of the erosive particle has a very strong effect on the wear process. If the velocity is very low then stresses at impact are insufficient for plastic deformation to occur and wear proceeds by surface fatigue [84]. When the velocity increases, the eroded material may deform plastically upon particle impact. In this regime, wear is caused by repetitive plastic deformation. At brittle wear response, wear proceeds by subsurface cracking. At very high particle velocities melting of the impacted surface may even occur (Fig. 1.3).

From medium to high velocities, a power law [84], can describe the relationship between wear rate and impact velocity:

$$dm/dt = kv^{n'} \qquad \text{.....(1.4)}$$

where m is the mass of the worn specimen, t is the duration of the process, k is an empirical constant, n' is a velocity exponent. The characteristics of the erodent and target material determine the value of the exponent n'. It has been stated that n' varies in the range of 2–3 for polymeric materials behaving in a ductile manner, while for polymer composites behaving in brittle fashion the value of n' is in the range of 3–5 [141].

Effect of impact angle

In respect to the impact angle (θ), solid particle erosion is divided in [50]:

- erosion at normal impact angles (θ ≈90°)
- erosion at oblique impact angles ($0^o < \theta < 90^o$)

A low impact angle favours wear processes similar to abrasion because the particles tend to track across the worn surface after impact. A high impact angle causes wear mechanisms which are typical of solid particle erosion (Fig. 1.4) [50]. It can be seen in Fig. 1.4 that in ductile mode of erosion the maximum material removal occurs at low impingement angles whereas maximum erosion is found at high impingement angles causing brittle mode of erosion.

Effect of erodent characteristics

A key aspect of the erosion problem is related to the erodent characteristics. Variations in particle size and shape can cause fundamental changes in the erosion response [84]. If the eroding particles are blunt or spherical then plastic deformation is favoured, if the particles are sharp then cutting and brittle fragmentation are more likely. A blunt particle has a mostly curved surface approximating to a spherical shape while a sharp particle consists of flat areas joined by corners with small radii which are critical to the process of wear [84].

It is assumed that the erosion rate is independent of particle size above a critical value [142, 143]. This critical value is observed between 100–200 μm, however, it is dependent on the exposure conditions and the particle target interaction [143]. Up to this

critical value, experimental results showed that with increasing size of the erodent also the erosion rate increases. The existence of this critical value has been attributed to a range of factors [143]. These factors are:

(i) Strain rate effects, due to small particles: it has been shown that strain rates are higher for smaller than for larger particles. This results in increased stresses of the target material when bombard with smaller particles.

(ii) Differential work hardening due to erodents of various particle sizes: It has been suggested that a surface layer of 50–100 μm "hardens" more than the bulk material. Hence, small particles will encounter a layer with a significantly higher flow stress than the bulk material, whereas large particles should penetrate in this layer. Above the critical size, the influence of this layer should be negligible.

The effect of erodent hardness depends mainly on the particular mode of erosive wear taking place, e.g., ductile or brittle. In the brittle mode the effect of particle hardness is much more pronounced than in the ductile mode. It is usually believed that hard particles cause higher wear rates than soft ones, but it is impossible to isolate hardness completely from other features of the particle (e.g., shape). Even if the particle is hard, but relatively blunt, then it is unlikely to cause severe erosive wear [84].

With respect to the size and type of the erodent material, two trends may hold for harder and/or more brittle material. The erosive wear increases the higher the hardness of the erodent and the larger the erosive particle size are (until a level of saturation is reached in both cases) [144]. In ductile polymers, however, the situation may be quite

different. Due to the relatively low hardness no pronounced effects of changes in the hardness of the usually much harder erodent materials should be expected [144].

1.6 Surface coatings

Solid particles transported in gas or liquid flows cause severe damage on industrial components and lead to expensive repair and part replacement [145]. Wastage associated with erosion has caused an increase in power plant down time due to increased maintenance, therefore reducing plant efficiency. This problem has led to various methods to combat solid particle erosion. One method to combat solid particle erosion is to select erosion resistant materials for use in components that are subject to an erosive environment and another is to apply coatings to the components subjected to erosive environments.

Coatings of a wide variety of materials are commonly applied to substrates for many purposes. These may include the enhancement of mechanical properties, visual appearance or corrosion resistance or may provide special magnetic and optical properties. Often, coatings are applied to improve tribological performance [146]. The plasma spray coatings are generally used for protection against wear and corrosion, to prevent erosion or cavitations, and to provide electrical insulation or conductivity. Plasma spraying is the most flexible and versatile thermal spray process with respect to the sprayed materials. Almost any material can be used for plasma spraying on almost any type of substrate [147].

Extensive research has been conducted to understand the mechanism of erosion of underwater parts, such as turbine blades, guide vanes and lyberinths [148]. It has been established that the intrinsic characteristics like microstructure and mechanical properties of the component material play an important role in the erosion behaviour. The effect of surface coatings on the erosion damages has not yet been systematically studied. Thermal spray coatings are being used on structural steels in energy conversion and utilization systems to prevent surface degradation by corrosion, erosion or combination of these phenomenons. The ability of the coatings to protect base material against erosion is related to their composition and processing; and especially to the structure of the coatings. Generally, the hardness of the coatings does not directly relate to their erosion resistance [149-151]. However, some data in the literature [152] suggests that the relative hardness values of the erodent particles and the target material might play a role in the erosion behaviour of brittle materials. It is reported that decreasing the ratio of the target material hardness to the hardness of the impacting particles resulted in an increase in the erosion rates, mainly when the ratio is in the range of unity.

Thermally sprayed coatings have emerged as a viable solution for a wide range of wear resistance applications to improve the service life of machine components. Tungsten carbide and chromium carbide-based coatings are frequently used for many of the applications in gas turbine, steam turbine, aero engine as well as hydro turbines to improve the resistance to sliding, abrasive and erosive wear [153-155]. For sliding wear and abrasive wear resistance, the carbide coatings are considered to be a viable

alternative to hard chrome plating due to the strict environmental regulations and cost concerns with regard to the electroplating process. These cermet coatings are deposited by plasma spray and high velocity processes namely high velocity oxy-fuel (HVOF) and detonation gun spray processes [59, 156, 157]. WC and Cr_3C_2 with different metallic binders like Co, Ni and Fe have been studied using different amounts of binder contents with Co and Ni most commonly used. Addition of Cr to the matrix has been found to improve the wear and oxidation resistance of these cermets [157]. The wear behavior of WC based coatings with varying amounts of Co content deposited by different thermal spray processes has been studied by a number of researchers [158-163].

It has been reported that the abrasive wear rate for the cermet coatings is controlled by several factors like the morphology of the starting powder, the size and distribution of the carbide particles, hardness of the carbide particles relative to the abrasive, properties of the matrix and its volume fraction and the coating process, which determines the coating characteristics like the phases, density, microhardness and the residual stresses. Even though tungsten carbide has a very high hardness of 2200 HV, the hardness of HVOF coating of WC–Co based powder is very low with 866 to 1226 HV [157, 160]. This hardness difference is due to the presence of metallic binder (Co, Ni, and Cr) and little amount of porosity in the coating. Various attempts have been made to improve the abrasion resistance like adding vanadium carbide powder (VC), chromium carbide (Cr_3C_2) etc. [164].

Chapter 2

Formulation of problem

Continuous demand of electrical energy in India has necessitated a smooth working of various hydro power plants in the Himalayan region, where the silt concentration is very high. It is seen that these power plants suffer a serious setback due to rapid erosion of underwater parts by silt laden water and cavitation. The erosion due to silt particles is a result of mechanical wear of components on account of dynamic action of silt flowing in water coming in contact with wearing surface. The flow handling parts of hydro turbine also suffer erosion due to cavitation, which forms in low pressure or high velocity areas. Extensive research has been done in the past few years on the mechanisms of erosion by silt laden water, cavitation and silt laden water as well as cavitation. In hydro turbine it has been seen that silt erosion is worsened by the presence of cavitation (synergetic erosion). Following solutions have been suggested to overcome the problem of erosion:

(i) Improvement in sedimentation technology

Sedimentation is a technique to reduce the silt concentration in the water flowing through the turbine by settling down the silt particles in a reservoir. This technique suffers from the limitation that particle concentration below 300 ppm cannot be eliminated. Another problem faced by the sedimentation is that a large percentage of the sediment is deposited in the reservoirs thus reducing the storage capacity. The technology

of silt separation by sedimentation now appears saturated and no further benefit is expected from sedimentation control techniques.

(ii) Improvement in repair welding technology

The eroded components of the hydro turbine can be repaired by welding at the site. This technique also has not proved too useful because welding of hydro turbine components require pre and post welding heat treatments, which are very difficult to perform at work site. The 13/4 martensitic stainless steel is currently being used in the fabrication of hydro turbine underwater parts. The hardness of this steel is of the order of 300-400 VHN, which is the chief cause of its good erosion resistance. The weldability of this steel is, however, poor and cracks are invariably formed in the weld metal and heat affected zone (HAZ). Further, carbides and various intermetallic particles may form in the HAZ. These particles are very sensitive to attack of silt laden water and also act as point of stress concentration resulting in acceleration in erosion rate in the HAZ portion. Very precise pre weld and post weld heat treatments are necessary to avoid formation of such particles, which are difficult to perform at work sites.

(iii) Development of alternative grades of steel

Since the silt erosion damage is on account of dynamic action of silt with the component, properties of silt, mechanical properties of the component in contact with the flow and the conditions of the flow are jointly responsible for the intensity and quantum of erosion. In view of good weldability and mechanical properties as well as

microstructure of the target material, nitronic steels appear as a suitable alternative to 13/4 martensitic steel.

(iv) Development of technology for protective surface coatings

Various attempts have been made in the development of protective surface coatings for the purpose of improving erosion resistance of underwater parts. From literature it has been observed that the erosion resistant coating should possess high hardness, low porosity and optimum volume fraction of hard phases in the matrix.

In this research attempts are made to develop an erosion resistant material called 21-4-N steel as an alternative to 13/4 steel. So far no investigation has been reported on the comparative study on erosion behaviour of 13/4 and 21-4-N steel. 21-4-N steel is a nitrogen strengthened austenitic stainless steel. The role of nitrogen in 21-4-N steel is to stabilize the austenitic structure at room temperature, strengthen the austenitic matrix by solid solution hardening and decrease the stacking fault energy, which results in improving the strain hardening ability. By alloying with nitrogen, the strength of the alloy can exceed that of martensitic steel. Due to higher strain hardening ability, the strength of nitronic steels can be enhanced by mechanical deformation.

21-4-N steel is a regular production of M/S Star Wire (India) Ltd. Ballabhgargh (Haryana) for the manufacture of inlet and exhaust valves in the automobiles, where it acts as an erosion resistant material due to the product of combustion. Hence it is expected to perform satisfactorily as a material for fabrication of underwater parts in

hydroelectric projects. In view of this, the austenitic 21-4-N steel has been studied for its suitability as a material for underwater parts. From literature it has also been reported that the erosion resistant material should have the microstructure that accumulates the strain caused by the impingement of erodent particles. In this context also the austenitic structure of 21-4-N steel should be preferred over martensitic structure of 13/4 steel.

Planning of experiments

Long bars of 13/4 and 21-4-N steels were received from M/S Star Wire (India) Ltd. Ballabhgargh (Haryana). The heat treatment and rolling (8% reduction in thickness) were performed on these steels to alter the microstructure as well as the mechanical properties. The samples for metallographic examination, mechanical testing and solid particle erosion were machined from the as received bars. The strain hardening coefficient and tensile toughness have been measured and correlated with the erosion behaviour. Erosion tests were performed in a near sonic high velocity air blast erosion rig at 30° and 90° impingement angles. The erosion behaviour of both the steels has been analyzed with respect to impingement angle, microstructure and mechanical properties.

The metallographic examination, mechanical testing and erosion testing were performed on the various heat treated samples of both the steels. The effects of heat treatment on the microstructure, mechanical properties and erosion behaviour of both the steels have been analyzed. In addition to the as cast steels, studies on hot rolled 21-4-N

steel were also conducted. The effects of rolling on as received steels on microstructure, mechanical properties and erosion behaviour have been analyzed.

The cavitation erosion behavior of 21-4-N steel in as cast and hot rolled conditions was investigated by means of an ultrasonic vibration processor and compared with that of as cast 13/4 steel.

Besides development of erosion resistant nitronic steel, the effect of surface coating on erosion behaviour has also been studied. D-gun spray provides very hard and dense coating as compared to other thermal spray coatings. So far no investigation has been carried out on the erosion of coatings on 21-4-N steel. For this purpose D-gun spray coatings of stellite-6, Cr_3C_2-NiCr and WC-Co-Cr were provided on the hot rolled 21-4-N steel and their performance under erosive environment has been studied.

Chapter 3

Experimental procedures

This chapter deals with the experimental techniques adopted in this study. Optical microscope was used for microstructural characterization. Conventional techniques were used for the measurements of mechanical properties; viz. tensile properties, impact energy and hardness. Air jet erosion test rig and ultrasonic processor were used for the erosion testing. Scanning electron microscope (SEM) was used to study the fracture behaviour and erosion mechanisms of the steels under investigation.

3.1 Material selection

The 13/4 martensitic and 21-4-N nitronic steels used in this investigation possess the chemical composition as given in Table 3.1. Long bars of 40 × 40 mm cross-section were received from M/s Star Wire (India) Ltd., Ballabhgarh (Haryana). Specimens for metallographic examination, tensile test, impact test and erosion tests were machined from these bars.

3.2 Heat treatments

3.2.1 Cast 13/4 martensitic stainless steel

A standard heat treatment was given to the cast 13/4 steel. The plates were heated at the austenitizing temperature of 1050°C for 4 hr and then quenched in oil. To avoid the

Table 3.1. Chemical composition of 13/4 and 21-4-N steels (wt %)

Steel	C	Si	Mn	Cr	Ni	N	S	Cu	Co	P	Mo	Fe
13/4	0.06	0.74	1.16	13.14	3.9	-	0.014	.088	0.035	0.015	0.61	Bal
21-4-N	0.56	0.25	9.90	23.42	4.28	0.38	0.001	0.16	0.06	0.041	-	Bal

warpage and cracking of martensitic steel, preheating was carried out from 550°C to 1050°C at the rate of 100°C per hr. Immediately after quenching; tempering was carried out at 620°C for 4 hr followed by oil quenching. Tempering temperature of 620°C was chosen because loss of impact strength occurs when martensitic steels are tempered within the range 370°C to 593°C [64].

3.2.2 Cast 21-4-N nitronic steel

Solution annealing treatment

Like conventional austenitic stainless steels, 21-4-N steel cannot be hardened by heat treatment but will harden as a result of cold working. The heat treatment of 21-4-N steel consisted of heating the steel up to austenitizing temperature; kept there for some time to allow the dissolution of carbides and then quenching in water to prevent the carbide precipitations. During annealing chromium carbides were dissolved. Since carbide precipitation can occur at temperatures between 425°C and 900°C, it is obviously desirable that the solution annealing temperature should be safely above this limit. Cooling from the annealing temperature must be rapid, but it must also be consistent with limitations of distortion. Whenever considerations of distortion permit, water quenching is used thus ensuring that dissolved carbides remain in solution.

The various solution annealing temperatures such as 950°C, 1000°C, 1050°C and 1100°C were selected for the solution annealing treatment of 21-4-N steel. The 21-4-N steel specimens were put in the furnace after attaining the annealing temperature and kept

there for 2 hr to ensure the dissolution of carbides. Then for rapid cooling, the specimens were quenched in water.

Aging

The aging of solution annealed 21-4-N was carried out at 700°C to determine the changes in the microstructure and mechanical properties of 21-4-N steel.

3.3 Rolling

3.3.1 Rolling of as cast 13/4 and 21-4-N steels

The rolling of 13/4 and 21-4-N steel was carried out on the two high mill type of rolling mill. The stock is returned to the entrance for further reduction by hand carrying. Due to very high hardness of both the steels, the rolling at room temperature was not possible. Therefore, the stocks were heated up to 700°C before rolling. In this way 8% reduction in thickness was obtained in both the steels. For metallographic examination, tensile testing, Charpy V-notch impact testing, hardness measurement and erosion testing, the required samples were cut from these rolled steels.

3.3.2 Hot rolling of 21-4-N steel

The hot rolled 21-4-N steel was received from M/S Star wire (India) Ltd. Ballabhgarh (Haryana). The flow chart of hot rolling 21-4-N steel is

Rolling from7" X 8" to 63 RCS

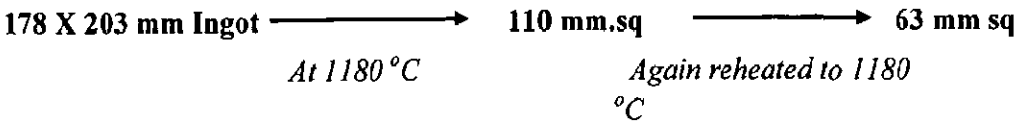

Rolling Temperature = 1180°C

Roliing finishing temperature = 1020°C

Percent reduction in cross-sectional area = 89

Average reduction ratio = 1:9

3.4 Metallographic study

13/4 and 21-4-N steels in as received as well as in heat treated and rolled conditions were prepared for microstructural examinations by conventional polishing techniques. The polished specimens were etched with aquarazia and Zeiss Axiovert 200 MAT inverted optical microscope was utilized for recording microstructures.

3.5 Determination of mechanical properties

3.5.1 Tensile testing

Standard cylindrical tensile specimens were prepared with a gauge length of 20 mm and gauge diameter of 4 mm as per **ASTM E8M-03** [165] specifications as shown in Fig. 3.1. The tensile tests were carried out on as received, heat treated and rolled samples of 13/4 and 21-4-N steels utilizing a Hounsfield H25K materials testing machine with a crosshead speed of 1 mm/min at room temperature.

3.5.2 Charpy V-notch impact testing

Standard Charpy V-notch impact specimens of dimension 10 × 10 × 55 mm were prepared as per **ASTM E23** [166] specification as shown in Fig. 3.2 and the test were performed at room temperature.

3.5.3 Hardness test

Hardness measurements were carried out on the Vickers hardness testing machine using a 30 kg load. Each hardness value reported is the mean of 10 indentations.

3.6 D-Gun (Detonation-Gun) spray surface coating

3.6.1 Substrate material

The substrate material selected for the study was a hot rolled 21-4-N steel. The chemical composition of the substrate material is given in Table 3.1. The specimens measuring 40 × 40 × 10 mm were polished and grit blasted before subjecting to coating by D-Gun.

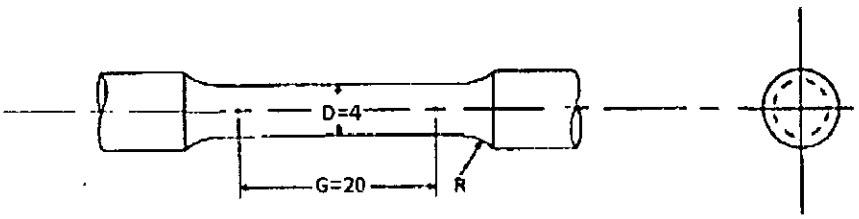

Fig. 3.1. Dimensions of tensile specimen (all dimensions in mm) [165]

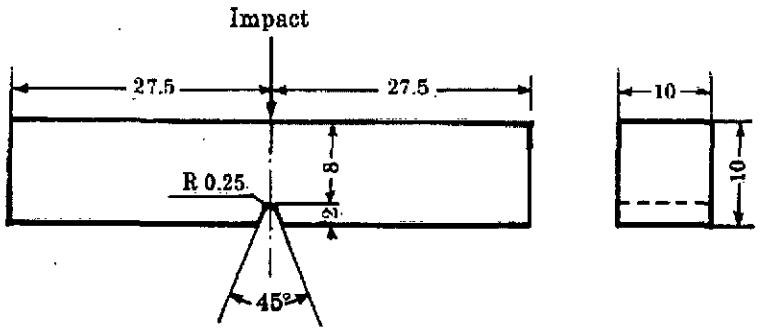

Fig. 3.2. Dimensions of Charpy V- notch impact test specimen (all dimensions in mm) [166]

Table 3.2. Composition of coating powders

Coating material	Composition (wt %)
Stellite-6	30 Cr-5Fe-6W-1C-Co (Bal)
Cr_3C_2-NiCr	$75Cr_3C_2$ -25 NiCr
WC-Co-Cr	86WC-10Co-4Cr

Table 3.3. D-Gun process parameters

Particle size	35-45 μm
Spray spot diameter	25mm
Spraying distance	200mm
Spraying atmosphere	air
Thickness per shot	5-6 μm
Shots/second	3
Total coating thickness	300μm

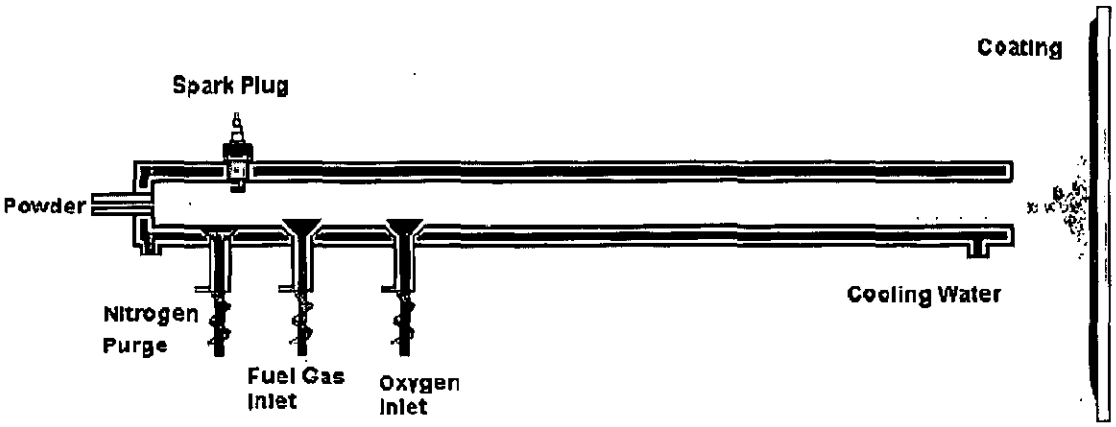

Fig. 3.3. Detonation-gun thermal spray coating process [167]

3.6.2 Surface coatings

Three types of powders were used in the study, the chemical compositions of which are reported in Table 3.2. D-Gun spray (Fig. 3.3) equipment having horizontal orientation was used for coating of the samples at the worksite of M/s Sai Surfacing Co, Hyderabad (India). The D-Gun spraying process parameters are given in Table 3.3.

3.6.3 Characterization of the as D-Gun sprayed coatings

The microstructural features of the coated specimens were studied using optical microscope. Porosity of coatings was measured using a Zeiss Axiovert 200 MAT inverted optical microscope fitted with imaging software Zeiss Axio Vision 4.1. Microhardness of the coatings was measured by Leitz's Hardness Tester Mini Load-2. Two hundred gram load was provided to the needle for penetration and the hardness value was determined based on the relation: $HV = 189.03 \times 10^3 \times (F/d^2)$, where F is the load in gram, and d is the mean of the indentation diagonal length in μm. For each hardness value, an average of ten measurements was taken. The XRD analysis was carried out using a Bruker AXS D-8 Advance Diffractometer with CuKα radiation.

3.7 Erosion test

3.7.1 Solid particle erosion test rig

The solid particle erosion test rig used for erosion testing was fabricated to accelerate solid particles to high velocities and for these particles to impinge on test specimens under controlled erosive conditions as per standard followed by **Wood and**

Wheeler [168] (Fig. 3.4). The photograph of the erosion testing rig is shown in Fig. 3.5. Silicon carbide particles of size ranging between 500-700 μm were used as erodent. The SEM of SiC particles are shown in Fig. 3.6. Erodent is fed into the rig from a hopper fitted with a mechanism to control the erodent flow. The erosion chamber has the facility to vary the sample to air jet impingement angle from 90 to 20^0 as well as the sample to acceleration tube standoff distance from 10 to 100 mm. A sample holder fitted on the sample stand holds the sample in place.

The erosion tests were conducted by fixing the feed screw for the feed rate of 5 g / min. The erosion test conditions utilized in the present study are listed in Table 3.4. A standard test procedure was employed for each erosion test. The samples were cleaned in acetone, dried, weighed to an accuracy of 1×10^{-4} g using an electronic balance, eroded in the test rig for 10 min and then weighed again to determine weight loss. The experiments were conducted at 30° and 90° impingement angles at room temperature. The cumulative weight losses as a function of time of erosion were plotted for the purpose of comparison of weight losses during two hr of erosion test. The ratio of this weight loss to the weight of the eroding particles causing the loss (i.e. testing time × particle feed rate) was then computed as the dimensionless incremental erosion rate. The erosion rates (g/g) versus cumulative weight of erodent were plotted for a comparison of the erosion rates of the steels under investigation. The eroded surfaces were studied on SEM to identify the mechanism of erosion. The cumulative weight losses were also interpreted as functions of microstructural and mechanical properties.

3.7.2 Cavitation erosion test

The cavitation erosion tests were conducted on as cast 13/4 and 21-4-N steels and hot rolled 21-4-N steel. The samples for cavitation erosion tests were cut by diamond cutter of 10 × 10 × 4 mm dimensions, ground and polished in order to obtain a surface free from scratches. Cavitation erosion resistance has been measured by means of an ultrasonic vibratory test. The ultrasonic vibratory test comprises of an electronic generator that generates 250 watt of average electrical energy. The transformer or velocity horn amplifies the small vibrations. It is attached to a pair of lead zirconate titanate transducer elements. This system uses a device to vibrate in the probe immersed in distilled water. The schematic of ultrasonic vibratory testing processor is given in Fig. 3.7 [169]. During half of each vibration cycle, a low pressure is created at the test specimen surface, producing cavitation bubbles. During the other half of the cycle, bubbles collapse at the specimen surface producing damage and erosion of the specimen. Although the mechanism for generating fluid cavitation in this method differs from that occurring in flowing systems and hydraulic machines, the nature of the material damage mechanism is believed to be basically similar. The method therefore offers a small scale, relatively simple and controllable test that can be used to compare the cavitation erosion resistance of different materials and to study the nature and progress of damage in a given material in detail. This standard test procedure for ultrasonic cavitation testing has been approved by the American Society for Testing and Materials (ASTM) as **ASTM G32-06** [20]. The test specimen was placed at a small distance of 1 mm below the tip of the

Table 3.4. Erosion parameters

Erodent material	**Silicon carbides**
Particle size (μm)	500-700
Particle velocity(ms^{-1})	120
Air pressure (kPa)	196
Impact angle (°)	30 and 90
Nozzle diameter (mm)	8
Feed rate (g/min)	5
Test time (min)	Cycles of 10 min
Working distance (mm)	10

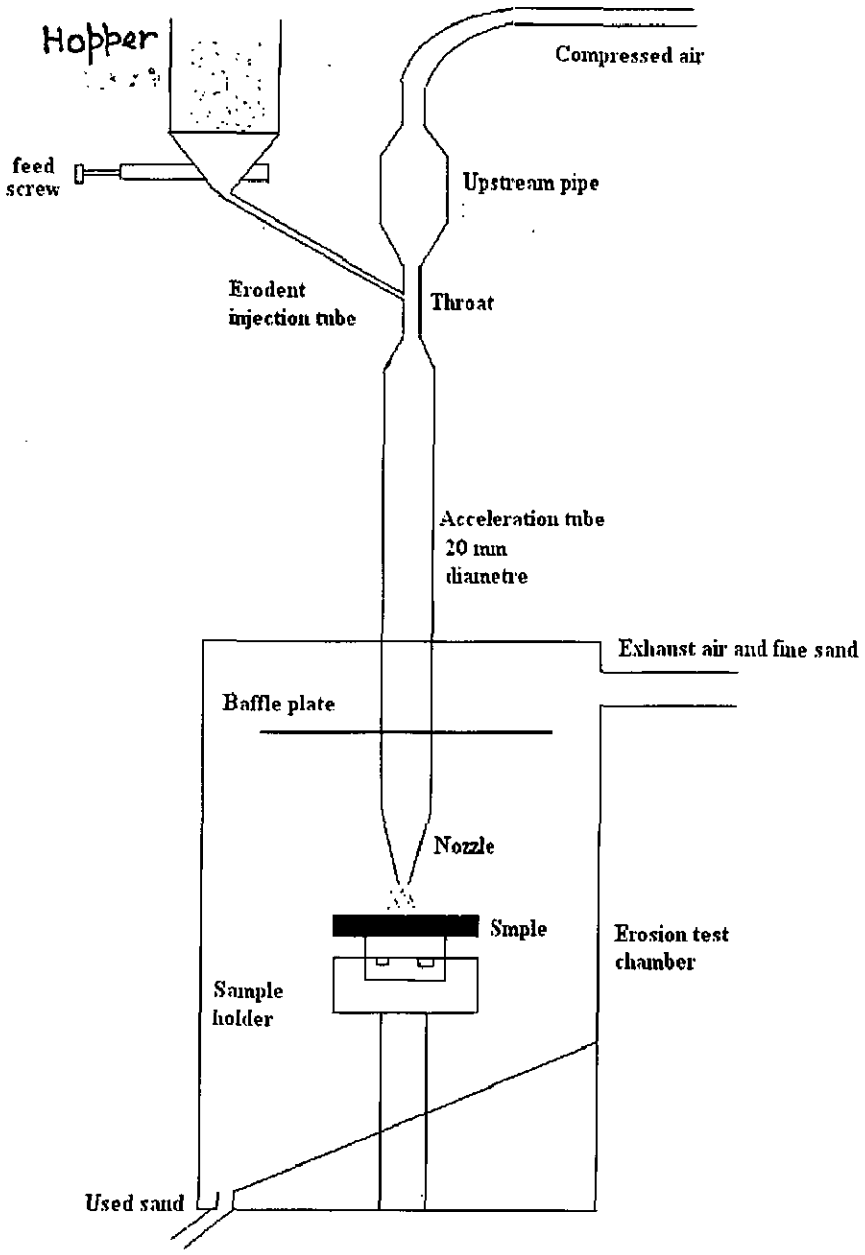

Fig. 3.4. Details of air jet erosion tester

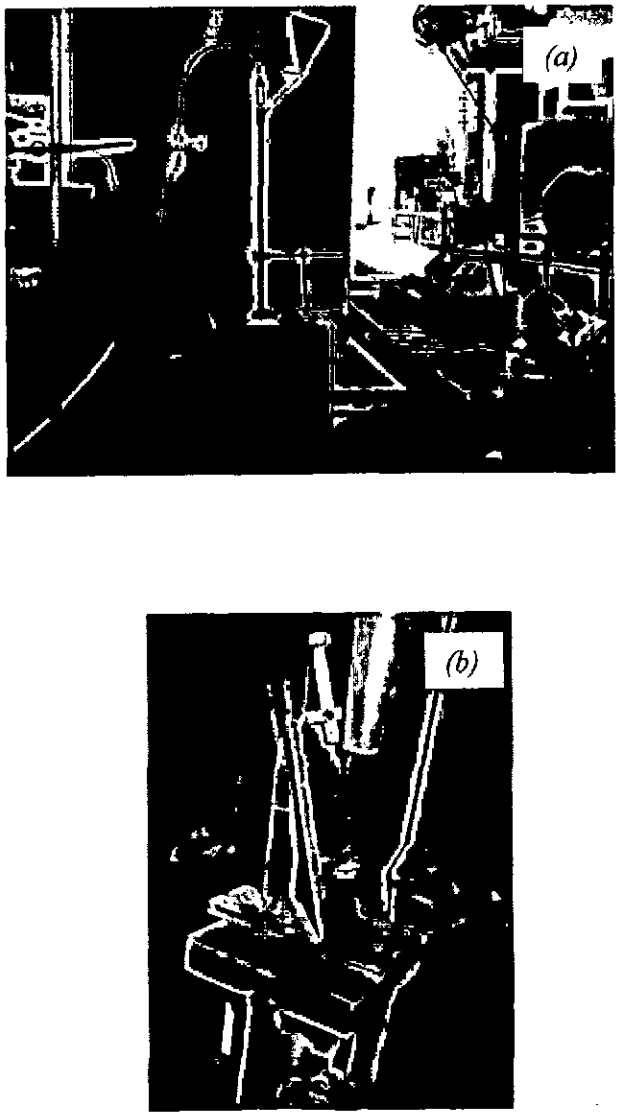

Fig. 3.5. (a) Photograph of erosion test rig and (b) assembly of nozzle and sample holding device

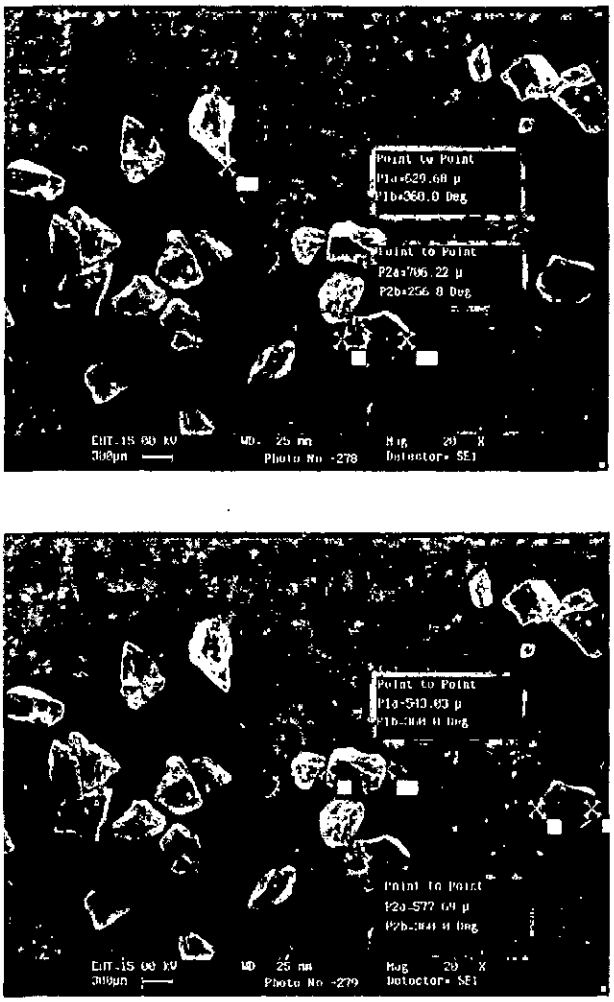

Fig. 3.6. Scanning electron micrographs of SiC particles

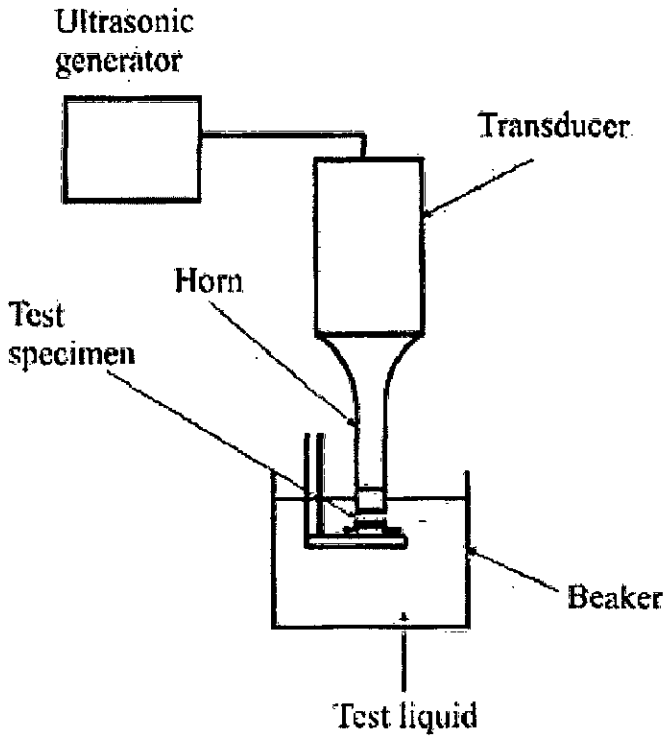

Fig. 3.7. Schematic of the ultrasonic vibratory test device [169]

ultrasonic probe. The cavitation erosion was conducted for a total duration of 32 hr each and weight loss was measured at every successive stage of 4 hr. The samples were cleaned in acetone, dried, weighed to an accuracy of 1×10^{-4} g using an electronic balance, eroded in the ultrasonic vibratory processor for 4 hr and then weighed again to determine weight loss. The eroded surfaces were studied on optical microscope and SEM to identify the mechanism of cavitation erosion. SEM study of eroded surfaces was conducted using FEI Quanta 2000 field emission scanning electron microscope (FESEM) at an accelerating voltage of 20 kV.

The primary result of a cavitation erosion test was the cumulative weight loss versus time of erosion curve. Although the raw data was in terms of the weight loss versus time, for analysis and reporting purposes this should be converted to a mean depth of erosion (MDE) versus time curve, since a volumetric loss is more significant than a weight loss when materials of different densities are compared. The MDE is calculated by dividing the weight loss measured by the density of the material and the affected cavitation area. For comparisons, the cavitated area is considered to be the horn tip area and for this setup, it is 1.638 cm^2. Thus MDE is given by Equation

$$MDE = \frac{\text{Erosion weight loss (g)}}{10 \times \text{Density (g. cm}^{-3}) \times \text{Cavitated area (cm}^2)} \quad \text{..... (3.1)}$$

3.8 Scanning electron microscopy

Extensive investigations were carried out on the fracture surfaces of impact and tensile specimens and on the eroded surfaces. A LEO 435 VP scanning electron

microscope and FEI Quanta 2000 field emission scanning electron microscope (FESEM) were utilized to study the fracture behaviour and erosion mechanisms.

Chapter 4

Characterization and erosive wear of 13/4 and 21-4-N steels

This chapter deals with characterization, erosion behaviour of 13/4 and 21-4-N hydro turbine steels in as cast conditions. The erosion behaviour is also analyzed as a function of impact angle, microstructure and mechanical properties.

4.1 Introduction

Erosion due to impact of hard and abrasive particles is a common phenomenon in hydro turbine underwater parts and many other industrial situations. Extensive investigations [170-172] have been carried out in the past to identify the factors responsible for severe erosive damages in hydro turbine underwater parts due to attack from silt laden water. A number of operating variables such as the impact angle and impact velocity affect the erosion process [50, 81, 89, 173]. The rate of erosion is influenced by the relative hardness of the target material and the particles impacting on the surface [50]. Ductile materials during erosion are considered to lose material through a cutting and ploughing mechanism at a low impact angle [89]. On the other hand, erosion damage of brittle materials is based on cracking, fragmentation and removal of flakes [81]. The erosion mechanism in terms of mechanical properties was presented by

Bitter [85]. He described that during impact, when the yield strength of the materials is locally exceeded, plastic deformation takes place in the vicinity of the impact. After multiple impacts, a plastically deformed surface layer may form near the eroded surface and, therefore, the yield strength of the material increases due to work hardening. **Sundararajan and Shewmon** [96] suggested that during erosion material loss from a metal surface occurs when a critical fracture strain is achieved at the surface. **Ball** [174] proposed that, in order to design a material to resist erosion, attention must be given to providing a microstructure that never accumulates the critical fracture strain under the stress that the impacting particles impose.

The cast martensitic stainless steels currently find wide applications in many hydro turbine and other industrial applications facing damages due to erosion. This is due to their good mechanical properties and resistance against corrosion and erosion. CA6NM steel containing 13% Cr and 4% Ni (also known as 13/4) is being used in fabrication of hydro turbine underwater parts. However, the maintenance repair of this steel is a primary cause of concern in its use. The quantity of martensite and its hardness are the main causes of weldability problems encountered with martensitic steels. Fully martensitic steels are air hardening and susceptible to hydrogen embrittlement. Austenitic stainless steel, on the other hand, has been widely preferred by industry due to its good mechanical properties, outstanding corrosion resistance in a wide range of environment and good weldability. However, there is a need to increase the strength level of this steel to meet the challenges forced by severe erosive conditions faced by hydro turbine

underwater parts. In raising the strength of austenitic stainless steel, N alloying has been gaining much attention; because N is a strong solid solution hardener, has higher solubility in austenite than C, and improves corrosion resistance. In addition, N increases grain size hardening [175]. Nitrogen solubility in austenite increases with Mn and Cr contents; the N alloying can be applied to Cr–Mn and Cr– Mn–Ni austenitic stainless steels.

4.2 Microstructure

Figs. 4.1 and 4.2 show the microstructures of 13/4 martensitic stainless steel and 21–4–N nitronic steel respectively in as cast condition. The microstructure of 13/4 martensitic stainless steel consists of packets of very fine, untempered lath/martensitic needles (Fig. 4.1). Apart from these packets, the structure exhibits a second phase, which is δ-ferrite. The as cast 21–4–N steel, which is a nitrogen strengthened austenitic stainless steel having low Ni and higher concentration of C, possesses predominantly austenitic phase along with the precipitates of carbides. The carbides may be any one or combinations of $M_{23}C_6$, MC, M_7C_3 and M_6C, where M can be Cr, Fe, Mo and Ni [176]. Among these carbides, the probability of formation of $M_{23}C_6$ appears low, since presence of N in the matrix is reported to suppress the precipitation of this carbide. The M_6C (M = Fe, Cr, Mo, W, Nb and V) carbides are often found in austenitic stainless steels containing Mo, W and Nb. The MC (M = Ti, Zr, Hf, V, Nb and Ta) carbides are very stable and invariably present in stabilized austenitic stainless steels such as AISI 321 (Ti

stabilized). The M_7C_3 carbides can only be found in austenitic stainless steels for very high C: Cr ratio. Since the 21–4–N steel has higher concentration of N and also possesses high C: Cr ratio, the carbide precipitated in this steel may be M_7C_3. In the microstructural examination of this steel, the massive core of carbides (dark portion) is surrounded by an eutectic, which according to **Padilha and Rios** [176] consists of austenite and carbides.

Identification of the microstructures with the help of Schaeffler diagram

The structure of 13/4 and 21-4-N steels is also determined with the help of Schaeffler diagram (Fig. 4.3) which is useful to predict the resulting microstructure of stainless steel after solidification [177]. For the 13/4 steel the chromium equivalent has been empirically determined using the most common ferrite forming elements:

$$\mathbf{Cr\ eq} = \mathbf{(Cr) + 2(Si) + 1.5(Mo) + 5(V) + 1.75(Nb) + 0.75(W)}$$

$$= 13.4 + 2(0.74) + 1.5(0.61) + 1.75\ (.003) + 0.75(0.55)$$

$$= 16.21$$

and the nickel equivalent has been determined with the familiar austenite-forming elements:

$$\mathbf{Ni\ eq} = \mathbf{(Ni) + (Co) + 0.5(Mn) + 0.3(Cu) + 25(N) + 30(C)}$$

$$= 3.9 + 0.035 + 0.5(1.16) + 0.3(.088) + 30\ (.06)$$

= 6.34

From Schaeffler diagram (Fig. 4.3), the values of Cr_{eq} and Ni_{eq} for 13/4 steel corresponds to the region of martensite plus δ-ferrite, which is in agreement with the microstructures of 13/4 steel as shown in Fig. 4.1. Apart from the packets of martensitic laths, the structure exhibits a second phase, which is δ-ferrite.

In case of 21-4-N steel the chromium equivalent has been empirically determined using the most common ferrite forming elements:

$$\mathbf{Cr_{eq}} = \mathbf{(Cr) + 2(Si) + 1.5(Mo) + 5(V) + 5.5(Al) + 1.75(Nb) + 1.5(Ti) + 0.75(W)}$$

$$= 23.42 + 2(.25) + 1.5(0) + 5(0) + 5.5(0) + 1.75\ (0) + 1.5(0) + 0.75\ (0)$$

$$= 23.92$$

and the nickel equivalent has likewise been determined with the familiar austenite-forming elements:

$$\mathbf{Ni_{eq}} = \mathbf{(Ni) + (Co) + 0.5(Mn) + 0.3(Cu) + 25(N) + 30(C)}$$

$$= (4.28) + (0.06) + 0.5(9.9) + 0.3(0.16) + 25(0.38) + 30(0.56)$$

$$= 35.63\ .$$

From Schaeffler diagram (Fig. 4.3), the values of Cr_{eq} and Ni_{eq} for 21-4-N steel correspond to the region of austenite, which is in agreement with the microstructure (Fig. 4.2)

4.3 Mechanical properties

Table 4.1 shows the mechanical properties of 13/4 martensitic stainless steel and 21–4–N nitronic steel studied in this investigation. The 13/4 martensitic stainless steel possesses significantly higher values of impact energy, YS and UTS than the corresponding values in the 21–4–N nitronic steel. The hardness and ductility (% elongation) in martensitic stainless steel are marginally lower in comparison to nitronic steel.

4.4 Erosion behaviour

Erosion tests as described earlier were conducted on both the steels for a total duration of 2 hr each and the weight loss was measured at every successive stage of 10 min. Fig. 4.4 gives the cumulative weight loss curves of the test materials at the impingement angles of 30° and 90°. The cumulative weight loss at 30° and 90° impingement angles is also shown in a bar chart diagram given in Fig. 4.5. It can be noticed that the cumulative weight loss of both steels under consideration, is maximum at 90° impingement angle, which normally corresponds to erosion of brittle materials [50, 54, 81, 86, 104, 159, 173, 174]. At both the impingement angles, the cumulative weight

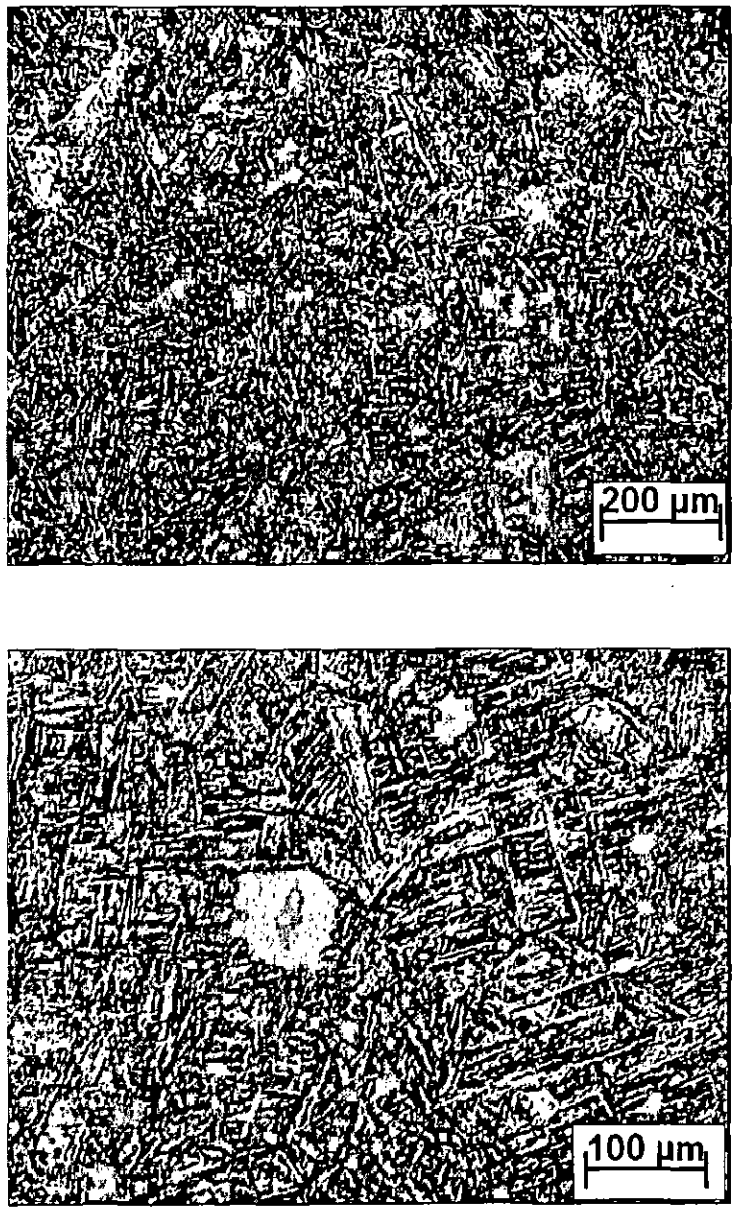

Fig. 4.1. Microstructures of as cast 13/4 martensitic stainless steel

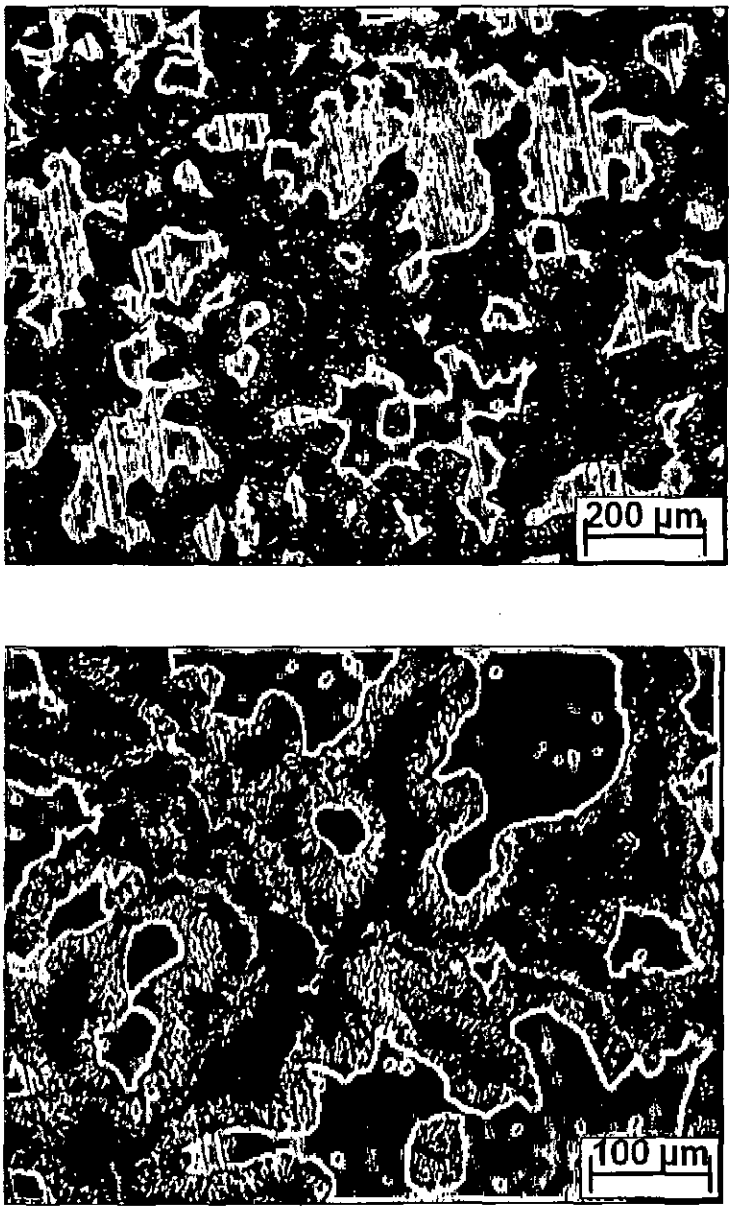

Fig. 4.2. Microstructures of as cast 21-4-N steel

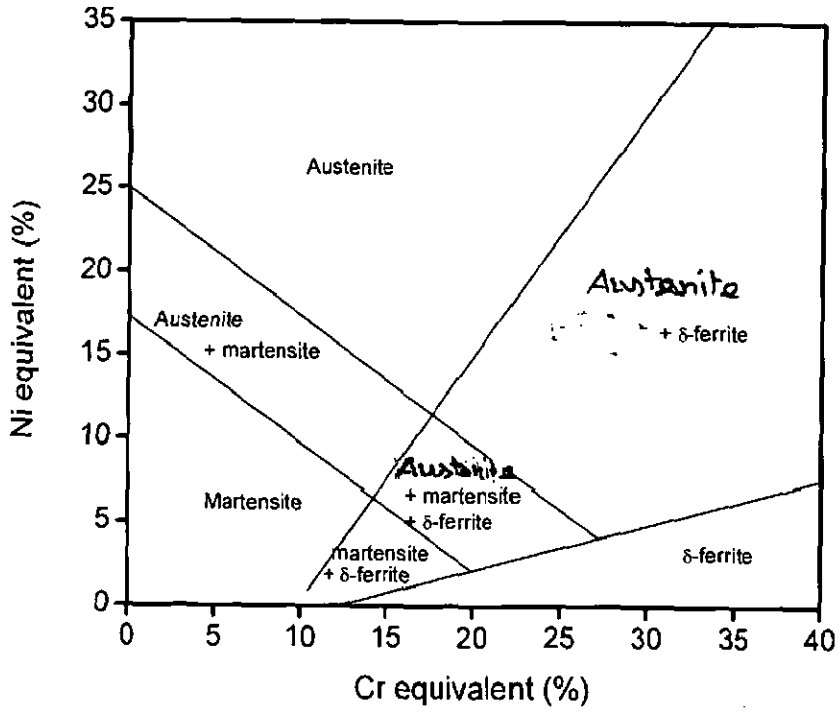

Fig. 4.3. Schaffler diagram [177]

Table 4.1. Mechanical properties of 13/4 and 21-4-N steels in as cast condition

Properties	13/4	21-4-N
Hardness (VHN)	305	320
Impact energy (J)	64	9
YS (MPa)	899	466
UTS (MPa)	930	676
Ductility (% elongation)	14	17

loss in martensitic stainless steel is more than that in nitronic steel. The slopes of erosion test curves given in Fig. 4.4 are almost constant except in case of nitronic steel at 90° impingement angle. Variations in the slope of erosion curve may indicate variations in the mechanism of erosion damages during the erosion test. At 30° impingement angle the erosion loss is primarily due to shear cutting of surface material, whereas at 90° impingement angle resultant erosion damage is due to strain hardening and embrittlement of target material. The 21–4–N nitronic steel, owing to an austenitic matrix, is likely to undergo significant strain hardening and subsequent embrittlement leading to material loss. Irregular interaction between strain hardening and embrittlement may lead to variations in the rate of material loss at various stages of erosion test. The 13/4 steel, being martensite, is less likely to undergo strain hardening and thus exhibits constant slopes at both 30° and 90° impingement angles.

4.5 SEM study of eroded surfaces

Figs. 4.6 and 4.7 show the scanning electron micrographs of eroded surfaces of 13/4 and 21–4–N steels at impingement angle of 30° and 90°, respectively. At 30° impingement angle the process of erosion involves a shear process. Thus the topography of eroded surfaces (Fig. 4.6) in both the steels indicates presence of ploughs, which are formed due to extrusion of platelets from the impact zone. Fig. 4.6 also shows that the ploughs in 13/4 martensitic stainless steel are much wider than those in 21–4– N steel, which indicates more erosion damages in the 13/4 martensitic stainless steel. At 90°

impingement angle, the eroded surfaces are almost free from ploughs. Deep surface cavities are instead observed (Fig. 4.7), which are created due to dislodging of material by hard hitting abrasive particles. Figure 4 also shows that at 90° impingement angle, the cavities in 13/4 martensitic stainless steel are much deeper than those in 21–4–N steel. This is in agreement with more erosion damages (weight loss) observed in 13/4 steel.

4.6 Discussion

4.6.1 Effect of microstructure

The microstructure of target material plays an important role in solid particle erosion. The better erosion resistance of 21–4–N steel is attributed to stabilized austenitic structure. 21–4–N steel contains a heterogeneous microstructure consisting of two metallurgical phases, i.e. austenite and precipitated carbides. In solid particle erosion, austenite is considered to be a beneficial constituent because (i) austenite is plastic and tough; (ii) the strength at the interface between carbide and austenite is high [134] and (iii) localized strength of austenite increases with strain hardening [135]. The better erosion resistance of 21–4–N steel is also due to the distribution of hard carbides (M_7C_3) in the matrix of austenite. In 21–4–N steel the austenitic matrix is continuous and the strength is high too, which are the beneficial parameters for erosion resistance [84].

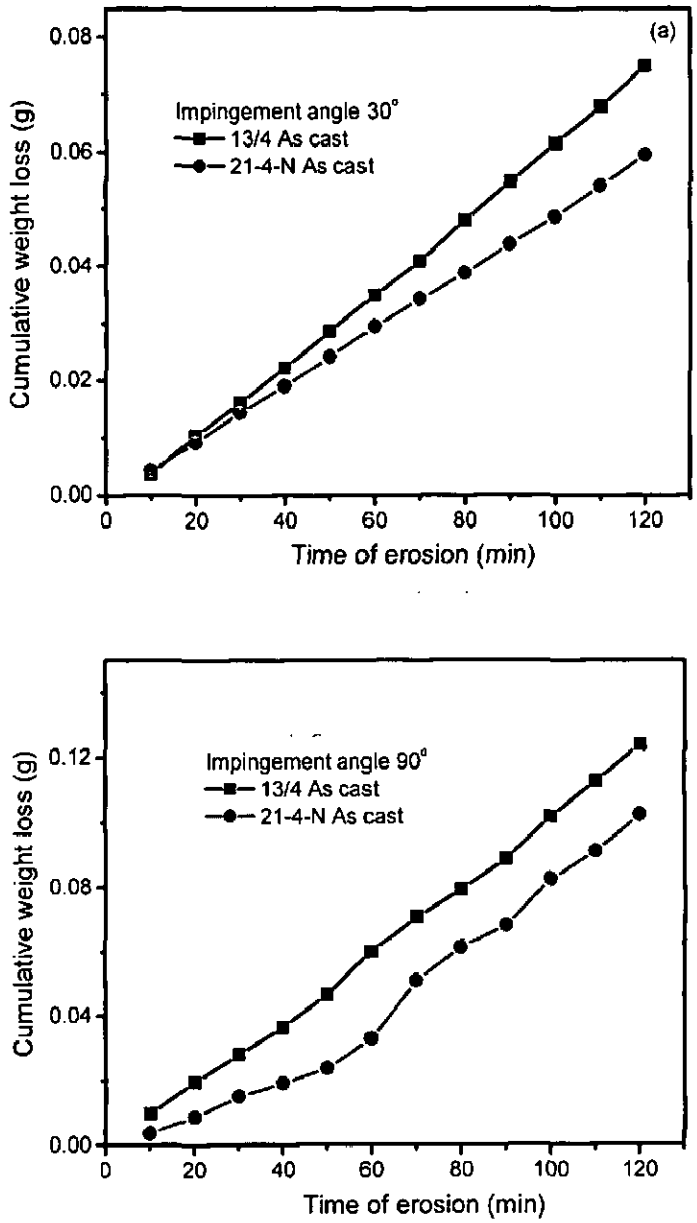

Fig. 4.4. Cumulative weight loss as a function of erosion time at impingement angles of (a) 30° and (b) 90°

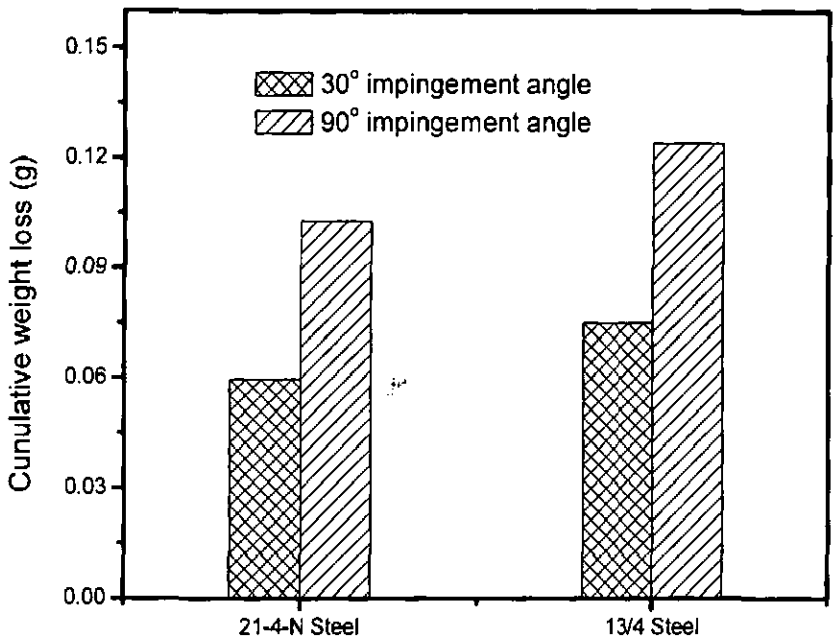

Fig. 4.5. Bar chart illustrating cumulative weight loss as a function of impingement angle

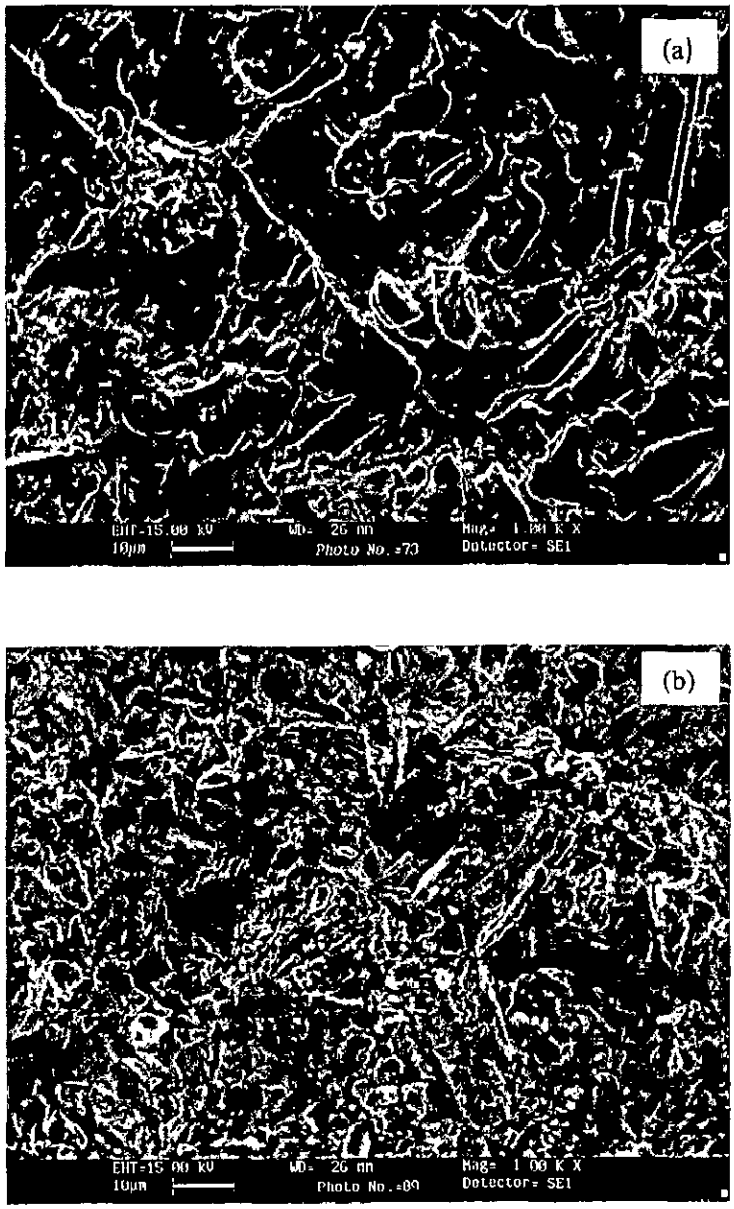

Fig. 4.6. Scanning electron micrographs of eroded surface of (a) 13/4 steel and (b) 21-4-N steel at 30° impingement angle

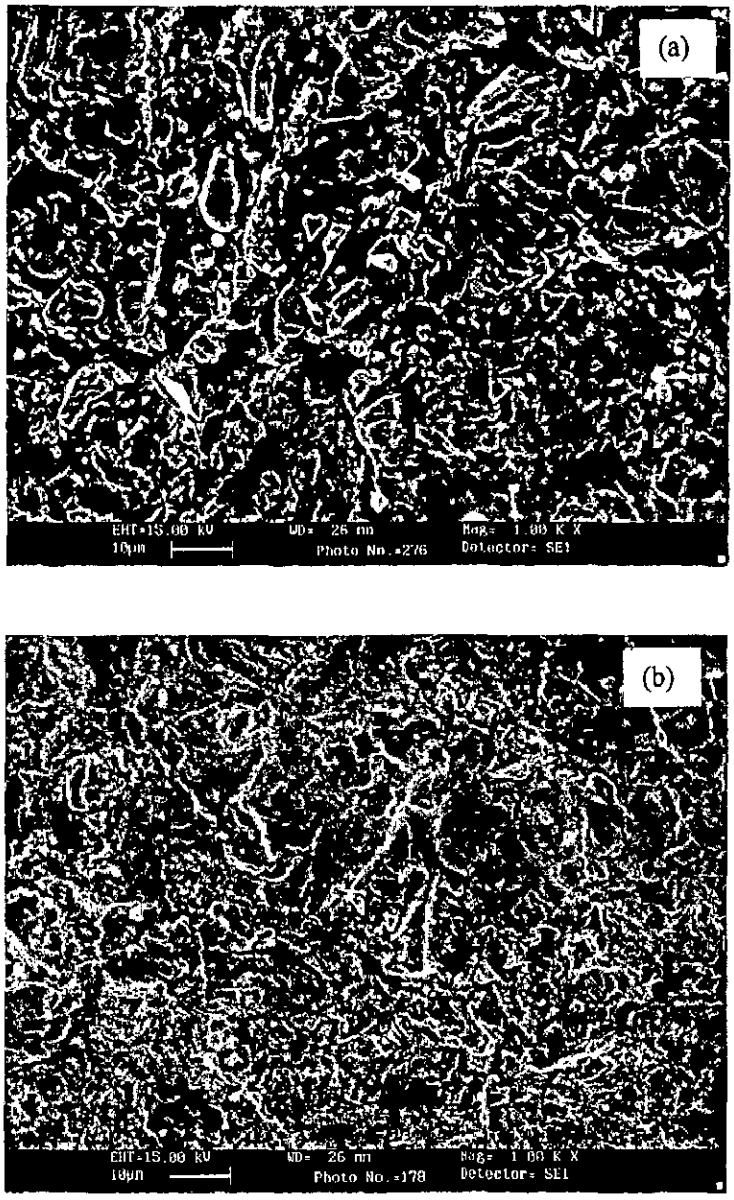

Fig. 4.7. Scanning electron micrographs of eroded surface of (a) 13/4 steel and (b) 21-4-N steel at 90° impingement angle

4.6.2 Effect of hardness and ductility

This investigation revealed that at both the impingement angles of 30° and 90° the erosion damages are more severe in 13/4 martensitic stainless steel as compared to the austenitic 21–4–N nitronic steel. The mechanical properties play a vital role in determining the resistance to erosion of a target material. Primarily the hardness and ductility have been identified as main properties affecting erosion behaviour [50]. High hardness coupled with high ductility leads to improved erosion resistance. High hardness is needed to counteract the effect of hard impinging particles. Ductility in the target material provides relief from high velocity particles by way of partial consumption of their kinetic energy in permitting localized deformation at impact sites, thus minimizing the chances of cracking. In the 21–4–N nitronic steel the observed hardness (320 VHN) and elongation (17%) values are higher than the corresponding values (305 VHN and 14%) in 13/4 martensitic stainless steel. This explains to a large extent the better erosion resistance observed in 21–4–N nitronic steel. The role of impact energy and tensile strength does not appear to be significant in affecting the erosion behaviour in the steels studied in this investigation.

4.6.3 Effect of tensile toughness

It is observed that higher erosion resistance of 21–4–N nitronic steel is also linked to its tensile toughness, which is higher than that of 13/4 steel. The eroded surface at 30° and 90° impingement angles assume elliptical and circular shapes respectively as seen in

the optical macrographs given in Fig. 4.8. The elliptical shape at 30° impingement angle suggests a greater role of tensile stresses in causing erosion loss as compared to that at 90° impingement angle. **Mishra et al** [178] also observed similar effects in the erosion study of plasma sprayed coatings on a Ni-base superalloy. Fig. 4.9 shows the engineering stress–strain diagram of both the steels. The tensile toughness of the 13/4 steel, as calculated from the area ABCD in the plastic range, is 68 MJm^{-3}, whereas for 21–4–N steel, as calculated from the area EFGH, it is 73 MJm^{-3}. The tensile toughness of a material is its ability to absorb energy in the plastic range. It is represented by the area below the engineering stress–strain curve between the YS and fracture stress. **Levin et al** [56] reported that tensile toughness is indicative of the ability of a material to absorb the energy of the abrasive particles impacted and have shown that a material having higher tensile toughness possesses higher erosion resistance. This goes to show that during silt impact the tensile stresses developed contribute significantly towards the mechanism of erosion. Further, the role of impact energy, as determined by Charpy V-notch test, appears to be insignificant in the erosion damages. The 21–4–N steel exhibits a better erosion resistance even though its impact energy (9 J) is much lower than that of the 13/4 steel (64 J).

4.6.4 Effect of strain hardening

The work hardening behaviour of the target material during solid particle impact also appears to be of critical importance. The austenitic grades of steels usually owe their

wear resistance to their work hardening characteristics [51, 179]. Development of wear resistant Hadfield steel, for example, is primarily based on its self work hardening characteristics. The flow curve of many metals in their plastic range can be explained by the simple power curve relation $\sigma=k\,\epsilon^n$, where n is the strain hardening exponent, k is the strength coefficient and σ and ϵ are, respectively true stress and true strain. The value of n can be calculated from the log–log plot of true stress and true strain curve after yielding. As seen in Fig. 4.10, the values of n so obtained are 0.07 and 0.46 for 13/4 steel and 21–4–N steel, respectively. A higher value of n in case of 21–4–N steel is an indication of a higher rate of work hardening in the steel as compared to that in 13/4 steel.

During erosion, impingement of silt particles causes localized elastic and plastic strains in the substrate material. These strains lead to *in situ* strain hardening in the sub surface region, which in turn causes resistance to wear and erosion. Steels with an austenitic matrix are more likely to develop *in situ* work hardening as compared to those with a martensitic structure. In this context, the stacking fault energy of the austenitic matrix plays an important role, as low stacking fault energy may cause a high rate of work hardening. In Fe–Cr–Ni alloys, **Schramm and Reed** [72] reported that Cr rapidly reduces the stacking fault energy. They have observed that Ni and C addition tend to increase the stacking fault energy while Cr, Si, Mn and N tend to decrease stacking fault energy in Fe–Cr–Ni austenitic alloys. The higher resistance to erosion in 21–4–N nitronic steel can, therefore, be attributed to the low stacking fault energy of its austenitic matrix.

During strain hardening, the gap between YS and UTS is also an important parameter, as it determines the stress range to which strain energy can be absorbed during plastic yielding prior to failure. As seen in Fig. 4.9, this stress range in 13/4 steel is 31 MPa against a stress range of 210 MPa in 21–4–N steel. This provides more opportunity for continued strain hardening and a better erosion resistance in 21–4–N steel in comparison to the 13/4 martensitic steel.

The SEM study shows that at 30° impingement angle the erosion damages are primarily due to formation of plough with shear lips. At 90° impingement angle the damages are due to dislodging of chunks of material in the surface layer of the target material. In both the cases *in situ* strain hardening due to impinging particles plays an important role. High rate of work hardening, as measured by the magnitude of work hardening index n, retards both ploughing and dislodging of particles from target surface. Thus high hardness coupled with high ductility as well as high strain hardening characteristics contribute significantly towards the erosion resistance of these steels.

The voids developed due to localization of strain in the target materials also appear to be an important parameter in determining the erosion resistance. The higher erosion rate of 13/4 steel corresponds to formation of large concentration of voids as compared to 21-4-N steel during fracture. It is seen that the strain rate developed in the target material due to erosion is totally different from that found in mechanical testing. The stresses induced in the target materials during solid particle erosion are of very high

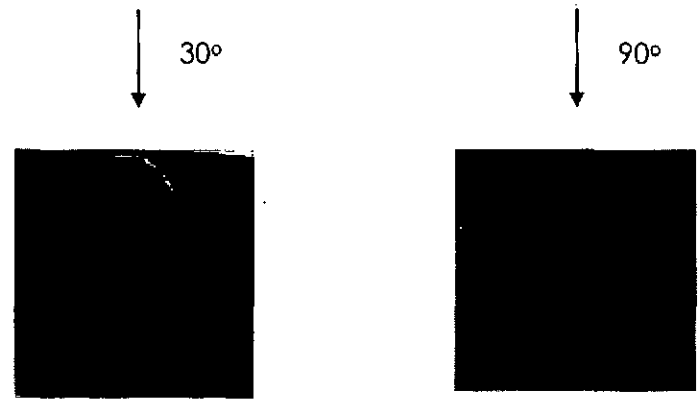

(a) 13/4 Steel

(b) 21-4-N steel

Fig. 4.8. Macrographs of eroded surface (a) 13/4 steel and (b) 21-4-N steel at 30° and 90° impingement angles

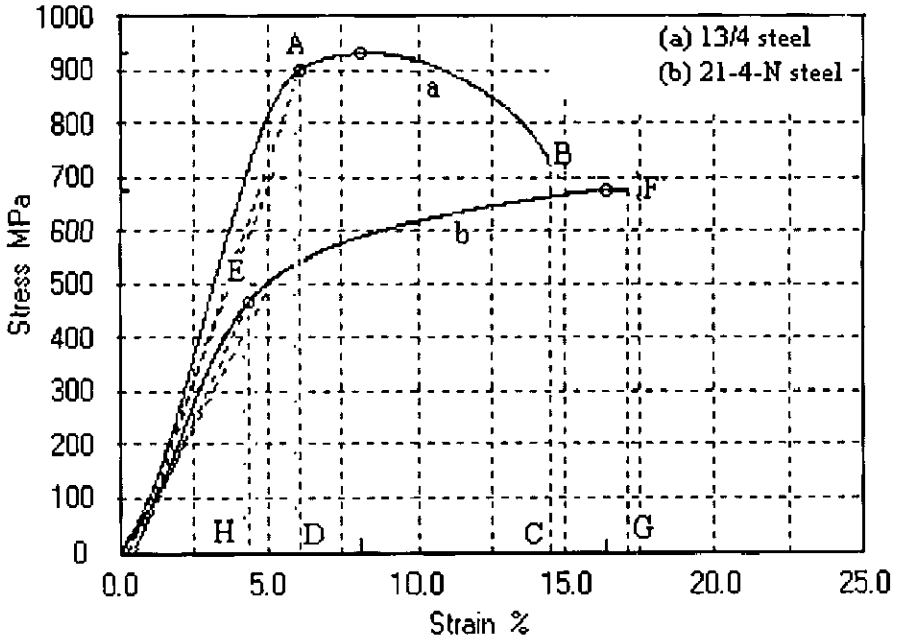

Fig. 4.9. Engineering stress–strain diagram of (a) 13/4 steel and (b) 21–4–N steel

magnitude as compared to those in normal tensile tests. Figs. 4.11 - 4.13 show the fracture appearance and SEM micrographs of fracture surfaces of 13/4 and 21-4-N steels after tensile testing. Fig. 4.13 and 4.14 shows the SEM micrographs of fracture surfaces of 13/4 and 21-4-N steels after Charpy V-notch impact test. It is clearly observed that large concentration of voids are nucleated in both low strain rate tensile tests and high strain rate Charpy V-notch impact tests of 13/4 steel. The voids are the results of extensive localization of strain. The martensite matrix of 13/4 steel is highly stressed and more prone to localization of strains in comparison to 21-4-N steel, which is also an important parameter causing higher erosion damages in 13/4 steel.

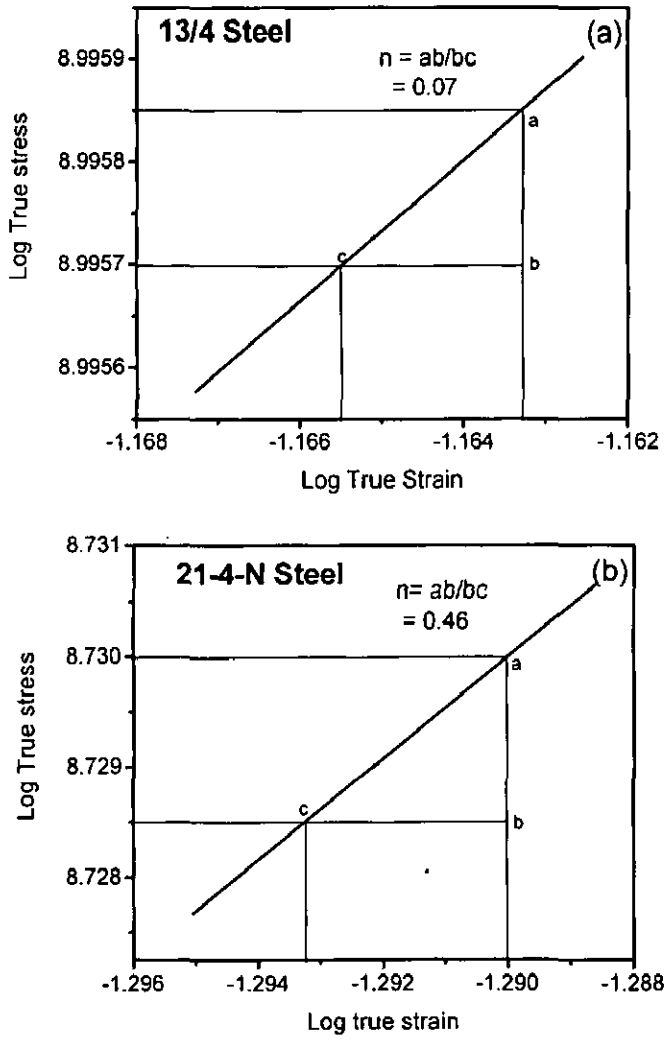

Fig. 4.10. Work hardening exponent of (a) 13/4 steel and (b) 21–4–N steel

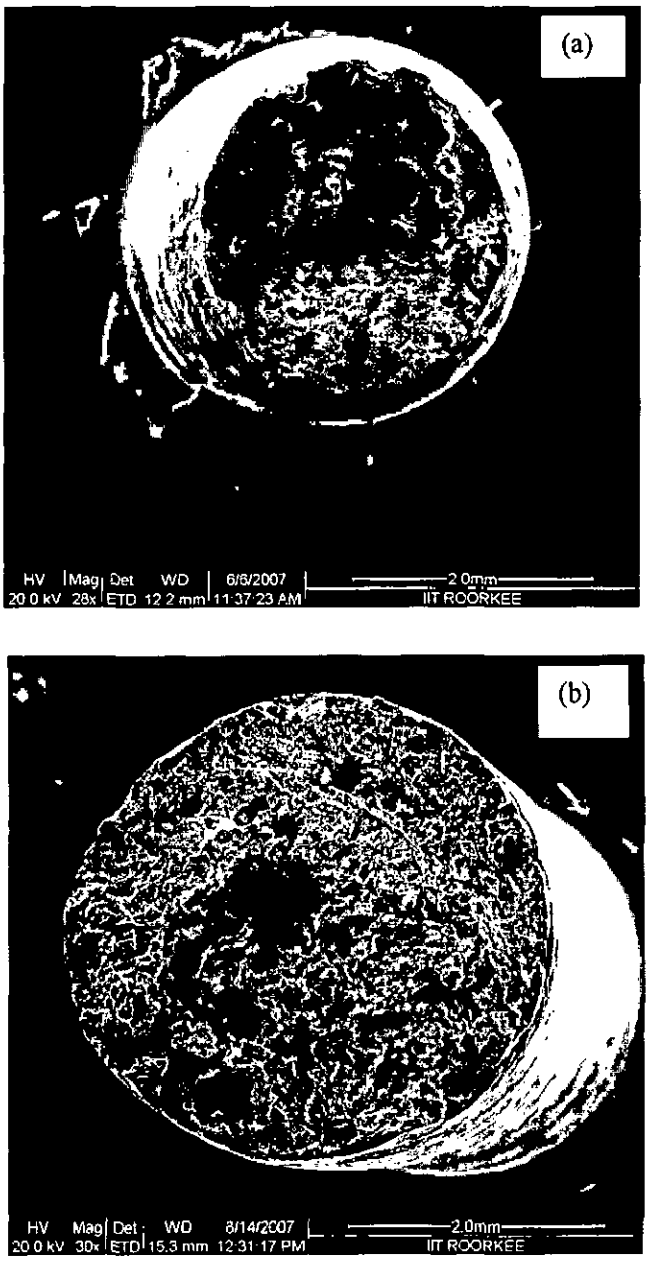

Fig. 4.11. Fracture appearance of fracture surfaces of (a) 13/4 steel and (b) 21-4-N steel after tensile test

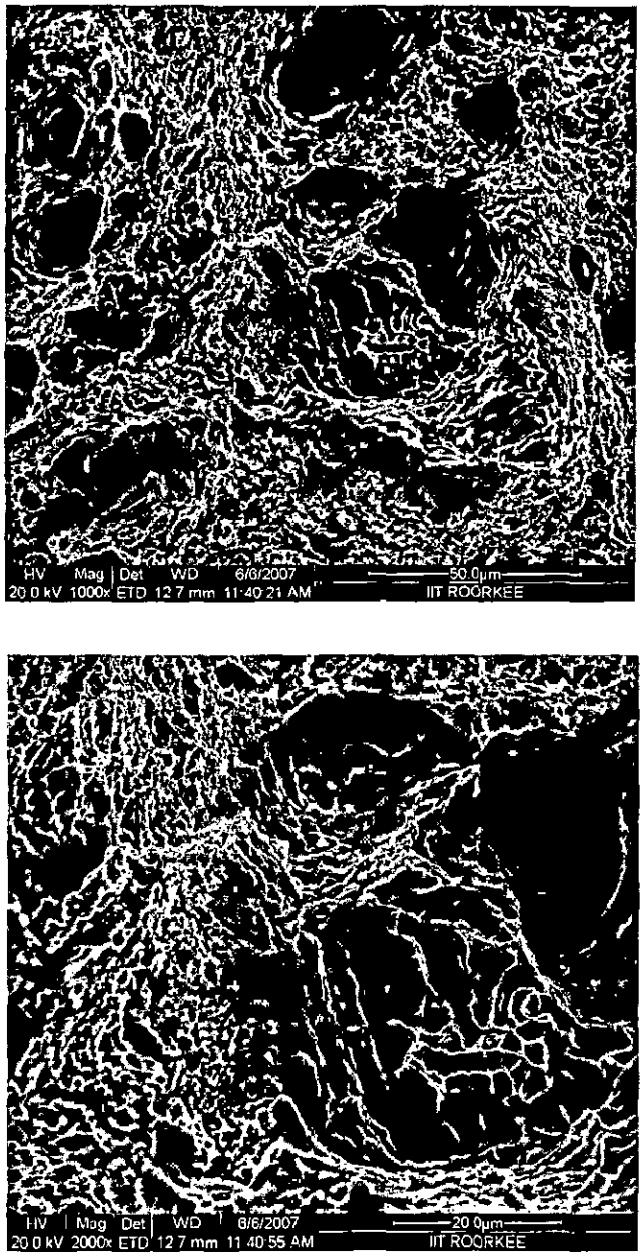

Fig. 4.12. SEM micrographs of fracture surface of 13/4 steel after tensile test

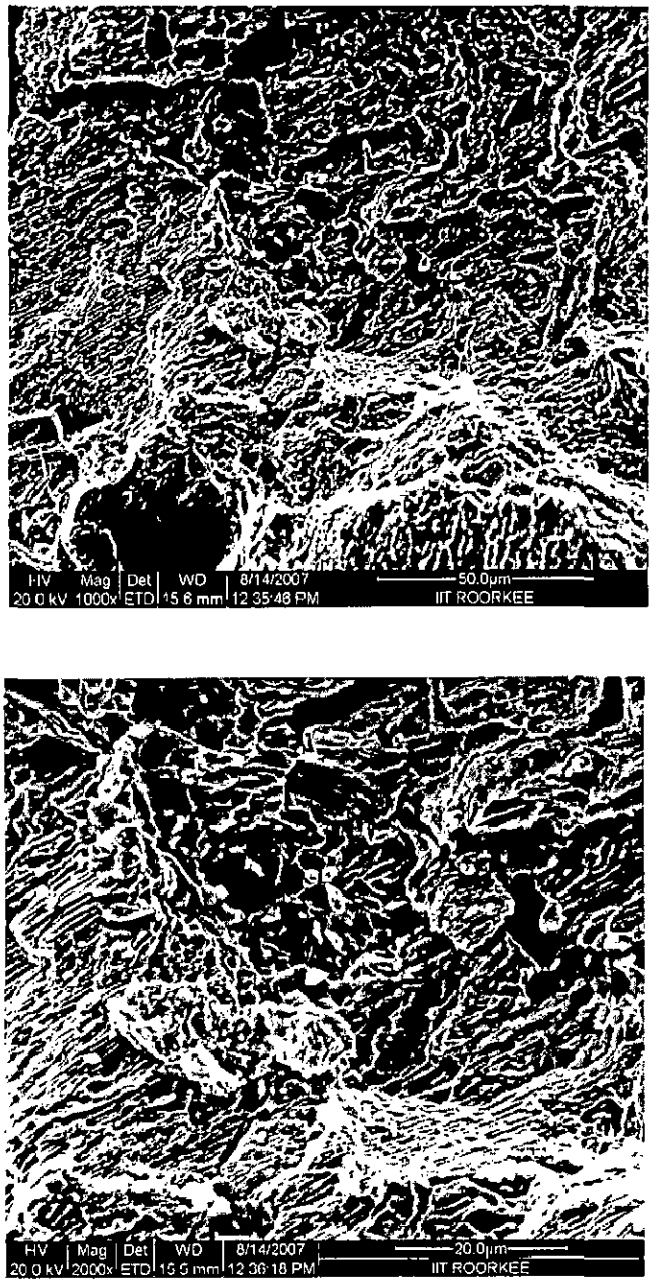

Fig. 4.13. SEM micrographs of fracture surface of 21-4-N steel after tensile test

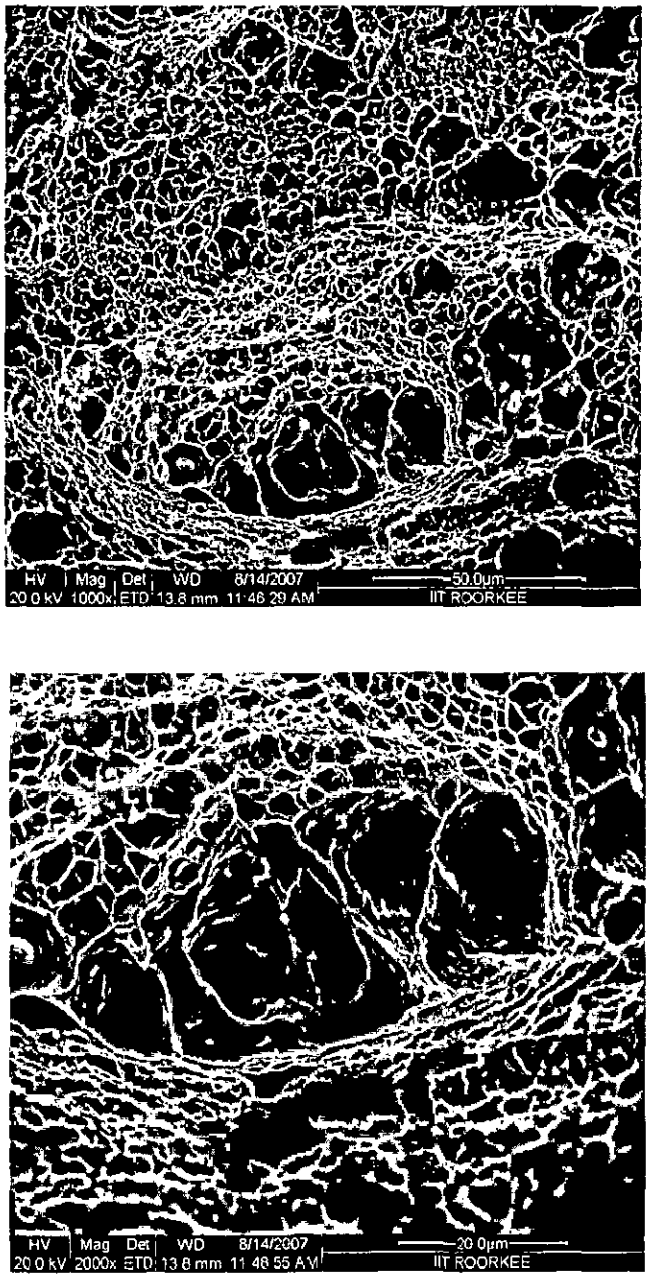

Fig. 4.14. SEM micrographs of fracture surface of 13/4 steel after Charpy V-notch impact test

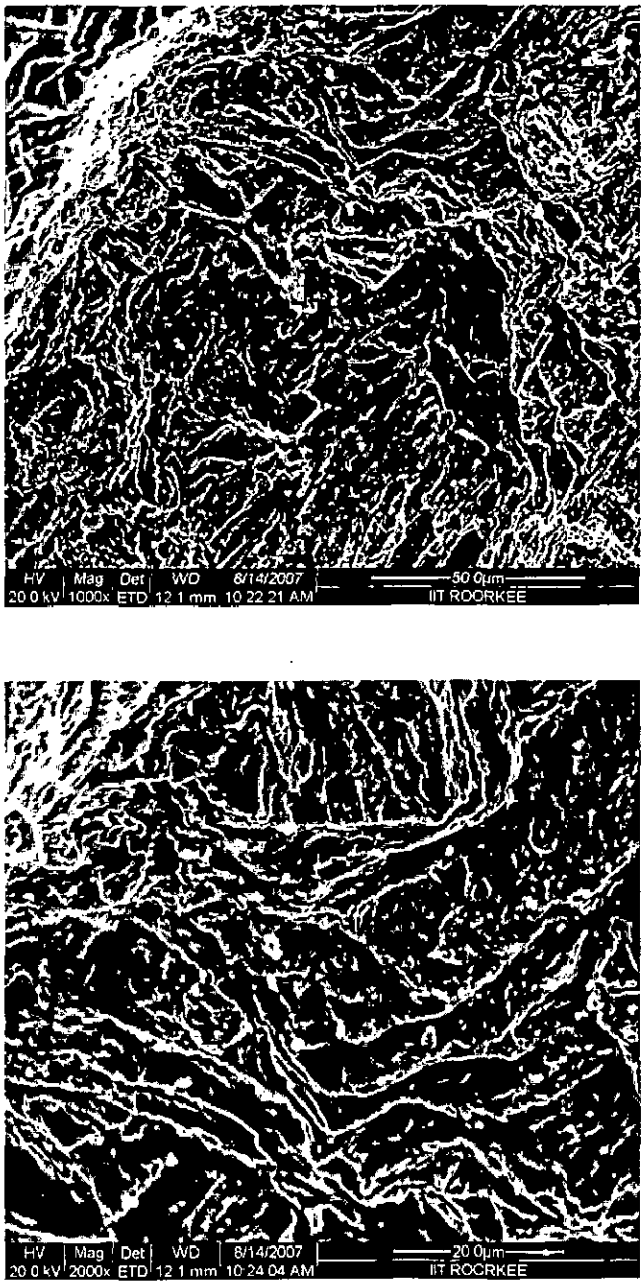

Fig. 4.15. SEM micrographs of fracture surface of 21-4-N steel after Charpy V-notch impact test

4.7 Conclusions

1. The erosion resistance of 21–4–N steel investigated by means of solid particle impingement is higher than that of 13/4 martensitic stainless steel.

2. From the microstructure view point, higher erosion resistance observed in 21-4-N steel is due to its austenitic matrix, which is less prone to erosion damages as compared to the stressed and untempered martensitic matrix of 13/4 steel.

3. Mechanical properties significantly affect the erosion resistance of target material. In 21–4–N steel, high resistance to erosion is due to (i) high hardness coupled with high ductility, (ii) high tensile toughness and (iii) high rate of strain hardening in comparison to 13/4 martensitic stainless steel.

Chapter 5

Effect of heat treatment on the erosion behaviour of 13/4 and 21-4-N steels

This chapter contains the results of heat treatment of 13/4 and 21-4-N steels. The effects of heat treatment on mechanical properties and solid particle erosion behaviour of 13/4 and 21-4-N steels have been analyzed in this chapter.

5.1 Introduction

Influence of various parameters such as microstructure and mechanical properties of target material on erosion damage caused by solid particle impact have been proposed by many investigators [50, 88, 105-110, 180-183]. **Levy** [88] has reported how specific steel microstructures affect the erosion. He observed that the erosion rate is directly related to the distribution of hard, brittle and soft, ductile phases in the alloy. He emphasized that within limits, the more continuous the ductile matrix, the lower the erosion rate is. However, when the ductile matrix becomes the predominant phase and the resulting strength of the steel is markedly reduced, strength and not ductility becomes the dominant factor in erosion.

Mechanical properties of the target material exert a strong effect on erosive wear. The erosive wear rates may increase when a material is deliberately hardened. An

illustration of this rule is provided by the comparison of the relative erosion resistance of metals as a function of impingement angle. When the impingement angle is shallow, hardened steel shows lower erosion than a soft steel; the converse is true at high impingement angles. Heat treatment of steel to increase hardness improves erosive wear resistance at low impact angles but lessens the erosive wear resistance at high impact angles. **Ball and Feng** [180] have attempted to define regimes of erosion of hard metals, ranging from "plasticity-dominated" to "fracture-dominated" behaviour. An analysis of their results reveals that for brittle materials, glass and alumina, the erosion rate is determined by kinetic energy, particle size and the relative hardness and toughness of erodents. However, for ductile materials, the shape and kinetic energy of erodents are the most important factors determining the erosion rate. They also reported that there is no significant effect of hardness and toughness of erodents on erosion.

Foley and Levy [184] have made an attempt to characterize the erosion behavior as it relates to the mechanical properties obtainable by conventional heat treatments. They observed that the ductility of the steels poses a significant effect on their erosion resistance which increases with increasing ductility and that hardness, strength, fracture toughness and impact strength pose little effect on erosion behavior. **Ninham** [182] has reported that the aging or work hardening treatments carried out on the high temperature alloys had essentially no effect on erosion rates. He also reported that the carbide particles which confer abrasion resistance to alloys are found to disrupt plastic flow

around the indentation, causing void formation and fracture and concluded that the carbides are thus deleterious to erosion performance.

5.2 Microstructures

Fig. 5.1 shows the microstructure of 13/4 steel after a standard heat treatment, which involved austenitizing followed by a tempering treatment. The microscopic study reveals that the heat treatment causes tempering of the martensitic laths. The lath size is observed to have thickened as compared to that in 13/4 steel in as cast condition (Fig. 4.1).

The microstructures of 21-4-N steel solution annealed at 950°C, 1000°C, 1050°C and 1100°C for 2 hr followed by water quenching are shown in Figs. 5.2 to 5.5. It is observed that the dissolution of carbides is higher with increasing the temperature of solution treatment; however, all carbides are not dissolved even at 1100°C. The microstructures of solution annealed at 950°C, 1000°C, 1050°C and 1100°C for 2 hr followed by water quenching consists of eutectic structures of austenite and carbides in the matrix of austenite, as in the case of the microstructure of as cast 21-4-N steel (Fig. 4.2). Since during water quenching very less amount of carbides was precipitated, at 1100°C solutionizing temperature, very less amount of carbide was precipitated along the grain boundary (Fig. 5.5). Since in annealing treatment the softening of material took place; the specimen solutionized at 1100°C exhibits more softness. Fig. 5.6 shows the

microstructures of 21-4-N steel solutionized at 1100°C followed by WQ, followed by aging at 700°C for 20 hr in which carbides are precipitated again.

5.3 Mechanical properties

The mechanical properties such as hardness, tensile and Charpy V-notch impact strength of different heat treated samples of as cast 13/4 and 21-4-N steels were determined as per standard describes earlier. The mechanical properties of the heat treated 13/4 and 21-4-N steels are given in Table 5.1. From Table 5.1, it is seen that in 13/4 steel the value of hardness decreases whereas the values of impact energy, YS and UTS increase after tempering treatment. However; the value of ductility of 13/4 steel remains almost unchanged after tempering. From the Table 5.1 it is seen that for 21-4-N steel the values of hardness decreases and the values of impact energy and ductility increase with increasing the annealing temperature. The values of YS and UTS of 21-4-N steel solution annealed at 1100°C are higher than those of cast 21-4-N steel (Table 4.1). The aging treatment of solution annealed 21-4-N steel was carried out at 700°C for 20 hr followed by WQ. It is observed that the value of hardness increases whereas the values of impact energy, YS, UTS and ductility decrease as a result of aging treatment.

In Chapter 4, it has been established that tensile toughness and strain hardening ability in addition to hardness and ductility of the target material also appear to play vital role in determining the erosion resistance. Thus the values of tensile toughness and strain

Fig. 5.1. Microstructures of 13/4 steel after solutionizing at 1050°C followed by tempering at 620°C

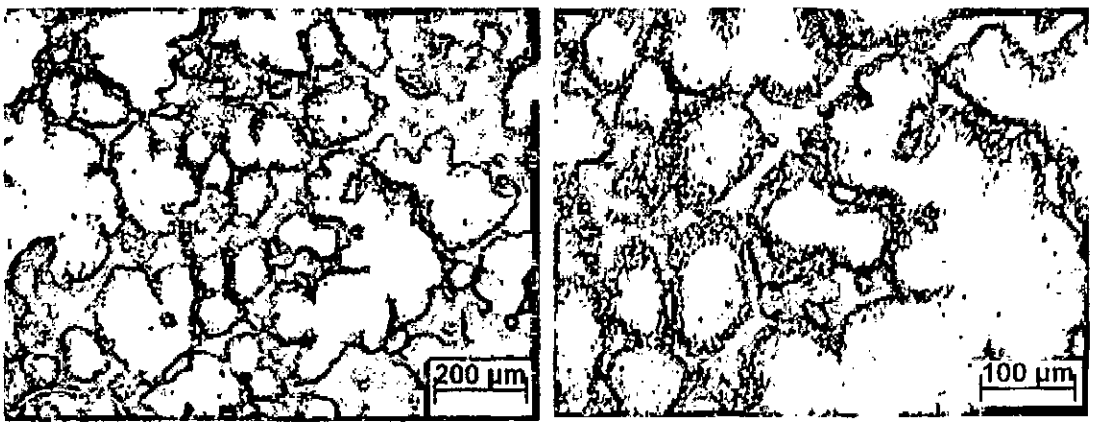

Fig. 5.2. Microstructures of 21-4-N steel after solutionizing at 950°C

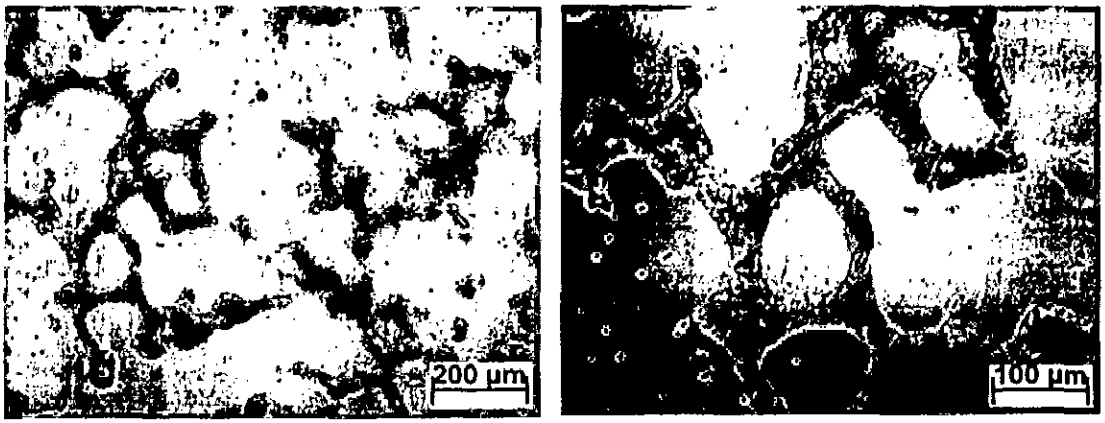

Fig. 5.3. Microstructures of 21-4-N steel after solutionizing at 1000°C

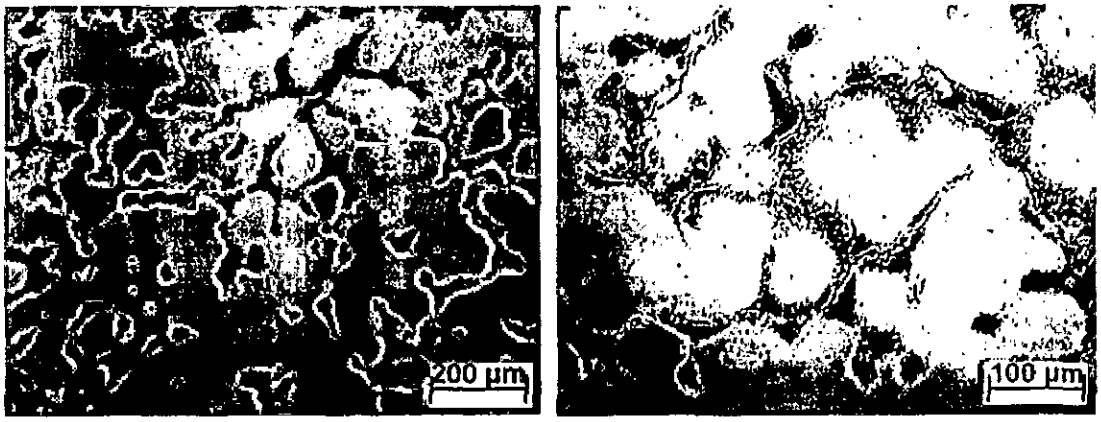

Fig. 5.4. Microstructures of 21-4-N steel after solutionizing at 1050°C

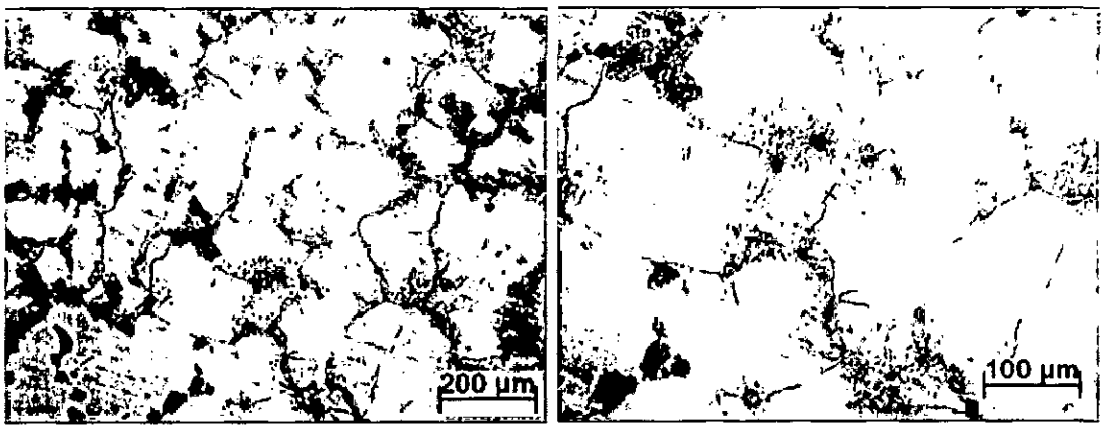

Fig. 5.5. Microstructures of 21-4-N steel after solutionizing at 1100°C

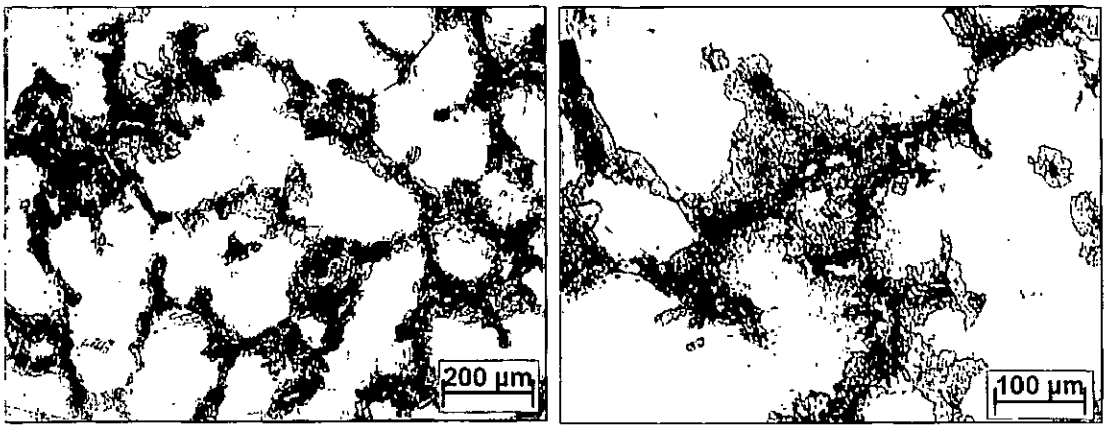

Fig. 5.6. Microstructures of 21-4-N steel after solutionizing at 1100°C, followed by aging at 700°C

hardening ability of tempered 13/4 and solution annealed and aged 21-4-N steel are determined as follows:

Tensile toughness

The tensile toughness is the ability of the target material to absorb the strain energy during plastic deformation. The tensile toughness is calculated from the area under stress-strain curve between YS and fracture stress. Fig. 5.7 shows the engineering stress-strain curves of 13/4 steel in as cast and tempered conditions. The values of tensile toughness of as cast and tempered 13/4 steel are calculated from the area ABCD and EFGH respectively from the respective engineering stress-strain diagram; and the corresponding values are 68 and 71 MJm^{-3}. The values of the tensile toughness of as cast, solution annealed and aged 21-4-N steel are determined from the area ABCD, EFGH and IJKL respectively from the respective engineering stress-strain curves as shown in Fig. 5.8. The values of tensile toughness of as cast, solution annealed and aged 21-4-N steel are 73, 117 and 72 MJm^{-3} respectively.

Strain hardening exponent

The strain hardening exponent is calculated from the slope of log-log plot of true stress - true strain curve after yielding. The values of strain hardening exponent of 13/4 and 21-4-N steel in cast condition have been evaluated in Chapter 4 as 0.07 and 0.46 respectively. The log-log plots of true stress - true strain curve after yielding for tempered

Table 5.1. Mechanical properties of 13/4 and 21-4-N steels after different heat treatments

Properties	13/4 Steel	21-4-N Steel				
	Solutionized at 1050 °C (4 hr) and Tempered at 620 °C (4 hr)	Solution annealed at				Sol. Annealed at 1100 °C (2 hr) followed by aging at 700°C (20 hr)
		950 °C	1000 °C	1050 °C	1100 °C	700°C
Hardness (VHN)	289	311	310	306	304	327
Impact energy (J)	78	11	11	12	13	7
YS (MPa)	1148	465	485	467	490	486
UTS (Mpa)	1181	686	732	713	716	685
Ductility (% elongation)	13.06	19	20	22	23	15

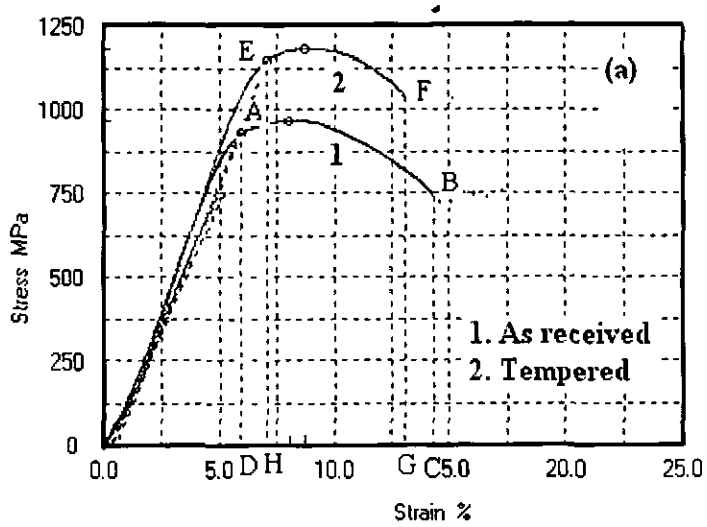

Fig. 5.7. Engineering stress-strain diagrams of 13/4 steel in as cast and tempered conditions

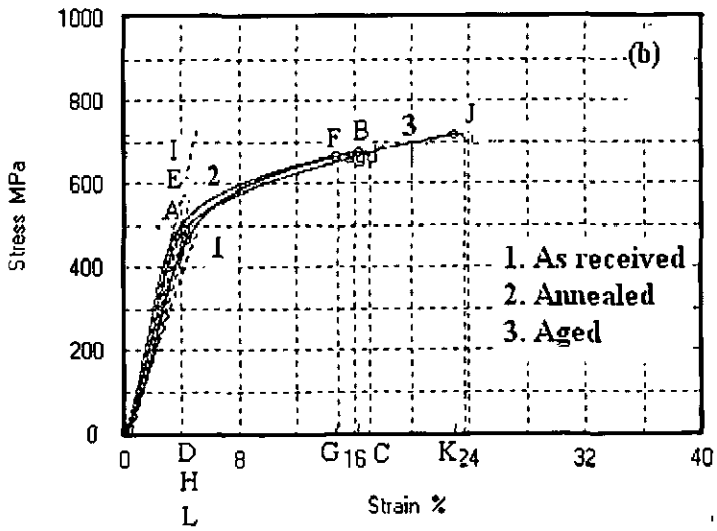

Fig. 5.8. Engineering stress-strain diagrams of 21-4-N steel in as cast, solution annealed and aged conditions

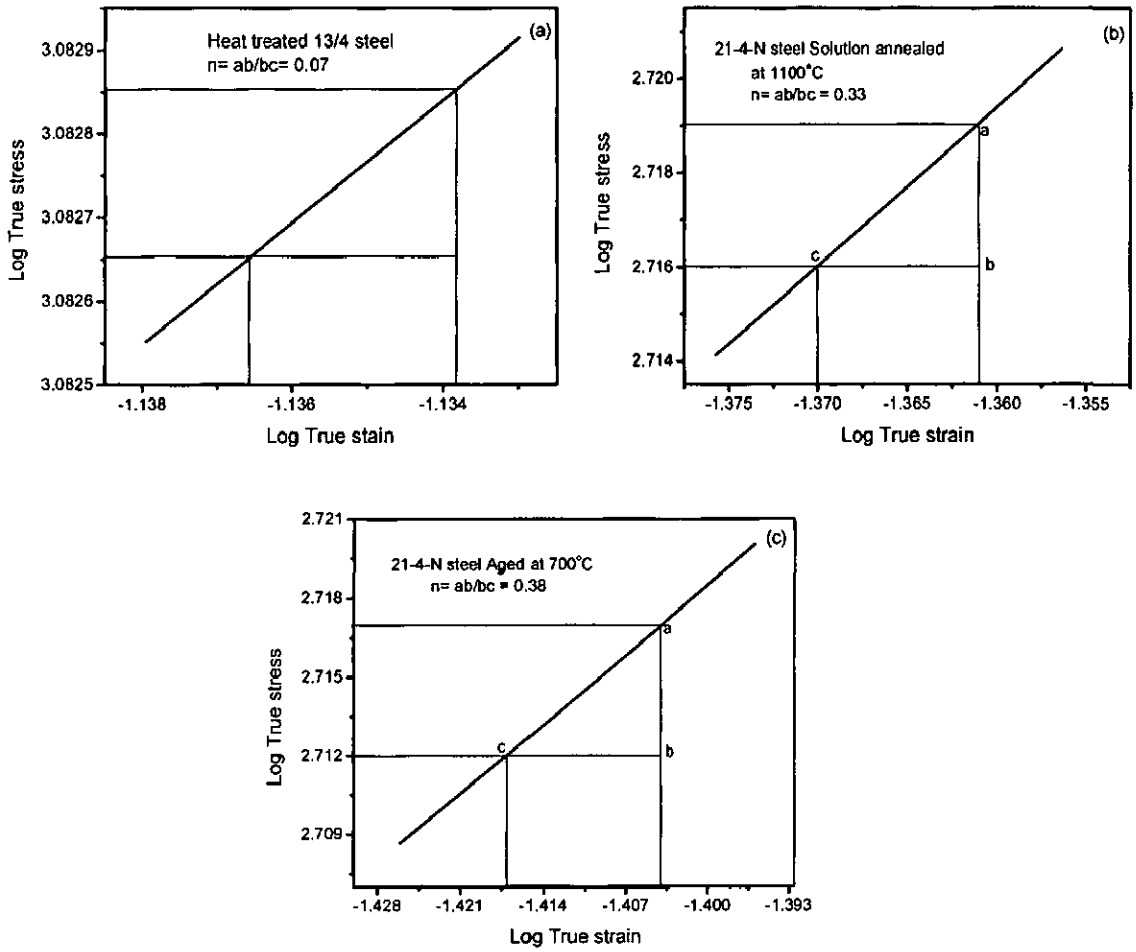

Fig. 5.9. Strain hardening exponents of (a) tempered 13/4 steel, (b) solution annealed 21-4-N steel and (c) aged 21-4-N steel

13/4 steel, solution annealed 21-4-N steel and aged 21-4-N steel are shown in Fig. 5.9. The values of strain hardening exponent of tempered 13/4 steel, solution annealed 21-4-N steel and aged 21-4-N steel are 0.07, 0.33 and 0.38 respectively.

5.4 Erosion behaviour

Figs 5.10 and 5.11 show respectively the cumulative weight loss as a function of time of erosion and erosion rate (g/g) as function of cumulative mass of erodent at impingement angles of 30° and 90°. At 30° impingement angle there is slight decrease in erosion resistance while substantial improvement in erosion resistance is observed at 90° impingement angle in 13/4 steel after tempering. Figs 5.12 and 5.13 show respectively the cumulative weight loss as a function of time of erosion and erosion rate (g/g) as function of cumulative mass of erodent at impingement angles of 30° and 90°. It is observed that there is improvement in erosion resistance in 21-4-N steel as a result of annealing treatment (Figs. 5.12 and 5.13) at both the impingement angles. It is also observed that there is deterioration in erosion resistance of 21-4-N steel after aging heat treatment (Figs. 5.12 and 5.13). However, the deterioration is less at 30° impingement angle as compared to that at 90° impingement angle.

The slopes of the cumulative weight loss curves of both 13/4 and 21-4-N steels in as cast as well as heat treated conditions (Fig. 5.10 and 5.12) are almost constant except in case of as cast and aged 21-4-N steel eroded at 90° impingement angle. From the erosion rate curves of both 13/4 and 21-4-N steels in as cast as well as heat treated

conditions (Fig. 5.11 and 5.13), it is observed that the erosion rate first increases and then become constant except in tempered 13/4 steel eroded at 90° impingement angle, which attained the steady state erosion rate very early during erosion test. 21-4-N steel eroded at 30° impingement angle also attained the steady state erosion rate. The constant slopes of erosion curve indicate the involvement of identical mechanisms of erosion during the erosion test. The variations in the slopes of erosion curves or zig-zag shape of erosion rate curves in as cast and aged 21-4-N steel may indicate variation in the mechanism of erosion damages during the erosion test. At 30° impingement angle the erosion is primarily due to shearing and cutting of the surface of the material, whereas at 90° impingement angle resultant erosion damage is due to plastic deformation, strain hardening and embrittlement of the target material. The 13/4 steel, being martensite, is less likely to undergo strain hardening and thus exhibits constant slopes at both 30° and 90° impingement angles. The 21-4-N steel owing to an austenitic matrix is likely to undergo significant strain hardening and embrittlement leading to erosion damage of the target material. Due to less amount of carbides in annealed 21-4-N steel, there is regular interaction between strain hardening and embrittlement leading to constant rate of material loss at various stages of erosion test and thus constant slopes are exhibited at both 30° and 90° impingement angles. Due to the presence of carbides in as cast and aged 21-4-N steel, there is irregular interaction between strain hardening and embrittlement, which leads to variation in the rate of material loss at various stages of erosion test, which

results in variation in the slopes of cumulative weight loss curves (Fig. 5.12) at 90° impingement angle.

5.5 SEM study of eroded surfaces

Fig. 5.14 shows the SEM micrographs of eroded surfaces of tempered 13/4 steel eroded at 30° and 90° impingement angles. It is seen that ploughs are observed in the SEM micrograph of tempered 13/4 steel eroded at 30° impingement angle; while at 90° impingement angle the surface is free from ploughs and consists of fragmented flakes. Longer ploughs are seen in the SEM of as cast 13/4 steel (Fig. 4.6a) in comparison to those in tempered 13/4 steel (Fig. 5.14a) eroded at 30° impingement angle. By comparison of the SEM micrographs of 13/4 steel in as cast (Fig. 4.7b) and tempered (Fig. 5.14b) conditions eroded at 90° impingement angle, it is observed that fragmentation of flakes in as cast 13/4 steel is more indicating more, erosion rate in as cast 13/4 steel at 90° impingement angle.

Fig. 5.15 shows the SEM micrographs of eroded surfaces of 21-4-N steel in solution annealed and aged conditions eroded at 30° impingement angle. It is observed that in both the samples, the erosion occurs by shearing and ploughing mechanisms. The deeper ploughs observed in the SEM micrograph of aged 21-4-N steel as compared to those in solution annealed 21-4-N steel indicate more erosion damage in aged 21-4-N steel. The cracks are seen in the SEM micrograph of eroded surface of aged 21-4-N steel

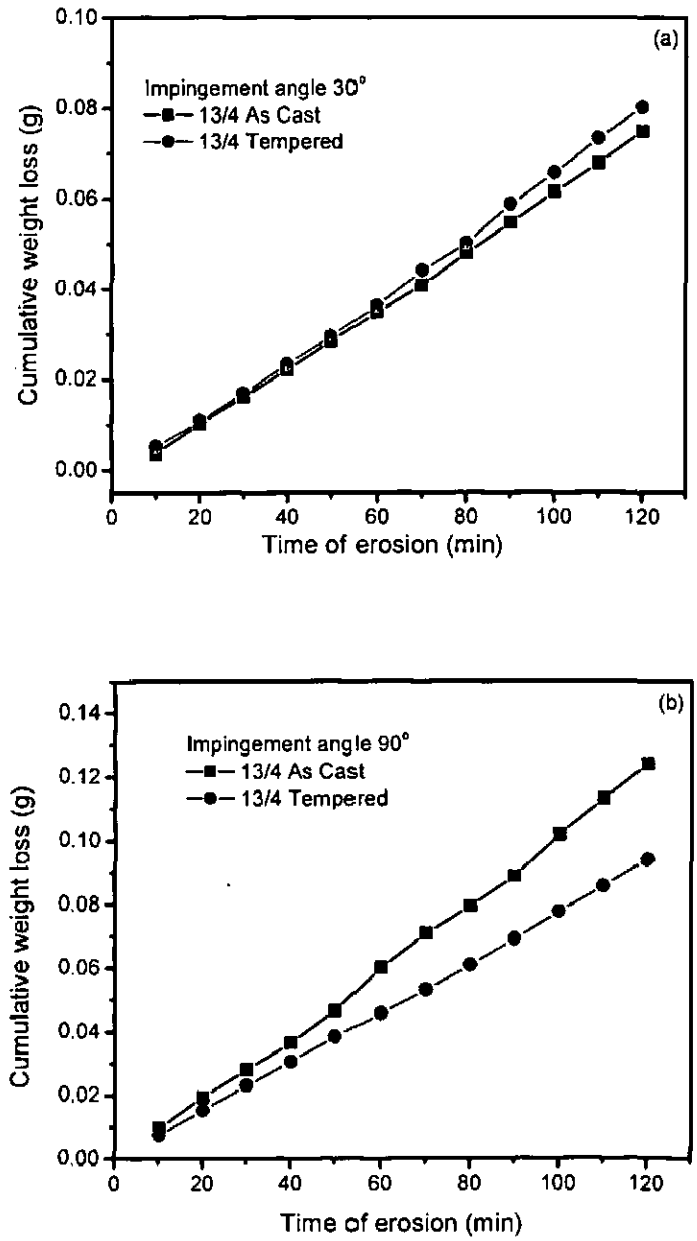

Fig. 5.10. Cumulative weight loss as function of time of erosion at impingement angles of (a) 30° and (b) 90°

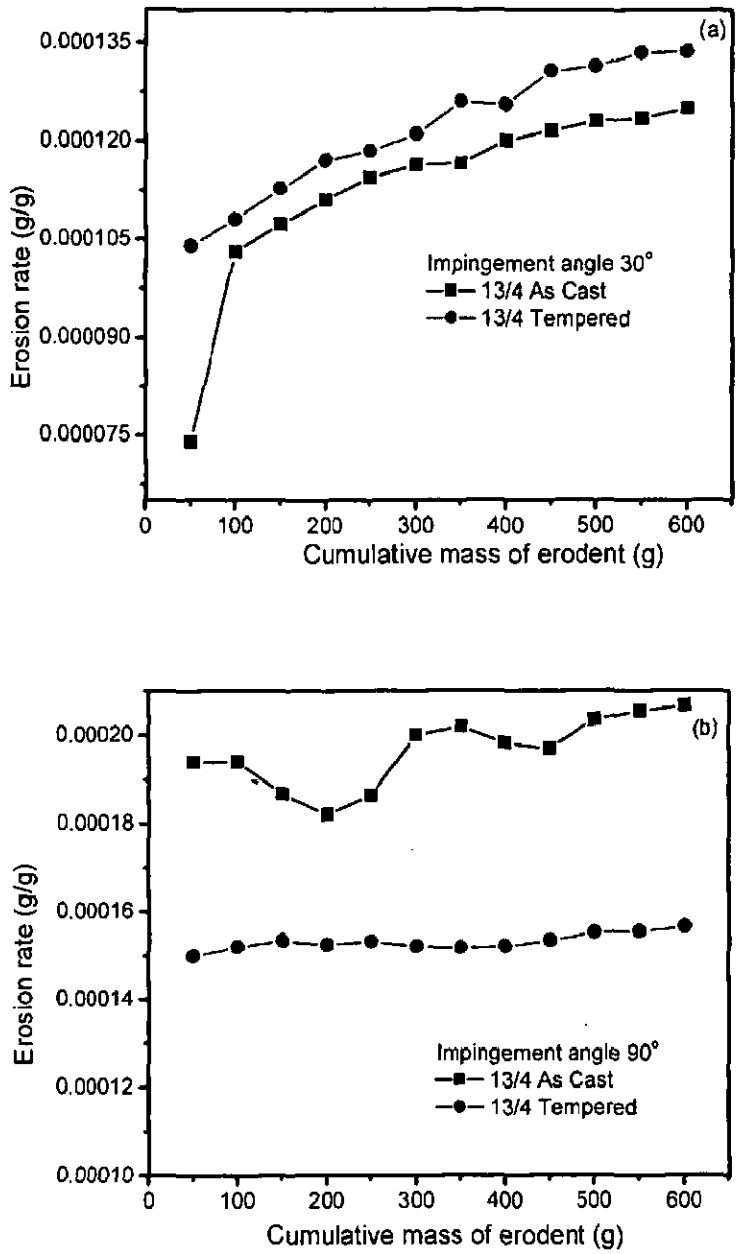

Fig. 5.11. Erosion rate as function of cumulative mass of erodent at impingement angles of (a) 30° and (b) 90°

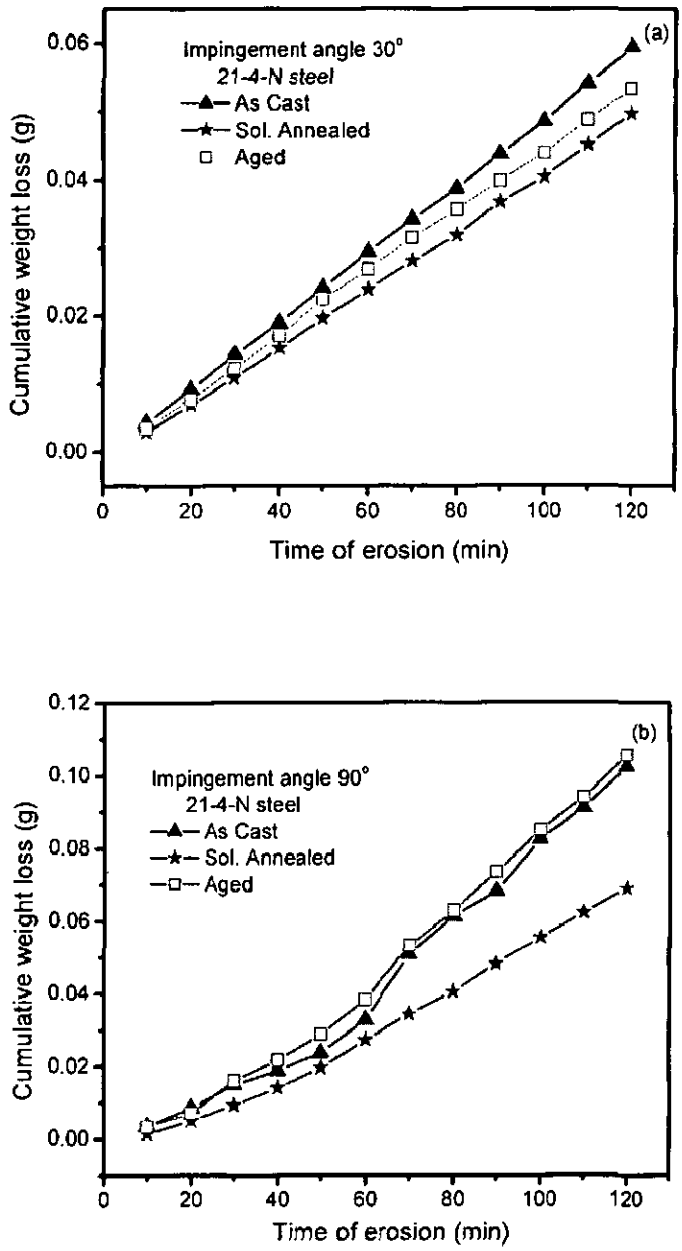

Fig. 5.12. Cumulative weight loss as function of time of erosion at impingement angles of (a) 30° and (b) 90°

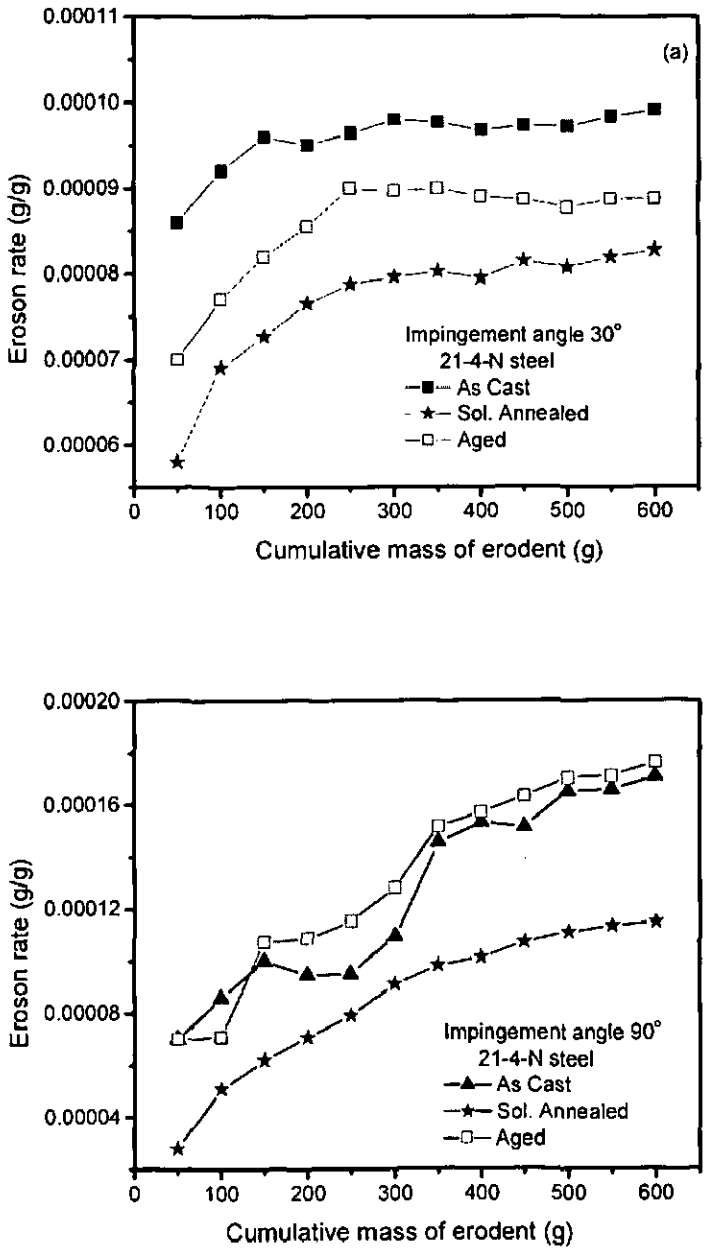

Fig. 5.13. Erosion rate as function of cumulative mass of erodent at impingement angles of (a) 30° and (b) 90°

(Fig. 5.14b), while the eroded surface of solution annealed 21-4-N steel is free from such cracks (Fig. 5.14a).

Fig. 5.16 shows the SEM micrographs of eroded surfaces of 21-4-N steel in solution annealed and aged conditions eroded at 90° impingement angle. It is observed that at 90° impingement angle, the erosion occurs due to formation of flakes and/or cracks and fragmentation of them. The deeper flakes observed in the SEM micrograph of aged 21-4-N steel (Fig. 5.16b) is in agreement with more erosion damage in aged 21-4-N steel as compared to that in solution annealed 21-4-N steel (Fig. 5.16a). By comparison of the SEM micrograph of eroded surface of as cast 21-4-N steel (Fig. 4.7b) with that of 21-4-N steel in solution annealed and aged conditions eroded at 90° impingement angle; it is observed that the formation of flakes and their fragmentation is more severe in 21-4-N steel in both as cast and aged conditions in comparison to solution annealed 21-4-N steel causing less erosion damage in solution annealed 21-4-N steel.

5.6 Discussion

The effect of heat treatment on the erosion of the steels under investigations are analyzed in terms of microstructure and mechanical properties, which were altered during heat treatment processes.

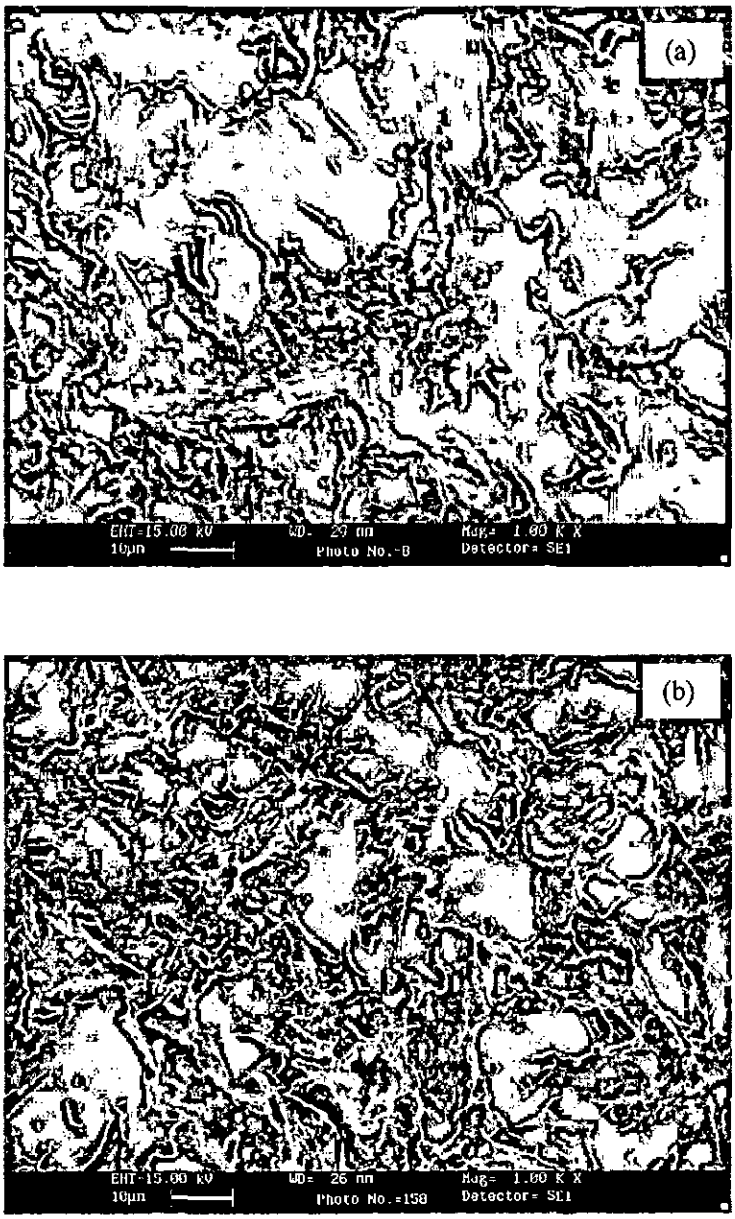

Fig. 5.14. Scanning electron micrographs of eroded surface of tempered 13/4 steel at impingement angles of (a) 30° and (b) 90°

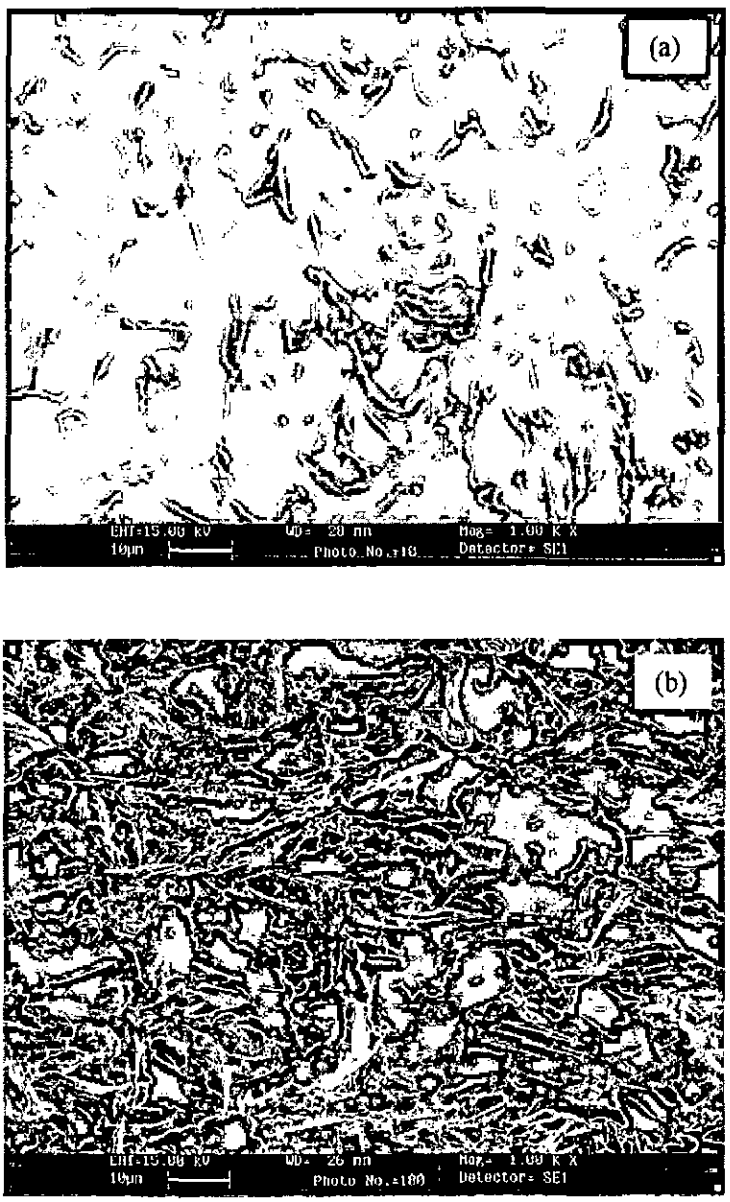

Fig. 5.15. Scanning electron micrographs of eroded surface of (a) solution annealed and (b) aged 21-4-N steel at impingement angle 30°

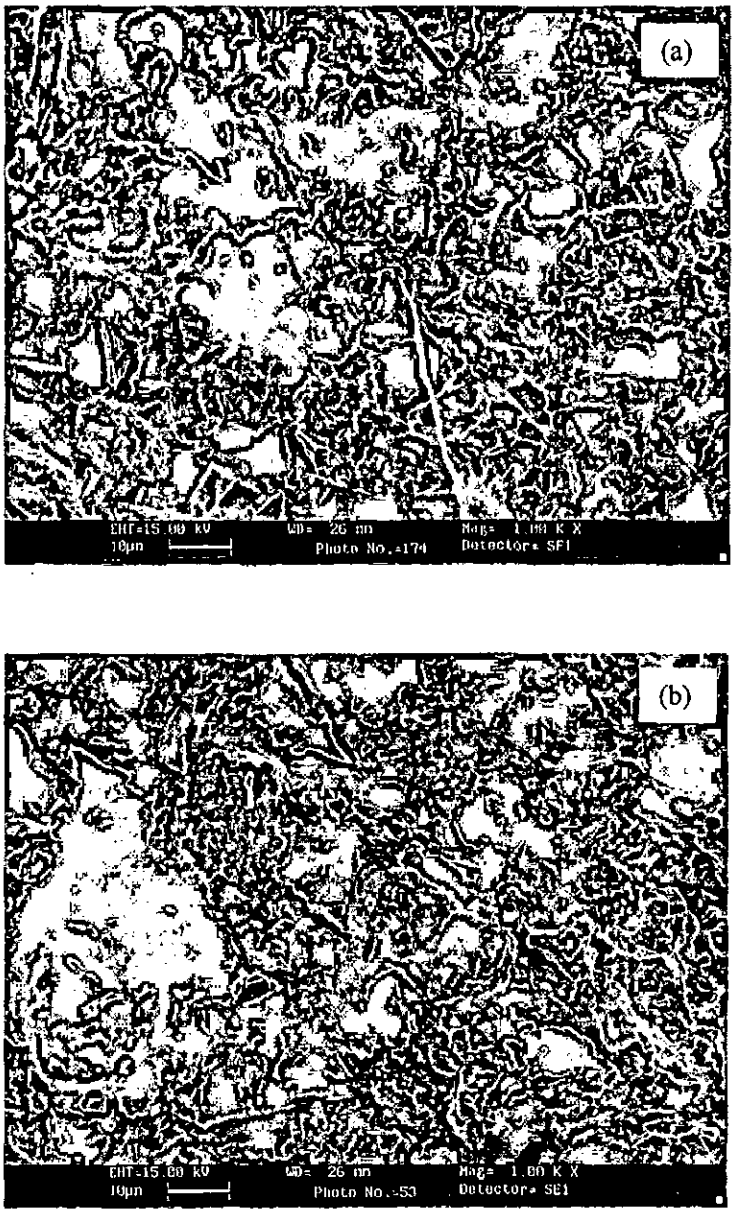

Fig. 5.16. Scanning electron micrographs of eroded surface of (a) solution annealed and (b) aged 21-4-N steel at impingement angle 90°

5.6.1 Effect of microstructure

By comparing the erosion behaviour of 13/4 steel in both as cast and tempered conditions, it is observed that as cast 13/4 steel shows better erosion resistance at 30° impingement angle; but at 90° impingement angle better erosion resistance is shown by tempered 13/4 steel (Figs. 5.10 and 5.11) in comparison to as cast condition. The result of erosion at 90° impingement angle is similar to that of **Kumar** [64], in which it is reported that in slurry erosion test, tempered 13/4 steel shows better erosion resistance than the as cast 13/4 steel at both the impingement angles. This is because the untempered martensitic laths are associated with internal stresses, which are relieved by solutionizing and tempering. At 30° impingement angle, the erosion is by cutting and shearing mechanisms. Therefore, the erosion damage (cutting) is somewhat more difficult in as cast 13/4 steel associated with internal stresses in comparison to tempered 13/4 steel. At 90° impingement angle, the erosion is by crack formation followed by propagation leading to fragmentation. It has been reported that the target material having ability to absorb more kinetic energy of the abrasive particle impacted normally erode less. The untempered martensitic laths of as cast 13/4 steel, which are already associated with internal stresses, absorb less kinetic energy of the abrasive particles as compared to that in tempered 13/4 steel and result in more erosion damage. At 90° impingement angle, the less erosion damage in tempered 13/4 steel is also due to thickened martensitic laths as compared to fine martensitic laths in as cast 13/4 steel, because the interfaces between the martensitic laths may be more prone to erosion damage.

In Chapter 4, it has been analyzed that the better erosion resistance of 21-4-N steel is due to stabilized austenitic structure and precipitates of carbides. Because of its plasticity and toughness and increase in localized strength with strain hardening, the austenitic structure is considered to be a beneficial parameter in solid particle erosion. At 30° impingement angle erosion damage in 21-4-N steel after solution annealing is less in comparison to that in as cast 21-4-N steel. In solution annealed 21-4-N steel, the C remains largely soluble in the matrix causing stabilization of the austenitic matrix. This causes more resistance to erosion. The similar observation was reported by **Levy** [88]. He observed that the erosion rate is directly related to the distribution of hard, brittle and soft, ductile phases in the alloy. **Levy** [88] reported that within limits, the more continuous the ductile matrix, the lower is the erosion rate. The erosion resistance is found to reduce in aged 21-4-N steel as compared to that in solution annealed 21-4-N steel. It is due to precipitation of carbides during aging at 700°C, which are deleterious to erosion resistance. In aged 21-4-N steel, the continuous ductile matrix of austenite also gets reduced and causes more erosion damages. At 90° impingement angle, the interfaces between the carbides and austenite as well as the carbides are more prone to erosion damages, because these are less able to absorb the kinetic energy of the erodent particles impacted as compared to the austenitic matrix. At 90° impingement angle, the least erosion damage is observed in solution annealed 21-4-N steel having very less precipitates of carbides. As cast as well as aged 21-4-N steel having higher amount of precipitates of carbides show higher erosion damage at 90° impingement angle.

5.6.2 Effect of mechanical properties

13/4 steel

It can be seen from the results obtained in this study that the erosion of all the specimens is higher at 90° impingement angle than that at 30° impingement angle, which corresponds to erosion of brittle materials [50, 54, 81, 86, 104, 159, 173, 174] and identical to the erosion of as cast 13/4 and 21-4-N steels reported in Chapter 4. The cumulative weight loss at 30° impingement angle of 13/4 steel in both conditions as function of various mechanical properties is shown in Fig. 5.17. In this study it is seen that tempered 13/4 steel shows slightly higher erosion damage as compared to that in as cast 13/4 steel at 30° impingement angle. In Chapter 4, it has been established that the values of hardness with retaining ductility, higher tensile toughness and higher strain hardening ability of the target material correspond to higher erosion resistance. From Fig. 5.17 it is observed that strain hardening exponent, ductility and tensile toughness remain almost unchanged and hardness decreases in 13/4 steel after tempering. At 30° impingement angle, the erosion is by cutting and ploughing mechanisms and scratching. At 30° impingement angle the decrease in hardness in 13/4 steel as a result of tempering enhances erosion rate, because with increasing hardness the erosion rate through cutting and ploughing mechanisms decreases. In soft material the erosion at 30° impingement angle through ploughing or scratching is easy as compared to hard material. The substantial decrease in hardness from 305 to 289 VHN causes considerable increase in

erosion damage, but cumulative effect of all mechanical properties as well as microstructure cause slight increase in erosion damage in 13/4 steel as a result of tempering.

At 90° impingement angle erosion is by lip formation followed by fragmentation. When a hard particle impacts on a target, the force produced by impacting is not only associated with the particles mass, velocity and impact angle; but also with properties of the target, such as its local hardness. The cumulative weight loss at 90° impingement angle of 13/4 steel in both conditions as function of various mechanical properties is shown in Fig. 5.18. It is observed that at 90° impingement angle the decrease erosion in rate corresponds to decrease in hardness as a result of tempering, because except hardness all the mechanical properties remain almost unchanged. The decrease in hardness of 13/4 steel as a result of tempering is accompanied by slight increase in tensile toughness (68 to 71 J) and increase in elastic deformation. The elastic deformation indicates the deformation without onset of fracture, which is more in tempered 13/4 steel and is one of the influential factors resulting in less erosion in tempered 13/4 steel.

The process of erosion by erodent particles impacted at 90° impingement angle is accompanied by two types of tresses produced along the surface layer of indentation. One is the normal stress and the other is tensile stress. The normal stress makes the target material move down along the normal direction of indentation and the tensile stress makes the material of the target surface layer elongate. Tempered 13/4 steel resists normal stresses more without fracture as compared to more brittle and already stressed as

cast 13/4 steel and thus results in lower erosion damage. The tensile stress will play an important role in deformation damage removal. Tempered 13/4 steel sustains higher tensile stress and higher elastic deformation as compared to as cast 13/4 steel (Fig. 5.7) and implies, during solid particle erosion, tempered 13/4 steel deforms more without dislodging of material, which again results in lower erosion damage.

21-4-N steel

It can be seen from the results obtained for 21-4-N steel in different conditions that, 21-4-N steel in as cast condition shows higher erosion at both the impingement angles; while least erosion is observed in solution annealed 21-4-N steel (Figs. 5.12 and 5.13). In 21-4-N steel the ductility in addition to hardness play vital role in determining the erosion resistance. **Divakar et al** [50] have shown that the erosion resistance increases with increasing the hardness provided the ductility remains constant. The ductility of the target material is necessary to relieve the stresses imposed by high velocity erodent particles. Figs. 5.19 and 5.20 show the cumulative weight loss of 21-4-N steel at 30° and 90^{0} impingement angles respectively as function of various mechanical properties. From Figs. 5.19, at 30° impingement angle the lower erosion damage in solution annealed 21-4-N steel as compared to as cast and aged 21-4-N steel is due to higher ductility and tensile toughness in the solution annealed condition. The decrease in

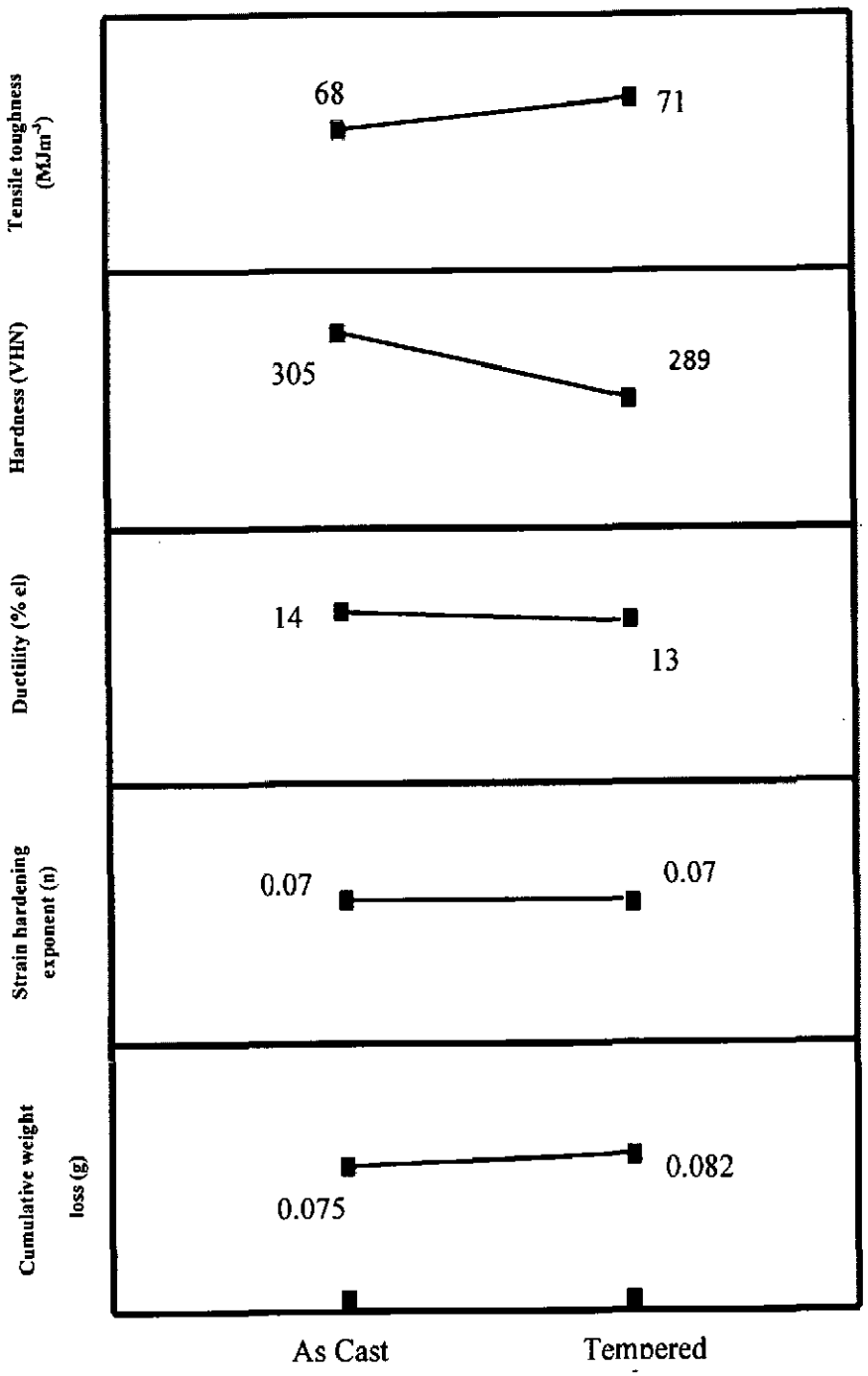

Fig. 5.17. Effect of mechanical properties on cumulative weight loss in 13/4 steel (impingement angle 30°)

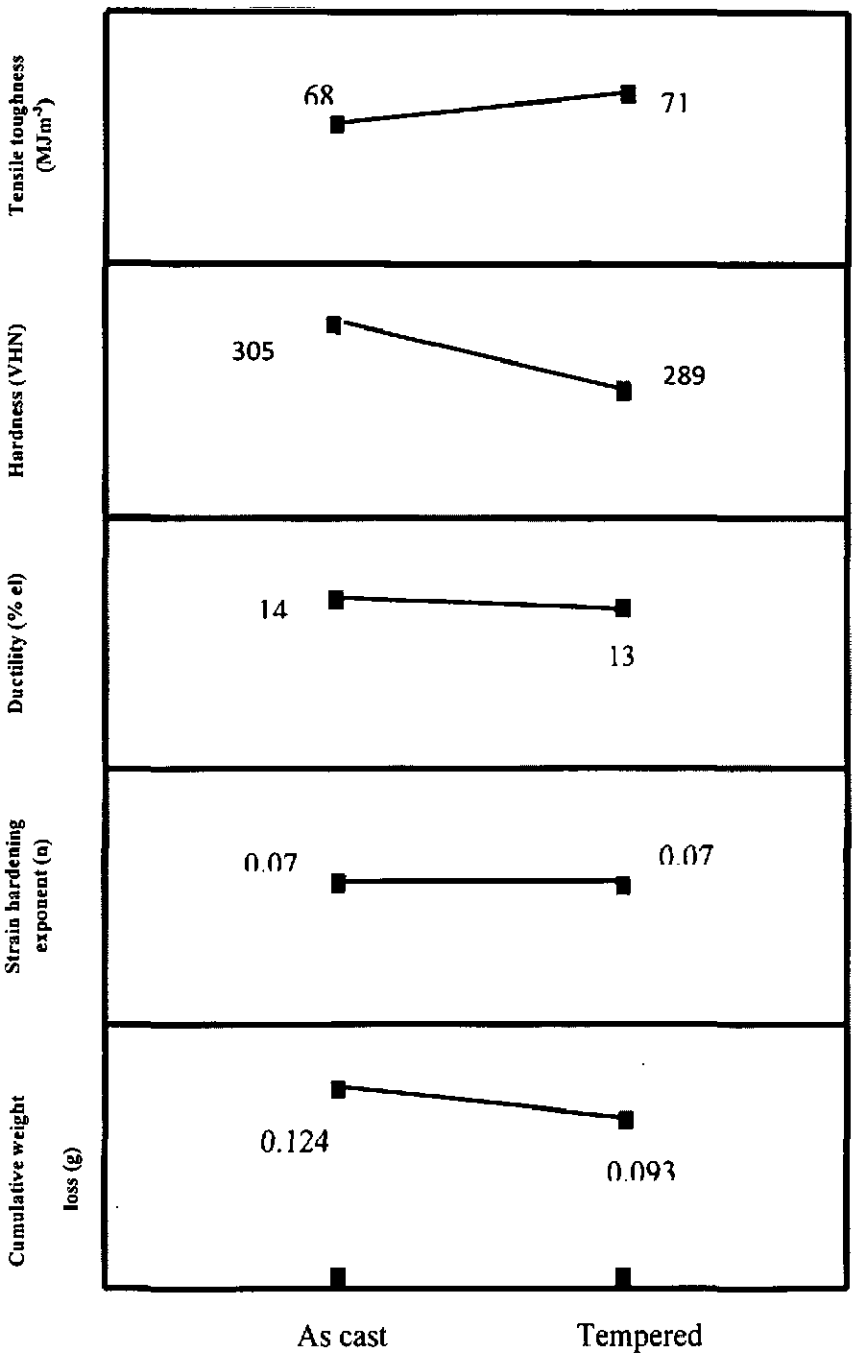

Fig. 5.18. Effect of mechanical properties on cumulative weight loss in 13/4 steel (impingement angle 90^0)

hardness and strain hardening ability in solution annealed 21-4-N steel cause increase in erosion damage through ploughing and scratching action, but cumulative effect of all the mechanical properties of solution annealed 21-4-N steel causes less erosion. The ploughs formed due to impingement of erodent particles at 30° impingement angle are elongated more in annealed 21-4-N steel, which indicates delay in the embrittlements and dislodging of the ploughs and results in lower erosion in solution annealed 21-4-N steel. The erosion damage increases in aged 21-4-N steel in which the ductility and tensile toughness decreases substantially whereas hardness and strain hardening exponent increases. The ploughs formed in this specimen are strain hardened and dislodged earlier due to lower ductility and tensile toughness.

Fig. 5.20 reveals that at 90° impingement angle again, solution annealed 21-4-N steel exhibits least erosion damage. Due to higher tensile toughness in solution annealed 21-4-N steel, more kinetic energy of the erodent particles is absorbed and the formation of strain hardened sub surface layer at the impact site is delayed. The higher ductility of solution annealed 21-4-N steel permits local plastic deformation of the subsurface region, which also causes delay in dislodging of the material due to erodent particles impacted. Solution annealed 21-4-N steel resists normal stresses imposed by the erodent particles by absorbing the kinetic energy due to higher tensile toughness. Solution annealed 21-4-N steel also sustains higher tensile stress and higher elastic-plastic deformation as compared to as cast and aged 21-4-N steel (Fig. 5.8) indicates, during solid particle erosion, solution annealed 21-4-N steel.

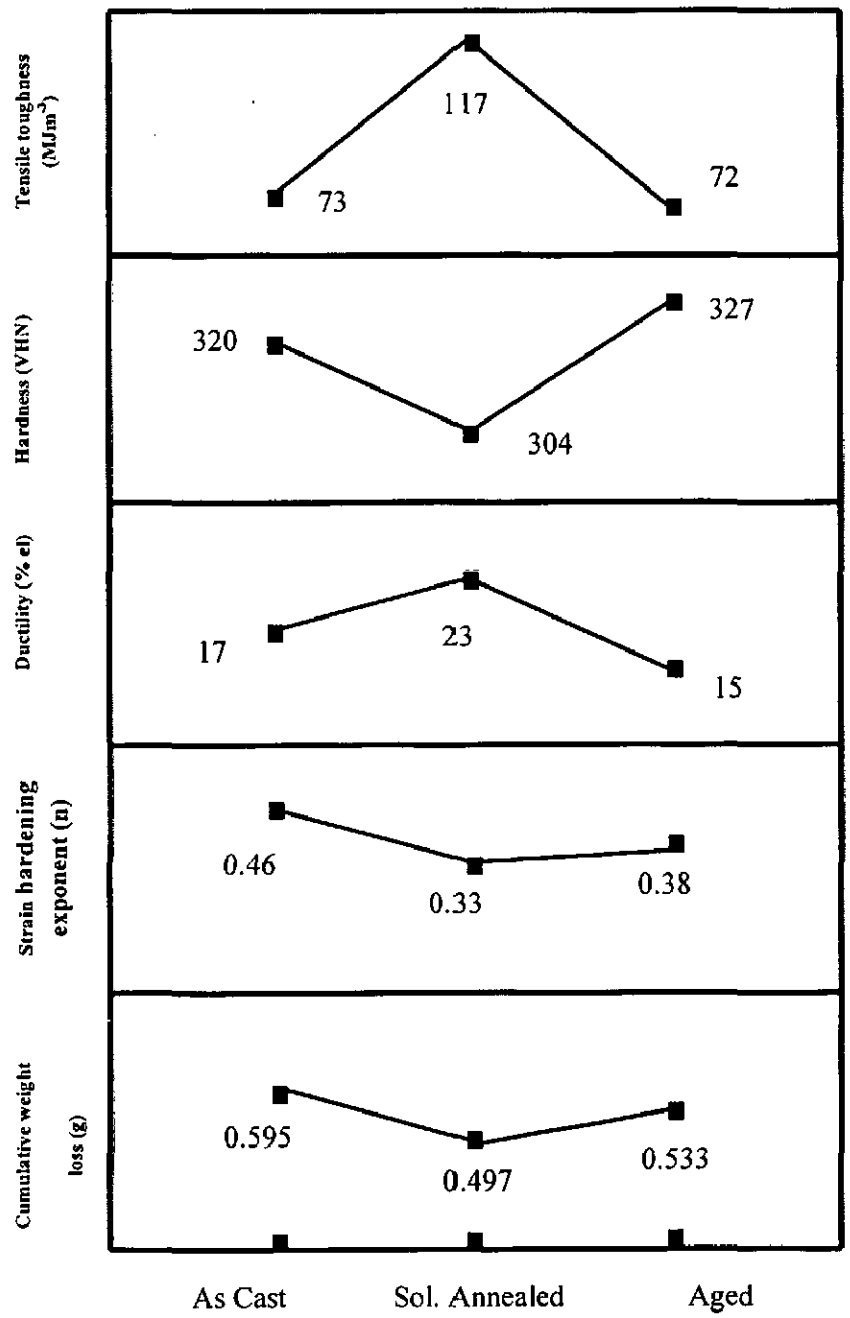

Fig. 5.19. Effect of mechanical properties on cumulative weight loss in 21-4-N steel (impingement angle 30°)

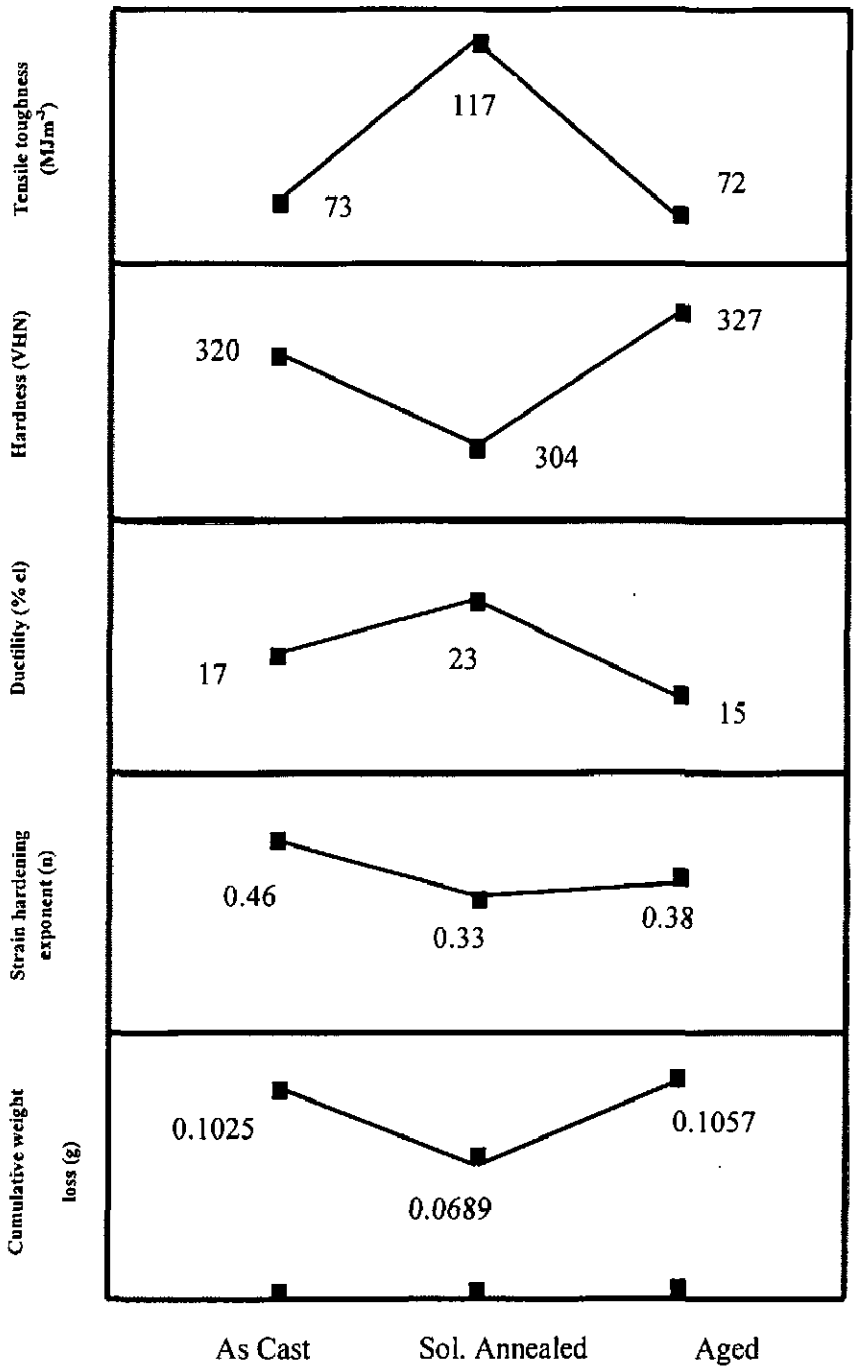

Fig. 5.20. Effect of mechanical properties on cumulative weight loss in 21-4-N steel (impingement angle 90°)

As described in Chapter 4, formation of voids due to localization of strain plays an important role in determining the erosion resistance of the target material. The higher erosion damage of as cast 13/4 steel at 90° impingement angle corresponds to large concentration of voids as compared to that in tempered 13/4 steel as well as 21-4-N steel in each conditions. At 90° impingement angle, the impacted erodent particles cause development of more cracks in as cast 13/4 steel because of severe localization of strain, which results in more void formation. Figs. 5.21-5.24 show the fracture appearance and SEM micrographs of fracture surfaces of tempered 13/4 steel, solution annealed 21-4-N steel and aged 21-4-N steel after tensile tests. Figs. 5.25-5.27 show the SEM micrographs of fracture surfaces of tempered 13/4 steel, solution annealed 21-4-N steel and aged 21-4-N steel after Charpy V-notch impact test. It is clearly observed that large number of voids is nucleated in both low strain rate tensile tests and high strain rate Charpy V-notch impact tests of as cast 13/4 steel. The untempered martensitic laths of as cast 13/4 steel are more prone to localization of strain in comparison to tempered 13/4 steel. It is also observed that the fracture mode of solution annealed 21-4-N steel is more ductile (Fig. 5.23) as compared to that in as cast (Fig. 4.13) and aged 21-4-N steel (Fig. 5.24) in tensile testing.

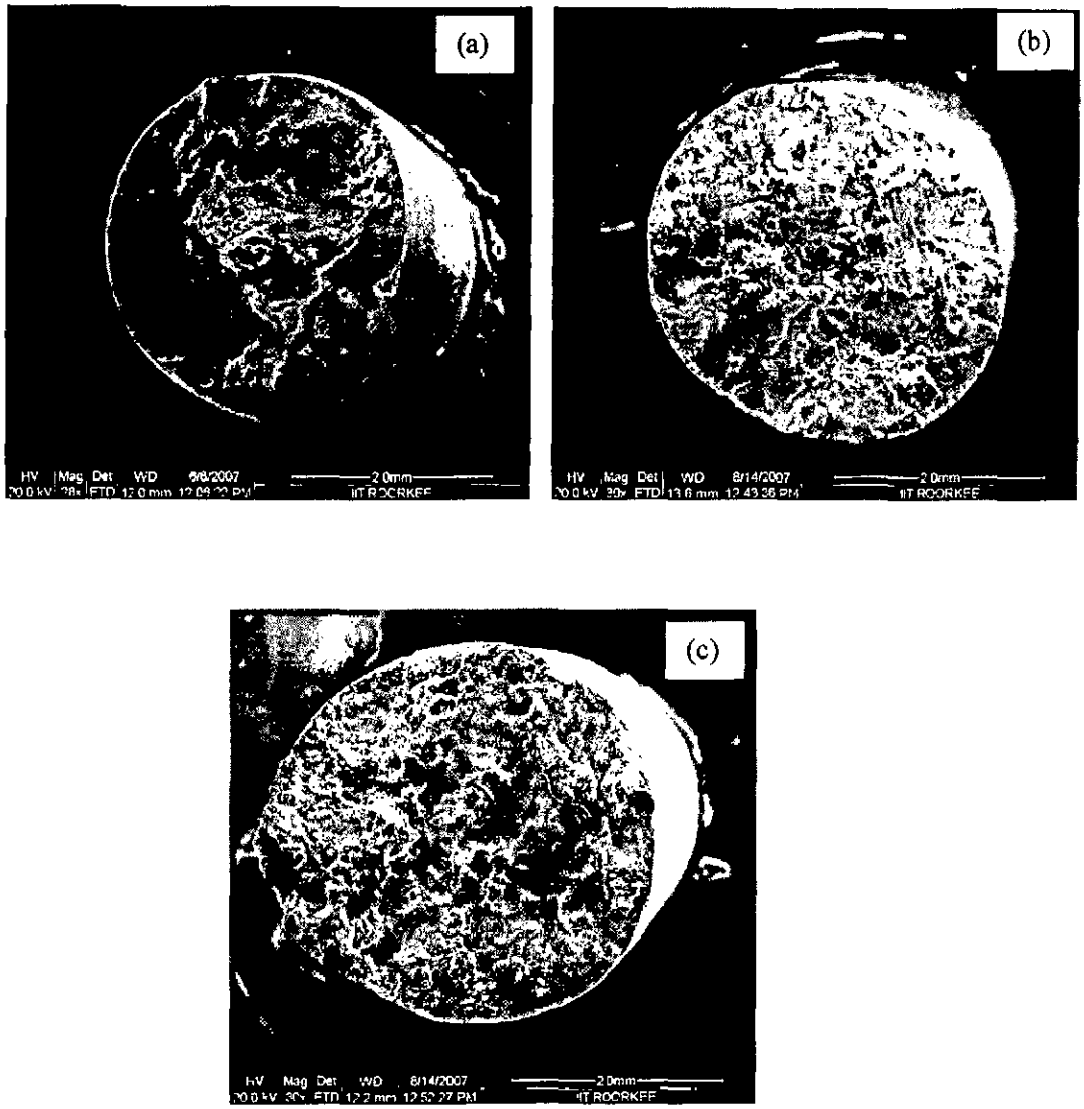

Fig. 5.21. Fracture appearance of fracture surface of (a) tempered 13/4 steel, (b) solution annealed 21-4-N steel and (c) aged 21-4-N steel after tensile testing

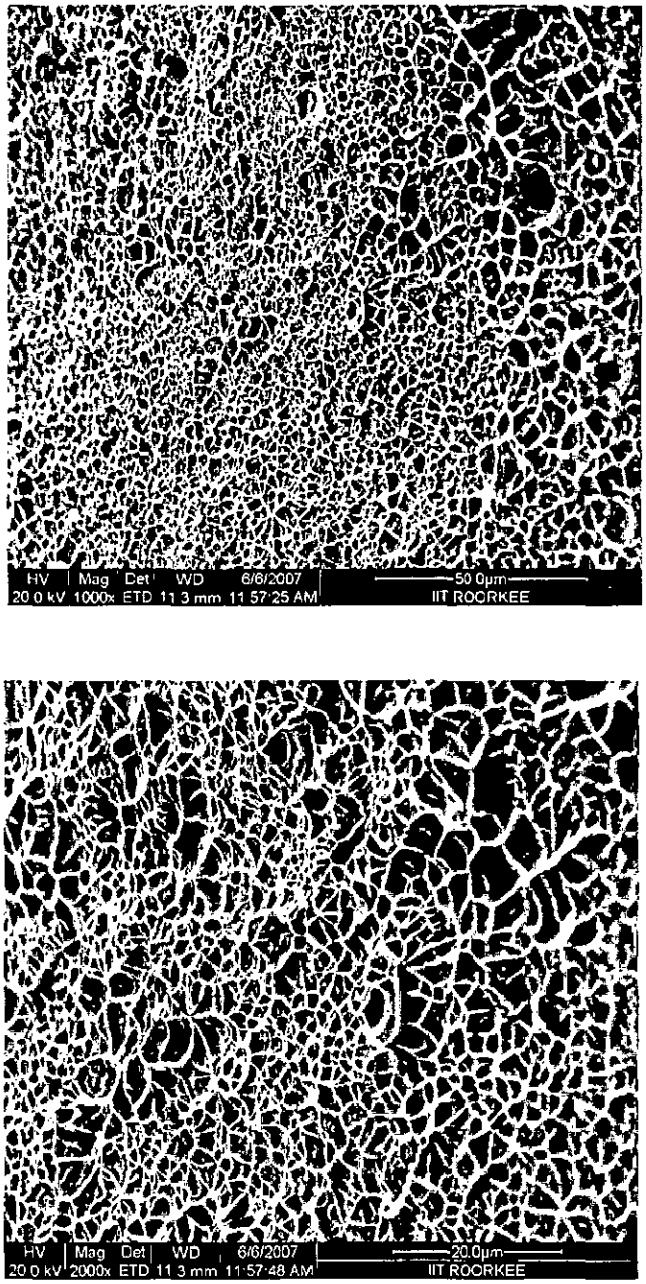

Fig. 5.22. SEM micrographs of fracture surface of tempered 13/4 steel after tensile testing

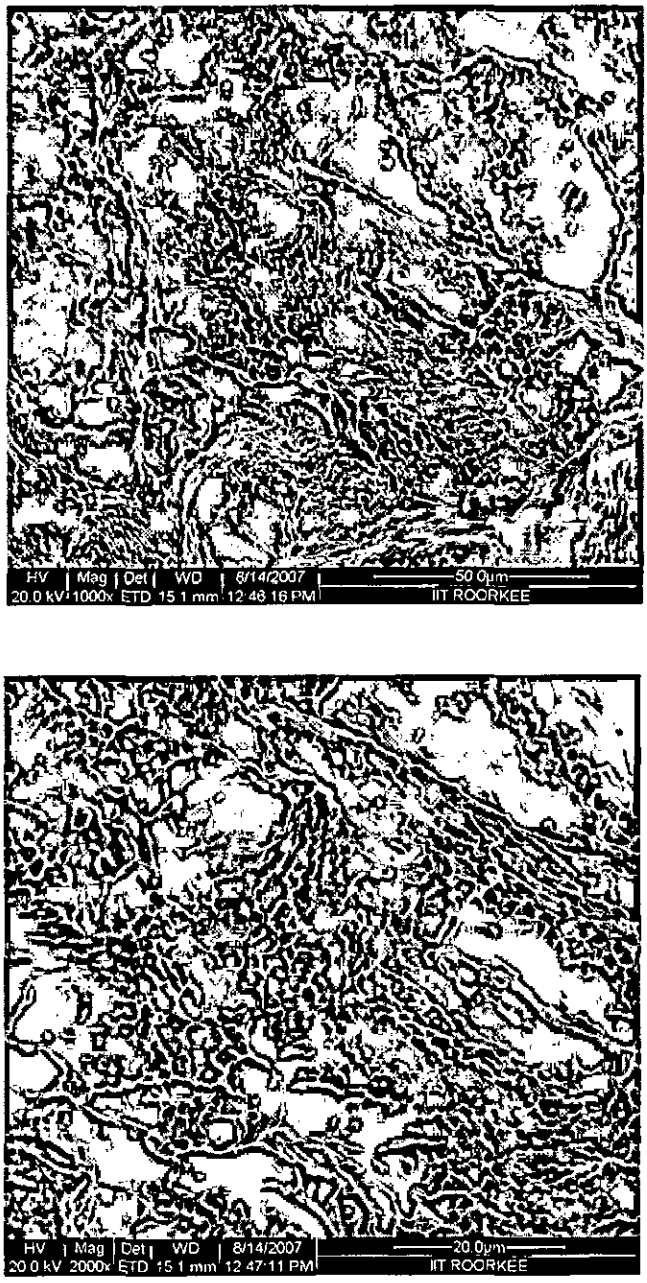

Fig. 5.23. SEM micrographs of fracture surface of solution annealed 21-4-N steel after tensile testing

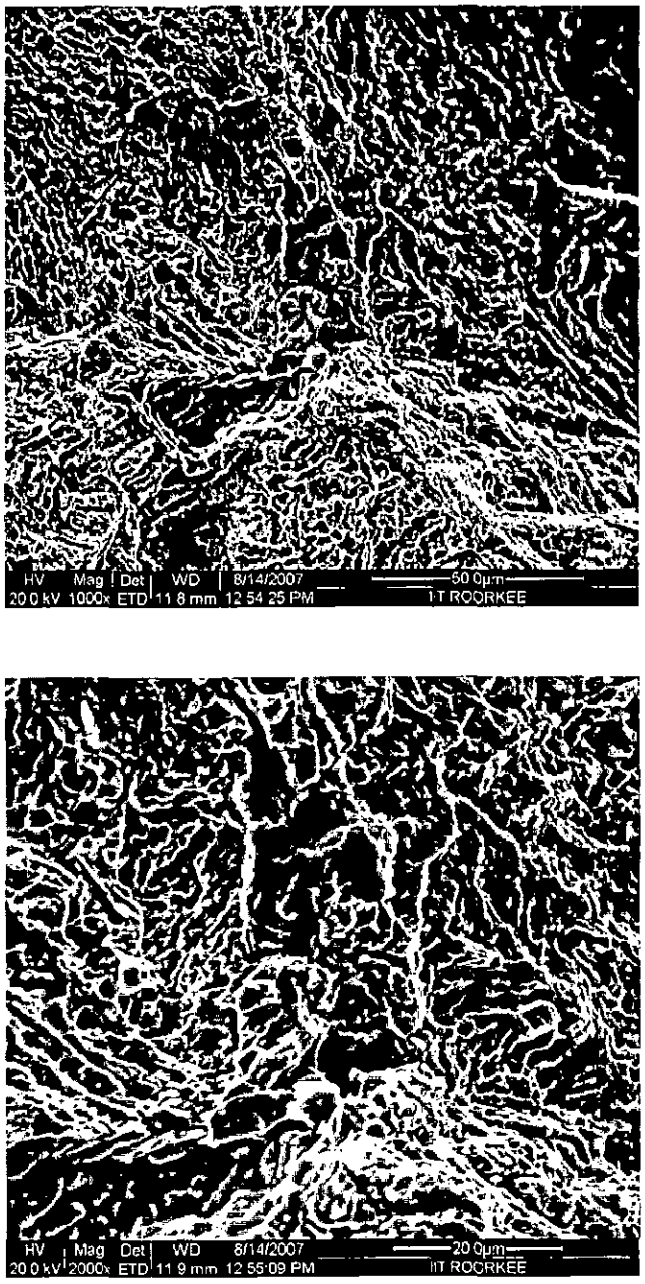

Fig. 5.24. SEM micrographs of fracture surface of aged 21-4-N steel after tensile testing

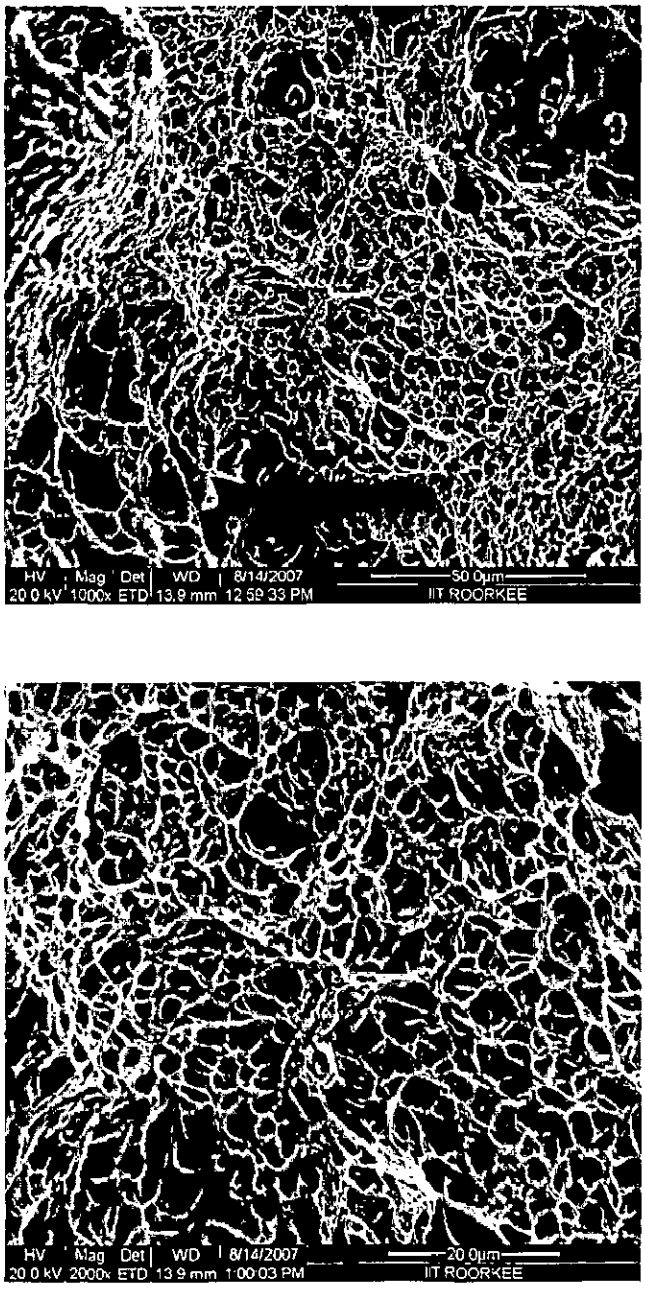

Fig. 5.25. SEM micrographs of fracture surface of tempered 13/4 steel after Charpy V-notch impact testing

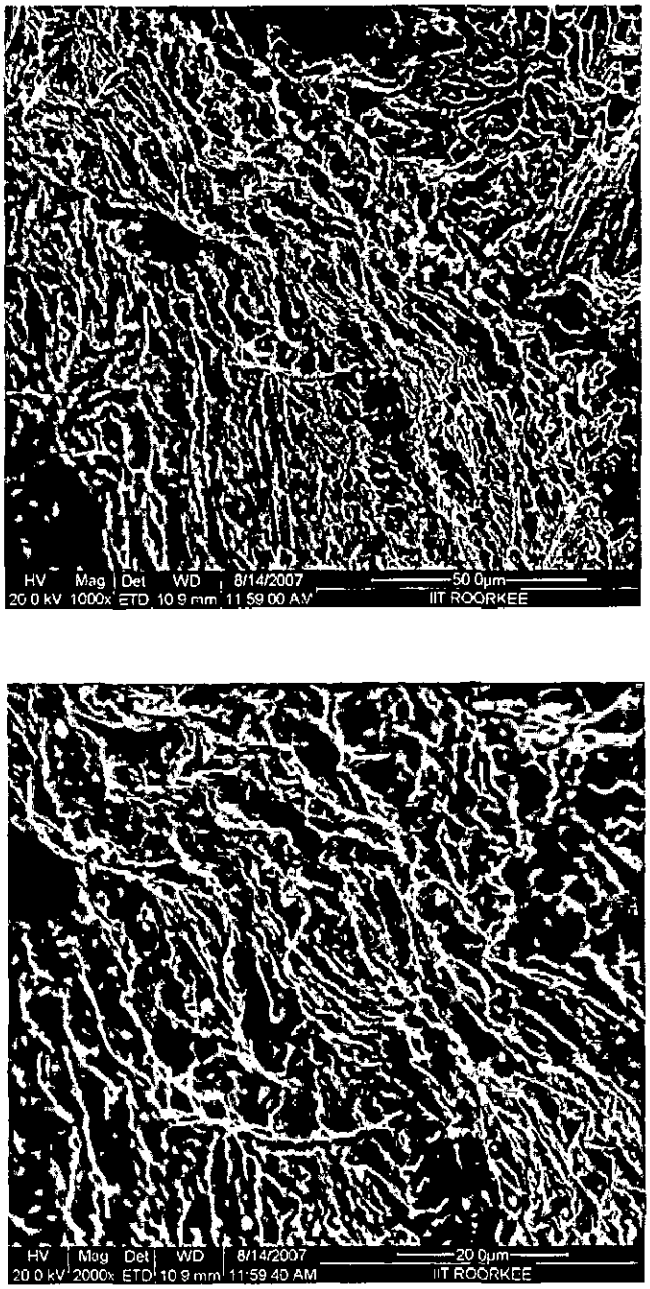

Fig. 5.26. SEM micrographs of fracture surface of solution annealed 21-4-N steel after Charpy V-notch impact testing

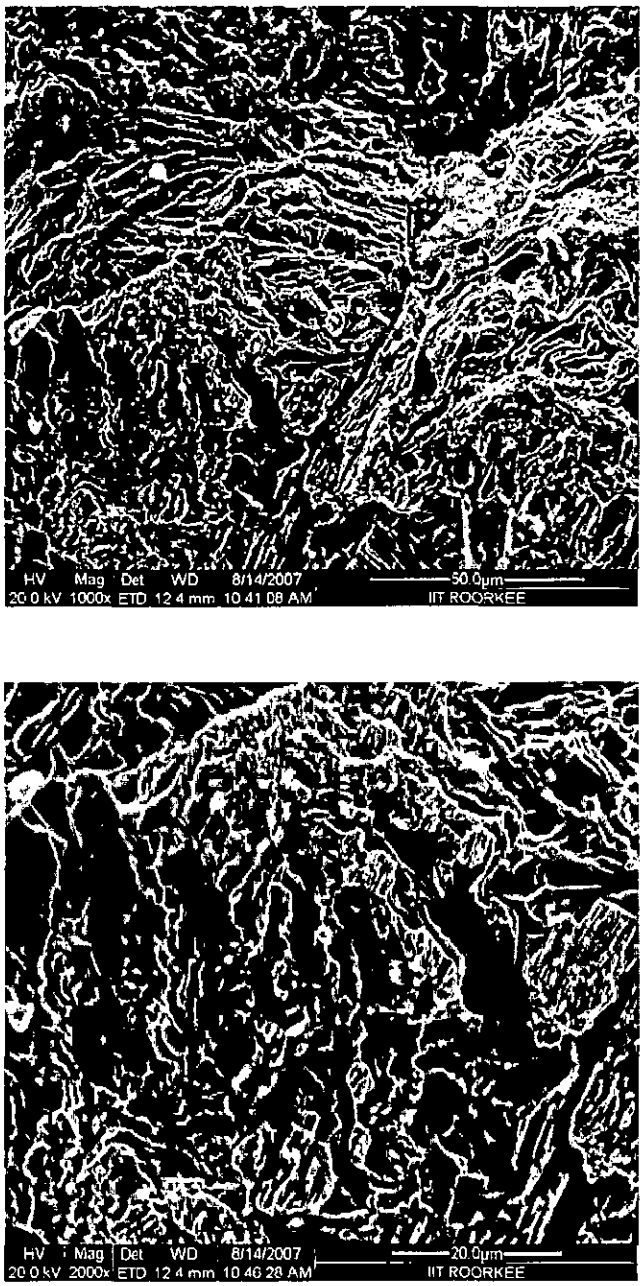

Fig. 5.27. SEM micrographs of fracture surface of aged 21-4-N steel after Charpy V-notch impact testing

5.7 Conclusions

1. Remarkable improvement in the erosion resistance of 13/4 steel at 30° impingement angle is observed; whereas erosion resistance slightly deteriorates at 30° impingement angle as a result of solutionizing at 1050 °C and tempering at 620 °C.

2. At 90° impingement angle the increased erosion resistance of 13/4 steel as result of tempering treatment is due to relieving of internal stresses and thickening of martensitic laths.

3. As a result of tempering there are a certain changes in mechanical properties of 13/4 steel. Due to tempering the hardness decreases from 305 to 289 VHN and the tensile toughness increases slightly (from 68 to 71 MJm^{-3}). The values of ductility and strain hardening exponent (n) almost remain unchanged. The decrease in erosion resistance at 30° impingement angle is attributed to decrease in hardness whereas increase in erosion resistance at 90° impingement angle is correlated with slightly increase in tensile toughness.

4. Substantial improvement in the erosion resistance of 21-4-N steel at both the impingement angles of 30° and 90° is observed as a result of solution annealing at 1100 °C. However, aging treatment of solution annealed 21-4-N steel causes deterioration in erosion resistance at both impingement angles.

5. The improved erosion resistance of 21-4-N steel as a result of solution annealing at 1100 °C is due to substantial dissolution of carbides in the austenitic matrix. Again

reprecipitations of carbides in the aged 21-4-N steel are responsible for decreased erosion resistance.

6. The mechanical properties significantly affect the erosion resistance of 21-4-N steel. The increased values of ductility and tensile toughness as a result of solution annealing of 21-4-N steel increase the erosion resistance. However, lowering of hardness and strain hardening ability of 21-4-N steel as result of solution annealing may cause reduction in erosion resistance; but cumulative effect of all mechanical properties results in increased erosion resistance.

7. SEM study shows that erosion at 30° impingement angle occurs by formation of ploughs, whereas at 90° impingement angle the erosion damage is caused by formation of cavities and cracks.

Chapter 6

Effect of deformation on the erosion behaviour of 13/4 and 21-4-N steels

This chapter contains the results of mechanical deformation (rolling) as described earlier and erosion behaviour of 13/4 and 21-4-N steels. The effects of rolling prior to erosion test on solid particle erosion behaviour of 13/4 and 21-4-N steels have been analyzed in this chapter. The as cast 13/4 and 21-4-N steels were subjected to 8% reduction in thickness by rolling at 700 °C. The as cast 21-4-N steel was also subjected to 89% reduction in cross sectional area by hot rolling at 1180 °C. Experimental studies were conducted to determine the changes in microstructure, mechanical properties and erosion behaviour of these steels as a result of deformation by rolling.

6.1 Introduction

Erosive wear usually occurs if the particle hardness is greater than the material hardness. The improvement in the hardness with ductility of the material results in increased resistance to erosion. Over the past years the solid particle erosive wear behavior of the materials by improving their erosion resistance by cold working has been discussed in detail [50]. **Sundararajan** [185] concluded neither heat treatment nor cold working of the target has any effect on erosion resistance. **Naim and Bahadur** [186] on the other hand reported that prior cold working of the target material increases the

incubation period for the onset of erosion. Also due to an increase in the initial level of cold working, a higher rate of erosion was observed for both the normal and the oblique impact conditions. **Goretta et al** [51] have investigated the erosion resistance of copper, nickel and 304 stainless steel with sharp alumina particles. They concluded that work hardening improved the erosion resistance of the copper, which has high ductility. Higher hardness also improves the erosion resistance of the material if it retains sufficient ductility. **Rao et al** [187] evaluated the resistance of a laser-surface-melted 0.4% C low alloy steel to solid particle erosion. They observed that the laser surface melting does not improve or impair the erosion resistance of a 0.4% C steel.

6.2 Microstructure

Fig. 6.1 shows the microstructures of 13/4 steel in 8% rolled condition, which consists of lath/martensitic needles along with a second phase, which is δ-ferrite. However, there is a difference between the microstructures of 13/4 steel in as cast (Fig. 4.1) and in rolled conditions, which is size of martensitic laths and δ-ferrites. The martensitic laths and δ-ferrites are coarser in rolled 13/4 steel as compared to those in as cast 13/4 steel.

Fig. 6.2 shows the microstructure of 21-4-N steel in 8% rolled condition. These microstructures are very similar to the microstructures of 21-4-N steel in as cast condition (Fig. 4.2). The microstructure consists of precipitates of carbides in the matrix of austenite. In 8 % rolled condition also, the carbides (dark portion) are surrounded by the

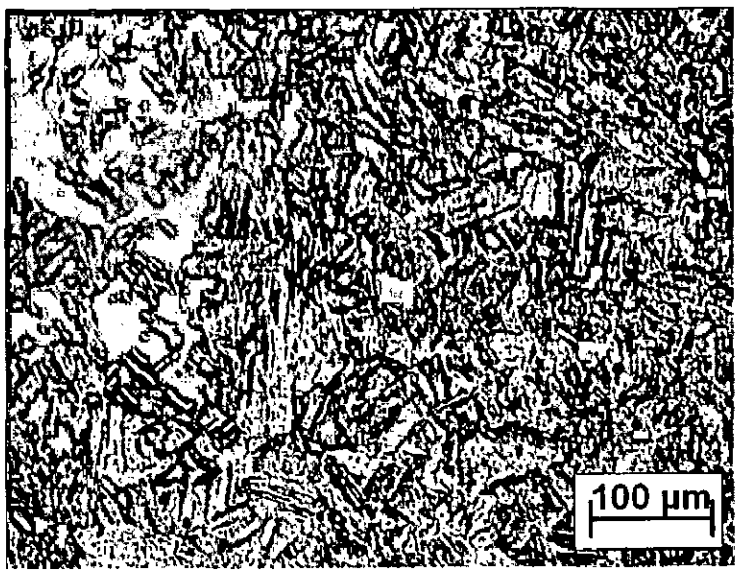

Fig. 6.1. Microstructure of 8% rolled 13/4 steel

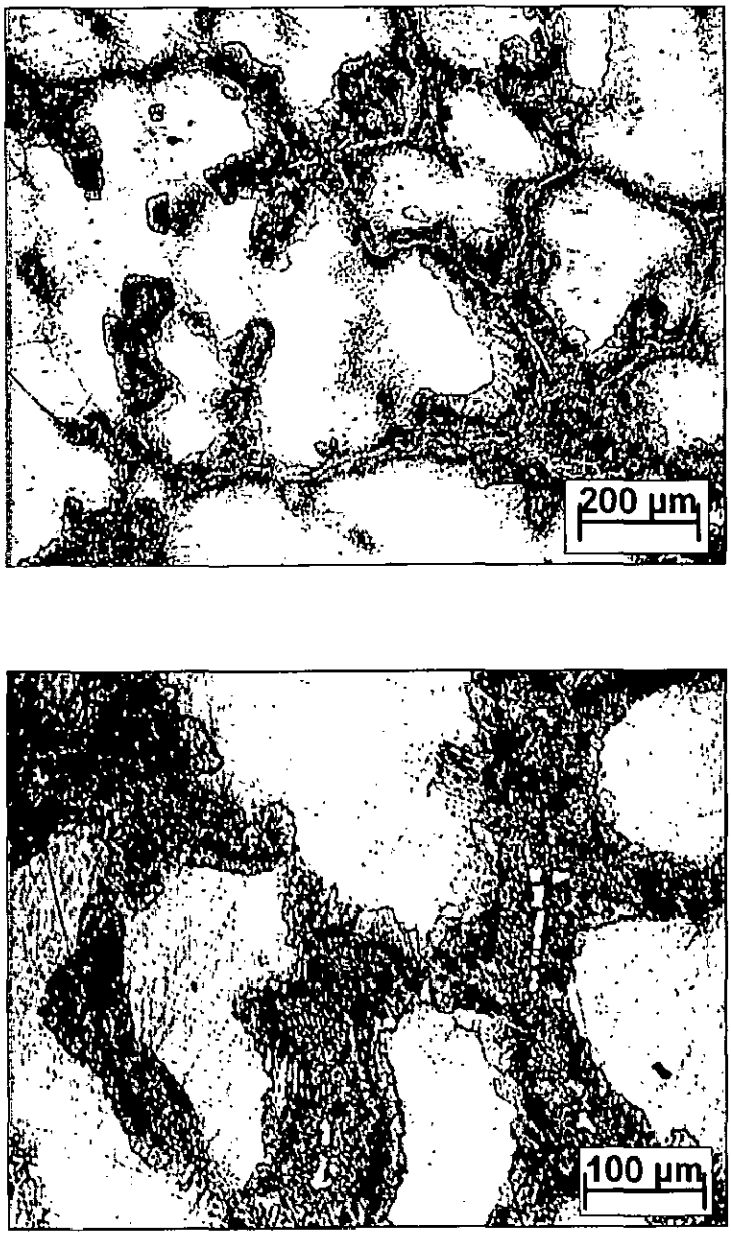

Fig. 6.2. Microstructure of 8% rolled 21-4-N steel

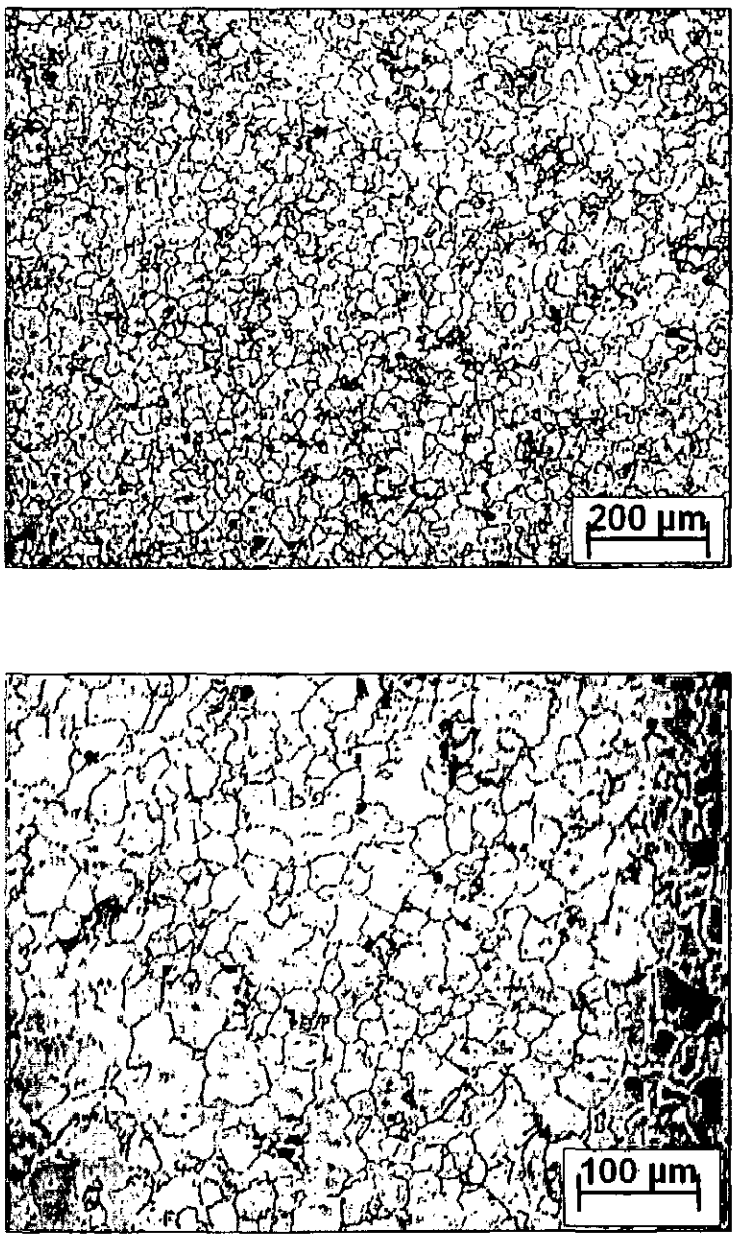

Fig. 6.3. Microstructure of hot rolled 21-4-N steel

eutectic of austenite and carbides (M_7C_3), as identified earlier, where M can be Cr, Fe and Ni. Fig. 6.3 shows the microstructure of hot rolled (at 1180 °C) 21-4-N steel, which consists of fine grains of austenite along with precipitates of carbides. Due to very high C:Cr ratio and higher concentration of N, the carbides are identified as M_7C_3 type, where M can be Cr, Fe and Ni.

6.3 Mechanical properties

The mechanical properties viz. hardness, YS, UTS, ductility and Charpy V-notch impact energy were determined for 13/4 and 21-4-N steels in 8% rolled condition and for hot rolled 21-4-N steel. The mechanical properties of these steel specimens are given in Table 6.1. It is seen that the after 8% rolling the hardness, YS and UTS increased significantly whereas impact energy and ductility reduced drastically in both the steels. In hot rolled 21-4-N steel it is observed that the values of hardness, impact energy, YS, UTS and ductility are higher as compared to those in as cast 21-4-N steel.

Tensile toughness

The tensile toughness is the ability of the target material to absorb the strain energy during plastic deformation and is calculated from the area under stress-strain curve between YS and fracture stress. Fig. 6.4 shows the engineering stress-strain curves of 13/4 steel in as cast and 8% rolled conditions. The values of tensile toughness of 13/4 steel in as cast and 8% rolled conditions are determined from the areas ABCD and EFGH respectively from the respective engineering stress-strain curves as shown in Fig. 6.4.

The values of tensile toughness for 13/4 steel in as cast and 8% rolled conditions are 68 and 15 MJm^{-3} respectively as given in Table 6.1. The values of the tensile toughness of as cast, 8% rolled and hot rolled 21-4-N steel are determined from the area ABCD, EFGH and IJKL respectively from the respective engineering stress-strain curves as shown in Fig. 6.5. The values of tensile toughness of as cast, 8% rolled and hot rolled 21-4-N steel are 73, 15 and 254 MJm^{-3} respectively.

Strain hardening exponent (n)

The strain hardening exponent is calculated from the slope of log-log plot of true stress - true strain curve after yielding. The values of strain hardening exponent of 13/4 and 21-4-N steel in cast condition have been evaluated in Chapter 4 as 0.07 and 0.46 respectively. The log-log plots of true stress - true strain curves after yielding for 8% rolled 13/4 steel, 8% rolled 21-4-N steel and hot rolled 21-4-N steel are shown in Fig. 6.6. The values of strain hardening exponent of 8% rolled 13/4 steel, 8% rolled 21-4-N steel and hot rolled 21-4-N steel are 0.06, 0.06 and 0.57 respectively.

Table 6.1. Mechanical properties of 13/4 and 21-4-N steels in rolled conditions

Properties	13/4 Steel 8% rolled at 700 °C	21-4-N Steel 8% rolled at 700 °C	21-4-N steel Hot rolled at 1180 °C
Hardness (VHN)	350	403	339
Impact energy (J)	32	4	20
YS (MPa)	1117	912	917
UTS (Mpa)	1124	950	1207
Ductility (% elongation)	8	8	29
Tensile toughness (MJm^{-3})	15	15	254
Strain hardening exponent (n)	0.06	0.06	0.57

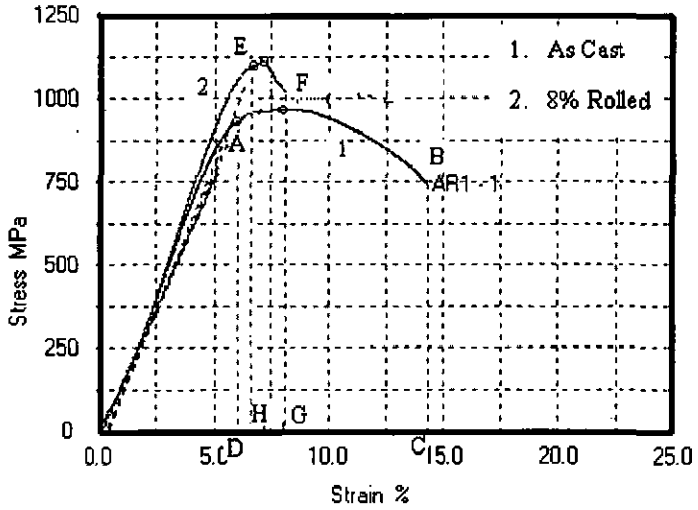

Fig. 6.4. Engineering stress-strain curves of 13/4 steel in as cast and 8% rolled conditions

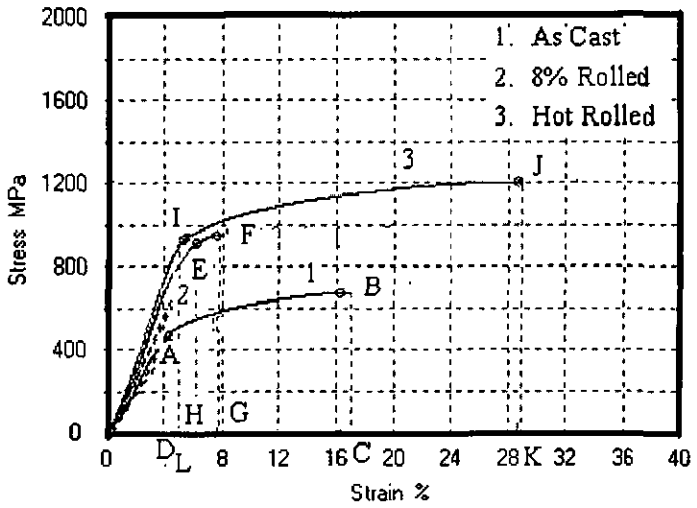

Fig. 6.5. Engineering stress-strain curves of 21-4-N steel in as cast, 8% rolled and hot rolled conditions

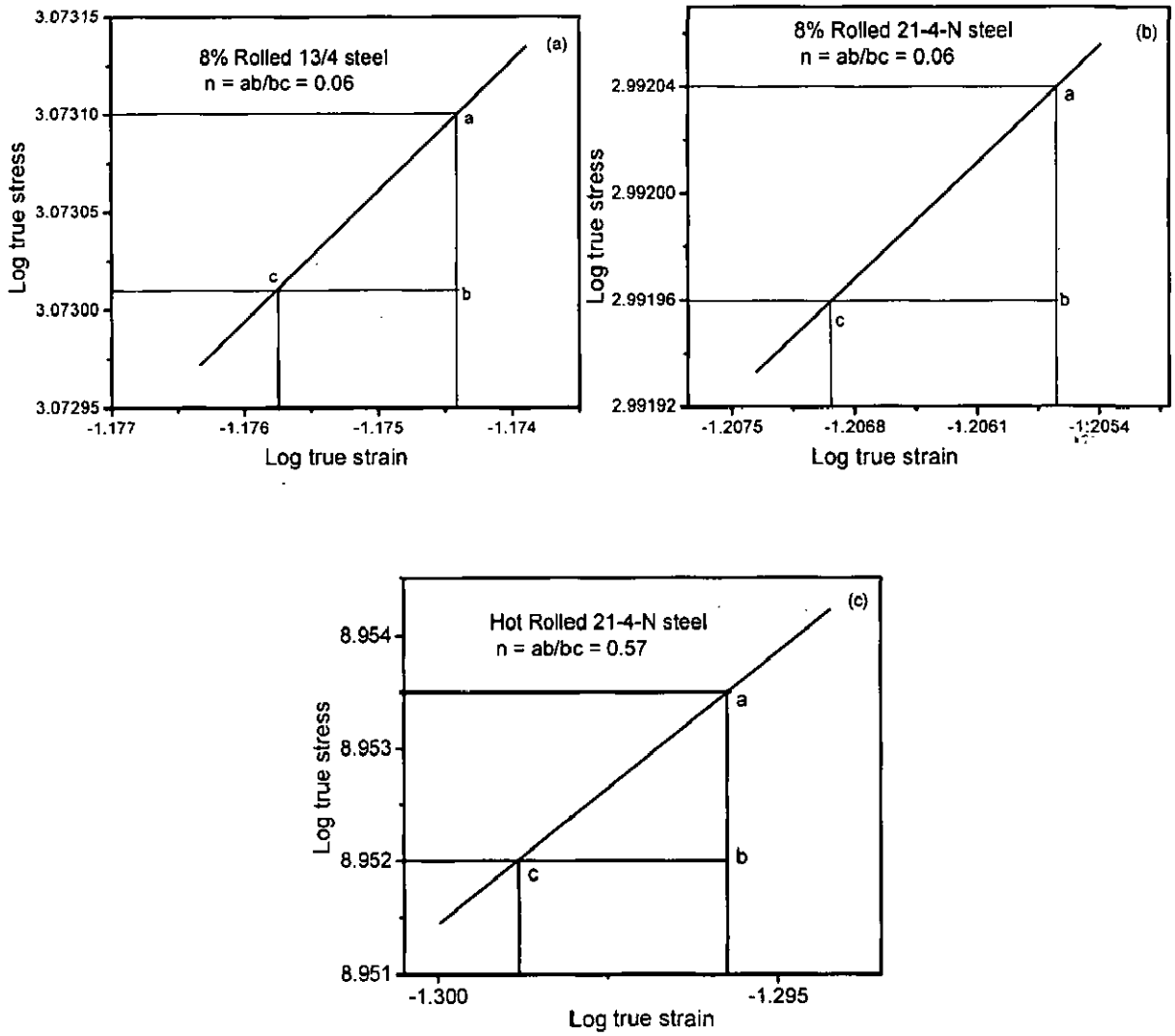

Fig. 6.6. Strain hardening exponents (n) of (a) 8% rolled 13/4 steel, (b) 8% rolled 21-4-N steel and (c) hot rolled 21-4-N steel

6.4 Erosion behaviour

Figs. 6.7 and 6.8 show respectively the cumulative weight loss versus time of erosion and erosion rates as function of mass of erodent in respect of 13/4 steel in as cast and 8% rolled conditions at the impingement angles of 30° and 90°. At 30° impingement angle, the cumulative weight loss is lower in 8% rolled condition in comparison to that in as cast condition, but at 90° impingement angle it is higher in 8% rolled condition than. that in as cast 13/4 steel. From Fig. 6.8 it is seen that erosion rate in as cast 13/4 steel is more at 30° impingement angle, but at 90° impingement angle it is less than that in 8% rolled 13/4 steel. It is also seen that the erosion rates in as cast as well as 8% rolled specimens at 30° impingement angle and in as cast specimen at 90° angle approach the steady state erosion rate, while in 8% rolled specimen at 90° impingement angle erosion rate increases continuously, indicating higher erosion rate of 8% rolled sample at 90° impingement angle.

Figs. 6.9 and 6.10 show respectively the cumulative weight loss versus time of erosion and erosion rates as a function of mass of erodent curves of 21-4-N steel in as cast, 8% rolled and hot rolled conditions at the impingement angles of 30° and 90°. The slopes of cumulative weight loss curves are almost constant for each specimen except in as cast 21-4-N steel at 90° impingement angle. The variation of slope in as cast 21-4-N steel at 90° impingement angle indicates variation in the mechanism of erosion whereas in other specimens the mechanisms of erosion are identical throughout the erosion test.

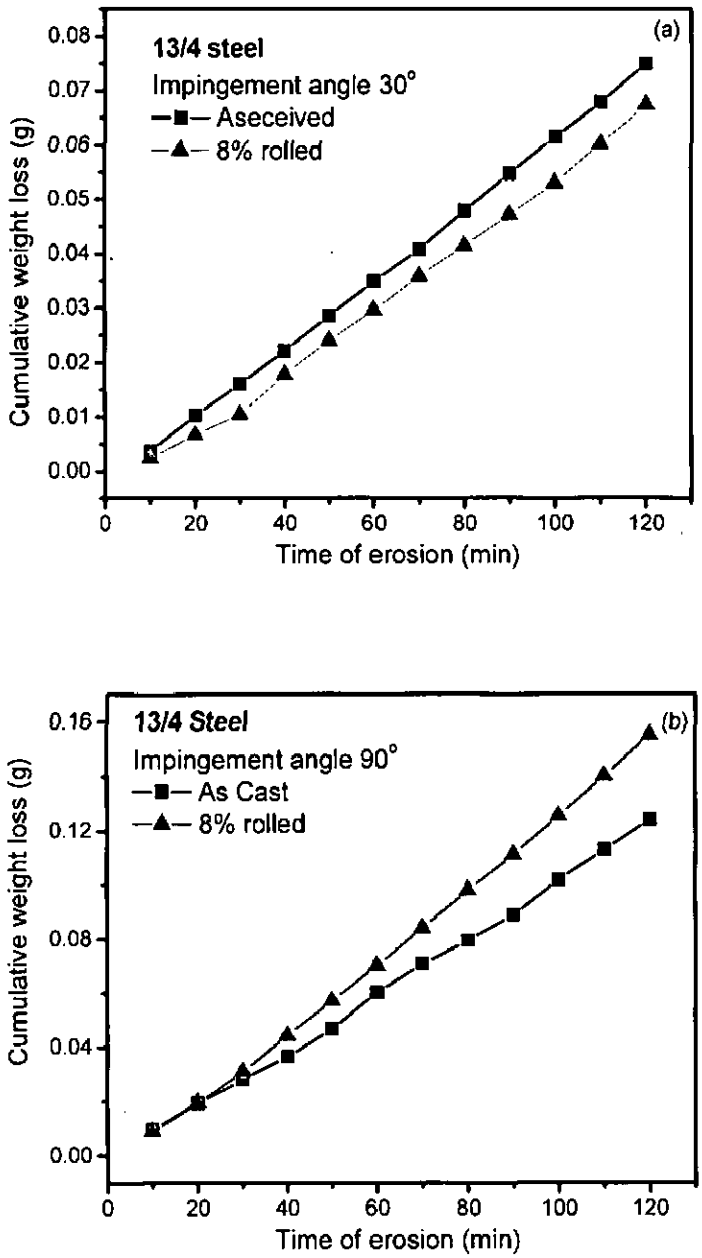

Fig. 6.7. Cumulative weight loss as function of time of erosion at impingement angles of (a) 30° and (b) 90°

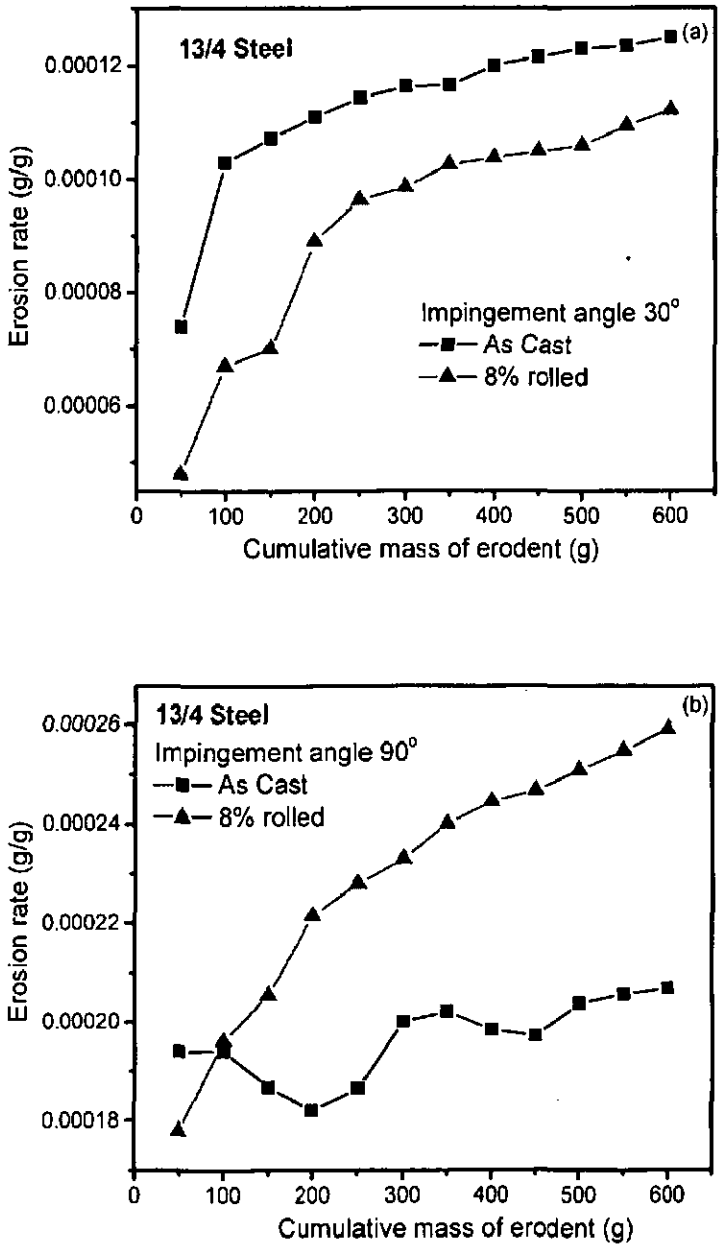

Fig. 6.8. Erosion rate as function of cumulative mass of erodent at impingement angles of (a) 30° and (b) 90°

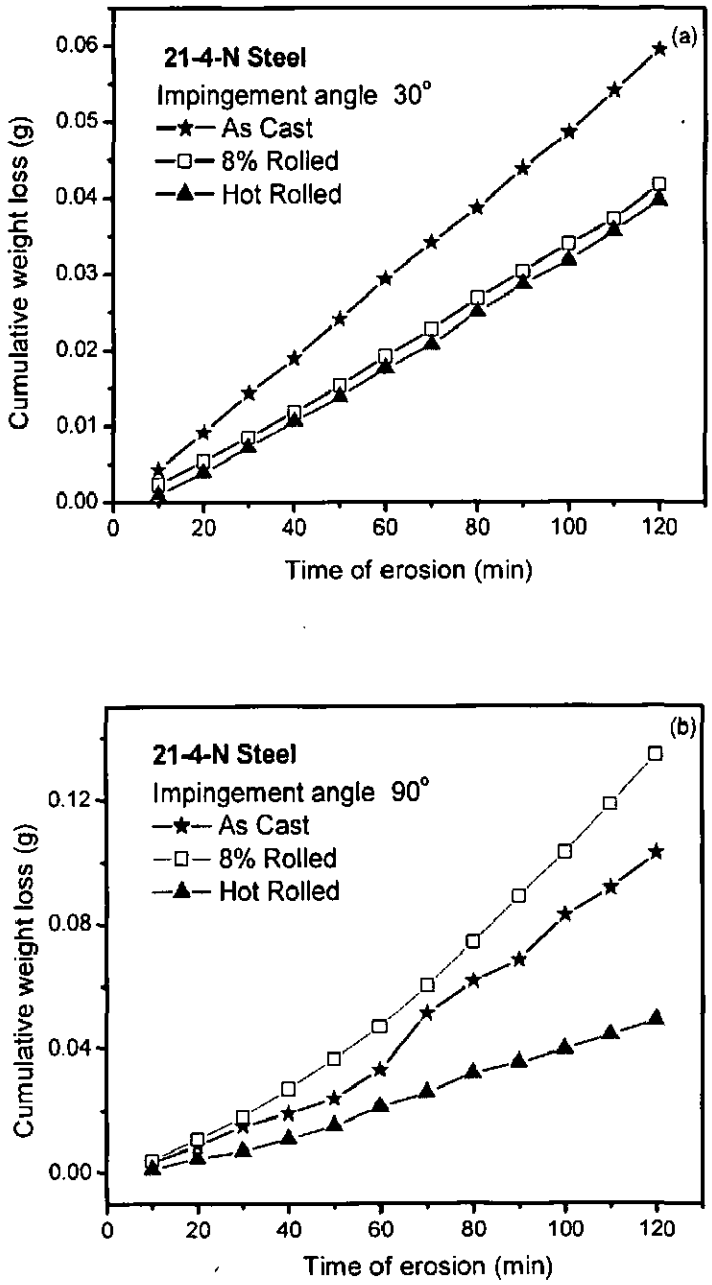

Fig. 6.9. Cumulative weight loss as function of time of erosion at impingement angles of (a) 30° and (b) 90°

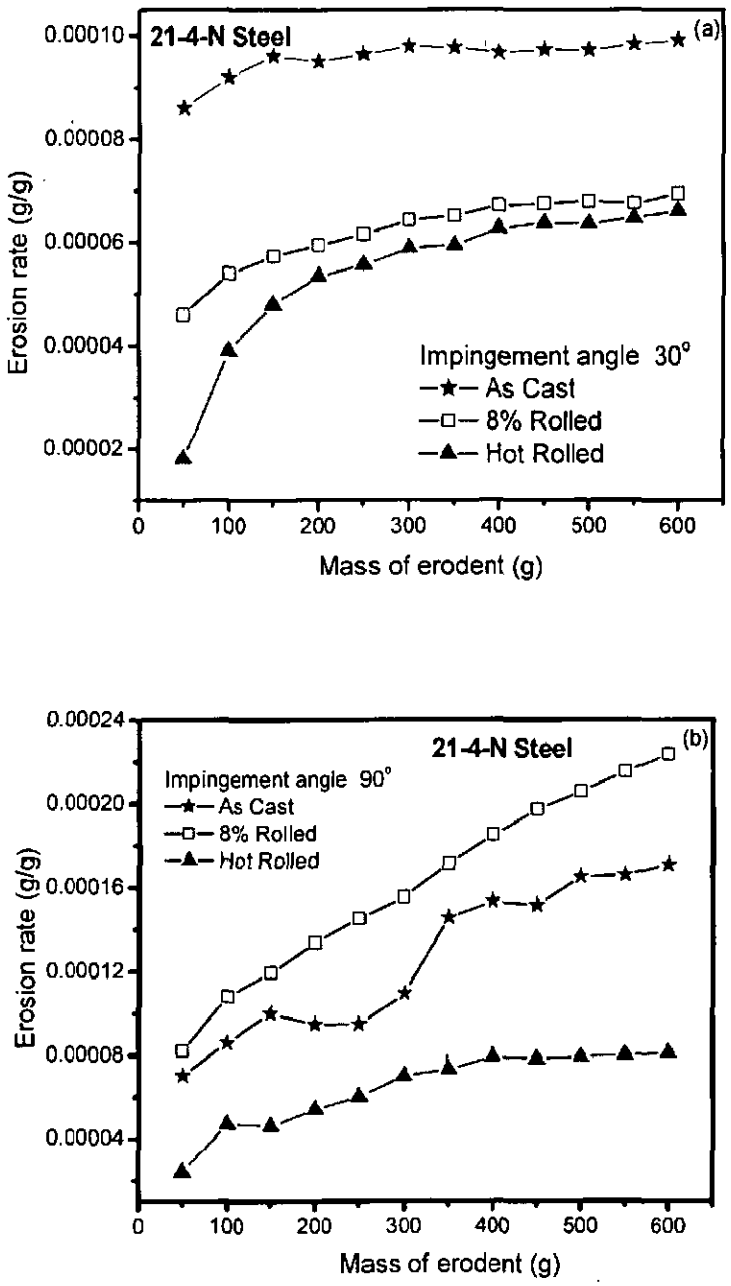

Fig. 6.10. Erosion rate as function of cumulative mass of erodent at impingement angles of (a) 30° and (b) 90°

At both the impingement angles lowest erosion is observed in hot rolled 21-4-N steel, whereas highest erosion is seen in as cast 21-4-N steel at 30° impingement angle and in 8% rolled 21-4-N steel at 90° impingement angle.

It can be seen that at 30° impingement angle the rate of erosion increases initially and then becomes almost constant; whereas at 90° impingement angle the erosion rate curves of as cast 13/4 and 21-4-N steel and hot rolled 21-4-N steel are of zig-zag type. The erosion rate of 13/4 and 21-4-N steel in 8% rolled condition at 90° impingement angle increases continuously throughout the erosion test. At 30° impingement angle, there is constant involvement of shear in the erosion process, which leads to a rate of erosion, which is almost constant. At 90° impingement angle the zig-zag shape of erosion curves of as cast 13/4 and 21-4-N steel and hot rolled 21-4-N steel may be due to irregular interaction between strain hardening and embrittlement at various stages of erosion. Rapid embrittlement of the sub surface layer of 13/4 and 21-4-N steel in 8% rolled condition by the erodent particles at 90° impingement angle may be contributory to the increasing erosion rate.

6.5 SEM study of eroded surfaces

Fig. 6.11 shows the SEM micrographs of eroded surfaces of 8% rolled 13/4 steel at 30° and 90° impingement angles. At 30° impingement angle the erosion involves a shear process as observed by the presence of ploughs (Fig. 6.11a). The ploughs in as cast condition are much wider (Fig. 4.6a) and longer than those in 8% rolled 13/4 steel. This

confirms more erosion damages in as cast 13/4 steel. At 90° impingement angle, the eroded surfaces are free from ploughs. Deep surface cavities are observed in the SEM micrograph (Fig. 6.11b), which are created due to fragmentation of strain hardened layer of material by the impingement of abrasive particles. At 90° impingement angle, the cavities are much deeper, wider and longer in 8% rolled 13/4 steel (Fig. 6.11b) than those in as cast 13/4 steel (Fig. 4.7a). This is in agreement with higher erosion damages observed in 8% rolled 13/4 steel than those in as cast 13/4 steel.

Figs. 6.12 and 6.13 show respectively the SEM micrographs of eroded surfaces of (a) 8% rolled and (b) hot rolled 21-4-N steel at impingement angles of 30° and 90°. At 30° impingement angle, the eroded surfaces consist of ploughs (Fig. 6.12) similar to those in as cast 21-4-N steel (Fig. 4.6b). The ploughs observed in as cast 21-4-N steel are of smaller size but deeper (Fig. 4.6b), than those in 8% rolled and hot rolled 21-4-N steel, that confirms higher erosion damages in as cast 21-4-N steel. The ploughs seen in the eroded surfaces of 8% rolled 21-4-N steel are shallower (Fig. 6.12a), while in hot rolled 21-4-N steel these are deeper but fewer, indicating more erosion damages in 8% rolled 21-4-N steel than that in hot rolled 21-4-N steel. From SEM micrographs it can also be inferred that at 30° impingement angle the 21-4-N steel in hot rolled condition presents lower erosion damages than that in as cast and 8% rolled conditions. At 90° impingement angle, the SEM micrographs exhibit cavities created due to dislodging of materials by hard hitting abrasive particles (Fig. 6.13). The deeper and larger cavities seen in the SEM micrograph of 8% rolled steel (Fig. 6.13a) confirms in this steel higher

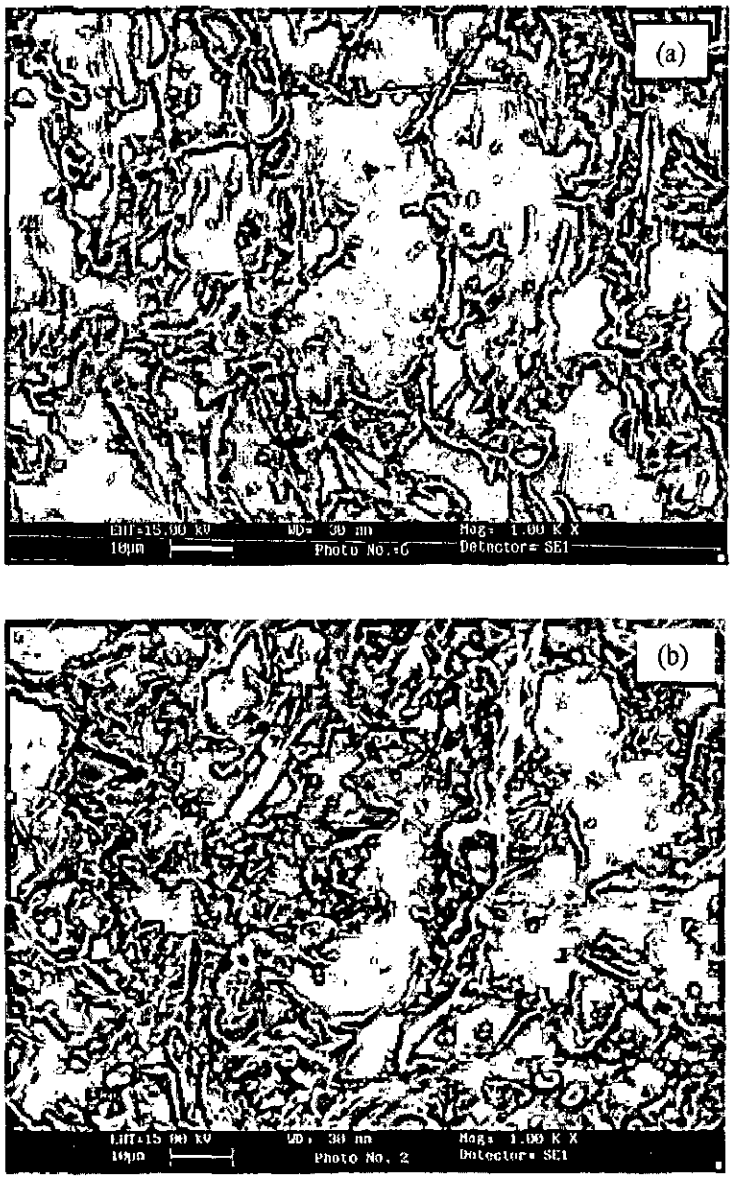

Fig. 6.11. SEM of eroded surface of 8% rolled 13/4 steel at (a) 30° and (b) 90° impingement angle

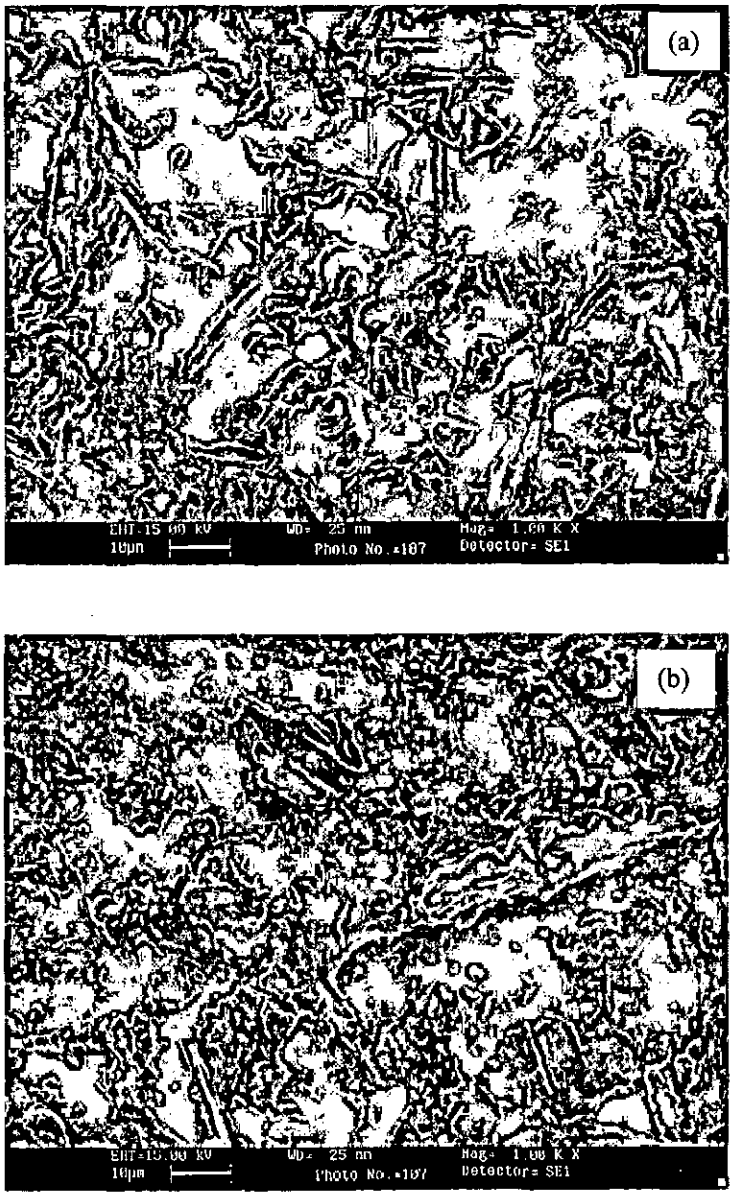

Fig. 6.12. SEM of eroded surface of (a) 8% rolled 21-4-N steel and (b) hot rolled 21-4-N steel at 30° impingement angle

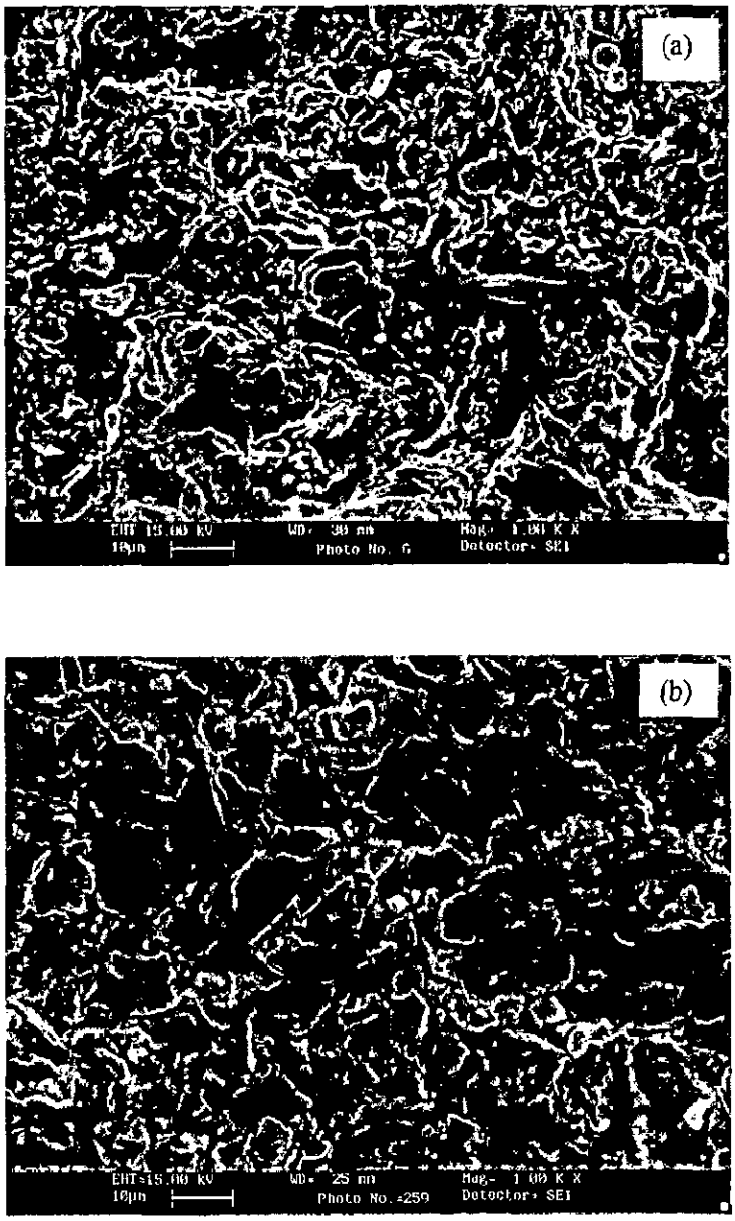

Fig. 6.13. SEM of eroded surface of (a) 8% rolled 21-4-N steel and (b) hot rolled 21-4-N steel at 90° impingement angle

erosion damages as compared to those in as cast (Fig. 4.7b) and hot rolled (Fig. 6.13b) conditions.

6.6 Discussion

6.6.1 Effect of microstructure on erosion

The microstructure of the target material plays an important role in solid particle erosion. It is observed that there is improvement in erosion resistance at 30° impingement angle, whereas it deteriorates at 90° impingement angle as a result of 8% rolling prior to erosion test. From the microstructural view point, the improvement in erosion resistance at 30° impingement angle in 13/4 steel is attributed to increased internal stresses as result of rolling prior to erosion test. These internal stresses pose resistance against ploughing or cutting by erodent particles, and results in lower erosion damage at 30° impingement angle. But at 90° impingement angle these internal stresses make the material less able to absorb the kinetic energy of the erodent particles, which results in very fast nucleation and propagation of cracks and finally increased erosion damages.

The matrix of 21-4-N steel becomes so hard and brittle as a result of 8% rolling and the austenite as well as carbides are heavily stressed. While hot rolling of 21-4-N at 1180 °C enables it to recrystallize during rolling, this results in refinement of the austenitic grain structure and dissolution of carbides too. The stresses associated with 8% rolled 21-4-N steel make the erosion process through ploughing mechanism difficult, which results in improvement in erosion resistance of 21-4-N steel at 30° impingement

angle. Due to stressed austenitic structure the 8% rolled 21-4-N steel is less able to absorb the kinetic energy of the erodent particles and local plastic deformation is also reduced, which results in increased erosion rate at 90° impingement angle. The better erosion resistance of hot rolled 21-4-N steel is attributed to its fine and stabilized austenitic structure. In solid particle erosion austenite is considered to be beneficial constituent because austenite is plastic and tough and localized strength of austenite increases with strain hardening. The better erosion resistance of hot rolled 21-4-N steel is also due to lesser amount of carbide in comparison to that in as cast and 8% rolled conditions.

6.6.2 Effect of mechanical properties on erosion

13/4 Steel

The cumulative weight loss at 30° impingement angle of 13/4 steel in both conditions as function of various mechanical properties is shown in Fig. 6.14. In this study it is seen that 8% rolled 13/4 steel shows higher erosion resistance as compared to that in as cast 13/4 steel at 30° impingement angle. In Chapter 4, it has been established that the values of hardness with retaining ductility, higher tensile toughness and higher strain hardening ability of the target material correspond to higher erosion resistance. From Fig. 6.14 it is observed that as a result of 8% rolling the impact energy decreases from 64 to 32 J, ductility decreases from 14 to 8% and tensile toughness decreases from 68 to 15 MJm^{-3}. The strain hardening exponent remains almost unchanged. However, there is increase in hardness from 305 to 350 VHN. In 13/4 steel at 30° impingement angle, the erosion, which occurs by ploughing mechanisms is reduced as a result of

rolling, because with increasing hardness the erosion rate through cutting and ploughing mechanisms becomes difficult. In soft material the erosion at 30^0 impingement angle through ploughing or scratching is easy as compared to hard material. Substantial increase in hardness makes the formation of ploughs too difficult by the erodent particles. Although the changes in impact energy, ductility, tensile toughness and strain hardening exponent suggest deterioration in erosion resistance at 30^o impingement angle, the overwhelming effect of hardness plays a greater role. Further, the SEM analysis shows smaller and finer ploughs suggesting that after rolling the formation of ploughs becomes difficult. The role of tensile toughness and strain hardening exponent comes only after ploughs are formed. Formation of ploughs becomes difficult due to increased hardness. Therefore the cumulative effect of all mechanical properties is reduction in erosion rate at 30^o impingement angle.

The cumulative weight loss at 90^o impingement angle of 13/4 steel in both conditions as function of various mechanical properties is shown in Fig. 6.15. The deterioration of erosion resistance of 13/4 steel is attributed to decrease in impact energy, ductility, tensile toughness and slight decrease in strain hardening exponent as a result of rolling. The decrease in impact energy implies that in 13/4 steel the ability of absorbing the energy of high velocity erodent particles decreases as a result of rolling. The decrease in ductility indicates that the 8% rolled 13/4 is less able to provide relief from high velocity erodent particles by way of partial consumption of their kinetic energy. The

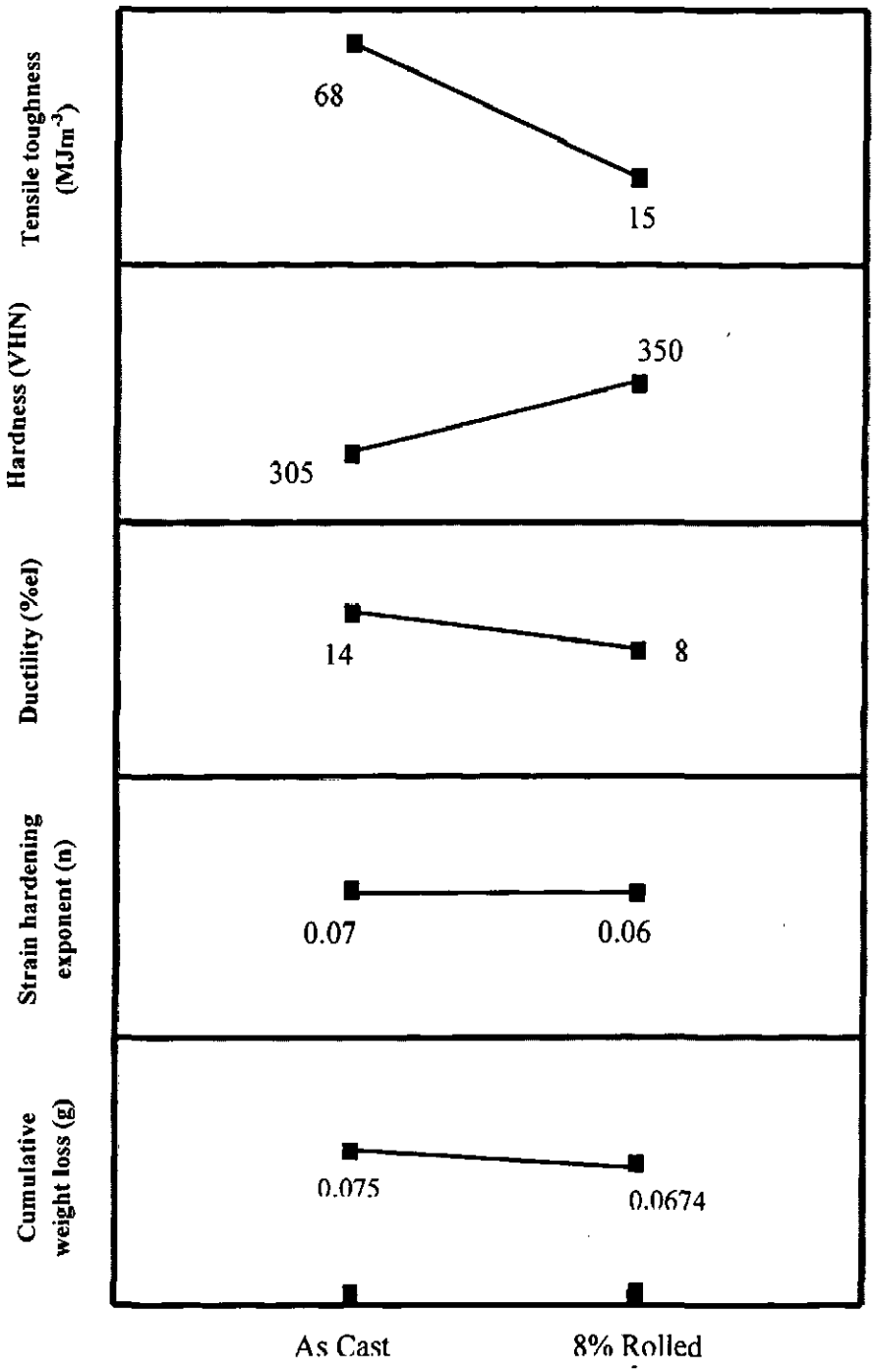

Fig. 6.14. Effect of mechanical properties on cumulative weight loss in 13/4 steel (impingement angle 30°)

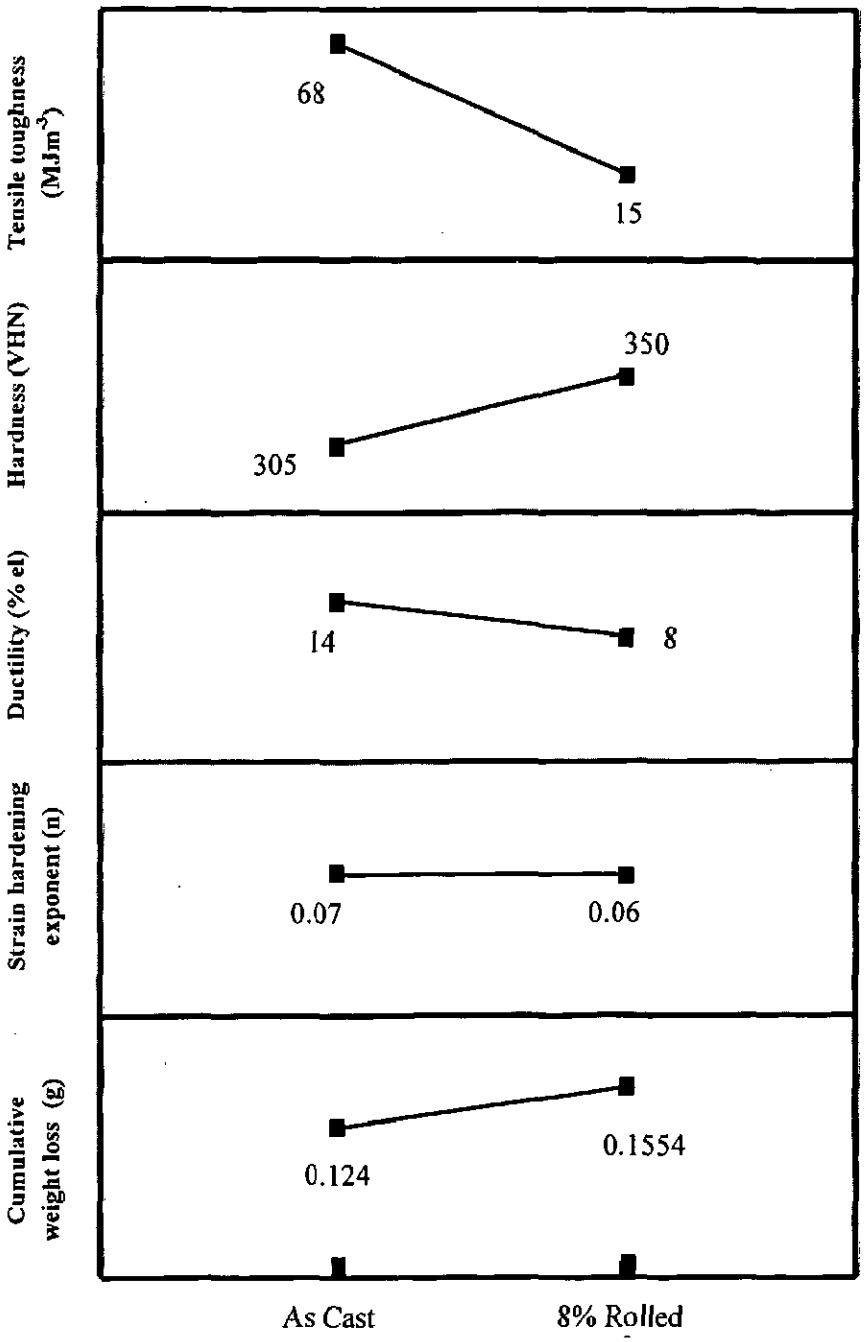

Fig. 6.15. Effect of mechanical properties on cumulative weight loss in 13/4 steel (impingement angle 90°)

decrease in tensile toughness implies that the 8% rolled 13/4 steel is unable to deform plastically and absorb the kinetic energy of the erodent particles and thus resulting in early formation of embrittled sub surface layer during erosion process. After 8% rolling, the ability of the 13/4 steel to plastic deformation decreases resulting in acceleration of erosion rate. Thus cumulative effect of all mechanical properties results in increased erosion rate at 90° impingement angle.

21-4-N steel

Figs. 6.16 and 6.17 show respectively the cumulative weight loss of 21-4-N steel as function of various mechanical properties at impingement angles of 30° and 90°. It can be seen from the results obtained for 21-4-N steel in as cast and rolled conditions that there is improvement in erosion resistance at 30° impingement angle, whereas at 90° impingement angle the erosion resistance deteriorates as a result of 8% rolling. The 8% rolling of 21-4-N steel results in lowering of ductility (17 to 8 %), tensile toughness (73 to 15 MJm^{-3}) and strain hardening exponent (0.46 to 0.06), whereas there is increase in hardness (320 to 400 VHN). The decreased values of ductility, tensile toughness and strain hardening ability showed cause reduction in erosion resistance at both impingement angles. But the substantial increase in hardness makes it too hard to erosion through cutting or ploughing by the erodent particles at 30° impingement angle resulting in reduction in erosion rate. The cumulative effect of all the mechanical properties results in increase in erosion resistance of 8 % rolled 21-4-N steel due to overwhelming effect

of hardness at 30° impingement angle. At 90° impingement angle, the erosion takes place through plastic deformation, strain hardening, embrittlement and finally dislodging of the chunk of material from the target surface. The increased value of hardness may cause decrease in erosion rate, but the dominating effects of reduction in ductility, tensile toughness and strain hardening exponent cause increased erosion rate at 90° impingement angle.

The hot rolling of 21-4-N steel results in increased values of ductility (17 to 29 %), hardness (320 to 339 VHN), tensile toughness (73 to 254 MJm^{-3}) and strain hardening ability (0.46 to 0.57). From Figs. 6.16 and 6.17 it is seen that cumulative weight loss is lowest in hot rolled 21-4-N steel at both the impingement angles. The decreased erosion rate at both the impingement angle is attributed to increased values of ductility, hardness, tensile toughness and strain hardening ability as a result of hot rolling of 21-4-N steel. The increased hardness and ductility in hot rolled 21-4-N steel respectively counteracts the effect of hard impinging erodent particles and the increased ductility provides relief from high velocity erodent particles by way of partial consumption of their kinetic energy in permitting localized deformation at impact sites, thus minimizing the chances of cracking. The higher value of tensile toughness in hot rolled 21-4-N steel enables it to absorb energy of the erodent particles in the plastic range. The increased work hardening ability of hot rolled 21-4-N steel increases the accumulation of elastic and plastic strains due to the impingement of erodent particles. These strains lead to *in situ* strain hardening in the sub surface region, which in turn

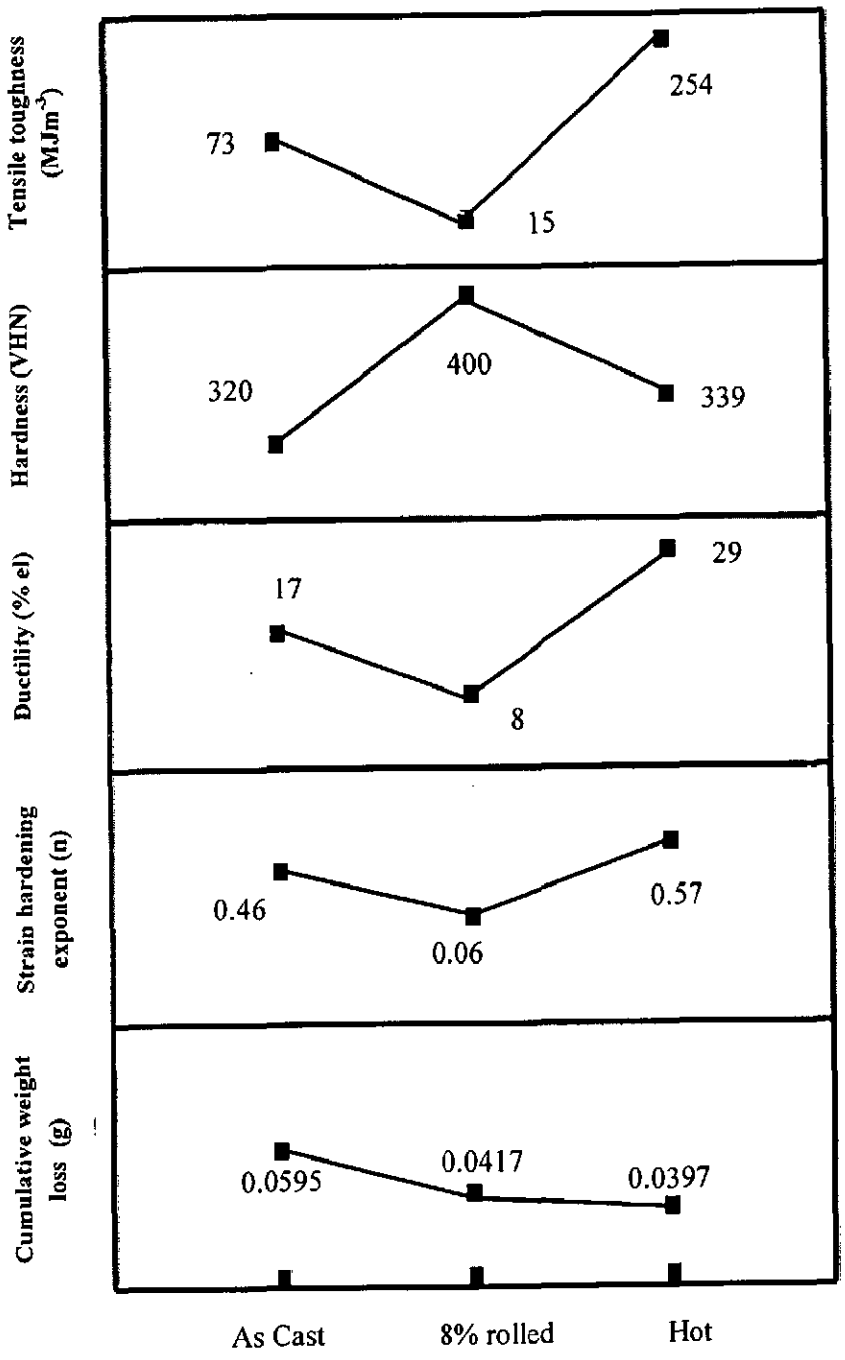

Fig. 6.16. Effect of mechanical properties on cumulative weight loss in 21-4-N steel (impingement angle 30°)

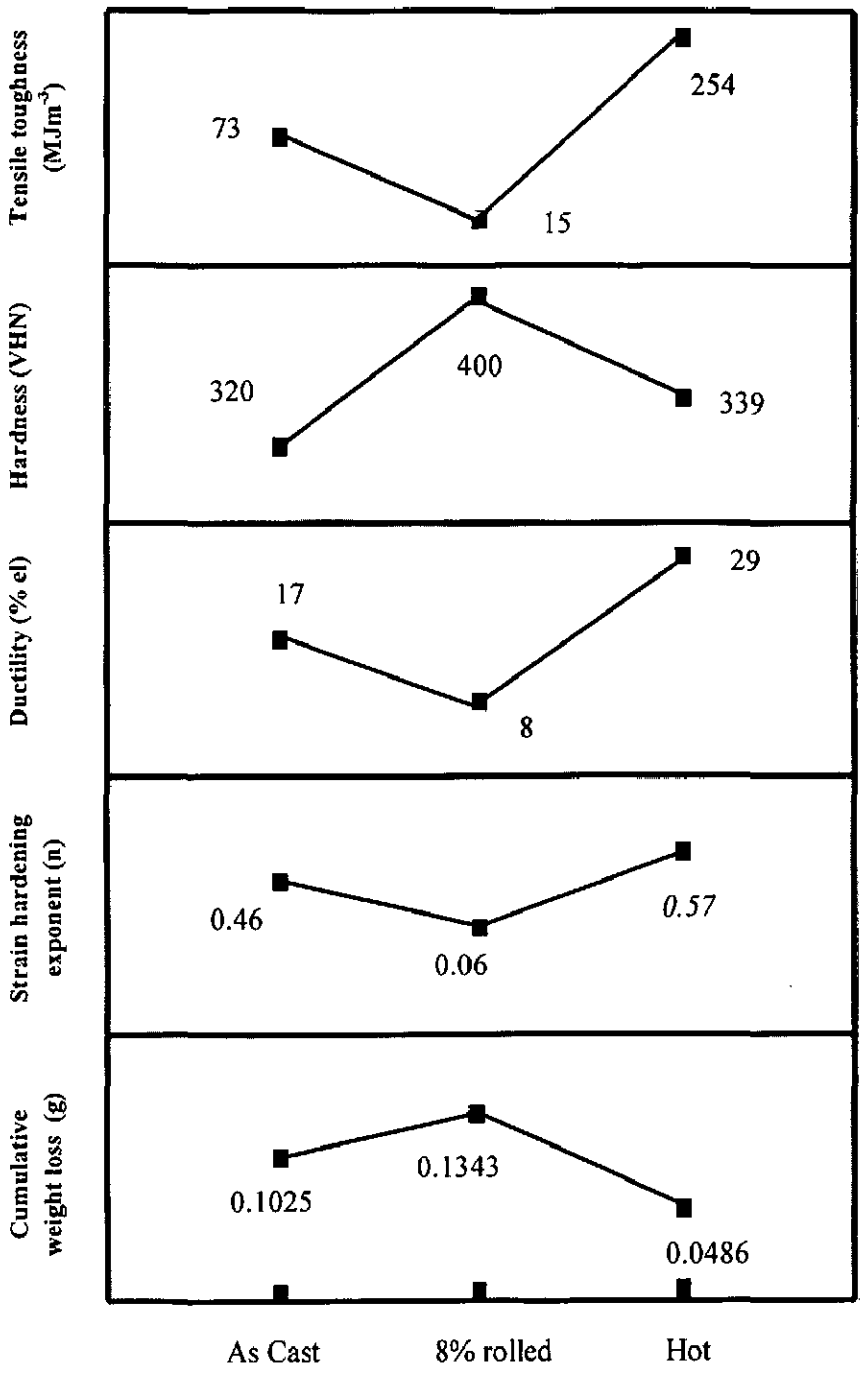

Fig. 6.17. Effect of mechanical properties on cumulative weight loss in 21-4-N steel (impingement angle 90°)

causes resistance to erosion. Thus increasing hardness without scarifying the ductility and tensile toughness by hot rolling of 21-4-N steel is the main factor for increasing erosion resistance. **Divakar et al** [50] have also shown that erosion resistance of AISI 316 steel increases with increasing hardness without impairing the ductility.

The SEM analysis of eroded surfaces of 13/4 steel eroded at 30° impingement angle show that the ploughs observed in 8% rolled 13/4 steel are smaller as compared to those in as cast 13/4 steel. The smaller ploughs observed in 8% rolled 13/4 steel are attributed to low values of ductility, tensile toughness and strain hardening exponent, because role of ductility, tensile toughness and strain hardening ability comes only after formation of ploughs. In 8% rolled 13/4 steel the formation of ploughs becomes difficult due to high hardness. However, once the ploughs form, the embrittlement and removal of lips is very rapid due to low values of ductility, tensile toughness and strain hardening exponent and this leads to formation of smaller ploughs.

The cavities and cracks observed in the SEM micrograph of 8% rolled 13/4 steel eroded at 90° impingement angle are deeper and wider as compared to those in as cast 13/4 steel suggesting more erosion damages in 8% rolled 13/4 steel. The deeper and wider cavities or cracks formed in 8% rolled 13/4 steel is due to lower values of ductility, tensile toughness and strain hardening exponent, which make it less able to absorb the kinetic energy of the erodent particles and this results in rapid embrittlement of sub surface layer, which leads to rapid erosion.

The SEM study of eroded surface of 21-4-N steel indicates that the ploughs formed at 30° impingement angle are shallower and the cavities are deeper and wider, which are created due to impingement of erodent particles at 90° impingement angle in 8% rolled steel as compared to those in as cast condition. The lowering of ductility, tensile toughness and strain hardening exponent in 21-4-N steel as a result of 8% rolling cause less elongation and rapid embrittlement of the lips nucleated due to erodent particles impinging at 30° impingement angle resulting in smaller ploughs. At 90° impingement angle the low values of ductility, tensile toughness and strain hardening exponent of 8% rolled 21-4-N steel make it less able to deform plastically and also decrease the capacity of absorbing the kinetic energy of the erodent particles. This results in rapid embrittlement of sub surface layers leading to higher erosion damage.

6.7 Conclusions

1. In 13/4 steel the martensitic laths are thickened as a result 8% reduction in thickness by rolling at 700 °C. The values of YS, UTS and hardness increase whereas the values of ductility, tensile toughness and impact energy decrease as a result of rolling. However, the strain hardening exponent remains almost unchanged.

2. In 21-4-N steel no significant change is observed in the microstructure; however considerable changes in mechanical properties are observed as a result of 8% rolling at 700 °C. The values of YS, UTS and hardness increase and the values of tensile toughness, ductility, impact energy and strain hardening exponent decrease as a result of 8% rolling.

and cracks created are deeper and larger in 8% rolled condition as comparison to those in as cast condition.

Chapter 7

Cavitation erosion resistance of 13/4 and 21-4-N steels

This chapter deals with the cavitation erosion behaviour of 13/4 and 21-4-N steels investigated by means of ultrasonic vibration processor as described in experimental procedures (Chapter 3). The cavitation erosion behaviour of 13/4 and 21-4-N steels has been analyzed as a function of microstructure, mechanical properties and alloying elements.

7.1 Introduction

Cavitation erosion is responsible for many machinery failures in the shipping and power generation industries. Cavitation erosion is a type of wear in systems in which a material comes into contact with a flowing liquid, e.g. hydro turbines, ship propellers etc. The bubble explode during cavitation generates very high and transient stresses [9], which strains the materials in a particular way. For efficient operation of a hydro turbine, it must have specific shape and contour. Cavitation erosion leaves behind cavities or pits which affect these important contours, creating obstacles to smooth flow of water through the turbine. This leads to a loss of operating efficiency of the turbine. Considering the cost of electrical energy, even a relatively small change in the operating efficiency can be very expensive. Cavitation causes surface penetration damage of up to 10 mm per year to critical components such as impellors, turbine blades, and casings [21]. The end result is

a reduction in energy extraction capacity that can lead to losses in terms of downtime, productivity, efficiency and money.

The martensitic chromium nickel stainless steel (13/4 or CA6NM steel) has wide application in hydro turbines, pumps and compressors. The erosion resistance of martensitic stainless steels can be attributed to the homogeneous distribution of deformation and the shorter effective mean free platelets of martensite [9]. It has been reported that the cavitation-erosion-resistance is related to the degree of solution hardening of the matrix and the quantity, the structure, hardness, super-elasticity and super – plasticity [188-191]. To overcome the problems of cavitation erosion, there is a need to develop a cavitation erosion resistant material for the fabrication of the underwater parts of hydro turbines. In the earlier chapters, the results on erosion by air-abrasive jets have been reported. In many critical applications, the net erosion loss is due to combined effect of erodent particles and cavitation. In this chapter results on study of erosion due to cavitation alone has been reported.

7.2 Cavitation erosion behaviour

The cumulative weight loss due to cavitation erosion for the samples in this investigation is plotted as function of time of cavitation erosion in Fig. 7.1, while Fig. 7.2 presents mean depth of erosion (MDE) versus time of erosion curve. MDE is calculated using equation 3.1. From Fig. 7.1 and 7.2 it is noticed that cumulative weight loss versus time of erosion curve and MDE as function of time of erosion curve are almost identical,

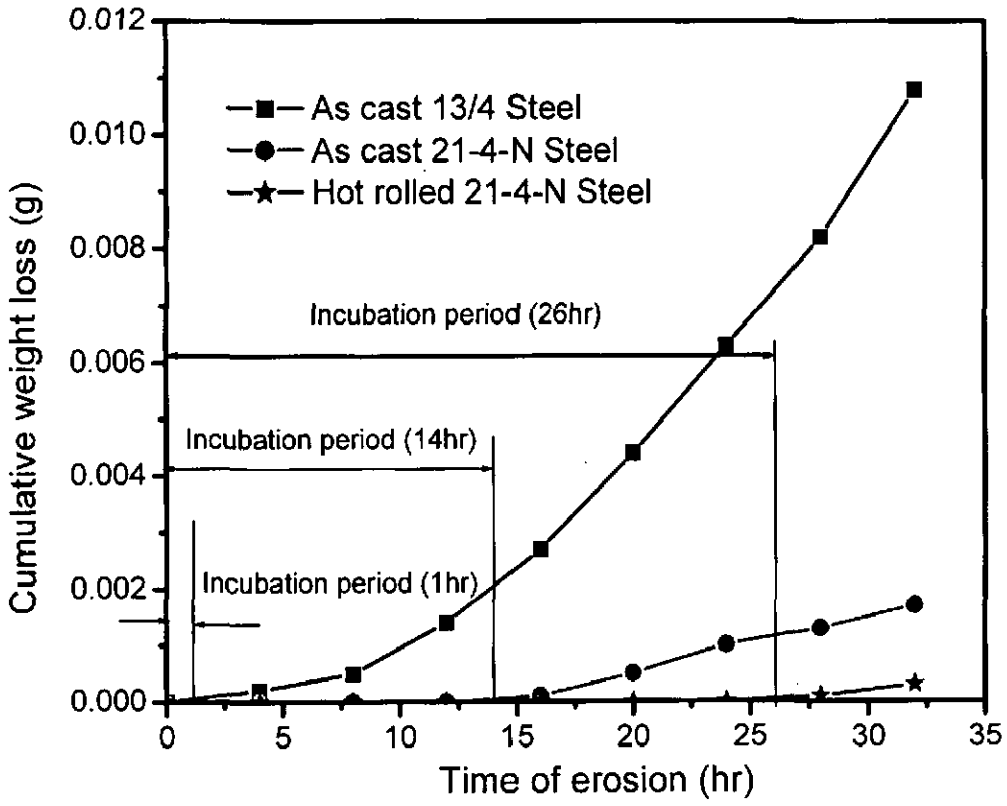

Fig. 7.1. Cumulative weight loss as function of time of cavitation erosion

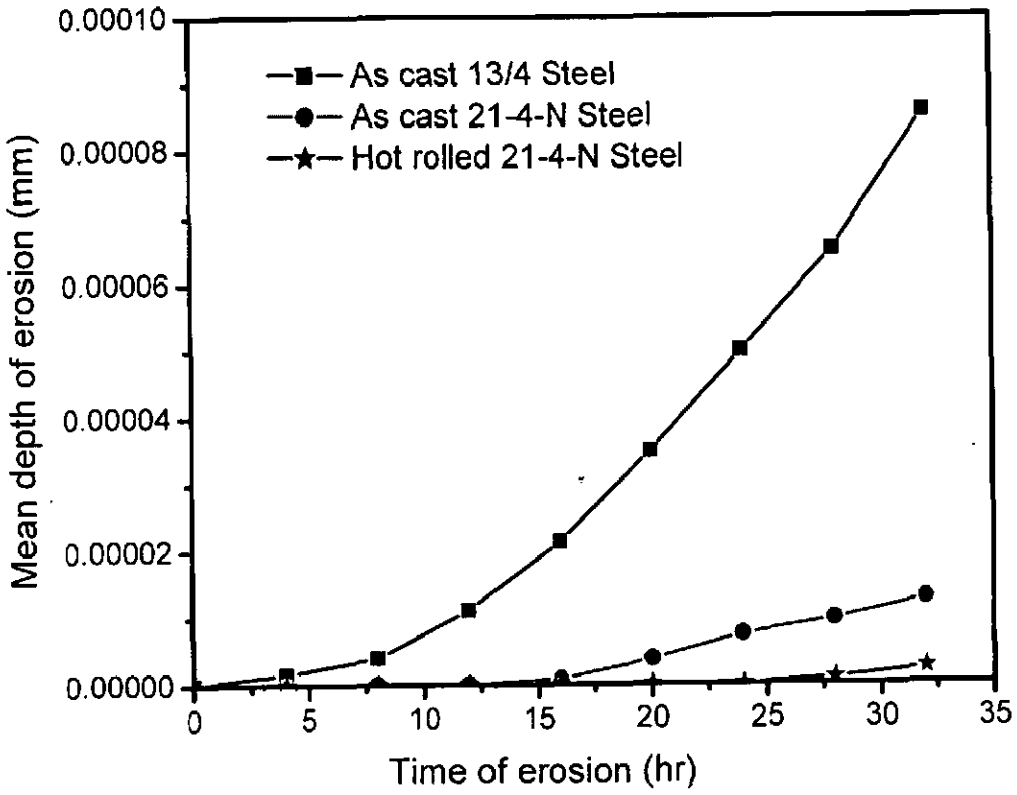

Fig. 7.2. Mean depth of erosion (MDE) as function of time of cavitation erosion

because of the marginal difference in the densities of 13/4 steel (7.795 gcm^{-3}) and 21-4-N steel (8.137 gcm^{-3}), which is the only variable in the determination of MDE in this investigation. The erosion rate in as cast 13/4 steel is more than that in 21-4-N steel in both as cast and hot rolled conditions similar to solid particle erosion rate as described in Chapters 4 and 6. However, the erosion resistance of 21-4-N steel in both as cast and hot rolled conditions in cavitation erosion is far better than that in solid particle erosion.

7.3 Morphology of eroded surfaces

Optical micrographs of the steels under investigation after different exposure of time during the test are shown in Figs. 7.3 - 7.5 and the SEM micrographs after 32 hr of cavitation erosion test are shown in Fig. 7.6. The material loss results presented in Fig. 7.1 and images obtained (Figs. 7.3 - 7.6) show a distinctive behavior as a function of cavitation erosion time that can be divided in two stages: the first stage is characterized by an incubation period during which very little material loss is detected and the second stage represents a steady state erosion condition, where there is almost constant rate of material removal from the surface of the eroded specimen. The incubation time seems to be dependent on the microstructure as well as strain hardening ability of the alloys. The incubation time for hot rolled 21-4-N steel is 26 hr, for as cast 21-4-N steel is 14 hr and for as cast 13/4 steel it is 1 hr. Very less incubation period possesses by 13/4 steel is because of its martensitic structure.

The micrographs shown in Fig. 7.3 are very similar to those reported by **Liu et al** [122] for 0Cr13Ni5Mo stainless steel. In 13/4 steel the deformation due to cavitation attack is restrained in martensitic laths during initial stages of cavitation erosion (Fig. 7.3b). Since the material is removed from the surface of 13/4 steel as cavitation erosion goes on, the martensitic laths are no more distinguished in a straight forward manner (Fig. 7.3c and d).

Contrary to 13/4 steel, the cavitation erosion morphologies of as cast 21-4-N steel are different due to its austenitic structure. There is no obvious damage in the surface of as cast 21-4-N steel after 8hr of cavitation erosion (Fig. 7.4). It can be seen that the damages develop mainly at austenite-carbide boundaries and this is a characteristic of cavitation, i.e. preferential attack on the weakest phase of a material. This observation is identical with that of **Okada et al** [120], in which it has been reported that the graphite inclusions provide the required crack initiation centers for rapid wear by brittle fracture. After 32 hr of cavitation erosion in the as cast 21-4-N steel the cavities are formed due to material removal at austenite-carbide boundaries (Fig 7.4d).

The cavitation erosion of hot rolled 21-4-N steel is different from that of the as cast condition due to its fine austenitic microstructure. This observation is similar to the observation reported by **Garzon et al** [192]. It has been reported that plastic deformation intensity in each grain is different due to both its own lattice spatial orientation and its neighbor's lattice spatial orientation. After 8 hr of cavitation erosion, no obvious eroded

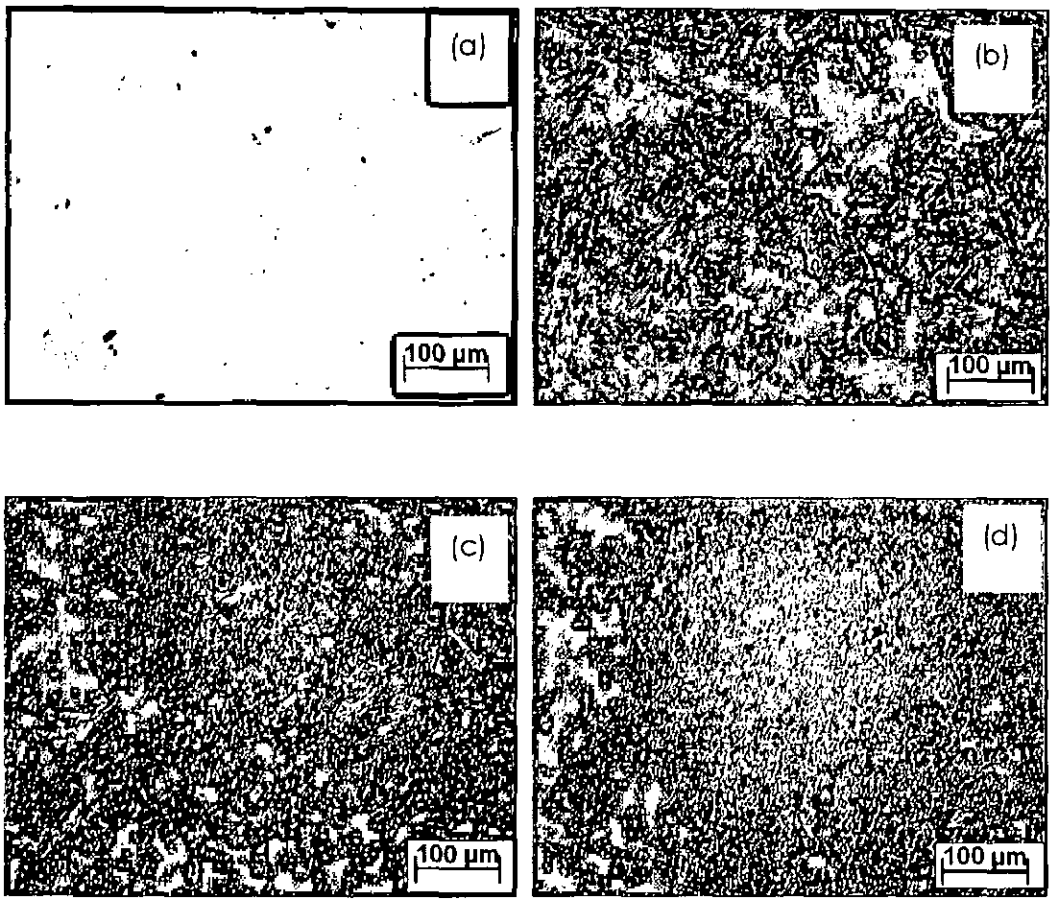

Fig. 7.3. Optical micrographs of as cast 13/4 steel (a) before cavitation erosion, (b) after 8 hr of cavitation erosion, (c) after 16 hr of cavitation erosion and (d) after 32 hr of cavitation erosion

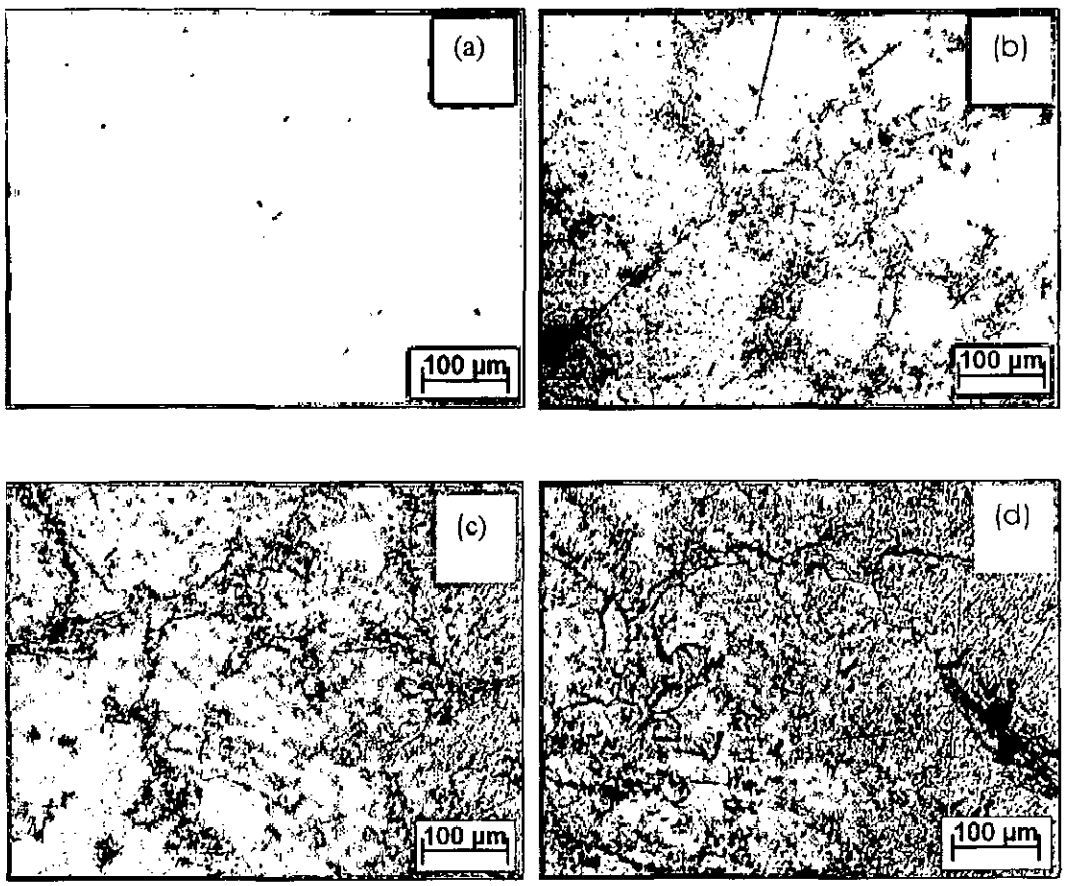

Fig. 7.4. Optical micrographs of as cast 21-4-N steel (a) before cavitation erosion, (b) after 8 hr of cavitation erosion, (c) after 16 hr of cavitation erosion and (d) after 32 hr of cavitation erosion

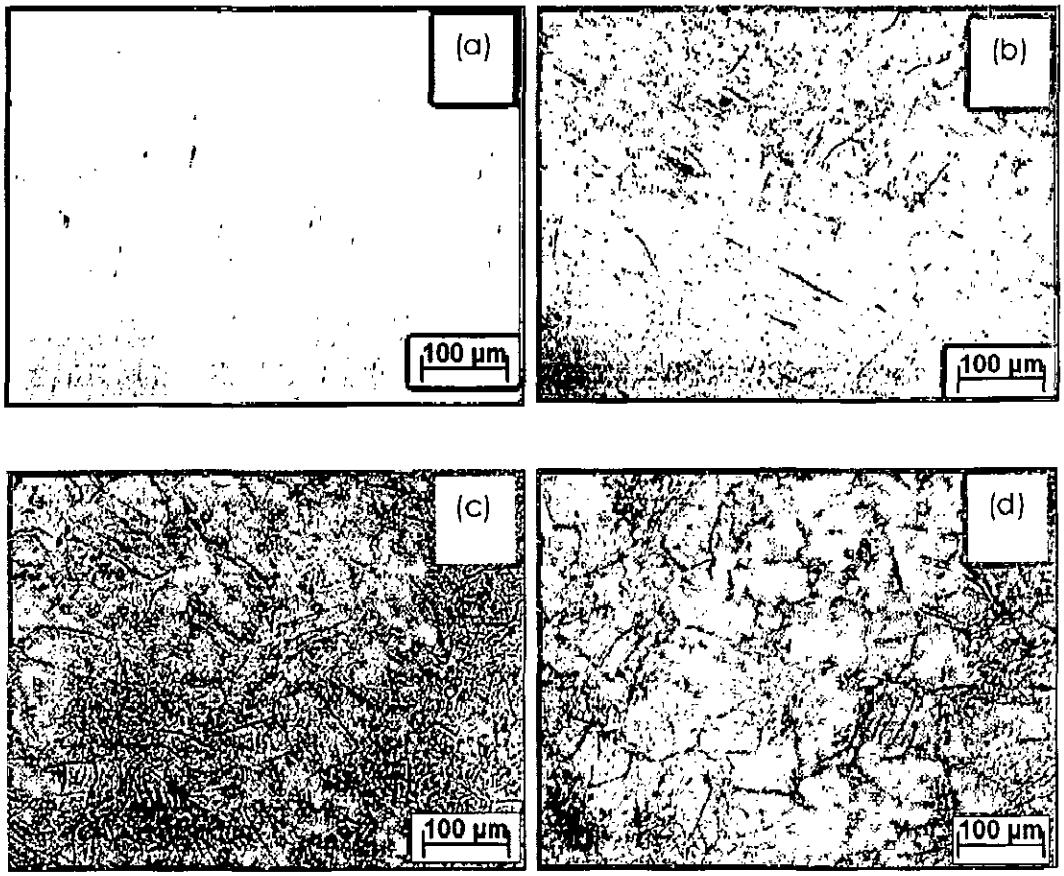

Fig. 7.5. Optical micrographs of hot rolled 21-4-N steel (a) before cavitation erosion, (b) after 8 hr of cavitation erosion, (c) after 16 hr of cavitation erosion and (d) after 32 hr of cavitation erosion

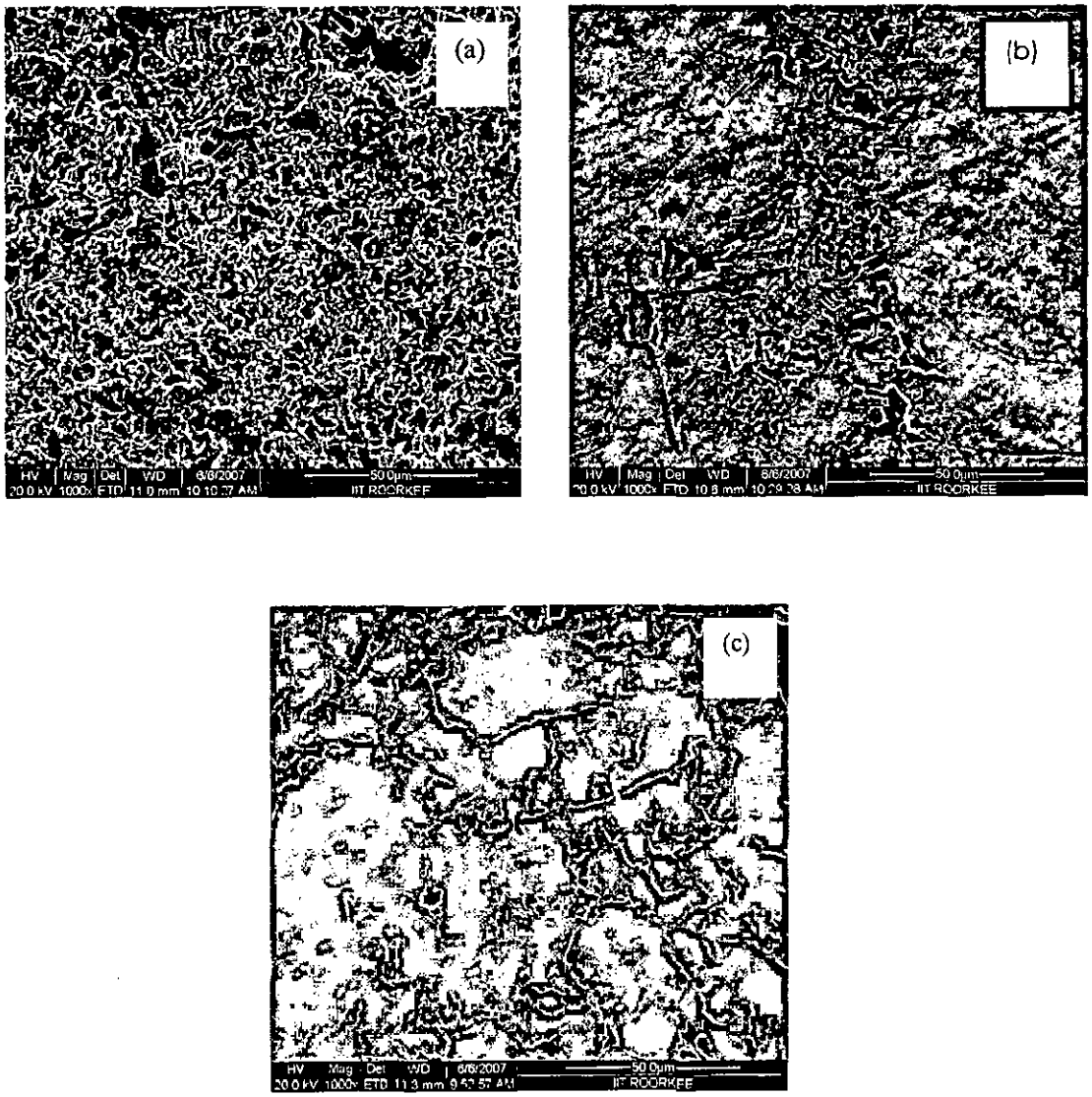

Fig. 7.6. SEM micrographs of eroded surface of (a) 13/4 steel, (b) as cast 21-4-N steel and (c) hot rolled 21-4-N steel

marks are seen in the surface (Fig. 7.5b). After cavitation erosion of 16 hr, the grain boundaries become visible (Fig. 7.5c). This indicates cavitation erosion occurs preferentially near carbide network located at grain boundaries. After 32 hr of cavitation erosion also the damages are observed along the austenite grain boundaries (Fig. 7.5d).

Fig. 7.6 shows the SEM micrographs of eroded surface of as cast 13/4 steel, as cast 21-4-N steel and hot rolled 21-4-N steel, after 32 hr of cavitation erosion test. The SEM micrograph of 13/4 steel, after 32 hr of cavitation erosion (Fig. 7.6a), is similar to the result of **Zhang et al** [193] for ZG06Cr13Ni5Mo. In this case cavitation holes are formed during 32 hr of cavitation erosion test and micro cracks are also observed. The SEM micrograph of eroded surface of as cast 21-4-N steel shows that the cavitation erosion starts along the interfaces between austenite and carbides (Fig. 7.6b). The cavitation holes are seen in the carbide regions. This may be due to the brittleness associated with carbides. The cavitation holes seen in the SEM micrograph of hot rolled 21-4-N steel may also be due to removal of carbide particles. The SEM micrographs of eroded surface of all the three specimens again suggest that higher erosion damage occurred in 13/4 steel.

7.4 Discussion

7.4.1 Effect of microstructure

The results of cavitation erosion test show that 21-4-N steel (as cast as well as hot rolled) because of its austenitic structure, gives more resistance against cavitation erosion

in comparison to 13/4 martensitic stainless steel. During cavitation erosion, the target material is subjected to very high repeated loading by cavitation impact wave. The microstructure of target material plays a vital role in cavitation erosion. In 13/4 steel the martensitic structure, which is less likely to develop *in situ* strain hardening, and δ-ferrite are the sources of cavitation attack. The austenitic matrix of 21-4-N steel, which is plastic and tough, is found to be beneficial parameters against cavitation erosion. **Xi and Zhou** [134] have reported in austenitic stainless steels, that the interface between carbide and austenite is associated with high stresses. As a result the interface between carbides and austenite is observed to be attacked severely in 21-4-N steel as compared to austenitic matrix. The interfaces are not able undergo strain hardening and consequently become brittle and fragmented by cavitation attack; while the localized strength of austenite increases with strain hardening during cavitation erosion. **Soussan and Degallaix** [135] have also analyzed that the localized strength of austenite in austenitic stainless steel increases with strain hardening. That is why, the austenite-carbide grain boundaries are attacked more in comparison to austenite grains of the as cast as well as hot rolled 21-4-N steel.

7.4.2 Effect of Mechanical properties

Due to the repeated attack by cavitation impact wave, the target material undergoes deformation plastically. The hot rolled 21-4-N steel possesses higher ductility than the corresponding value for as cast 13/4 and 21-4-N steels. As a result the former is

able to sustain load for longer duration than the latter for given value of deformation. 13/4 steel shows highest erosion damage (weight loss) of the three samples. The as cast 13/4 and 21-4-N steels having low ductility (14 and 17% respectively) show more erosion damage than that in hot rolled 21-4-N steel having higher ductility (29 %). Primarily the hardness and ductility have been identified as main properties affecting erosion behavior [50]. The hardness of the target material is detrimental to cavitation erosion resistance. Hot rolled 21-4-N steel possesses high hardness (339 VHN) as compared to as cast 21-4-N steel (320 VHN) and 13/4 steel (305 VHN) may erode rapidly, but cumulative effect of hardness and ductility results in less erosion damage. The high ductility and hardness of hot rolled 21-4-N steel are responsible for more cavitation erosion resistance.

The cavitation erosion resistant materials should also absorb the energy of the cavitation impact wave, which delays the nucleation of cracks. The tensile toughness of a material is its ability to absorb energy in the plastic range. The tensile stresses induced in the material is not equivalent to the stresses developed in the tensile test described earlier since the strain rate is very high during cavitation erosion test. However, a correlation can be established from the cavitation erosion test results and tensile toughness. The values of tensile toughness are 68, 73 and 254 MJm^{-3} as determined in earlier chapters from the area under their respective stress-strain curve between YS and fracture stress. It can be inferred that higher tensile toughness corresponds to more cavitation erosion resistance.

The higher tensile toughness of hot rolled 21-4-N steel enables it to deform plastically due to repeated loading of cavitation attack and also absorbs more strain energy.

7.4.3 Effect of strain hardening

Steels with an austenitic matrix are more likely to develop *in situ* work hardening as compared to those with a martensitic structure. In this context, the stacking fault energy of the austenitic matrix plays an important role, as low stacking fault energy may cause a high rate of work hardening. In Fe-Cr-Ni alloys **Schramm and Reed** [72] have reported that Cr rapidly reduces the stacking fault energy. They have observed that Ni and C addition tend to increase the stacking fault energy while Cr, Si, Mn and N tend to decrease stacking fault energy in Fe-Cr-Ni austenitic alloys. The higher resistance to cavitation erosion in 21-4-N steel (as cast and hot rolled) can therefore, be attributed to the low stacking fault energy of its austenitic matrix.

From stress-strain diagram, it is noticed that severe *in situ* strain hardening occurs during tensile testing in both as cast (Fig. 4.9) and hot rolled (Fig. 6.5) 21-4-N steel, whereas less strain hardening takes place during tensile testing of 13/4 steel (Fig. 4.9). During cavitation erosion high strain hardening exponent of 21-4-N steel corresponds to higher cavitation erosion resistance in comparison to 13/4 steel possessing lower strain hardening exponent. From the SEM study of eroded surfaces (Fig. 7.6a), it can be inferred that the martensitic laths of 13/4 steel embrittled earlier than austenite matrix in 21-4-N steel in both as cast and hot rolled conditions. The austenite matrix of 21-4-N

steel (Fig. 7.6b and c) deforms plastically and *in situ* strain hardening occurs, which delays the nucleation of cracks. This is in agreement with the results reported by **Liu et al** [122]. The austenite carbide boundaries of as cast 21-4-N steel are not able to undergo *in situ* strain hardening and become the sources of initiation of cracks. Therefore as cast 21-4-N steel is erode more in comparison to hot rolled 21-4-N steel.

7.5 Conclusions

1. The cavitation erosion resistance of 13/4 steel investigated by means of ultrasonic vibration processor is less than that of 21-4-N steel in both as cast and hot rolled conditions. However, hot rolled 21-4-N steel exhibits excellent cavitation erosion resistance.

2. From the microstructure view point, the untempered martensitic laths of 13/4 steel erode more rapidly than the austenitic structure of 21-4-N steel. The martensitic laths, already associated with internal stresses, are less able to absorb the strain energy due to transient stresses in the material induced by cavitation impact wave. It can also be inferred that the carbides present in 21-4-N steel are detrimental to cavitation erosion resistance leading to more erosion in as cast condition.

3. In 21-4-N steel in both as cast and hot rolled conditions, the cavitation erosion damages occur along the grain boundaries and the carbides are the first to be dislodged from the specimens.

4. In 21-4-N steel higher resistance to cavitation erosion is due to high hardness coupled with high ductility, high tensile toughness and high strain hardening exponent in comparison to those in 13/4 steel.

Chapter 8

Erosive wear of surface coated hot rolled 21-4-N steel

In the present investigation stellite-6, Cr_3C_2-NiCr and WC-Co-Cr coatings were deposited by D-Gun on a hot rolled 21-4-N steel meant for fabrication of hydro turbine underwater parts. The coatings have been characterized for microstructure, porosity, microhardness and crystalline nature. The erosion experiments were carried out using an air jet erosion test rig at a velocity of 120 ms^{-1} and impingement angles of 30° and 90°. Silicon carbide particles of size ranging between 500-700 μm were used as erodent. Scanning electron microscopy (SEM) technique was used to analyze the nature and mechanism of erosion.

8.1 Introduction

The loss of material caused by the impingement of tiny solid particles, which have a high velocity and impact on the material surface at defined angles, is called erosive wear. Erosion is a serious problem in many engineering systems, including steam and hydro turbines, pipelines and valves used in slurry transportation of matter, and fluidized bed combustion systems. Coatings of wide variety of materials are commonly applied for many purposes, especially to improve tribological performance; that include the enhancement of mechanical properties, visual appearance or corrosion resistance and optical properties. It has been reported that the thermal spray is a technique that produces

a wide range of coatings for various applications [194]. Erosion tests on coatings have been widely reported [59, 60, 146, 178, 195-198]. The mechanisms of coating damage in such tests depend on the coating material and its thickness, the properties of the interface, the substrate material and the test conditions [146].

Among the commercially available thermal spray coating techniques, detonation spray and high velocity oxy fuel spray are the best choices to get hard, dense and consequently wear resistant coatings [59-61]. Thermally sprayed coatings of thickness of 200-400μm offer an effective and economic method of conferring wear resistance without compromising other attributes of the component. Detonation Gun (D-Gun) spraying has shown to be one of the best methods for depositing coatings because of the higher velocities and lower temperatures experienced by the powder particles [199, 200]. **Wang** [60] examined the chromium carbide-nickel chromium coatings on mild carbon steel with different volume fractions of carbides and verified that the coatings with 75% carbide were dense with good bonding to substrate.

8.2 Characterization of coatings

8.2.1 Microstructures and XRD spectra

Figs. 8.1 and 8.2 show the XRD spectra and optical micrographs respectively of stellite-6 coating. From the peaks in XRD spectra (Fig. 8.1), it is observed that the stellite-6 coating consists of $Cr_{23}C_6$ and Co (γ or fcc), of which chromium carbide ($Cr_{23}C_6$) is the dominating hard phase. The microstructure of stellite as shown in Fig. 8.2

consists of fine chromium carbides in the austenitic matrix of Co. Some of the dark etching regions may also be due to porosity. Identical observation has been reported by **Singh et al** [201] for plasma sprayed stellite-6 coating on Fe-based superalloy.

Figs. 8.3 and 8.4 show the XRD spectra and optical micrograph of the Cr_3C_2-NiCr coating. From the peaks in XRD spectra (Fig. 8.3), it is observed that the Cr_3C_2-NiCr coating is made up of carbides and oxide phases, including Cr_3C_2, Cr_3Ni_2 and Cr_2O_3. In HVOF Cr_3C_2–NiCr coating, apart from Cr_3C_2 carbide particles, the carbides Cr_7C_3 and $Cr_{23}C_6$ might be also present according to the reported results through X-ray diffraction analyses [202]. It is likely that these carbides are formed through decarburization of Cr_3C_2. However, it is further pointed out that the presence of Cr_7C_3 and $Cr_{23}C_6$ in the as-sprayed Cr_3C_2–NiCr coating cannot be proven solely by X-ray diffraction approach because their main diffraction peaks coincide with the lines referring to the NiCr and Cr_3C_2. As seen in Fig. 8.4, the microstructure of Cr_3C_2-NiCr coating is characterized by bright phases as the binding matrix in which the dark/gray regions are carbides of type Cr_3C_2 and/or chromium oxide (Cr_2O_3). The very dark points observed in the binding matrix may be due to porosity. The similar observations have been reported by **Wang et al** [200]

Figs. 8.5 and 8.6 show the XRD spectra and optical micrograph of the WC-Co-Cr coating. From the peaks in XRD spectra (Fig. 8.5), it is observed that the WC-Co-Cr coating contains Co_3W_3C, WC, W_2C and CrCo, of which Co_3W_3C and WC are the major

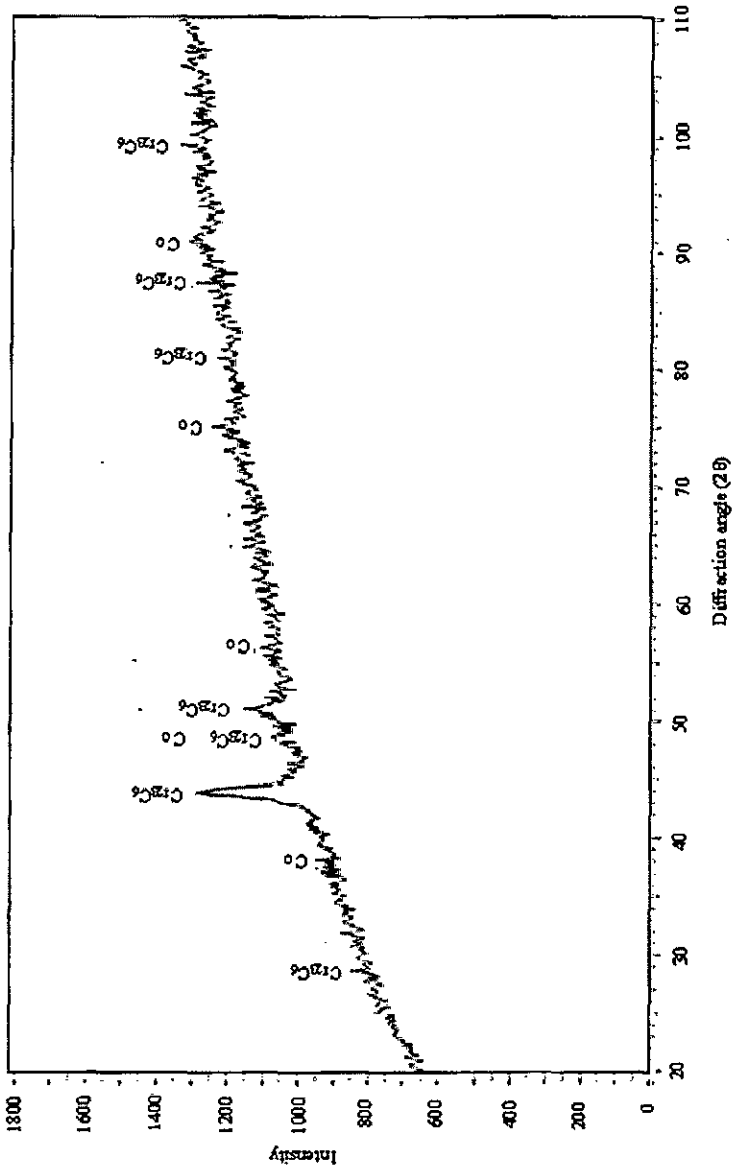

Fig . 8.1. XRD spectra of stellite-6 coating

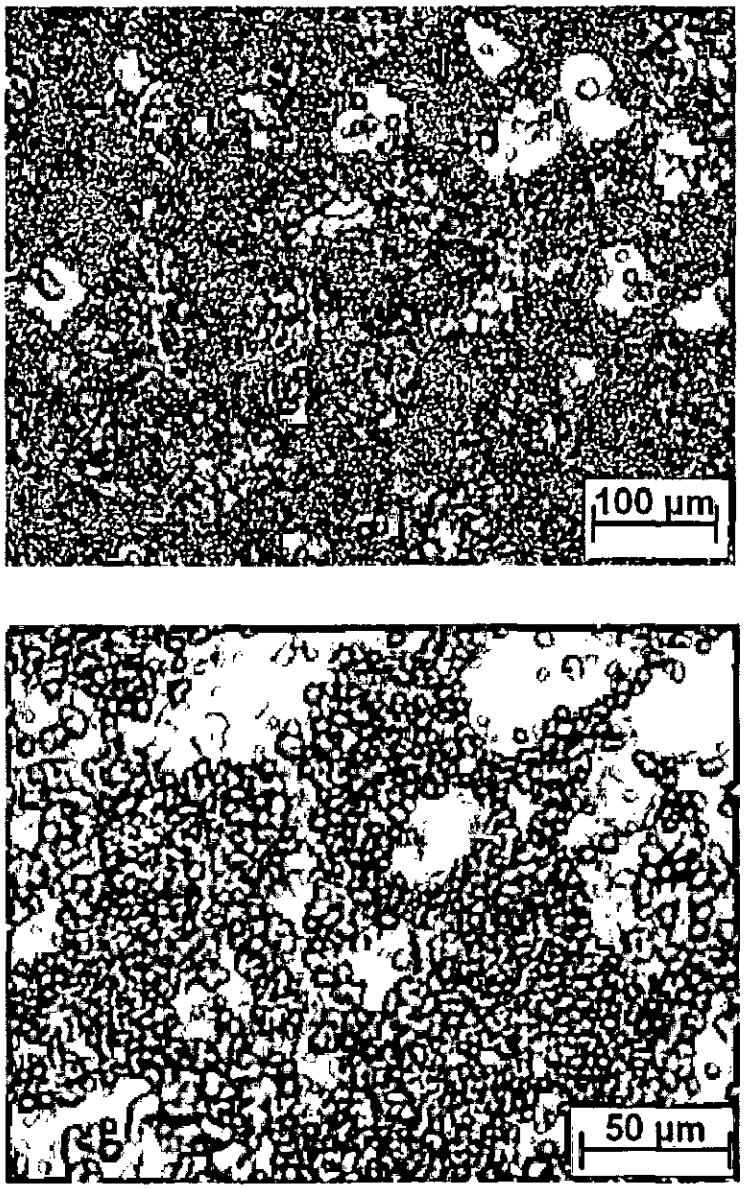

Fig. 8.2. Optical micrographs of stellite-6 coating

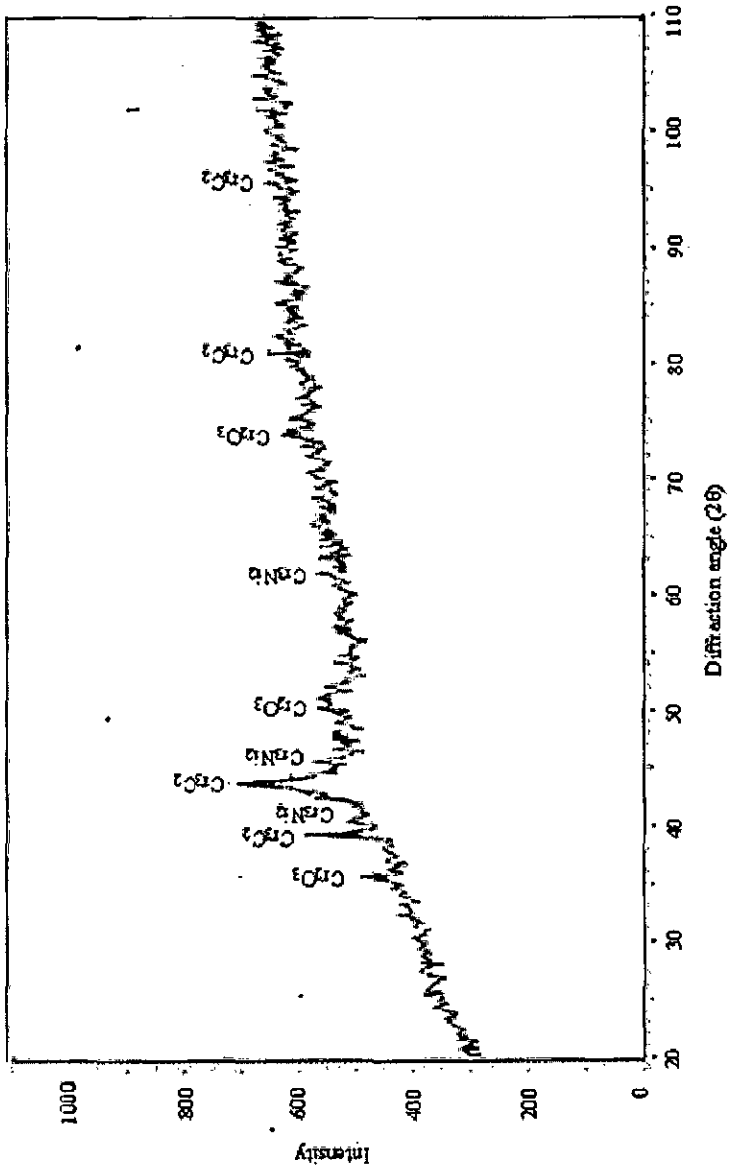

Fig. 8.3. XRD spectra of Cr_3C_2-NiCr coating

hard phases. The presence of W_2C phase in this coating indicates the decarburization of WC during coating process. Chromium addition to WC-Co inhibits the decarburization of WC to metallic tungsten. The similar XRD peaks have also been reported by **Sahraoui et al** [203] **and Zhang et al** [193]. As seen in Fig. 8.6 the microstructure of WC-Co-Cr coating consists of carbides well distributed and bonded within the Co based binding matrix. Bright/gray areas indicate binding matrix in which WC is dissolved in solution. Dark particles of carbides are seen in blocks of bright etching binding matrix. Identical observations have been reported by **Murthy et al** [159].

8.2.2 Porosity and microhardness measurements

The average porosity and microhardness of the D-Gun sprayed coatings are given in Table 8.1. The average porosity of the D-Gun sprayed coatings is found to be in the range of 0.03–0.29%. The stellite-6 coating exhibits highest hardness of 1098 HV, as also reported by **Zhang** [204] **and Zhao et al** [205]. This coating, however, suffered from maximum porosity of 0.29%. The porosity as well as microhardness of the stellite-6 coating is observed to be highest of the three coatings. The porosity of WC-Co-Cr coating is found to be lowest of the three coatings, whereas the minimum value of the average microhardness is shown by Cr_3C_2-NiCr coating. The measured values of porosities of Cr_3C_2-NiCr and WC-Co-Cr coatings in this investigation are much less as compared to the observations of **Sahraoui et al** [203] for HVOF coatings.

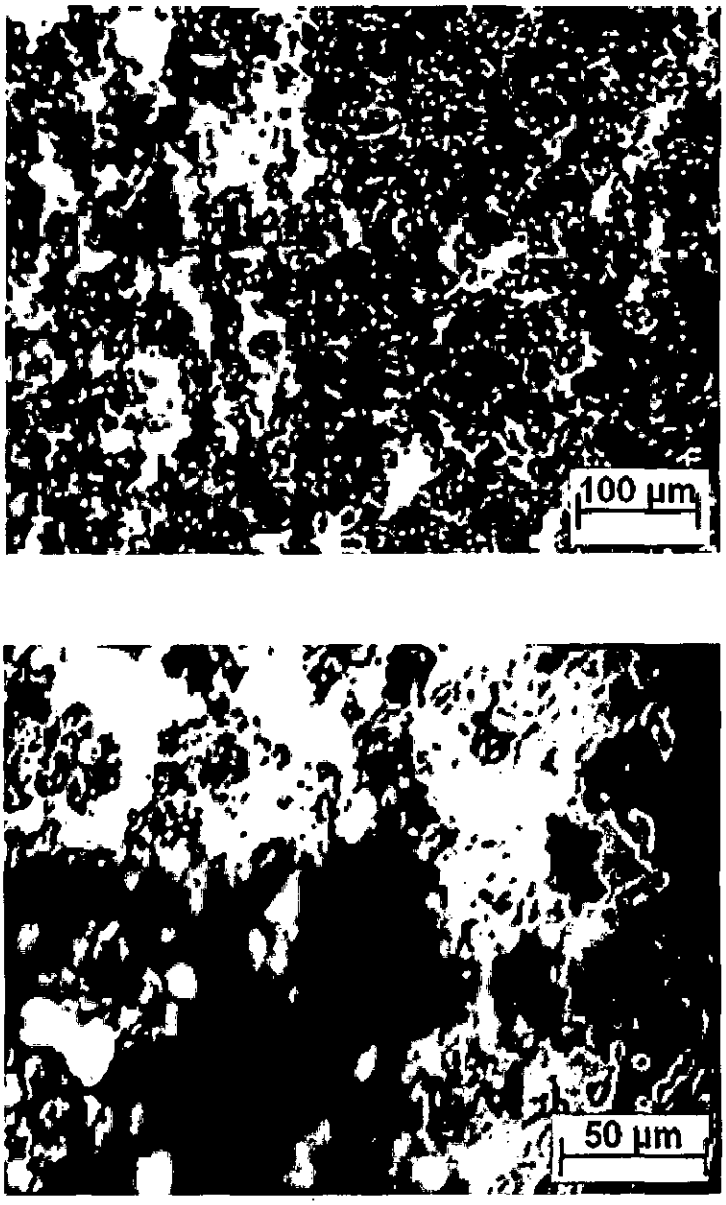

Fig. 8.4. Optical micrographs of Cr_3C_2-NiCr coating

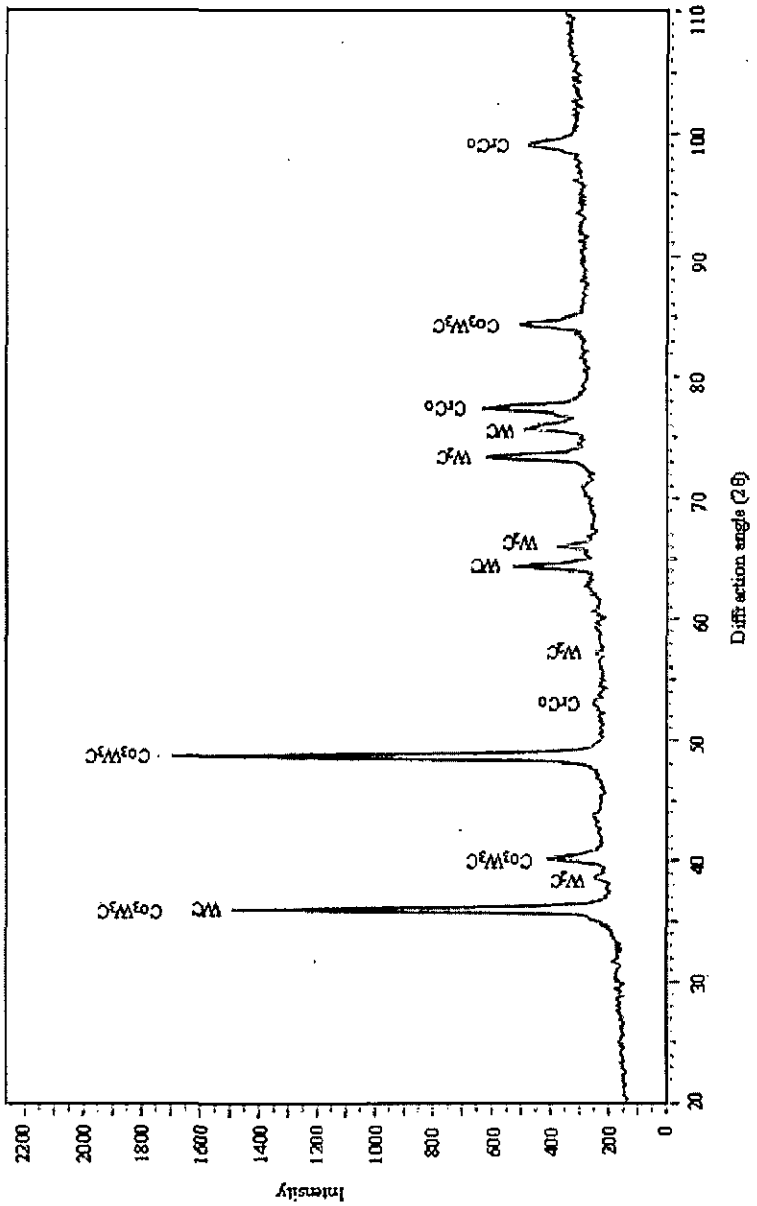

Fig. 8.5. XRD spectra of WC-Co-Cr coating

Table 8.1. Porosity and microhardness of coatings

Coating material	Average Porosity %	Microhardness ($HV_{0.2}$)
Stellite-6	0.29	1098
Cr_3C_2-NiCR	0.10	824
WC-Co-Cr	0.03	990

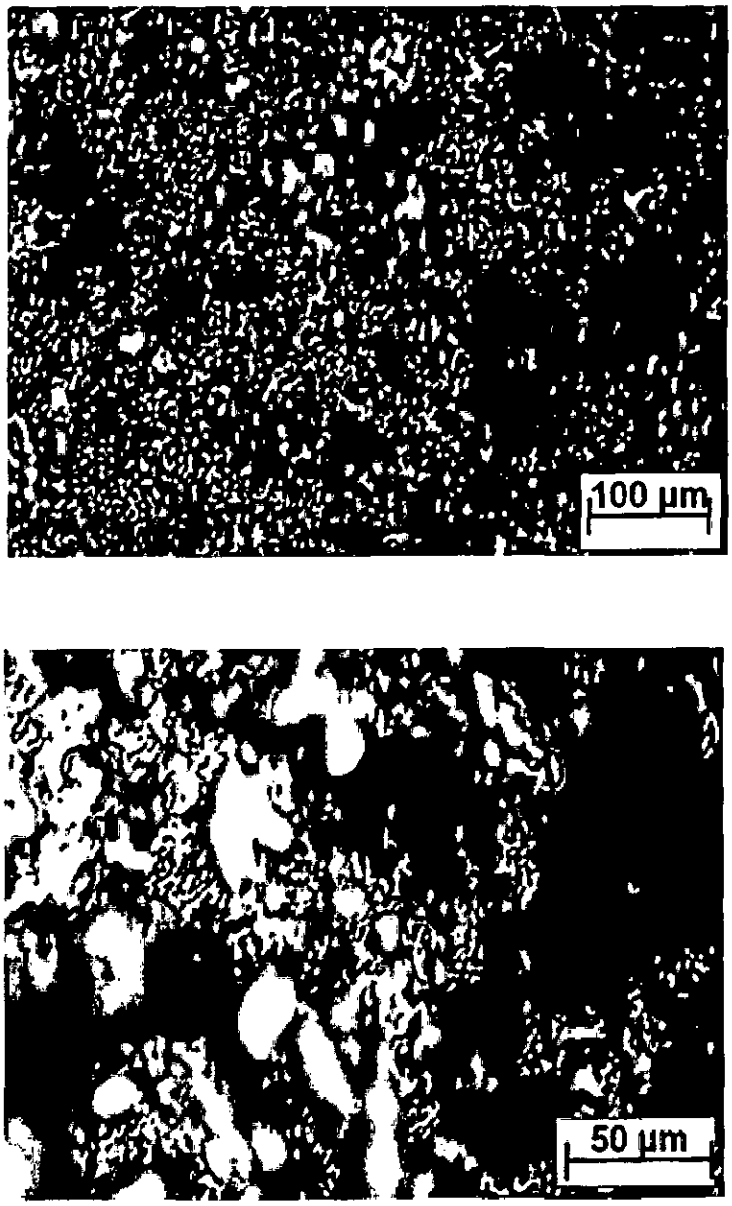

Fig. 8.6. Optical micrographs of WC-Co-Cr coating

8.3 Erosion behaviour

Erosion tests were conducted at impingement angles of 30° and 90° using silicon carbide particles as erodent. It is seen that at both impingement angles the erosion rate of the substrate material first increases rapidly and then becomes almost constant. The erosion rates of coated specimens at 30° impingement angle also increases rapidly in the beginning and become almost constant (Fig. 8.7a). At 90° impingement, however, the erosion rates of coatings initially decreases rapidly before attaining steady state values, as seen in Fig. 8.7b. From the plots (Fig. 8.8) of cumulative weight loss (g) versus time of erosion (min), it is observed that in all the coatings as well as in the substrate, cumulative weight loss increases linearly with time of erosion at both impingement angles. It is also observed that at both 30° and 90° impingement angles, the stellite-6 coating exhibits in general the maximum erosion rate. In all cases the 30° impingement angle yields lower erosion rates in comparison to 90° impingement. The lowest erosion rate is observed in the WC-Co-Cr coating at 30° impingement angle.

The erosion damages in terms of cumulative weight loss at the end of erosion test duration of 120 min are given in bar chart form in Fig. 8.9, which also shows lower erosion damages at 30° impingement angle. At 30° impingements angle the erosion loss is primarily due to shear cutting of surface material, whereas at 90° impingement angle erosion damage is due to strain hardening and embrittlement of target material. The

erosion at 90° impingement angle normally corresponds to erosion of brittle material without any involvement of shear cutting process and thus occurs at high speeds.

The influence of various parameters affecting erosion rate of surface coated materials poses a very complex problem. In general, it is expected that the erosion rate should decrease with increase in hardness and decrease in porosity of the coating [178]. The erosion rate should also decrease with increased involvement of shear process in the surface cutting of target material. In the presence of all these parameters, it is not possible to quantify the influence of individual parameters on the erosion rate. Hence the results obtained in this study do not exhibit any well defined relationship between hardness, porosity and the erosion rate. For example, as seen in Figs. 8.7 and 8.8 the stellite-6 coating exhibits maximum erosion damages, even though it possesses maximum hardness. Figs. 8.10 and 8.11 show the plots of cumulative weight loss as functions of micro hardness and porosity at impingement angles of 30° and 90° respectively. It is observed that there is no fixed pattern of the variation of cumulative weight loss with the hardness and porosity of the various coatings. **Levy** [88] **and Mishra et al** [178] have reported that in plasma sprayed coatings, the greater the porosity of the coating, the easier it is for the erodent particles to knock out pieces from the exposed surface, and greater is the removal rate. The porosity thus plays an overwhelming influence on the erosion behaviour of target material.

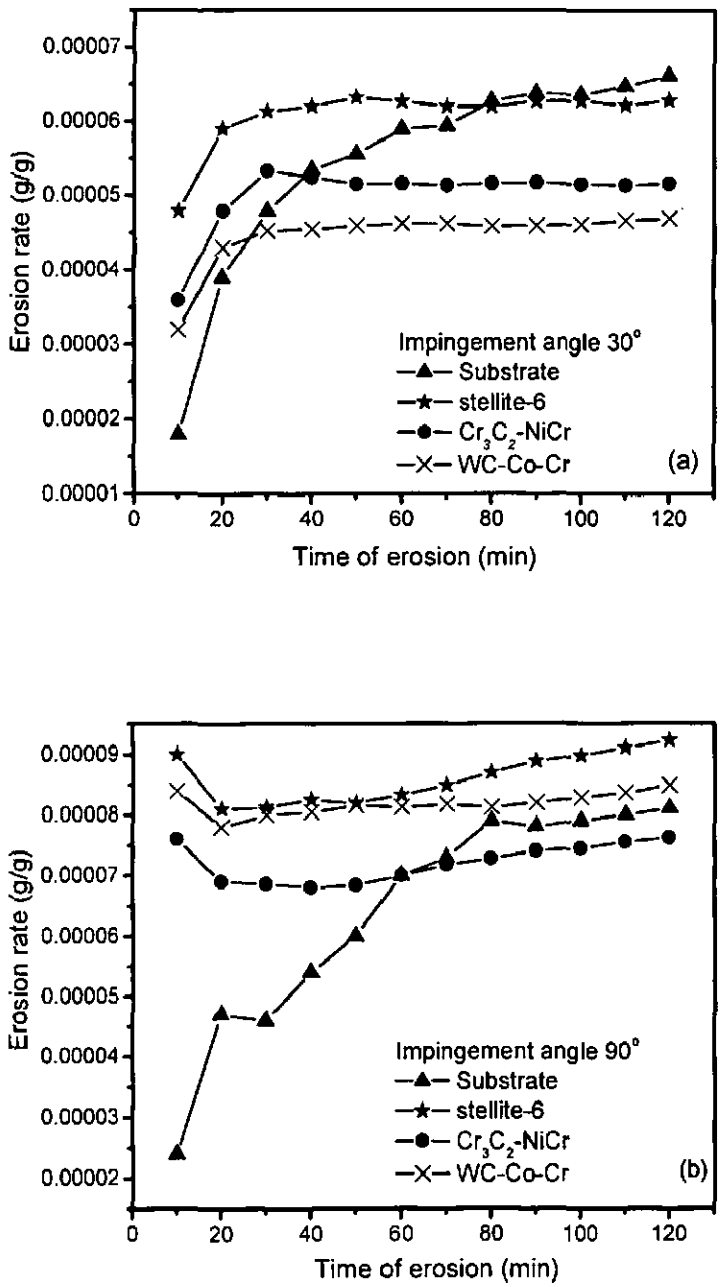

Fig. 8.7. Erosion rate (g/g) as function of erosion time for substrate material as well as for various coatings at impingement angles (a) 30° and (b) 90°

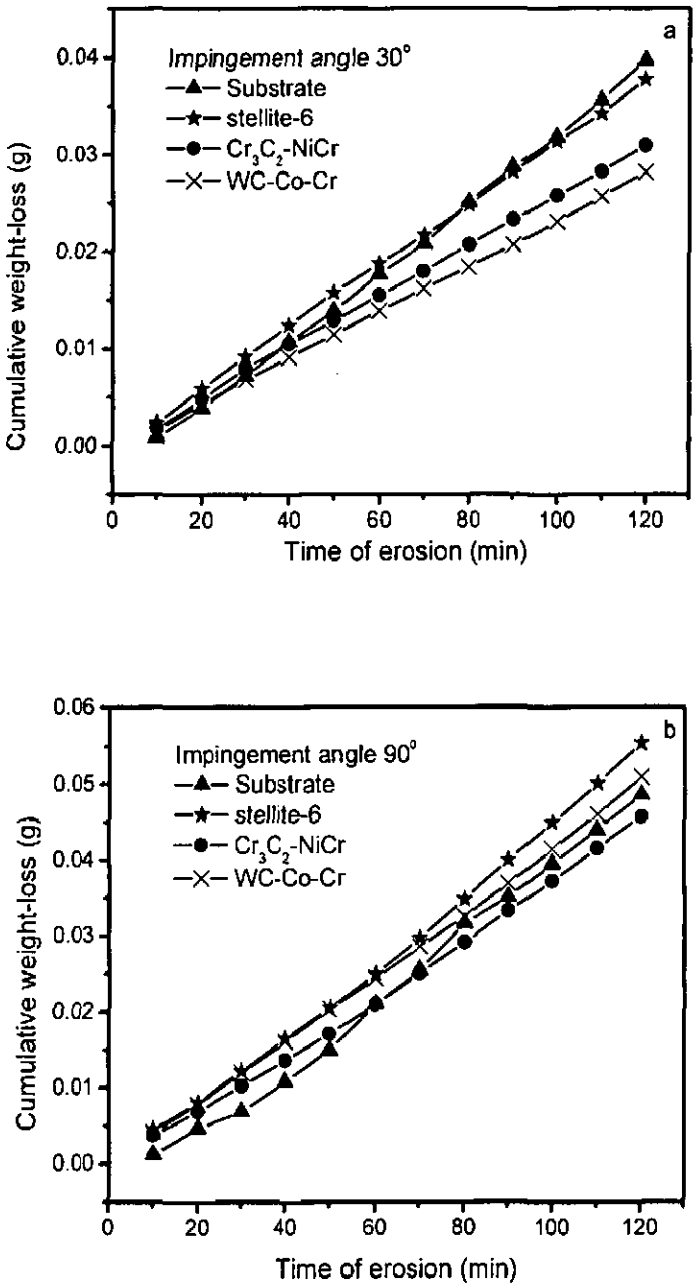

Fig. 8.8. Cumulative weight loss (g) as function of erosion time for substrate material as well as for various coatings at impingement angles (a) 30° and (b) 90°

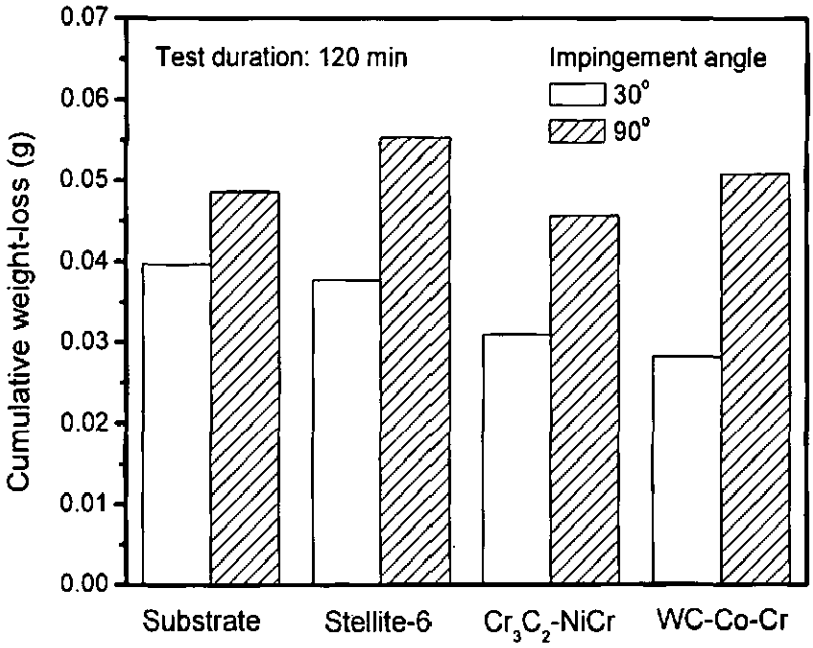

Fig. 8.9. A histogram illustrating cumulative weight loss of substrate (hot rolled 21-4-N steel) and different D-Gun sprayed coatings

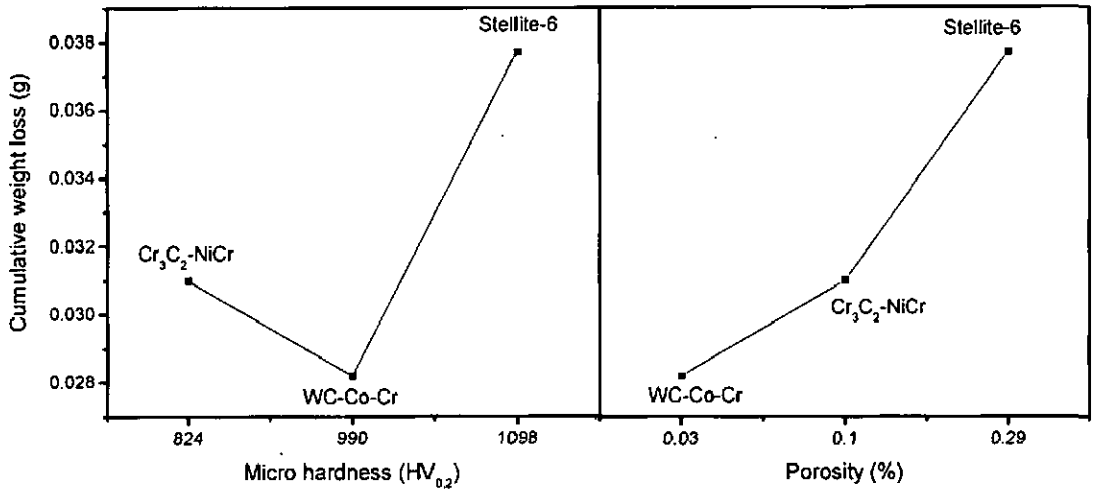

Fig. 8.10. Cumulative weight loss as functions of micro hardness and porosity content of the various coating at 30° impingement angle

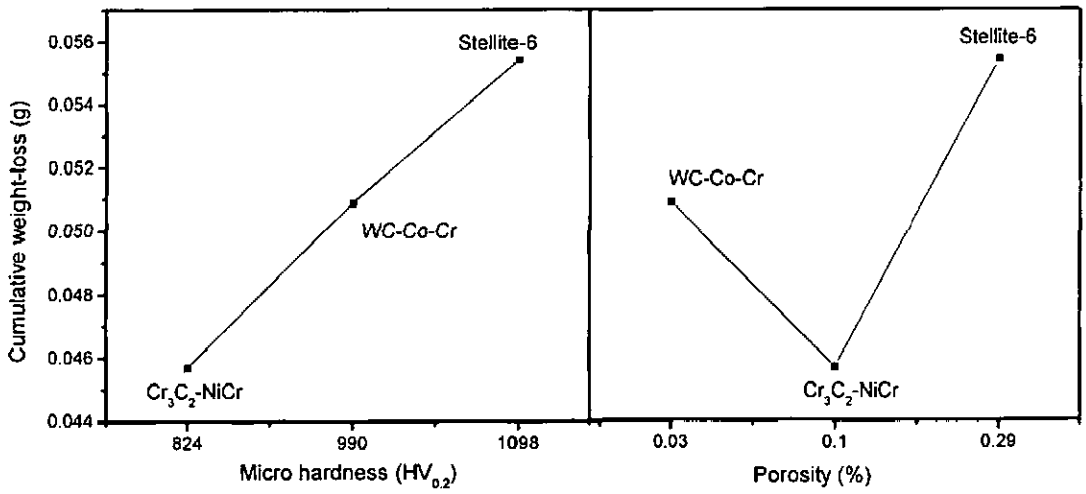

Fig. 8.11. Cumulative weight loss as functions of micro hardness and porosity content of the various coating at 90° impingement angle

8.4 Morphology of eroded surfaces and mechanisms of erosion

Figs. 8.12 and 8.13 show the scanning electron micrographs of eroded surfaces of substrate material, stellite-6, Cr_3C_2-NiCr and WC-Co-Cr coatings at impingement angles of 30° and 90° respectively. At 30° impingement angle the process of erosion involves a shear process. Thus the topography of eroded surfaces in the substrate as well as the coatings indicates presence of ploughs, which are formed due to extrusion of platelets from the impact zone (Fig. 8.12). The erosion is characterized by intense localized plastic flow producing lips and ploughs around the crater periphery as suggested by **Hearley et al** [196]. Wide ploughs are observed in substrate (Fig. 8.12a) and stellite-6 coating (Fig. 8.12b), which is indicative of high erosion damages. At 30° impingement angle, cutting due to impinging particle starts in the ductile matrix of stellite-6 around the $M_{23}C_6$ carbide grains leading to acceleration in erosion damages. The Cr_3C_2-NiCr and WC-Co-Cr coatings are continuous and are sufficiently hard to resist cutting due to the impacting erodent particles at 30° impingement angle. This mechanism of erosion of Cr_3C_2-NiCr and WC-Co-Cr coatings is supported by the scanning electron micrographs (Figs. 8.12c and d). At 90° impingement angle, the eroded surfaces in all cases are in general free from ploughs (Fig. 8.13). Deep craters are instead observed which are created due to dislodging of material by hard hitting erodent particles. The craters as revealed in SEM study are deepest in the stellite-6 coating (Fig. 8.13b) in comparison to other coatings. The deep craters observed in the scanning electron micrograph of eroded stellite-6

coating correspond to the removal of large chunks of carbides due to high level of porosity.

8.5 Analysis of performance of different coatings

The performance of a coating under erosion tests can be analyzed on the basis of (i) binding of the coating with the substrate, which is affected by its alloying nature, (ii) reinforcement of hard carbides in the binding matrix of the coating, (iii) hardness and (iv) porosity level. An analysis of the erosion behaviour of different coatings thus poses a complex problem.

8.5.1 Stellite-6 coating

The near-fusion line microstructure of the stellite deposit reveals a complex multi-phase microstructure consisting of: (a) a martensite-like structure with hexagonal intra 'lath ε Co-type precipitates ~10 to 30 nm in length adjacent to the fusion line; (b) a body centered cubic (bcc) Fe-Co-enriched α phase with an interconnected Cr-enriched α' phase located beyond the martensitic phase; and(c) fine (~20 to 150 nm) M23C6 carbides within the fcc stellite matrix [206]. The Cr-enriched phase exhibits a morphology and size consistent with α' bcc phase formed during aging in Fe-Cr-Co alloys (associated with severe hardening and embrittlement). The Fe-Cr-Co system contains a metastable miscibility gap, so that the single-phase bcc α alloy aged within the gap spinodally decomposes into the Fe/Co rich α and Cr-rich α' phases. **Burke et al** [207] have reported that the interfacial region contains significant amounts of Fe, Co and Cr. The Fe dilution

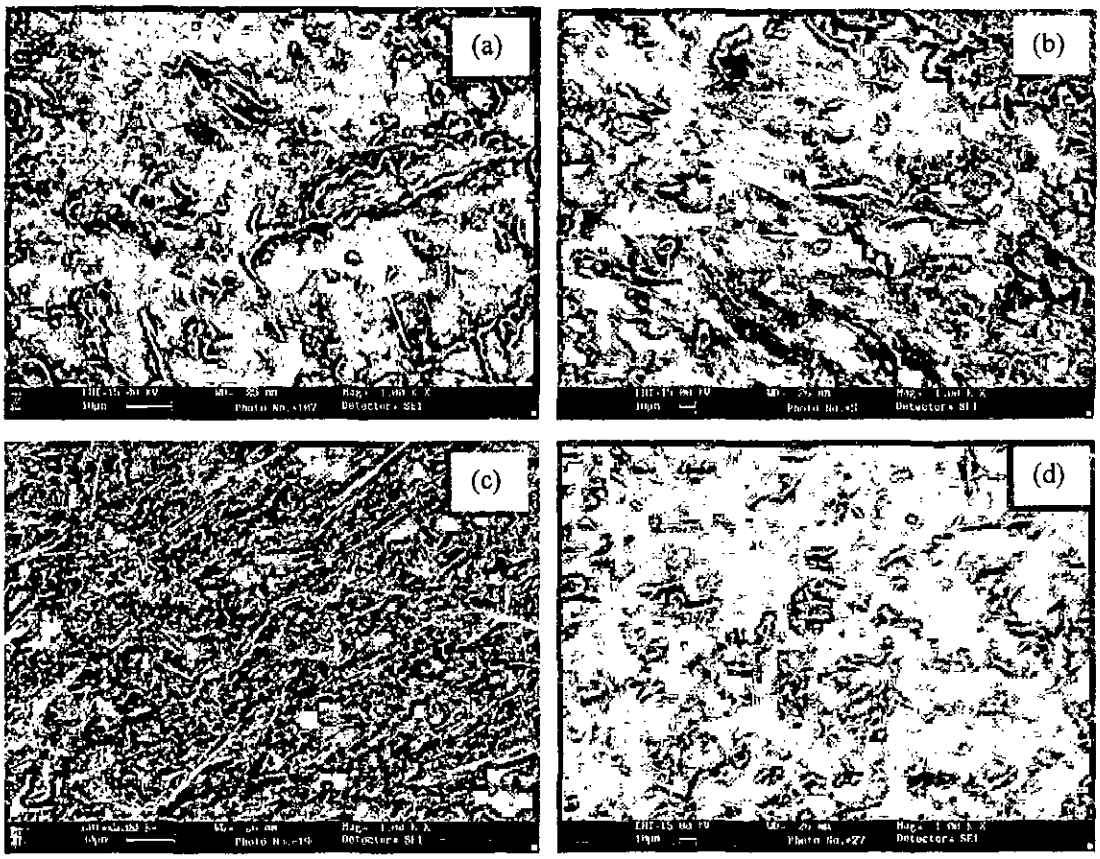

Fig. 8.12. Scanning electron micrographs of eroded surfaces of (a) substrate material (hot rolled 21-4-N steel), (b) stellite-6, (c) Cr_3C_2-NiCr and (d) WC-Co-Cr coatings after 120 min of erosion test at 30° impingement angle

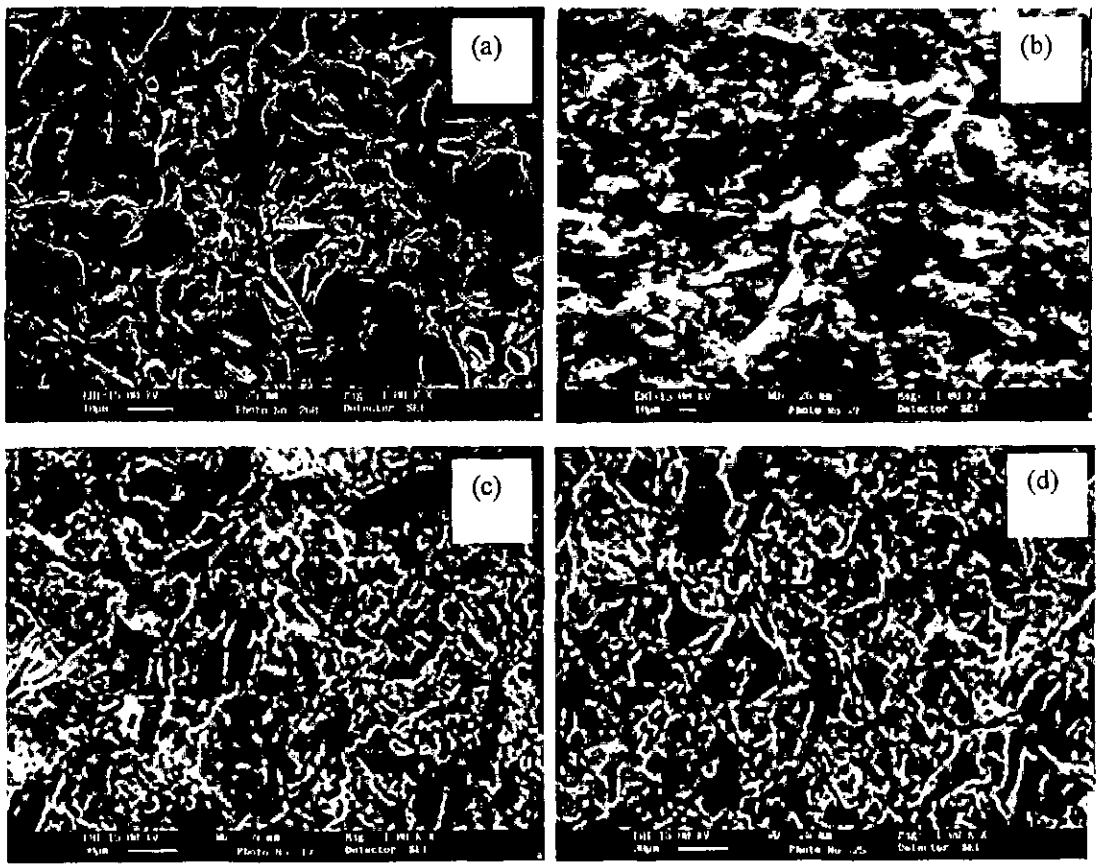

Fig. 8.13. Scanning electron micrographs of eroded surfaces of (a) substrate material (hot rolled 21-4-N steel), (b) stellite-6, (c) Cr_3C_2-NiCr and (d) WC-Co-Cr coatings after 120 min of erosion test at 90° impingement angle

into the stellite extends over 20 μm into the hard facing deposit. It is this Fe dilution that promotes the complex multi-phase microstructure in the near-fusion line zone.

8.5.2 Cr_3C_2-NiCr Coating

Wang et al [200] have reported that the microstructure of Cr_3C_2-NiCr consists of dense skeletal network of Chromium carbide (Cr_3C_2) and chromium oxides bound within the ductile matrix of NiCr. The microstructure contains the metallic binding matrix, chromium carbides and / or chromium oxides formed as a result of oxidation occurring during particle exposures to the high temperature of the spraying process. For HVOF coating of Cr_3C_2-NiCr powder, **Zhang et al** [193] have reported that the Cr_3C_2 -NiCr coating is made up of carbide and metallic phase with high hardness, including Cr_7C_3, Cr_3C_2, Cr_3Ni_2, C, Ni and CrO. **Staia et al** [208] observed that XRD analysis of the plasma sprayed coatings consists of Ni–Cr and mixtures of orthorhombic Cr_3C_2 and carbo-nitride phases based on Cr_3C_2.

8.5.3 WC-Co-Cr coating

During spraying process some tungsten carbide melts and reacts with the metal binder to form ternary carbide Co_3W_3C. Secondary carbides W_2C form due to decarburization of WC. Binding phase contains tungsten, cobalt and carbon. As the powder grains travel through the flame, they melt to different extent depending on their size and flight velocity. The molten cobalt dissolves partially (or completely) in the WC grains with respect to the local temperature. Carbon loss occurs by diffusion through the

liquid phase followed by reaction with the oxygen contained in the flame at the droplets surface. Then the droplets impinge on the solid surface and the nano-crystalline binder is formed through rapid solidification of their liquid part.

8.5.4 Effect of volume fraction of carbides on the erosion

Sapate and Rao [209] have reported that under mild erosion conditions, erosion rate decreases with increasing carbide volume fractions. With silica sand particles the erosion rate increases with carbide volume fractions under severe erosion conditions, whereas they further observed the beneficial effect of large volume fractions of carbides at 30° impingement angle under moderately severe erosion conditions. They also found that with alumina particles large volume fractions of carbides prove detrimental to erosion resistance under moderately severe erosion condition. Alumina particles are able to plastically indent and cause lateral fracture of carbide particles. Gross fracture of carbides is observed with silica sand particles at normal impact angle, whereas at lower impact angles material from the carbides is removed by small scale chipping induced by micro-fracture. **Sapate and Rao** [209] also reported that with increasing severity of erosion conditions, erosion rate shows stronger dependence on the ratio of hardness of erodent particle and that of the target material.

Zhou et al [210] have studied the effect of volume fraction of WC particles on erosion resistance of WC reinforced iron matrix surface composites. They reported that with increasing volume fraction of WC carbide particles, the wear rates first decrease, but

then increase after 36 vol% WC. **Zhou et al** [210] have identified a critical volume fraction of WC carbides in the WC reinforced iron matrix composites which gives minimum wear rate. If the volume fraction of carbide particles in coating is less than 36%, the erosion rates tend to decrease, and for volume fraction of carbides greater than 36%, there is a tendency for erosion rate to increase. The WC particles in the coating are 2.1 times harder than the abrasive silica particles. However, the content of the binding matrix also is important to hold the WC particles intact. At volume fraction of WC carbide particles less than 36%, erosion damages result in formation of surface sinks at the sites of binding matrix and protrusions at the WC sites. At larger concentration of WC, the carbides become loose and easily get detached from the surface leading to higher rate of erosion. The observations of **Zhou et al** [210] have also been supported by **Verdon et al** [211] who observed that there exists an optimum amount of transformation of carbides which ensures an optimum wear resistance for given erosion conditions. The diagram in Fig. 8.14 illustrates this interpretation.

8.5.5 *Effect of hardness and porosity on the erosion*

The hardness of materials is usually associated with erosion or abrasion resistance, it is generally admitted that soft materials possess resilience to resist particle impact at 90° and hard materials have ceramic phases making them able to deflect low angle impacting particles. The significance of hardness with regards to the wear behavior cannot be drawn directly. Admittedly, all materials contain hard and soft phases and

hardness measurements do not give any indication of the actual resistance of material against erosion. Previous work on weld overlay coatings has shown that an increase in coating hardness may lead to an increase in abrasion resistance. However, other workers have shown that hardness does not affect the erosion resistance [150].

The relative comparison of porosity contents of the coatings and respective erosion rates of coatings suggest negative effect of porosity content on the erosion rate of the HVOF sprayed coatings. **Levy and Buqian** [149] have suggested that the greater the porosity of the coating, the easier it is for the erodent particles to knock off pieces of exposed surface and the greater is the removal rate. Further **Vicenzi et al** [212] reported in their study on HVOF coatings against high temperature (300°C) erosion that the porosity acts to reduce the mechanical strength as well as modulus of elasticity, which further reduce the amount of energy required for the removal of parts of the surface. **Hearley et al** [196] have also reported that porosity not only influences the strength of inter-lamella bonding but may also initiate micro cracking leading to loss of lamellae and thus removal of coating.

8.5.6 Effect of impingement angle

It can be seen from the results obtained in this study that the erosion rate of stellite-6 is higher at both the impingement angles despite of having highest hardness

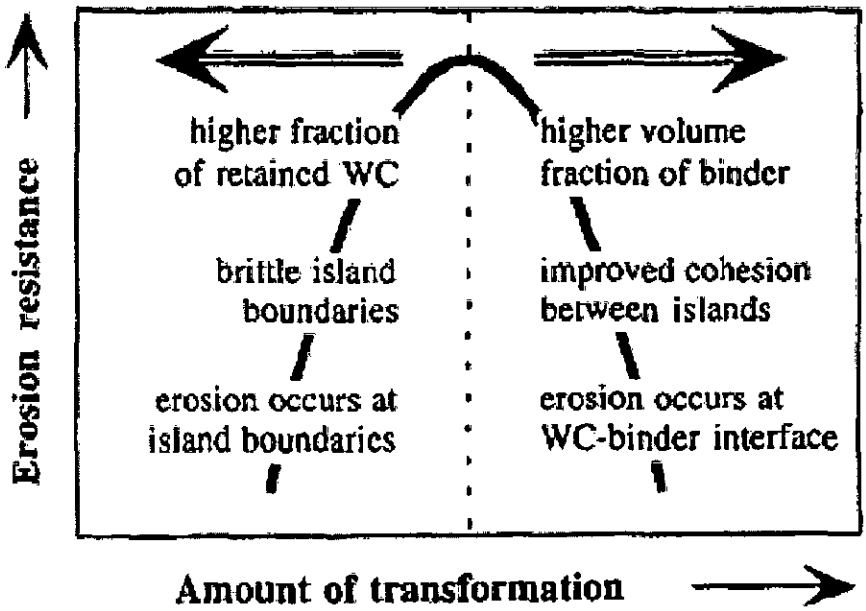

Fig. 8.14. Schematics of the dependence of the erosion resistance of WC-Co coatings on the transformations that occur during HVOF spraying [211]

(Figs. 8.7 to 8.11). At 30° impingement angle the erosion is due to shear cutting by the erodent particles. The higher erosion rate of stellite-6 coating may be due to higher volume fraction of fine and uniformly distributed grains of carbides in the matrix of Co and highest porosity content (Fig. 8.10). The higher erosion rate of stellite-6 coating than that of WC-Co-Cr coating is also due to austenitic matrix of Co since austenitic matrix is more prone to shear in comparison to the binding matrix (W, Co and C) of WC-Co-Cr coating and the hardness of chromium carbide ($Cr_{23}C_6$) (1200-1600 HV) of stellite-6 coating is less than that of the silicon carbide (SiC) particles (2100-2600 HV). At 30° impingement angle, cracks nucleated due to impingement of SiC particles in binding matrix as well as at the chromium carbide particles intersect readily each other and chunk of material knock out off the bulk of the coating. Due to this reason wider ploughs are observed in the scanning electron micrographs of stellite-6 coating (Fig. 8.12b).

The Cr_3C_2-NiCr coating presents lower erosion rate than that of stellite-6 coating at 30° impingement angle. This is due to delay in formation of ploughs in the binding matrix of Cr_3C_2-NiCr coating, since the proportion of binding matrix in Cr_3C_2-NiCr coating is higher i.e. volume fraction of chromium carbide (Cr_3C_2) is less than that of the carbides in stellite-6 coating. The higher erosion resistance of WC-Co-Cr coating is due to reinforcement of the binding matrix by WC particles which deflects the SiC particles because WC and SiC particles are of almost equal hardness, whereas the chromium carbides in Cr_3C_2-NiCr coating are cut by the SiC particles because of lower hardness of chromium carbides as compared to SiC particles. The longer ploughs in the Cr_3C_2-NiCr

coating in comparison to WC-Co-Cr coating as revealed from the scanning electron micrographs (Figs. 8.12c and d) are in agreement with the above assumption. When SiC particles are used as erodent less hard chromium carbide and binding matrix of Cr_3C_2-NiCr coating erode simultaneously while the binding matrix of WC-Co-Cr coating erode first followed by knock out off WC particles, resulting in lower erosion rate of WC-Co-Cr coating.

At 90° impingement angle the interfaces between carbide particles and the matrix act as the sources of initiation of cracks. The highest erosion rate of stellite-6 is attributed to higher volume fraction chromium carbides, higher grain boundary areas higher hardness and higher porosity as compared to other coatings. Due to higher volume fraction of chromium carbides ($Cr_{23}C_6$) in stellite-6 coating as seen in the optical micrographs (Fig. 8.2), the matrix between the carbide particles becomes too little and easily gets detached from the bulk of the coating by the high velocity SiC particles. The volume fraction of carbides in the matrix of Cr_3C_2-NiCr coating is lowest, whereas in the case WC-Co-Cr coating it is in between Cr_3C_2-NiCr and stellite-6 coatings. The lowest erosion rate of Cr_3C_2-NiCr coating at 90° impingement angle is attributed to its lower volume fraction of carbides. Since ductile binding matrix (NiCr) absorbs more kinetic energy of the high velocity SiC particles in comparison to stellite-6 and WC-Co-Cr coatings. Very high hardness of carbides in a coating may also result in embrittlement. Accordingly the higher hardness of WC in comparison to chromium carbides (Cr_3C_2) is

also responsible for higher erosion rate in WC-Co-Cr coating as compared to that in Cr_3C_2-NiCr.

8.6 Conclusions

I. The stellite-6 coating on 21-4-N steel substrate exhibits maximum damage due to erosion at 30° and 90° impingement angles. Minimum erosion losses are observed in WC-Co-Cr coating at 30° impingement angle.

2. The analysis of the influence of various parameters on erosion behaviour poses a complex problem. It is not possible to quantify the role of individual parameters like microstructural features, microhardness and porosity in affecting the erosion behaviour of coating. It is, however, observed that the nature and extent of porosity affect to a large extent the erosion rate of coatings. Maximum concentration of porosity is observed in stellite-6 coating.

3. The erosion damage at 90° impingement angle is more severe in comparison to erosion loss at 30° impingement angle.

4. Scanning electron microscopic study reveals that at 30° impingement angle erosion occurs by a shear process involving formation of lips and ploughs on the target surface. Existence of deep craters in the SEM micrographs at 90° impingement angle indicate knocking out of chunk of material from the target surface resulting in high rates of erosion.

Chapter 9

Conclusions and suggestions for future work

9.1 Conclusions

The following conclusions emerge from the present study:

1. The erosion resistance of as cast 21–4–N steel investigated by means of solid particle impingement is higher than that of as cast 13/4 martensitic stainless steel, because of its austenitic matrix, which is less prone to erosion damages as compared to the stressed and untempered martensitic matrix of 13/4 steel. Mechanical properties significantly affect the erosion resistance of target material. In 21–4–N steel, high resistance to erosion is due to (i) high hardness coupled with high ductility, (ii) high tensile toughness and (iii) high rate of strain hardening in comparison to 13/4 martensitic stainless steel.

2. Remarkable improvement is observed at 90° impingement angle in the erosion resistance of as cast 13/4 steel; whereas erosion resistance slightly deteriorates at 30° impingement angle as a result of solutionizing at 1050 °C and tempering at 620 °C. At 90° impingement angle the increased erosion resistance of 13/4 steel as result of tempering treatment is due to relieving of internal stresses and thickening of martensitic laths.

3. As a result of tempering at 620 °C there are certain changes in mechanical properties of 13/4 steel. Due to tempering the hardness decreases from 305 to 289 VHN and the tensile toughness increases slightly (from 68 to 71 MJm^{-3}). The values of ductility and strain hardening exponent (n) almost remain unchanged. The decrease in erosion resistance at 30° impingement angle is attributed to decrease in hardness whereas increase in erosion resistance at 90° impingement angle is correlated with slightly increase in tensile toughness.

4. Substantial improvement in the erosion resistance of 21-4-N steel at both the impingement angles of 30° and 90° is observed as a result of solution annealing at 1100 °C. However, aging treatment of solution annealed 21-4-N steel causes deterioration in erosion resistance at both impingement angles. The improved erosion resistance of 21-4-N steel as a result of solution annealing at 1100 °C is due to substantial dissolution of carbides in the austenitic matrix. Again reprecipitations of carbides in the aged 21-4-N steel are responsible for decreased erosion resistance.

5. The mechanical properties resulting from solution annealing significantly affect the erosion resistance of 21-4-N steel. The increased values of ductility and tensile toughness as a result of solution annealing of 21-4-N steel increase the erosion resistance. However, lowering of hardness and strain hardening exponent of 21-4-N steel as result of solution annealing may cause reduction in erosion resistance; but cumulative effect of all mechanical properties results in increased erosion resistance.

6. Mechanical working (by rolling) significantly affects properties and erosion resistance of 13/4 and 21-4-N steels. In 13/4 steel the martensitic laths are thickened whereas in 21-4-N steel no significant change is observed in the microstructure as a result of 8% rolling at 700 °C. The values of YS, UTS, and hardness increase and the values of tensile toughness, ductility, impact energy and strain hardening exponent in both 13/4 and 21-4-N steels as a result of 8% rolling at 700 °C.

7. The microstructure of 21-4-N steel develops fine grains of austenite as a result of 89% reduction in cross sectional area by hot rolling at 1180 °C. The values of hardness, impact energy, YS, UTS, tensile toughness and strain hardening exponent increase in 21-4-N steel as a result of hot rolling.

8. As a result of 8% reduction in thickness by rolling, for both 13/4 and 21-4-N steels there is improvement in erosion resistance at 30° impingement angle, whereas at 90° impingement angle there is a deterioration in the erosion resistance. Hot rolling to 21-4-N steel causes improvement in erosion resistance at both impingement angles. By 8% rolling the improved erosion resistance of 13/4 and 21-4-N steel at 30° impingement angle is attributed to overwhelming effect of increased hardness; whereas, the deterioration in erosion resistance of both the steels at 90° impingement angle is attributed to decreased values of ductility, tensile toughness and strain hardening exponent, in addition to internal stresses induced during rolling.

9. By hot rolling at 1180 °C the improved erosion resistance of 21-4-N steel at both 30° and 90° impingement angles is attributed to (i) fine grain structure of austenite and (ii) increased values of hardness, ductility, tensile toughness and strain hardening exponent.

10. In both the steels, the SEM studies show that the ploughs formed at 30° impingement angle are smaller and finer, whereas at 90° impingement angle the cavities and cracks created are deeper and larger in 8% rolled condition in comparison to those in as cast condition.

11. The cavitation erosion resistance of 13/4 steel investigated by means of ultrasonic vibration processor is less than that of 21-4-N steel in both as cast and hot rolled conditions. However, hot rolled 21-4-N steel exhibits excellent cavitation erosion resistance.

12. From the microstructure view point, the untempered martensitic laths of 13/4 steel exhibit more cavitation erosion than the austenitic structure of 21-4-N steel. The martensitic laths, already associated with internal stresses, are less able to absorb the strain energy due to transient stresses in the material induced by cavitation impact wave. It can also be inferred that the carbides present in 21-4-N steel are detrimental to cavitation erosion resistance leading to more erosion in as cast condition. In 21-4-N steel in both as cast and hot rolled conditions, the cavitation erosion damages occur along the grain boundaries and the carbides are the first to be dislodged from the specimens.

13. In 21-4-N steel higher resistance to cavitation erosion is associated with high hardness coupled with high ductility, high tensile toughness and high strain hardening exponent in comparison to those in 13/4 steel.

14. The stellite-6 coating on 21-4-N steel substrate exhibits maximum damage due to erosion at 30° and 90° impingement angles. Minimum erosion losses are observed in WC-Co-Cr coating at 30° impingement angle.

15. The analysis of the influence of various parameters on erosion behaviour of surface coatings poses a complex problem. It is not possible to quantify the role of individual parameters like microstructural features, microhardness and porosity in affecting the erosion behaviour of coating. It is, however, observed that the nature and extent of porosity affect to a large extent the erosion rate of coatings. Maximum concentration of porosity is observed in stellite-6 coating.

16. Scanning electron microscopic study of eroded surfaces on coated components reveals that at 30° impingement angle erosion occurs by a shear process involving formation of lips and ploughs on the target surface. Existence of deep craters in the SEM micrographs at 90° impingement angle indicate knocking out of chunk of material from the target surface resulting in high rates of erosion.

9.2 Suggestions for future work

1. The present study has shown that in 21-4-N nitronic steel there is a strong tendency of carbide formation. These carbides are undesirable from the view point of erosion resistance. Even a solution annealing treatment at 1100 °C is not able to completely dissolve all the matrix carbides. Aging at 700 °C after solution annealing again deteriorates the resistance to erosion due to carbide precipitation. Hence investigations need to be undertaken to develop the austenitic matrix free of carbides. An approach in this direction is to reduce the C content in nitronic steels. The steel investigated in this study possesses 0.56% C. Studies on erosion behaviour with lower C concentration may provide useful results.

2. In this investigation erosion tests have involved use of abrasive particles plus air jet as the erosive medium. Separate tests on cavitation erosion have also been conducted using water only without any erodent particles. To simulate actual field conditions in hydroelectric projects, investigations need to be taken up to study the erosion behaviour of nitronic steel in silt-water slurry with varying parameters.

3. Best performance against erosion has been observed in 21-4-N nitronic steel after 89% reduction by hot rolling at 1180 °C. This treatment provides a fine grain austenitic matrix free of carbides. Hot rolling of this steel is rather difficult and it may not be possible to fabricate various underwater components by hot rolling / forging at such a high temperature. To obtain a fine grain matrix free of carbides, investigations may be

undertaken on low C nitronic steels microalloyed with grain refining elements like B, Al, V and Ti.

4. This investigation has revealed that all mechanical properties play vital role in influencing the erosion behaviour of nitronic steel. It is well known that some of the mechanical properties, like impact energy, tensile toughness and ductility are strongly temperature dependent. In this study, all the mechanical properties have been determined at room temperature, whereas in certain critical applications, like underwater parts in hydroelectric projects, erosion occurs at sub zero temperatures. Hence studies need to be undertaken to correlate the erosion behaviour with mechanical properties determined at low temperatures.

5. *In situ* strain hardening occurring during erosion applications has been identified as an important parameter contributing resistance to erosion in nitronic steel. In this study the tendency of strain hardening has been correlated with strain hardening coefficient n determined from the slope of log true stress – log true strain diagram. Investigations on the nature and depth of *in situ* hardening may provide useful information on its actual role in erosion behaviour. This may require study of nature of sub surfaces undergoing erosion damages by optical metallography, transmission electron microscopy and X-ray analysis.

6. An important aspect in the development of a steel for a specific application is availability of complete know how of its manufacturing and fabrication technology. Although the foundry practices of nitronic steel is well established, studies need to be

conducted on its weldability, which is of vital importance for the maintenance of partially damaged components. Welding parameters need to be standardized and studies on development of suitable welding electrodes need to be undertaken. Similarly the practice of hot working by rolling / forging is also to be well established.

References

[1] Naidu B.S.K., *Uprating and refurbishment of silt affected hydro power plants*, Hydro power an Indian perspective, CBS Publishers and distributors, **(2001)** 289-311.

[2] Chattopadhyay R., *High silt wear of hydro turbine runners*, Wear, 162-164 **(1993)** 1040-1044.

[3] Mann B.S., Reddy D.M., Ramadass N., Somasundaram R., *Ceramics and coatings to prevent wear of hydro turbine components*, Proc. All India Seminar on Metallurgical Problems in Power project; The Institution of Engineers (India), UP State Centre, Lucknow **(1987)** 152-158.

[4] Sakhujja V.S., Paul T.C., Dhillon G.S., *Combating sediment problems in hydropower plants*, Proc. All India Seminar on Metallurgical Problems in Power project; The Institution of Engineers (India), UP State Centre, Lucknow **(1987)** 94-103.

[5] Li S., *Cavitation enhancement of silt erosion—An envisaged micro model*, Wear 260 **(2006)** 1145-1150.

[6] Zheng Y., Yao Z., Wei X., Ke W., *The synergistic effect between erosion and corrosion in acidic slurry medium*, Wear 186–187 **(1995)** 555–561.

[7] ASTM G76-02, *Standard test method for conducting erosion tests by solid particle impingement using gas jets*, West Conshohocken, PA **(2003)**.

[8] ASTM G40, *Standard terminology relating to wear and erosion, West Conshohocken*, PA **(2003)**.

[9] Karimi A., Martin J.L., *Cavitation erosion of materials*, Int. Met. Rev. 31 **(1986)** 1-26.

[10] Kwok C.T., Man H.C., Cheng F.T., *Cavitation erosion and pitting corrosion behaviour of laser surface-melted martensitic stainless steel UNS S42000*, Surf. Coat. Tech. 126 **(2000)** 238-255.

[11] Wu C.Z., Chen Y.J., Shih T.S., *Phase transformation in austempered ductile iron by micro et impact*, Mat. Charact. 48 **(2002)** 43–54.

[12] Zhang Y., Wang Z., Cui Y., *The cavitation behavior of metastable Cr–Mn–Ni steel*, Wear 240 **(2000)** 231–234.

[13] Krella A., Czyzniewski A., *Cavitation erosion resistance of Cr–N coating deposited on stainless steel*, Wear 260 **(2006)** 1324–1332.

[14] Hattori S., Mori H., Okada T., *Quantitative evaluation of cavitation erosion*, J. Fluids Eng. 120 **(1998)** 179–185.

[15] Krella A., *Influence of cavitation intensity on X6CrNiTi18-10 stainless steel performance in the incubation period*, Wear 258 **(2005)** 1723–1731.

[16] Di Schino A., Kenny J.M., Mecozzi M.G., Barteri M., *Development of high nitrogen, low nickel, 18% Cr austenitic stainless steels*, J. Mat. Sci. 35 **(2000)** 4803–4808.

[17] Mills D.J., Knutsen R.D., *An investigation of the tribological behaviour of a high-nitrogen Cr–Mn austenitic stainless steel*, Wear 215 **(1998)** 83–90.

[18] Preininger D., *Modelling of the effect of precipitates on work-hardening, ductility and impact behaviour of ferritic–martensitic Cr steels*, J. Nuclear Mat. 307–311 **(2002)** 514–520.

[19] Bregliozzi G., Di Schino A., Haefke H., Kenny J. M., *Cavitation erosion resistance of a high nitrogen austenitic stainless steel as a function of its grain size*, J. Mat. Sci. Letters 22 **(2003)** 981– 983.

[20] ASTM G32-06, *Standard test method for cavitation erosion using vibratory apparatus*, West Conshohocken, PA **(2007)**.

[21] Simoneau R., *The optimum protection of hydraulic turbines against cavitation erosion*, 12th IAHR Symposium, Stirling, UK, **(1984)** 27-30.

[22] Mann B. S., *Boronizing of cast martensitic chromium nickel stainless steel and its abrasion and cavitation-erosion behaviour*, Wear 208 **(1997)** 125-131.

[23] Panwar S., Kumar S., Goel D.B., *Effect of heat treatment on erosive wear of 13/4 martensitic stainless steel*, Sixteenth National Convention of Mechanical Engineers and All India Seminar on Future Trends in Mechanical Engineering

Research and Development, Department of Mech. and Ind. Eng., UOR, Roorkee , Sept. 29-30 **(2000)**.

[24] Deng T., Bradley M.S.A., Bingley M.S., *An investigation of particle dynamics within a centrifugal accelerator type erosion tester*, Wear 247 **(2001)** 55–65.

[25] Lindsley B.A., Marder A.R., *The effect of velocity on the solid particle erosion rate of alloys*, Wear 225–229 **(1999)** 510–516.

[26] Burnett A.J., Bradley M.S.A., O'Flynn D.J., Deng T., Bingley M.S., *Anomalies in the results obtained from rotating disc accelerator erosion testers: a discussion of possible causes*, Wear 233–235 **(1999)** 275–283.

[27] Deng T., Bingley M.S., Bradley M.S.A., *The influence of particle rotation on the solid particle erosion rate of metals*, Wear 256 **(2004)** 1037–1049.

[28] Desale G.R., Gandhi B.K., Jain S.C., *Effect of erodent properties on erosion wear of ductile type materials*, Wear 261 **(2006)** 914-921.

[29] Gandhi B.K., Singh S.N., Seshadri V., *Study of the parametric dependence of erosion wear for the parallel flow of solid–liquid mixtures*, Tribol Int. 32 **(1999)** 275–282.

[30] Mack R., Drtina P., Lang E., *Numerical prediction of erosion on guide vanes and in labyrinth seals in hydraulic turbines*, Wear 233–235 **(1999)** 685–691.

[31] Roman J.M., Xin L.Y., Hui W.M., Reginensi J.P., *Dealing with abrasive erosion in hydro turbine*, Hydro Power Dams 3 **(1997)** 67–71.

[32] Papini M., Spelt J.K., *Impact of rigid angular particles with fully plastic targets. Part II. Parametric study of erosion phenomena*, Int. J. Mech. Sciences 42 **(2000)** 1007–1025.

[33] Dhar S., Krajac T., Ciampini D., Papini M., *Erosion mechanisms due to impact of single angular particles*, Wear 258 **(2005)** 567–579.

[34] L'opez D., Congote J.P., Cano J.R., Toro A., Tschiptschin A.P., *Effect of particle velocity and impact angle on the corrosion–erosion of AISI 304 and AISI 420 stainless steels*, Wear 259 **(2005)** 118–124.

[35] Burstein G.T., Sasaki K., *Effect of impact angle on the slurry erosion–corrosion of 304L stainless steel*, Wear 240 **(2000)** 80–94.

[36] Toro A., Sinatora A., Tanaka D.K., Tschiptschin A.P., *Corrosion– erosion of nitrogen bearing martensitic stainless steels in seawater– quartz slurry*, Wear 251 **(2001)** 1257–1264.

[37] Sasaki K., Burstein G.T., *Erosion–corrosion of stainless steel under impingement by a fluid jet*, Corrosion Sci. 49 **(2007)** 92–102.

[38] Habib M.A., Badr H.M., Ben-Mansour R., Kabir M.E., *Erosion rate correlations of a pipe protruded in an abrupt pipe contraction*, Int. J. of Impact Eng. 34 **(2007)** 1350–1369.

[39] Das S.K., Godiwalla K.M., Mehrotra S.P., Sastry K.K.M., Dey P.K., *Analytical model for erosion behaviour of impacted fly-ash particles on coal-fired boiler components*, Sadhana 31 **(2006)** 583–595.

[40] Gee M.G., Gee R.H., McNaught I., *Stepwise erosion as a method for determining the mechanisms of wear in gas borne particulate erosion*, Wear 255 **(2003)** 44-54.

[41] Lee B.E., Fletcher C.A.J., Behnia M., *Computational prediction of tube erosion in coal-fired power utility boilers*, J. Eng. Gas Turbines Power 121 **(1999)** 746–750.

[42] Chang L.C., Hsui I.C., Chen L.H., Lui T.S., *Effects of heat treatment on the erosion behavior of austempered ductile irons*, Wear 260 **(2006)** 783–793.

[43] Dai W.S., Chen L.H., Lui T.S., *A study on SiO_2 particle erosion of flake graphite and spheroidal graphite cast irons*, Wear 239 **(2000)** 143-152.

[44] Hung F.Y., Chen L.H., Lui T.S., *A study on the particle erosion of upper bainitic austempered ductile iron*, Wear 252 **(2002)** 985-991.

[45] Chen D., Sarumi M., Al-Hassani S.T.S., *Computational mean particle erosion model*, Wear 214 **(1998)** 64-73.

[46] Chen Q., Li D.Y., *Computer simulation of solid particle erosion*, Wear 254 **(2003)** 203-210.

[47] Davies A.R., Field J.E., *The solid particle erosion of free-standing CVD diamond*, Wear 252 **(2002)** 96–102.

[48] Walley S.M., Field J.E., *The contribution of the Cavendish Laboratory to the understanding of solid particle erosion mechanisms*, Wear 258 **(2005)** 552–566.

[49] Sugiyama K., Harada K., Hattori S., *Influence of impact angle of solid particles on erosion by slurry jet*, Wear 265 **(2008)** 713–720.

[50] Divakar M., Agarwal V.K., Singh S.N., *Effect of the material surface hardness on the erosion of AISI316*, Wear 259 **(2005)** 110-117.

[51] Goretta K.C., Arroyo R.C., Wu C.T., Routbort J.L., *Erosion of work-hardened copper, nickel, and 304 stainless steel*, Wear 147 **(1991)** 145-154.

[52] Hutchings I.M., *A model for the erosion of metals by spherical particles at normal incidence*, Wear 70 **(1981)** 269-281.

[53] Naim M., Bahadur S., *Work hardening in erosion due to single particle impacts*, Proc. Int. Conf on Wear of Materials, Ed. Ludena, K.C., New York **(1985)** 340-345.

[54] Finnie I., *The mechanism of erosion of ductile metals*, Proc. of 3rd U.S. National congress of Applied Mechanics **(1958)** 527-532.

[55] Chen Y.M., Mongis J., *Cavitation wear in plain bearing: case study*, Mecanique & Industries 6 **(2005)** 195-201.

[56] Levin B.F., Vecchio K.S., DuPont J.N., Marder A.R., *Modeling solid-particle erosion of ductile alloys*, Metall. Mat. Trans. A 30A **(1999)** 1763-1774.

[57] Sidky B.S., Hocking M.G., *Reviewing of organic coatings and coating processes for reducing wear and corrosion*, British Corrosion J. 34 **(1999)** 171-183.

[58] Stringer J., *Coatings in the electricity supply industry: past, present, and opportunities for the future*, Surf. Coat. Tech. 108-109 **(1998)** 1-9.

[59] Barbezat G., Nicoll A.R., Sickinger A., *Abrasion, erosion and scuffing resistance of carbide and oxide ceramic thermal sprayed coatings for different applications*, Wear 162-164 **(1993)** 529-537.

[60] Wang Y., *Friction and wear performances of detonation-gun- and plasma-sprayed ceramic and cermet hard coatings under dry friction*, Wear 161 **(1993)** 69–78.

[61] Semenov S.Y., Cetegen B.M., *Experiments and modeling of the deposition of nano-structured alumina–titania coatings by detonation waves*, Mat. Sci. Eng. A 335 **(2002)** 67–81.

[62] Verma M.C., *Silt friendly design of turbine and other under water components*, Proc. of the First International Conference on Silting Problems in Hydro Power Plants, CBIP New Delhi **(1999)** IV (1 –19).

[63] Naidu B.S.K., *Silting problems in hydro power plants*, Proc. of the Second International Conference on Silting Problems in Hydro Power Plants, Bangkok **(2001)** 1 –16.

[64] Kumar Mukesh., *Effect of Welding parameters on the structures, properties and silt erosion of 13/4 martensitic stainless steel*, Ph.D. Thesis, University of Roorkee **(1996)**.

[65] McCaul C., *CA6NM for sulfide service*, Mat. News Letter 6 **(2007)** 1-5.

[66] Srinivasan V.S., Nagesha A., Valsan M., Rao K. B. S., Mannan S. L., Sastry D. H., *Effect of hold-time on low cycle fatigue behaviour of nitrogen bearing 316L stainless steel*, Int. J. Pressure Vessels and Piping 76 **(1999)** 863-870.

[67] Bose S.C., Singh Kulvir., Ray A.K., Ghosh R.N., *Effect of thermal ageing on mechanical properties and microstructures of a standard G-X 12 CrMoVWNbN 1011 grade of cast steel for turbine casing*, Mat. Sci. Eng. A 476 **(2008)** 257-266.

[68] Speidel M.O., *High nitrogen steels*, Proc. of the 2nd Int. Conf. on High-Nitrogen Steels, HNS 90, Aachen, Germany **(1990)** 128-131.

[69] Mudali U.K., *Nitrogen-A boon to metals industry*, Mat. Manufacturing Processes 19 **(2004)** 1-5.

[70] Malakondaiah G., Srinivas M., Rao P. R., *Ultrahigh-strength low-alloy steels with enhanced fracture toughness*, Progress in Mat. Sci. 42 (1997) 209-242.

[71] Katada Y., *Current research activities on high nitrogen steel in Japan*, Mat. Sci. Forum 539-543 **(2007)** 114-118.

[72] Schramm R.E., Reed R.P., *Stacking fault energies of seven commercial austenitic stainless steels*, Metall. Mat. Trans. A 6A **(1975)** 1345-1351.

[73] Mullner P., Solenthaler C., Uggowitzer P.J., Spiedel M.O., *Brittle fracture in austenitic steel*, Acta. Metall. 42 **(1994)** 2211-2217.

[74] Hanninen H., Romu J., Ilola R., Tervo J., Lantenane A., *Effects of processing and manufacturing of high nitrogen-containing stainless steels on their mechanical, corrosion and wear properties*, J. Mat. Proc. Tech. 117 **(2001)** 424-430.

[75] Sumita M., Hanawa T., Teoh S.H., *Development of nitrogen-containing nickel-free austenitic stainless steels for metallic biomaterials*, Mat. Sci. Eng. C 24 **(2004)** 753-760.

[76] Balachandran G., Bhatia M.L., Ballal N.B., Rao P.K., *Some teoretical apects on dsigning nckel fee high ntrogen astenitic sainless seels*, ISIJ Int. 41 **(2001)** 1018–1027

[77] Pickering F.B., *Physical Metallurgy and Design of Steels*, 1st Ed., Applied Sci. Pub., London, **(1978)**, 226-241.

[78] Hertzman S., Jarl M., *Thermodynamic analysis of the Fe-Cr-N system*, Metall. Trans., 18A **(1987)** 1745-1752.

[79] Uggovitzor P., Magdowski R., Speidel M.O., *Nickel fee high ntrogen austenitic seels*, ISIJ Int. 36 **(1996)** 901-908

[80] Burns H., *Manufacture and application of high ntrogen seels*, ISIJ Int. 36 (1996) 909-914

[81] Finnie I., *Erosion of surfaces by solid particles*, Wear 3 **(1960)** 87-103.

[82] Ruff A.W., Wiederhorn S.M., *Erosion by solid particle impact*, Treatise on Mat. Sci. Tech. 16 **(1979)** 69-126.

[83] Meng H.C., Ludema K.C., *Wear models and prediction equations: their form and content*, Wear 181-183 **(1995)** 443-457.

[84] Stachowiak G.W., Batchelor A.W., *Abrasive, erosive and cavitation wear*, Eng. Tribology (Third Edition) **(2006)** 501-551.

[85] Bitter J.G.A., *A study of erosion phenomena: Part I*, Wear 6 **(1963)** 5-21.

[86] Bitter J.G.A., *A study of erosion phenomena: Part II*, Wear 6 **(1963)** 169-190.

[87] Tilly G.P., *A two stage mechanism of ductile erosion*, Wear 23 **(1973)** 87-96.

[88] Levy A.V., *The solid particle erosion behaviour of steel as a function of microstructure*, Wear 68 **(1981)** 269-287.

[89] Sheldon G.L., Kanhere A., *An investigation of impingement erosion using single particles*, Wear 21 **(1972)** 195-209.

[90] Hutchings I.M., Winter R.E., *Particle erosion of ductile metals: A mechanism of material removal*, Wear 27 **(1974)** 121-128.

[91] Winter R.E. Hutchings I.M., *Solid particle erosion studies using single angular particles*, Wear 29 **(1974)** 181-194.

[92] Winter R.E. Hutchings I.M., *The role of adiabatic shear in solid particle erosion*, Wear 34 **(1975)** 141-148.

[93] Christman T., Shewmon P.G., *Erosion of a strong aluminum alloy*, Wear 52 **(1979)** 57-70.

[94] Hutchings I.M., *Some comments on the theoretical treatment of erosive particle impact*, Proc. of the Annual Industrial Pollution Conference **(1979)** 1-36.

[95] Sundararajan G., *An analysis of the localization of deformation and weight loss during single-particle normal impact*, Wear 84 **(1983)** 217-235.

[96] Sundararajan G., Shewmon P.G., *A new model for the erosion of metals at normal incidence*, Wear 84 **(1983)** 237-258.

[97] Brach M.R., *Impact dynamics with applications to solid particle erosion*, Int. J. Impact Eng. 7 **(1988)** 37-53.

[98] Hutchings I.M., Levy A.V., *Thermal effects in the erosion of ductile metals*, Wear 131 **(1989)** 105-121.

[99] Sundararajan G., *An analysis of the erosion-oxidation interaction mechanisms*, Wear 145 **(1991)** 251-282.

[100] Sundararajan G., Shewmon P.G., *The oblique impact of a hard ball against ductile, semi-infinite target materials—experiment and analysis*, Int. J. Impact Eng. 6 (1987) 3-22.

[101] Sheldon G.L., Finnie I., *The mechanism of material removal in the erosive cutting of brittle materials*, Trans. ASME 88B **(1966)** 393-400.

[102] Evans A.G., Wilshaw T.R., *Quasi-static particle damage in brittle solids - I: oservations, aalysis and iplications*, Acta Metall. 24 **(1976)** 939-956.

[103] Zambelli G., Levy A.V., *Particulate erosion of NiO scales*, Wear 68 **(1981)** 305-331.

[104] Hutchings I.M., *Tribology: Friction and wear of egineering materials*, First Published in Great Britain **(1992)** 171-197.

[105] Gahr K.H.Z., *Modelling of two-body abrasive wear*, Wear 124 **(1988)** 87-103.

[106] Arnold J.C., Hutchings I.M., *The mechanisms of erosion of unfilled elastomers by solid particle impact*, Wear 138 **(1990)** 33-46.

[107] Rao P.V., Buckley D.H., *Angular particle impingement studies of thermoplastic materials at normal incidence*, ASLE Transactions 29 **(1986)** 283-298.

[108] Sargent G.A., Saigal D., *Erosion of low-carbon steel by coal particles*, ASLE Transactions 29 **(1986)** 256-266.

[109] Shah S.M., Verhoeven J.D., Bahadur S., *Erosion behavior of high silicon bainitic structures: I: Austempered ductile cast iron*, Wear 113 **(1986)** 267-278.

[110] Shah S.M., Bahadur S., Verhoeven J.D., *Erosion behavior of high silicon bainitic structures : II: High silicon steels*, Wear 113 **(1986)** 279-290.

[111] Dular M., Stoffel B., Širok B., *Development of a cavitation erosion model*, Wear 261 **(2006)** 642-655.

[112] Avellan F., Farhat M., *Shock pressure generated by cavitation vortex collapse*, Proc. of the Third International Symposium on Cavitation Noise and Erosion in Fluid systems, FED-vol. 88, ASME Winter Annual Meeting, San Francisco, CA **(1989)** 119–125.

[113] Philipp A., Lauterborn W., *Cavitation erosion by single laser-produced bubbles*, J. Fluid Mechanics 361 **(1998)** 75–116.

[114] Karimi A., Avellan F., *Comparison of erosion mechanisms in different types of cavitation*, Wear 113 **(1986)** 305-322.

[115] Trethewey K.R., Haley T.J., Clark C.C., *Effect of ultrasonically induced cavitation on corrosion behaviour of a copper-manganese-aluminum alloy*, British J. Corrosion, 23 **(1988)** 55-60.

[116] Preece C.R., Brunton J.H., *A comparison of liquid impact erosion and cavitation erosion*, Wear 60 **(1980)** 269-284.

[117] Jin H., Zheng F., Li S., Hang C., *The role of sand particles on the rapid destruction of the cavitation zone of hydraulic turbines*, Wear 112 **(1986)** 199-205.

[118] Hattori S., Kishimoto M., *Prediction of cavitation erosion on stainless steel components in centrifugal pumps*, Wear (In Press) **(2008)** doi.1016/j.wear.2008.04.045

[119] Rao P.V., *Evaluation of epoxy resins in flow cavitation erosion*, Wear 122 **(1988)** 77-96.

[120] Okada T., Iwai Y., Yamamoto A., *A study of cavitation erosion of cast iron*, Wear 84 **(1983)** 297-312.

[121] Heathcock C.J., Ball A., Protheroe B.E., *Cavitation erosion of cobalt-based stellite alloys, cemented carbides and surface-treated low alloy steels*, Wear 74 **(1981)** 11-26.

[122] Liu W., Zheng Y.G., Liu C.S., Yao Z.M., Ke W., *Cavitation erosion behavior of Cr–Mn–N stainless steels in comparison with 0Cr13Ni5Mo stainless steel*, Wear 254 **(2003)** 713-722.

[123] Fu W., Zheng Y., He X., *Resistance of a high nitrogen austenitic steel to cavitation erosion*, Wear 249 **(2001)** 788-791.

[124] Zhang X.F., Fang L., *The effect of stacking fault energy on the cavitation erosion resistance of alpha- phase aluminum bronzes*, Wear 253 **(2002)** 1105-1110.

[125] Head W.J., Harr M.E., *The development of a model to predict the erosion of materials by natural contaminants*, Wear 15 **(1970)** 1-46.

[126] Naim M., Bahadur S., *Effect of microstructure and mechanical properties on the erosion of 18 Ni (250) maraging steel*, Wear, 112 **(1986)** 217 - 234.

[127] Goretta K.C., Thompson A.C., Routbort J.L., *Erosion of heat-treated AISI 4140 steel*, Mat. Sci. Eng. A161 **(1993)** L7-L10.

[128] Richman R.H., McNaughton W.P., *Correlation of cavitation erosion behavior with mechanical properties of metals*, Wear, 140 **(1990)** 63-82.

[129] Zhou R., Lu D.H., Jiang Y.H., Li Q.N., *Mechanical properties and erosion wear resistance of polyurethane matrix composites*, Wear 259 **(2005)** 676–683

[130] O'Flynn D.J., Bingley M.S., Bradley M.S.A., Burnett A. J., *A model to predict the solid particle erosion rate of metals and its assessment using heat-treated steels*, Wear 248 **(2001)** 162-177.

[131] Kishore, Sampathkumaran P., Seetharamu S., *Erosion and abrasion characteristics of high manganese chromium irons*, Wear 259 **(2005)** 70–77.

[132] Pugsley V.A., Allen C., *Microstructure / property relationships in the cavitation erosion of tungsten carbide–cobalt*, Wear 233–235 **(1999)** 93–103.

[133] Wang B.Q., Geng G.Q., Levy A.V., *Effect of microstructure on the erosion-corrosion of steel*, Wear 151 **(1991)** 351-364.

[134] Xi Z.T., Zhou Q.D., *Influence of retained austenite on the wear resistance of high chromium cast iron under various impact loads*, Wear 162–164 **(1993)** 83–88.

[135] Soussan A., Degallaix S., *Work-hardening behaviour of nitrogen-alloyed austenitic stainless steels*, Mat. Sci. Eng. A142 **(1991)** 169–176.

[136] Kwok C.T., Man H.C., Cheng F.T., *Cavitation erosion and damage mechanisms of alloys with duplex structures*, Mat. Sci. Eng. A242 **(1998)** 108–120.

[137] Bregliozzia G., Di Schinob A., Ahmed S.I.U., Kenny J.M., Haefke H., *Cavitation wear behaviour of austenitic stainless steels with different grain sizes*, Wear 258 **(2005)** 503–510.

[138] Telling R.H., Field J.E., *The erosion of diamond, sapphire and zinc sulphide by quartz particles*, Wear 233–235 **(1999)** 666–673.

[139] Jiang Z., Guan Z., Lian J., *Effects of microstructural variables on the deformation behaviour of dual-phase steel*, Mat. Sci. Eng. A190 **(1995)** 55-64.

[140] Hodgson P.D., *Microstructure modelling for property prediction and control*, J. Mat. Proc. Tech. 60 **(1996)** 27-33.

[141] Roy M., Vishvanathan B., Sundararajan G., *The solid particle erosion of polymer matrix composites*, Wear 171 **(1994)** 149-161.

[142] Hutchings I.M., *Ductile-brittle transitions and wear maps for the erosion and abrasion of brittle materials*, J. Phys. D: Appl. Phys. 25 **(1992)** A212-A221.

[143] Stack M. M., Pungwiwat N., *Slurry erosion of metallics, polymers, and ceramics: particle size effects,* Mat. Sci.. Tech. 15 **(1999)** 337-344.

[144] Friedrich K., *Erosive wear of polymer surfaces by steel blasting.* J. Mat. Sci. 21 **(1986)** 3317–3332.

[145] Mishra S.B, Chandra K., Prakash S., Venkataraman B., *Erosion performance of coatings produced by shrouded plasma spray process on a Co-based superalloy*, Surf. Coat. Tech. 201 **(2006)** 1477-1487.

[146] Shipway P.H., Hutchings I.M., *Measurement of coating durability by solid particle erosion*, Surf. Coat. Tech. 71 **(1995)** 1-8.

[147] Pfender E., *Fundamental studies associated with the plasma spray process*, Surf. Coat. Tech. 34 **(1988)** 1-14.

[148] Goel D.B., *Metallurgical solutions to erosion problems in hydroelectic plants*, Hydro Power an Indian Perspective, CBS Publishers & Distributors, New Delhi, **(2001)** 229-245.

[149] Levy A.V., Buqian W., *Erosion of hard material coating systems*, Wear 121 **(1988)** 325-346.

[150] Levy A.V., *The erosion-corrosion behavior of protective coatings*, Surf. Coat. Tech. 36 **(1988)** 387-406.

[151] Shui Z.R., Wang B.Q., Levy A.V., *Erosion of protective coatings*, Surf. Coat. Tech. 43-44 **(1990)** 875-887.

[152] Srinivasan S., Scattergood R.O., *Effect of erodent hardness on erosion of brittle materials*, Wear 128 **(1988)** 139-152.

[153] Jeanine T., DeMasi-Marcin, Gupta D. K., *Protective coatings in the gas turbine engine*, Surf. Coat. Tech. 68-69 **(1994)** 1-9.

[154] Rhys-Jones T.N., *Thermally sprayed coating systems for surface protection and clearance control applications in aero engines*, Surf. Coat. Tech. 43-44 **(1990)** 402-415.

[155] Mann B.S., Arya V., *Abrasive and erosive wear characteristics of plasma nitriding and HVOF coatings: their application in hydro turbines*, Wear 249 **(2001)** 354-360.

[156] Karimi A., Verdon C., Barbezat G., *Microstructure and hydro abrasive wear behaviour of high velocity oxy-fuel thermally sprayed WC-Co (Cr) coatings*, Surf. Coat. Tech. 57 **(1993)** 81-89.

[157] Murthy J.K.N., Venkataraman B., *Abrasive wear behaviour of WC–Co-Cr and Cr_3C_2–20(NiCr) deposited by HVOF and detonation spray processes*, Surf. Coat. Tech. 200 **(2006)** 2642-2652.

[158] Stewart D.A., Shipway P.H., McCartney D.G., *Abrasive wear behaviour of conventional and nano composite HVOF-sprayed WC–Co coatings*, Wear 225-229 **(1999)** 789-798.

[159] Murthy J.K.N., Rao D.S., Venkataraman B., *Effect of grinding on the erosion behaviour of a WC–Co–Cr coating deposited by HVOF and detonation gun spray processes*, Wear 249 **(2001)** 592-600.

[160] Sudaprasert T., Shipway P.H., McCartney D.G., *Sliding wear behaviour of HVOF sprayed WC–Co coatings deposited with both gas-fuelled and liquid-fuelled systems*, Wear 255 **(2003)** 943-949.

[161] Mann B.S., Arya V., *HVOF coating and surface treatment for enhancing droplet erosion resistance of steam turbine blades*, Wear 254 **(2003)** 652-667.

[162] Wang B.Q., Shui Z.R., *Hot erosion behavior of carbide–metal composite coatings*, J. Mat. Proces. Tech. 143-144 **(2003)** 87-92.

[163] Sugiyama K., Nakahama S., Hattori S., Nakano K., *Slurry wear and cavitation erosion of thermal-sprayed cermets*, Wear 258 **(2005)** 768-775.

[164] Machio C.N., Akdogan G., Witcomb M.J., Luyckx S., *Performance of WC–VC–Co thermal spray coatings in abrasion and slurry erosion tests*, Wear 258 **(2005)** 434-442.

[165] ASTM E8M-03, *Standard test methods for tension testing of metallic materials,* West Conshohocken, PA **(2003)**.

[166] ASTM E23-07, *Standard test methods for notched bar impact testing of metallic materials,* West Conshohocken, PA **(2007)**.

[167] http://www.gordonengland.co.uk/ds.htm **(13 March, 2008)**

[168] Wood R.J.K., Wheeler R., *Design and performance of a high velocity air–sand jet impingement erosion facility,* Wear 220 **(1998)** 95-112.

[169] Drozdz D., Wunderlich R.K., Fecht H.J., *Cavitation erosion behaviour of Zr-based bulk metallic glasses,* Wear 262 **(2007)** 176–183.

[170] Ness E., Zibbell R., *Abrasion and erosion of hard materials related to wear in the abrasive water jet,* Wear 196 **(1996)** 120-125.

[171] Mann B.S., *Erosion visualization and characteristics of a two dimensional diffusion treated martensitic stainless steel hydrofoil,* Wear 217 **(1998)** 56-61.

[172] Mann B.S., *High-energy particle impact wear resistance of hard coatings and their application in hydro turbines,* Wear 237**(2000)** 140-146.

[173] Oka Y.I., Okamura K., Yoshida T., *Practical estimation of erosion damage caused by solid particle impact: Part 1: Effects of impact parameters on a predictive equation,* Wear 259 **(2005)** 95-101.

[174] Ball A., *On the importance of work hardening in the design of wear-resistant materials,* Wear 91 **(1983)** 201-207.

[175] Ikegami Y., Nemoto R., *Effect of thermo-mechanical treatment on mechanical properties of high-nitrogen containing Cr-Mn-Ni austenitic stainless steels*, ISIJ Int. 36 **(1996)** 855-861.

[176] Padilha A.F., Rios P.R., *Decomposition of austenite in austenitic stainless steels*, ISIJ Int. 42 **(2002)** 325-337.

[177] Klueh R.L., Maziasz P.J., Lee E.H., *Manganese as an austenite stabilizer in Fe-Cr-Mn-C steels*, Mat. Sci. Eng. 102 **(1988)** 115-124.

[178] Mishra S.B., Prakash S., Chandra K., *Studies on erosion behaviour of plasma sprayed coatings on a Ni-based superalloy*, Wear 260 **(2006)** 422–432.

[179] Kumar Subodh., Goel D.B., *Micralloying of hadfield Mn steel for improved mechanical properties and wear characteristics*, Proc. of 37th Annual Convention, The Institute of Indian Foundrymen 17-19 Feb **(1989)** New Delhi 59-65.

[180] Ball A., Feng Z., *The erosion of four materials using seven erodents — toward an understanding*, Wear 233–235 **(1999)** 674–684.

[181] Zhou J., Bahadur S., *The effect of material composition and operational variables on the erosion of alumina ceramics*, Wear 150 **(1991)** 343-354.

[182] Ninham A., *The effect of mechanical properties on erosion*, Wear 121 **(1988)** 307 – 324.

[183] Hussainova I., Kubarsepp J., Pirso J., *Mechanical properties and features of erosion of cermets*, Wear 250 **(2001)** 818–825.

[184] Foley T., Levy A., *The erosion of heat-treated steels*, Wear 91 **(1983)** 45 – 64.

[185] Sundararajan G., *The solid particle erosion of metals and alloys*, Transact. Ind. Inst. Metals 36 **(1983)** 474–495.

[186] Naim M., Bahadur S., *The significance of the erosion parameter and the mechanisms of erosion in single-particle impacts*, Wear 94 **(1984)** 219–232.

[187] Rao D.R.K., Venkataraman B., Asundi M.K., Sundararajan G., *The effect of laser surface melting on the erosion behavior of low alloy steel*, Surf. Coat. Tech. 58 **(1993)** 85–92.

[188] Heathcock C.J., Protheroe B.E., Ball A., *Cavitation erosion of stainless steels*, Wear 81 **(1982)** 311-327.

[189] Sang K., Li Y., *Cavitation erosion of flame spray weld coating of nickel-base alloy powder*, Wear 189 **(1995)** 20-24.

[190] Huang W.H., Chen K.C., He J.L., *A study on the cavitation resistance of ion-nitrided steel*, Wear 252 **(2002)** 459-466.

[191] Stoltz R.E., Vander S.J.B., *The Effect of nitrogen on stacking fault energy of Fe-Ni-Cr-Mn Steels*, Met. Trans 11A **(1980)** 1033-1037.

[192] Garzon C.M., Thomas H., Santos J.F., Tschiptschin A.P., *Cavitation erosion resistance of a high temperature gas nitrided duplex stainless steel in substitute ocean water*, Wear 259 **(2005)** 145-153.

[193] Zhang P., Jiang J., Ma A., Wang Z., Wu Y., Lin P., *Cavitation erosion resistance of WC-Cr-Co and Cr_3C_2-NiCr coatings prepared by HVOF*, Advanced Mat. Research 15-17 **(2007)** 199-204.

[194] Herman H., Sampath S., Thermal spray coatings, *metallurgical and ceramic protective coatings*, K.H. Stern (Ed.), Chapman and Hall, London, **(1996)** 261-289.

[195] Takeda K., Ito M., Takeuchi S., Sudo K., Koga M., Kazama K., *Erosion resistance coating by low pressure plasma spraying*, ISIJ Int.33 **(1993)** 976–981.

[196] Hearley J.A., Little J.A., Sturgeon A.J., *The erosion behaviour of NiAl intermetallic coatings produced by high velocity oxy-fuel thermal spraying*, Wear 233–235 **(1999)** 328-333.

[197] Wang B., Lee S.W., *Erosion–corrosion behaviour of HVOF NiAl–Al_2O_3 intermetallic-ceramic coating*, Wear 239 **(2000)** 83-90.

[198] Sidhu H.S., Sidhu B.S., Prakash S., *Solid particle erosion of HVOF sprayed NiCr and Stellite-6 coatings*, Surf. Coat. Tech. 202 **(2007)** 232–238.

[199] Fagoaga I., Viviente J.L., Gavin P., *Multilayer coatings by continuous detonation system spray technique*, J. Thin Solid Films 317 **(1998)** 259-265.

[200] Wang J., Zhang Li, Sun B., Zhou Y., *Study of the Cr_3C_2–NiCr detonation spray coating*, Surf. Coat. Tech. 130 **(2000)** 69–73.

[201] Singh H., Puri D., Prakash S., *Studies of plasma spray coatings on a Fe-base superalloy, their structure and high temperature oxidation behaviour*, Anit-Corrosion Methods and Mat. 52 **(2005)** 84-95.

[202] Ji G. C., Li C. J., Wang Y. Y. Li W. Y., *Microstructural characterization and abrasive wear performance of HVOF sprayed Cr_3C_2–NiCr coating*, Surf. Coat. Tech. 200 **(2006)** 6749-6757.

[203] Sahraoui T., Fenineche N., Montavon G., Coddet C., *Structure and wear behaviour of HVOF sprayed Cr_3C_2–NiCr and WC–Co coatings*, Mat. and Design 24 **(2003)** 309-313.

[204] Zhang K., *Wear of cobalt-based alloys sliding in molten zinc*, Wear 255 **(2003)** 545-555.

[205] Zhao L., Zwick J., Lugscheider E., *HVOF spraying of Al_2O_3-dispersion-strengthened NiCr powders*, Surf. Coat. Tech. 182 **(2004)** 72-77.

[206] Zhu F., Wendt H., Haasen P., *Atom probe field ion microscopy of a Fe-Cr-Co permanent magnet alloy*, Scripta Meta.16 **(1982)** 1175-1180.

[207] Burke M.G., Hicks T.G., Phaneuf M.W., *Microstructure of stellite / steel clad interface*, Microsc Microanal 11 **(2005)** 2014-2015.

[208] Staia M.H., Valente T., Bartuli C., Lewis D.B., Constable C.P., *Part I: Characterization of Cr_3C_2-25% NiCr reactive plasma sprayed coatings produced at different pressures,* Surf. Coat. Tech. 146-147 **(2001)** 553-562.

[209] Sapate S.G., Rao A.V.R., *Effect of carbide volume fraction on erosive wear behaviour of hardfacing cast irons,* Wear 256 **(2004)** 774-786.

[210] Zhou R., Jiang Y., Lu D., *The effect of volume fraction of WC particles on erosion resistance of WC reinforced iron matrix surface composites,* Wear 255 **(2003)** 134-138.

[211] Verdon C., Karimi A., Martin J. L., *A study of high velocity oxy-fuel thermally sprayed tungsten carbide based coatings. Part 1: Microstructures,* Mat. Sci. Eng. A 246 **(1998)** 11-24.

[212] Vicenzi J., Villanova D.L., Lima M.D., Takimi A.S., Marques C.M., Bergmann C.P., *HVOF-coatings against high temperature erosion (~300 °C) by coal fly ash in thermoelectric power plant,* Mat. and Des. 27 **(2006)** 236-242.

Appendix I

Publications

1. **Chauhan** A.K., Goel D.B., Prakash S., Erosion behaviour of hydro turbine steels, Bulletin of Material Science, 31 (2008) 115–120.

2. **Chauhan A.K.,** Goel D.B., Prakash S., Solid particle erosion behaviour of 13Cr–4Ni and 21Cr–4Ni–N steels, Journal of Alloys and compounds, (in Press 2008). doi:10.1016/j.jallcom.2007.12.053

3. **Chauhan** A.K., Goel D.B., Prakash S., Erosive wear of surface coated hydro turbine steel, Bulletin of Material Science, (Under review).